JPRS-53498

JPRS 53498

1 July 1971

PROTECTION FROM PENETRATING RADIATION OF A NUCLEAR EXPLOSION

By

V. I. Kukhtevich, I. V. Goryachev, et al.

- USSR -

JOINT PUBLICATIONS RESEARCH SERVICE

NOTE

Unless otherwise indicated items are complete textual translations of the original.

The contents of this publication in no way represent the policies, views, or attitudes of the U.S. Government.

PROCUREMENT OF PUBLICATIONS

JPRS publications may be ordered from the National Technical Information Service, Springfield, Virginia 22151. In ordering, it is recommended that the JPRS number, title, date and author, if applicable, of publication be cited.

Current JPRS publications are announced in U.S. Government Research & Development Reports issued semi-monthly by the National Technical Information Service, and are listed in the Monthly Catalog of U.S. Government Publications issued by the Superintendent of Documents, U.S. Government Printing Office, Washington, D.C. 20402.

Correspondence pertaining to matters other than procurement may be addressed to Joint Publications Research Service, 1000 North Glebe Road, Arlington, Virginia 22201.

JPRS 53498

1 July 1971

UDC: 699.887:621.039.9

PROTECTION FROM PENETRATING RADIATION OF A NUCLEAR EXPLOSION

Translation of the Russian-language book by V. I. Kukhtevich, I. V. Goryachev, and L. A. Trykov, edited by Doctor of Physical and Mathematical Sciences V. I. Kukhtevich: Zashchita ot Pronikayushchey Radiatsii Yadernogo Vzryva, Moscow, Atomizdat Press, 1970, 190 pages.

CONTENTS

[I - USSR - K]

FOREWORD

During the quarter century since the creation of the first atomic bomb, a tremendous number of nuclear and thermonuclear warheads of various sizes have been accummulated in the world. Various transport systems have been created, allowing delivery of nuclear warheads to any point on the earth. Although an agreement was signed in 1963, forbidding the testing of nuclear weapons in the atmosphere, in space and underwater, some countries still continue to perform nuclear weapons tests. American strategic aircraft fly regularly with nuclear bombs onboard.

Some countries, desiring to develop their own nuclear weapons, are delaying in signing the treaty.

Therefore, the problem of protection of the population from the effects of the radiation of nuclear explosions is a problem of prime importance.

The creation of shielding effective against the radiation of nuclear explosions is a difficult and interesting scientific task. Although in principle the design of shielding from the radiation of nuclear explosions is no different from the design of the biological shielding of nuclear reactors, it has a number of peculiarities resulting from the specific geometric conditions and quality of the radiation involved.

Over the past few years, books have been published relating to various aspects of the phenomena accompanying nuclear explosions. The monographs of O. I. Leypunskiy Gamma-Izlucheniye Atomnogo Vzryva [The Gamma Radiation of a Nuclear Explosion] (Atomizdat Press, 1959) and P. A. Yampol'skiy Neytrony Atomnogo Vzryva [The Neutrons of an Atomic Explosion] (Gosatomizdat Press, 1961) are dedicated to description of the physical processes involved in the propagation of gamma radiation and neutrons in a nuclear explosion; the spatial distribution of the doses of neutrons and γ radiation during nuclear explosions are

analyzed. Problems of shielding from radiation are hardly discussed in these books.

The book Deystviye Yadernogo Oruzhiya [The Effects of Nuclear Weapons] (Translated from the English, Voyenizdat Press, 1963) presents a general description of all aspects of nuclear explosions and shielding against damaging effects. However, this book is descriptive in nature and is more an introduction to the problem than a practical guide.

The book of R. V. Petrov et al. Zashchita Ot Radioaktivnykh Osadkov [Protection From Radioactive Fallout] (Medgiz Press, 1963) and that of L. V. Spenser Zashchita Ot Gamma-Izlucheniya Radioaktivnykh Vypadeniy [Protection From the Gamma Radiation of Radioactive Fallout] (Translated from the English, Atomizdat Press, 1965) contain valuable material on protection from the radiation of radioactive fallout. The book of Petrov analyzes the general radiation situation arising when radioactive fallout occurs following an explosion. The book of Spenser presents an approximate method of designing shielding against γ radiation, corresponding to the specific geometric conditions which obtain when areas and structures are contaminated with radioactive fallout.

Thus, as yet no one has discussed the design of shielding from the primary radiation of a nuclear blast, and only one book has presented a method for approximate design of shielding of structures from the radiation of radioactive fallout.

However, many publications have appeared in the periodical literature in the past six or seven years concerning both clarification of the propagation of penetrating radiation in the atmosphere and its transmission through shielding. These data have not yet been systemitized in order to allow their use for the design of shielding from the radiation of nuclear explosions.

The use of these data is important, since correct design requires detailed knowledge of the characteristics of the field of ionizing radiation.

Actually, the dose within a protective structure can be calculated if we know the spectral and angular distributions of radiation on the outer surfaces of its walls. In a nuclear explosion, the field of radiation consists of radiation scattered in the air and radiation reflected from the earth, with complex spectral and angular characteristics. Equally detailed information is required on the radiation passing through the shielding.

In order to prevent this information in a small book, along with characteristics of the attenuation of radiation in shielding and a calculation method, the authors have omitted general definitions and physical interpretation of certain phenomena. The authors assume that the basic concepts of the physics of shielding have been sufficiently fully covered in certain monographs, for example B. Price, K. Horton and K. Spinney Zashchita Ot Yadernykh Izlucheniy [Shielding Against Nuclear Radiation] (Translated from the English, Foreign Literature Press, 1959); G. Goldstein Osnovy Zashchity Reaktorov [Principles of Reactor Shielding] (Gosatomizdat Press, 1961); and Yu. A. Kazanskiy et al. Fizicheskiye Issledovaniya Zashchity Reaktorov [Physical Studies of Reactor Shielding] (Atomizdat Press, 1966).

The principle of the arrangement of the book should be clear from the Table of Contents and requires no explanation.

Keeping in mind the fact that the planning of shielding structures involves both specialists in the area of nuclear equipment and construction engineers, practical calculations are presented in two versions. A simplified version is presented for an approximate solution, requiring no computer equipment. Precise design of complex structures requires the use of electronic computers. In these cases, calculation methods are presented in this book.

The authors hope that the book will be useful to a broad range of scientific workers and engineers working in the area of radiation protection, as well as persons directly involved in the development of protective structures.

CHAPTER 1. A NUCLEAR EXPLOSION AS A SOURCE OF IONIZING RADIATION

§ 1. Brief Description of Phenomena Accompanying a Nuclear Explosion

The explosion of a nuclear warhead is accompanied by liberation of a tremendous quantity of energy, concentrated in a small volume, over an extremely brief period of time. The colossal energy density causes heating of the material in the area of the explosion to temperatures on the order of tens of millions of degrees.

Matter heated to these high temperatures emits energy in the form of electromagnetic radiation over an extremely broad spectrum -- from x-rays to long wave electromagnetic energy.

A large portion of this energy is absorbed by the outer layers of the weapon. These layers, being heated, begin to glow and transmit energy outward. The energy radiated at these high temperatures is absorbed in the air, heating the layers of air adjacent to the bomb. The area of air surrounding the weapon begins to glow, forming the so-called atomic explosion fireball. As the air is increased in temperature, its pressure increases as well. The fireball grows very rapidly due to radiant transfer of energy.

As the fireball grows, the temperature of its outer areas decreases. Whereas at high temperatures the increase in size of the fireball results from radiant heat conductivity, during later stages the transfer of energy is achieved by displacement of the air mass from the area of increased density outward.

In the initial stage following the blast, the leading edge of the shock wave (area of sharp pressure, density and temperature gradient) corresponds with the boundary of the fireball. As the temperature drops, the moment arrives when the shock wave separates from the boundary of the fireball and moves further away from the blast center, while the fireball, expanding slowly, continues to glow for several more tenths of a second.

After passage of the shock wave, the pressure behind the wave equalizes; therefore, in the high temperature area adjacent to the blast center, the density of the air is less than atmospheric: an area of low density is formed. This area, due to its low density, rises upward.

The radioactive cloud containing the remains of the bomb rises upward, but soon the heavy particles begin to drop out of the cloud and fall to the ground along the path of movement of the cloud, forming a radioactive wake.

The most important factors in the damaging effects of a nuclear blast are the shock wave, light radiation and ionizing radiation. The quantity of energy in these damaging forms extending for various distances from the center of the blast depends on the type of nuclear warhead and the medium in which the blast occurs. If the blast occurs in the atmosphere at an altitude of less than 30 km, 35 % of the total blast energy is expended in the form of light radiation. Under these conditions, about 50% of the energy of nuclear fission is expended in the formation of the shock wave. The remaining 15% is liberated in the form of ionizing radiation. Of this radiation, about 5% is the initial radiation, acting during the first one minute following the moment of the blast, while 10% of the total energy of the nuclear explosion makes up the residual radiation, which appears over an extended period of time. The residual radiation results almost entirely from radioactive fission products. In a thermonuclear explosion, in which only about one-half of the total explosive energy is liberated as a result of the fission reaction, residual radiation amounts to only 5% of the energy liberated by the blast.

The portion of the energy of ionizing radiation is a small fraction of the total energy liberated in a nuclear blast; however, due to the great penetrating capacity and difficulty of detecting ionizing radiation, this radiation may have a damaging effect even at great distances from the radiation source and even in shelters. Therefore, ionizing radiation is an important damaging factor of a nuclear weapon.

Depending on the nature of the object and the purpose of the atomic attack, a nuclear blast may be performed in the air, at the surface of the ground (water) or underground (underwater). Therefore, atmospheric, surface and underground (underwater) explosions are differentiated.

Usually, an atmospheric nuclear explosion is used to destroy city or industrial buildings, to damage personnel and equipment on the field of battle. Under these conditions, it is set off at an altitude of several hundreds or thousands of meters over the ground, depending on

the power of the blast. A surface blast is designed to destroy strong surface structures, railroad junctions, heavy shelters, airfields, and to damage surface ships. It may be performed at an altitude of a few tens of meters over the surface or directly at the surface (contact explosion).

An underground nuclear blast may be used to damage especially strong underground structures. In certain cases, a surface or underground explosion may be used for radioactive contamination of the terrain in the enemy rear area as well.

The external picture of the blast, as well as the effects of its damaging factors, depend on the position of the blast center in relationship to the surface of the earth. During an atmospheric blast, the fireball does not touch the surface of the earth at the moment of its maximum brightness, and its dimensions depend on the power of the blast. The maximum radii of the fireball for atmospheric and surface explosions of the same power do not differ very greatly. The mean radius of the fireball can be described approximately by the following expression:

$$r_{fb} = 33.6q^{0,4}\text{m}, \qquad (1.1)$$

where q is the power of the explosion, kt.

The maximum size of the fireball is not immediately achieved, although the rate of growth of the fireball is rather great, so that it can be considered that it does not rise to any significant height above the point of the explosion during the time of its formation. Therefore, the height of a blast at which the fireball will not contact the surface of the earth is determined by its radius [see (1.1)].

If the distance between the blast center and surface of the earth (water) is not over r_{fb}, the external picture of the explosion is essentially the same as for an explosion occurring directly on the surface. Therefore, blasts occurring both directly on the surface and at a slight altitude above the surface are both considered surface blasts. With increasing altitude of the explosion, an intermediate position develops, in which the fireball does not contact the surface of the earth, but the column of dust and soil rising from the earth catches up with the rising cloud of fission products and is connected to it. This type of explosion is looked upon as a low altitude atmospheric blast.

During the period when the fireball glows, its temperature is so high that, at least in its interior, all of the matter of which the nuclear weapon is made is in the vapor state. This matter includes the radioactive fission products, uranium (or plutonium) which has not fissioned, the envelope around the charge and other parts of the nuclear weapon.

At the moment of an explosion, a mass of gas flies outward from the explosion center. A hollow sphere is formed in the center, the dimensions of which depend on the power of the explosion. After the departure of the shock wave, the pressure within the fireball returns to normal, but the density of the gas becomes near zero, since the temperature within the fireball is extremely high.

It is this significant difference between the densities within and without the fireball which leads to the rise of the radioactive cloud.

§ 2. The Neutrons of a Nuclear Explosion

During a nuclear explosion, the primary source of neutrons consists of the prompt fission neutrons emitted in the first few tenths of a microsecond.

Upon fission of nuclei of U^{235} or other fissionable material, the energy spectrum of prompt neutrons can be described by the following formula [1]:

$$\Phi_0(E_n) = \sqrt{E_n}\, e^{-\frac{3}{2}\frac{E_n}{\varepsilon}}. \qquad (1.2)$$

In this expression, parameter ε depends on the energy of excitation of the fission fragments which is related in turn to the mean number of neutrons ν per fission event. This relationships is expressed by the following dependence:

$$\varepsilon \approx 0{,}78 + 0{,}621\,(\nu + 1)^{1/2} \text{ MeV}. \qquad (1.3)$$

The value of ν for fission by thermal neutrons is well known for most fissionable nuclei:

$$U^{235} - \nu = 2{,}47 \pm 0{,}03;$$

$$U^{233} - \nu = 2{,}51 \pm 0{,}03;$$

$$Pu^{239} - \nu = 2{,}90 \pm 0{,}04.$$

This indicates that when U^{233} is split by thermal neutrons, the value of ε is 0.02 MeV higher than for the fission of U^{235}; for Pu^{239}, the increase is 0.07 MeV. Thus, for thermal neutron fission, the spectrum of Pu^{239} contains 30% more neutrons with energies of 10 MeV than the spectrum accompanying fission of U^{235}.

It is known that ν increases approximately linearly with the energy of the neutrons causing fission, and that the increase for U^{235} is 0.15 per 1 MeV. This change in ν, together with the relationship (1.3) between ε and ν presented above indicates that the mean energy of fission neutrons for U^{235} increases by 0.04 MeV as the energy of the neutrons causing fission is increased by 1 MeV. This slight change in the energetic characteristics of the fission neutrons with a change in the energy of neutrons causing fission or the energy of the nuclei undergoing fission can be ignored.

During a thermonuclear explosion based on reactions with lithium deuteride and the products of this reaction, the following main reactions occur [2]:

$$D + D \rightarrow He^3 + n + 3{,}25 \text{ MeV};$$
$$D + D \rightarrow T + p + 4{,}0 \text{ MeV};$$
$$n + Li^6 \rightarrow He^4 + T + 4{,}8 \text{ MeV};$$
$$T + D \rightarrow He^4 + n + 17{,}6 \text{ MeV}.$$

The probability of the last two reactions is approximately 100 times higher than the probability of the first two reactions; therefore, explosions of this type characteristically emit neutrons with energies of around 14 MeV. These neutrons interact with the structural elements of the bomb and the unreacted nuclear fuel. The higher energy of neutrons in this case results in the nuclear reaction (n, 2n). Furthermore, the reaction of inelastic scattering of neutrons on the heavy nuclei of the structural elements of the weapon is quite probable, resulting in the formation of neutrons with most probable energy around 4 MeV [3].

The spectrum of neutrons formed upon explosion of a bomb based on the fission-synthesis-fission principle, ignoring the moderation of neutrons within the material of the bomb, should be approximately as shown on Figure 1.1. This hypothetical spectrum consists of three main components: fission neutrons with most probable energy around

800 KeV (curve 1), neutrons developing as a result of inelastic scattering of 14 MeV neutrons, with most probable energy about 4 MeV (curve 2) and the 14 MeV neutrons (curve 3). The relationship between the various groups of neutrons can be significantly changed, depending on the share of power in the energy balance of the explosion attributed to fission and to thermonuclear reactions, as well as the design of the bomb.

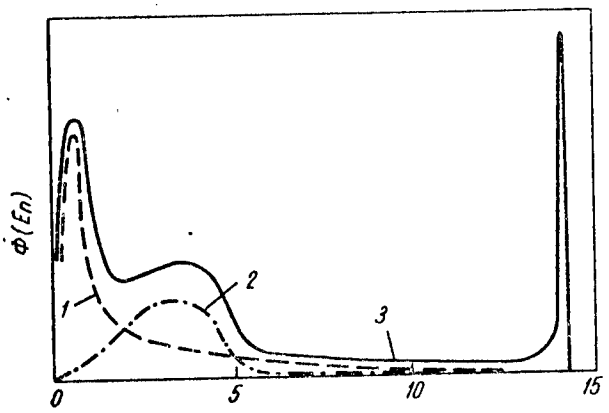

Figure 1.1. Probable Spectrum of Neutrons Formed Upon Explosion of a Weapon Operating According to the Fission-Synthesis-Fission Principle (Ignoring Moderation in the Shell):

1, fission neutrons; 2, neutrons resulting from inelastic scattering of neutrons with energy 14 MeV; 3, neutrons with energy 14 MeV developing in the synthesis reaction

The actual spectrum of neutrons formed by explosion of a bomb operating according to the fission-synthesis-fission principle will be softer and smoother, as a result of moderation of neutrons in the materials and structure of the warhead.

The distribution of neutrons leaving the shell of a nuclear weapon by energies is determined by the structural characteristics of the weapon, i. e. the quantities characterizing the permeability of the outer portions of the weapon. The problem of transformation of the spectrum of fission neutrons as they penetrate through the shell of a weapon was discussed in detail in [4].

Calculation of the spectrum of neutrons (density 2 g/cm^3) is presented in [4] and its results are shown on Figure 1.2.

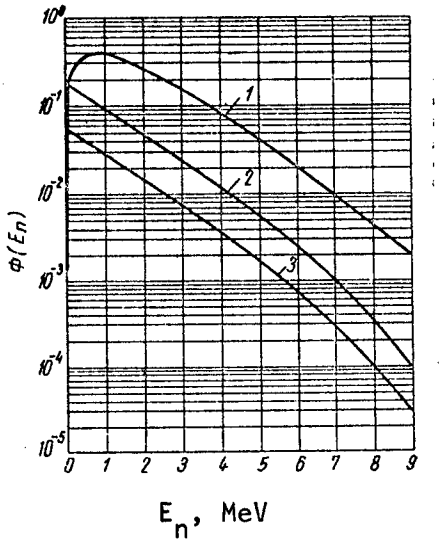

Figure 1.2. Spectrum of Neutrons Formed Upon Explosion of Weapon Based on Fission-Synthesis-Fission Principle:

1, spectrum of fission neutrons; 2, spectrum of neutrons leaving shell with radius of 25 cm; 3, spectrum of neutrons leaving shell with radius 50 cm

As we can see, the spectrum of neutrons leaving the shell is quite different from the spectrum of the primary fission neutrons. The spectrum of the scattered neutrons includes a significant fraction of neutrons at low energies. Figure 1.2 also indicates that the forms of the spectra of neutrons leaving shells of various thicknesses correspond, differing only in the absolute quantity of neutrons emitted during the process of moderation.

In addition to the fission neutrons, a small quantity (less than 1%) of so-called delayed neutrons is formed in the chain reaction of fission of uranium or plutonium; these neutrons are emitted from the strongly excited nuclei with excess neutrons.

Table 1.1 shows the basic data characterizing the delayed neutrons which develop upon fission of uranium and plutonium [5]. The yields of neutrons for each group are presented in the form of the fraction of the total number of delayed neutrons represented by the delayed neutrons emitted in each group.

Table 1.1

DELAYED NEUTRONS EMITTED DURING FISSION

Group	Half Life, sec	Mean Energy, KeV	Share of Delayed Neutrons, $a_i/\Sigma a_i$					
			Th^{232}	U^{233}	U^{235}	U^{238}	Pu^{239}	Pu^{240}
1	54,5	250	0,034	0,086	0,038	0,013	0,038	0,025
2	21,8	460	0,150	0,274	0,213	0,137	0,280	0,270
3	6,0	405	0,155	0,228	0,188	0,162	0,216	0,184
4	2,2	450	0,446	0,316	0,407	0,388	0,328	0,359
5	0,50	520	0,172	0,073	0,128	0,225	0,103	0,135
6	0,18	—	0,043	0,023	0,026	0,075	0,035	0,027
Total yield per fission event			0,0496 ±0,0020	0,0070 ±0,0004	0,0165 ±0,0005	0,0412 ±0,0017	0,0063 ±0,0003	0,0088 ±0,0006
Total yield per neutron emitted during fission			—	0,0029	0,0067	—	0,0021	—

For the fissionable elements U^{235} and Pu^{239}, the half life periods of delayed neutrons correspond within the measurement errors, since the delayed neutrons are formed from the same fragments. The yields of individual groups of delayed neutrons differ, since the curve of the distribution of fragments is different for the different isotopes.

The total yield of delayed neutrons increases with increasing mass number of fissionable material. The greater yield of delayed neutrons in U^{238} and Th^{232} apparently results from the presence of longer decay chains.

The mean energy of delayed neutrons is on the order of 0.5 MeV or less (significantly lower than the energy of prompt fission neutrons). However, we must also note for further analysis that in

contrast to prompt neutrons, the delayed neutrons are formed after the shell has been blown away and therefore do not experience its moderating influence as they fly outward.

In addition to the sources of neutrons during fission and synthesis which we have mentioned, two more should be noted: photoneutrons and activation neutrons.

Photoneutrons are formed by the reaction (γ-n), when the energy of photons exceeds the binding energy of a neutron. For most nuclei, the binding energy is greater than 7 MeV. Significant formation of photoneutrons can be expected only in the nuclei D, Be^9, C^{13} and Li^6, the threshold energies of photons of which are 2.23, 1.67, 4.9 and 5.3 MeV respectively. The values of photoneutron cross sections can be found in [6].

The only reaction in which activation neutrons can arise is the reaction O^{17} (n, p)N^{17}. The nucleus of the isotope N^{17} decays with a half life of 4.14 sec, forming the isotope O^{17}. Most of the neutrons emitted by O^{17} have energies of 1±0.2 MeV.

The reaction threshold of O^{17}(n, p)N^{17} is about 8.0 MeV, and its cross section for neutrons in the fission spectrum is on the order of 3.2 μbarn. Therefore, the contribution of this reaction to the total yield of delayed neutrons is apparently quite slight and will be ignored in this work.

Let us now determine the total number of neutrons leaving a nuclear weapon at the moment of the explosion.

As we know, upon fission of nuclei of the material used as nuclear fuel (U^{235} or Pu^{239}), each fission event liberates approximately $2.8 \cdot 10^{-4}$ erg of energy. As we know, detonation of one g TNT liberates an energy of $4.18 \cdot 10^{10}$ erg (1000 cal); this indicates that a nuclear explosion acccompanied by the liberation of energy equivalent to the energy of detonation of 1 Kt of TNT involves $N \approx 1.5 \cdot 10^{23}$ fission events. If we consider the number of neutrons required to maintain the chain reaction, the fission of N nuclei liberates $N(\nu - 1)$ free neutrons. For example, for a plutonium bomb, assuming $\nu \approx 3$, the number of neutrons liberated upon explosion of a weapon with a power of 1 Kt will be approximately $3 \cdot 10^{23}$.

Thus, the number of neutrons liberated in the fission chain reaction is determined by the power of the explosion, i. e. the

quantity of fissioning material; however, the number of neutrons flying outward depends also on the design of the weapon. The number of neutrons liberated upon explosion of a purely thermonuclear bomb corresponds approximately with the number of neutrons liberated upon explosion of a bomb of the same power, based on the fission reaction.

When a three-phase bomb is exploded, the thermonuclear reaction is used as an intermediate process, which initiates high energy neutrons, causing fission of U^{238} atoms included in the composition of the shell. Therefore, a significant portion of the energy of the explosion of this type of bomb is the energy of fission of the uranium nuclei. As studies performed in [7] have shown, the mean number of neutrons ν produced by fission of U^{238} by neutrons with an energy of 14 MeV is 4.5±0.32 per fission event. Knowledge of the value of ν for U^{238} allows us to estimate the number of neutrons liberated upon explosion of a three-phase thermonuclear bomb. It corresponds approximately to the yield of neutrons by a weapon operating according to the fission principle and is approximately $(2\text{-}2.5)\cdot 10^{26}$ n/Mt.

§ 3. γ Radiation of a Nuclear Explosion

The γ radiation observed upon explosion of a nuclear weapon consists of many components differing in their origin and the time of radiation, energy of quanta and radiated energy, all related to the origin.

The γ radiation formed in a nuclear explosion can be subdivided into primary and secondary as to its origin. Primary γ radiation is emitted in each fission event with the products (fragments). Secondary γ radiation includes the γ quanta developing upon interaction of neutrons with the materials of the charge and the matter making up the surrounding medium (such as air or soil).

As to time, γ radiation from a nuclear explosion is divided into prompt and delayed. Prompt (short-lived) γ radiation includes that emitted by the material of the bomb before it evaporates and flies outward (about 10^{-5} sec). In this classification, prompt γ radiation includes: the γ quanta produced directly in the process of fission and with slight delays, a portion of the radiation from short-lived fission products, the photons formed upon capture and inelastic scattering of neutrons by the materials of the nuclear charge. The delayed γ radiation results from short-lived (with half life $>10^{-5}$ sec) and long-lived decay products, and capture of moderated neutrons in the surrounding medium. Let us study the characteristics of these types of radiation in greater detail.

Figure 1.3 shows the energy spectrum of prompt fission γ quanta [8]. In the range from 1 to 7 MeV, this spectrum can be represented by the simple exponential rule $\Phi(E_\gamma) = 8.0 \cdot e^{-1.1E_\gamma}$ MeV^{-1} with an accuracy of ±40%, while in the area of energies from 1 to 4.5 MeV, the error is less, ±15%. Below energies of 1 MeV the experimental data are higher than what would be indicated by this formula; in this area, the formula $26.8e^{-2.30E_\gamma}$ provides a better fit. However, the γ quanta at low energies are easily absorbed by the shell of the weapon and are therefore insignificant radiation sources.

It was experimentally established in [9] that the form of the γ spectrum accompanying the fission of nuclei of U^{233} and Pu^{239} does not differ significantly from the γ spectrum formed upon fission of U^{235}. As concerns the total yield of energy of prompt γ quanta upon fission, in the interval of energies from 0.3 to 10 MeV it is 7.2±0.8 MeV, and in this area of energies 7.4±0.8 quanta are emitted per fission event [7]. In other words, the mean energy of instantaneous γ quanta from fission is approximately 1 MeV. The data presented relate to the case of fission of nuclear fuel by thermal neutrons. In [10, 11], the dependence of the total energy of γ radiation of fission on the energy of excitation of fissionable nuclei is studied. The comparison of the spectrum and number of γ quanta upon fission of U^{235} by thermal neutrons with energies of 2.8 and 14.7 MeV performed in these works showed that the energy of γ radiation and the yield of γ quanta are retained within limits of 15%. For comparison, Figure 1.3 shows data characterizing the energy composition of γ radiation arising in U^{238} under the influence of neutrons with an energy of 14 MeV. As we can see, the spectrum is almost the same as the spectrum of γ radiation developing upon fission of U^{235} by thermal neutrons. The instantaneous γ radiation is significantly attenuated in the materials of which the nuclear charge is made, since its time of luminescence is approximately 100 times less than the time required for the bomb to burst. The degree of attenuation of the prompt γ radiation within the weapon can be estimated by the following method.

Let us analyze a nuclear charge in the form of a sphere of radius r_0 at the moment of the explosion. In order to simplify our calculations, we will make the following assumptions: the sources of γ quanta (i. e. the fissioning nuclei) are distributed evenly throughout the entire volume of the charge; the instantaneous γ radiation is monoenergetic; the absorption of γ radiation in the material of the charge occurs exponentially. These assumptions are apparently physically justified in this analysis.

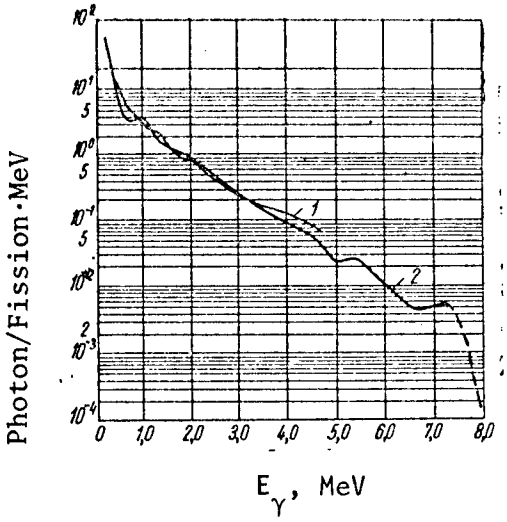

Figure 1.3. Spectrum of γ Radiation Arising in U^{238} Under the Influence of Neutrons With 14 Mev Energy (Curve 1), and Energy Spectrum of Prompt γ Quanta Emitted Upon Fission of U^{235} or Pu^{239} by Thermal Neutrons (Curve 2)

We would like to know the number of times by which the dose of γ radiation at some distance from the weapon is decreased due to self-absorption in the material of the charge in comparison to the case when a source of the same total intensity is concentrated at the center of the charge.

Let us look at Figure 1.4. Distance x, over which absorption of γ radiation from an elementary radiating volume occurs

$$dv = r^2 \cos\theta d\theta d\varphi dr, \qquad (1.4)$$

is determined by the relationship

$$x = c - d.$$

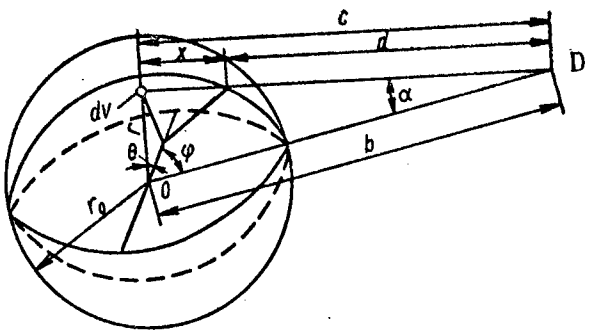

Figure 1.4. Calculation of Self-Absorption of γ Quanta of Fission in Charge Material

From the equation

$$d^2 - 2db\cos\alpha + b^2 - r_0^2 = 0 \tag{1.5}$$

considering the limits of change of the quantity

$$b - r_0 \leqslant d \leqslant b\cos\alpha \tag{1.6}$$

we find

$$d = b\cos\alpha - \sqrt{r_0^2 - b^2\sin^2\alpha}. \tag{1.7}$$

From the expression

$$r^2 = c^2 + b^2 - 2bc\cos\alpha \tag{1.8}$$

we determine

$$\cos\alpha = \frac{b - r\cos\theta\cos\varphi}{\sqrt{r^2 + b^2 - 2rb\cos\theta\cos\varphi}}.$$

Then

$$d = \frac{b^2 - rb\cos\theta\cos\varphi - \sqrt{r_0^2(r^2 + b^2 - 2rb\cos\theta\cos\varphi) - r^2b^2(1 - \cos^2\theta\cos^2\varphi)}}{\sqrt{r^2 + b^2 - 2rb\cos\theta\cos\varphi}}; \tag{1.9}$$

and

$$x = \frac{r^2 - rb\cos\theta\cos\varphi}{\sqrt{r^2 + b^2 - 2rb\cos\theta\cos\varphi}} + \\ + \frac{\sqrt{r_0^2(r^2 + b^2 - 2rb\cos\theta\cos\varphi) - r^2b^2(1 - \cos^2\theta\cos^2\varphi)}}{\sqrt{r^2 + b^2 - 2rb\cos\theta\cos\varphi}}. \quad (1.10)$$

Introducing the new variable $m = r/r_0$ and $p = b/r_0$, we can write the expression for x in the form

$$x = r_0 \frac{m^2 - mp\cos\theta\cos\varphi}{\sqrt{m^2 + p^2 - 2mp\cos\theta\cos\varphi}} + \\ + r_0 \frac{\sqrt{m^2 + p^2 - 2mp\cos\theta\cos\varphi - m^2p^2(1 - \cos^2\theta\cos^2\varphi)}}{\sqrt{m^2 + p^2 - 2mp\cos\theta\cos\varphi}}. \quad (1.11)$$

Then the desired attenuation of the dose or flux of instantaneous γ radiation due to self-absorption can be calculated as follows:

$$K(p, \mu r_0) = \int_0^1 \int_0^{\pi/2} \int_0^{\pi} \frac{e^{-\mu x} m^2 \cos\theta\, dm\, d\theta\, d\varphi}{m^2 + p^2 - 2mp\cos\theta\cos\varphi}. \quad (1.12)$$

The results of integration of this expression are shown in Table 1.2.

In this table, the dimensions of the charge of nuclear fuel are represented by the radius of the uranium sphere (in free path lengths -- μr_0 -- of fission γ quanta). The size of the nuclear charge can be judged on the basis of the critical mass necessary to initiate an explosive fission reaction. Data on the critical masses of fissionable elements have been published in the foreign literature. The most detailed data have been presented for charges consisting of U^{235}. For example, it is reported in [2] that the critical mass of a spherical charge (93.5% U^{235} and 6.5% U^{238}) with a density of 18.8 g/cm^3 is 48 Kg. The radius of a sphere of this mass is about 8.5 cm. For γ quanta with an energy of 1 MeV, corresponding to the average of the spectrum of prompt γ radiation, expressed in free path lengths this is $\mu r_0 \approx 12$. Turning to Table 1.2, we note that with this size nuclear charge, the dose of prompt γ radiation at the surface of the weapon will be attenuated by approximately 100-1000 times due to

internal self-absorption[1].

Therefore, although the number of prompt fission γ quanta and γ radiation of fission products are approximately equal, the contribution of prompt γ radiation during a nuclear explosion can be ignored.

The γ radiation of fission products is emitted mainly during the later stages of the explosion, after the material of the shell of the weapon has evaporated. Therefore, during the first minute following the explosion the quantity of γ radiation of fission products is approximately 100 times greater than the quantity of prompt γ radiation included in the composition of the initial ionizing radiation observed at equal distances from the center of the explosion. The production of fragments is a statistical process. The fission of U^{235} and Pu^{239} produces about 60 isotopes. With asymmetrical fission, the most probable reactions involve the formation of fragments with mass numbers 95 and 140. The yield of fragments as a function of mass number varies by a factor of 10^5. It has been established that during fission of uranium and plutonium, fragments are produced with mass numbers from A = 72 to A = 161. The change in mass number of fissionable material from 233 to 238 is accompanied by a significant change in the production of fragments with mass numbers from A = 105 to A = 115. The group of heavy fragments experiences no significant change in yield.

Data on the yields of various fragments formed by fission of U^{235}, U^{238} and Pu^{239} by fission neutrons, neutrons with energies of 14 MeV and neutrons from a thermonuclear explosion are presented in [12].

Each fragment formed undergoes an average of three β decay events with various periods. Thus, the fission fragments include about 200 radioactive nuclei with half lives from fractions of a second to decades. Many of the decay events are accompanied by γ radiation.

Since nuclei with various half lives participate in the radiation, the rate of decrease of γ activity of radiation with time does not follow a simple exponential rule. The effective half life increases as time passes, since the short-lived isotopes decay and only the longer-lived fragments remain.

---

[1]In this estimated calculation, the accummulation factor can be ignored, since its magnitude $\approx$ 5.

Table 1.2

ATTENUATION OF PROMPT γ RADIATION OF FISSION IN URANIUM, CALCULATED FROM FORMULA (1.12)

p	RADIUS OF URANIUM SPHERE IN FREE PATH LENGTHS μr_0						
	0,4	0,8	2,0	4,0	8,0	10	15
1,25	$6{,}011 \cdot 10^{-1}$	$4{,}733 \cdot 10^{-1}$	$2{,}718 \cdot 10^{-1}$	$1{,}528 \cdot 10^{-1}$	$8{,}526 \cdot 10^{-2}$	$7{,}244 \cdot 10^{-2}$	$5{,}725 \cdot 10^{-2}$
1,5	$3{,}923 \cdot 10^{-1}$	$3{,}082 \cdot 10^{-1}$	$1{,}763 \cdot 10^{-1}$	$9{,}869 \cdot 10^{-2}$	$5{,}446 \cdot 10^{-2}$	$4{,}598 \cdot 10^{-2}$	$3{,}580 \cdot 10^{-2}$
2,0	$2{,}094 \cdot 10^{-1}$	$1{,}642 \cdot 10^{-1}$	$9{,}366 \cdot 10^{-2}$	$5{,}255 \cdot 10^{-2}$	$2{,}922 \cdot 10^{-2}$	$2{,}474 \cdot 10^{-2}$	$1{,}930 \cdot 10^{-2}$
3,0	$9{,}000 \cdot 10^{-2}$	$7{,}045 \cdot 10^{-2}$	$4{,}000 \cdot 10^{-2}$	$2{,}233 \cdot 10^{-2}$	$1{,}230 \cdot 10^{-2}$	$1{,}036 \cdot 10^{-2}$	$7{,}992 \cdot 10^{-3}$
5,0	$3{,}190 \cdot 10^{-2}$	$2{,}495 \cdot 10^{-2}$	$1{,}414 \cdot 10^{-2}$	$7{,}857 \cdot 10^{-3}$	$4{,}306 \cdot 10^{-3}$	$3{,}625 \cdot 10^{-3}$	$2{,}803 \cdot 10^{-3}$
10	$7{,}924 \cdot 10^{-3}$	$6{,}197 \cdot 10^{-3}$	$3{,}511 \cdot 10^{-3}$	$1{,}947 \cdot 10^{-3}$	$1{,}054 \cdot 10^{-3}$	$8{,}807 \cdot 10^{-4}$	$6{,}695 \cdot 10^{-4}$

internal self-absorption[1].

Therefore, although the number of prompt fission γ quanta and γ radiation of fission products are approximately equal, the contribution of prompt γ radiation during a nuclear explosion can be ignored.

The γ radiation of fission products is emitted mainly during the later stages of the explosion, after the material of the shell of the weapon has evaporated. Therefore, during the first minute following the explosion the quantity of γ radiation of fission products is approximately 100 times greater than the quantity of prompt γ radiation included in the composition of the initial ionizing radiation observed at equal distances from the center of the explosion. The production of fragments is a statistical process. The fission of U^{235} and Pu^{239} produces about 60 isotopes. With asymmetrical fission, the most probable reactions involve the formation of fragments with mass numbers 95 and 140. The yield of fragments as a function of mass number varies by a factor of 10^5. It has been established that during fission of uranium and plutonium, fragments are produced with mass numbers from A = 72 to A = 161. The change in mass number of fissionable material from 233 to 238 is accompanied by a significant change in the production of fragments with mass numbers from A = 105 to A = 115. The group of heavy fragments experiences no significant change in yield.

Data on the yields of various fragments formed by fission of U^{235}, U^{238} and Pu^{239} by fission neutrons, neutrons with energies of 14 MeV and neutrons from a thermonuclear explosion are presented in [12].

Each fragment formed undergoes an average of three β decay events with various periods. Thus, the fission fragments include about 200 radioactive nuclei with half lives from fractions of a second to decades. Many of the decay events are accompanied by γ radiation.

Since nuclei with various half lives participate in the radiation, the rate of decrease of γ activity of radiation with time does not follow a simple exponential rule. The effective half life increases as time passes, since the short-lived isotopes decay and only the longer-lived fragments remain.

---

[1]In this estimated calculation, the aceummulation factor can be ignored, since its magnitude $\approx$ 5.

Table 1.2

ATTENUATION OF PROMPT γ RADIATION OF FISSION IN URANIUM, CALCULATED FROM FORMULA (1.12)

p	RADIUS OF URANIUM SPHERE IN FREE PATH LENGTHS μr_0						
	0,4	0,8	2,0	4,0	8,0	10	15
1,25	$6{,}011 \cdot 10^{-1}$	$4{,}733 \cdot 10^{-1}$	$2{,}718 \cdot 10^{-1}$	$1{,}528 \cdot 10^{-1}$	$8{,}526 \cdot 10^{-2}$	$7{,}244 \cdot 10^{-2}$	$5{,}725 \cdot 10^{-2}$
1,5	$3{,}923 \cdot 10^{-1}$	$3{,}082 \cdot 10^{-1}$	$1{,}763 \cdot 10^{-1}$	$9{,}869 \cdot 10^{-2}$	$5{,}446 \cdot 10^{-2}$	$4{,}598 \cdot 10^{-2}$	$3{,}580 \cdot 10^{-2}$
2,0	$2{,}094 \cdot 10^{-1}$	$1{,}642 \cdot 10^{-1}$	$9{,}366 \cdot 10^{-2}$	$5{,}255 \cdot 10^{-2}$	$2{,}922 \cdot 10^{-2}$	$2{,}474 \cdot 10^{-2}$	$1{,}930 \cdot 10^{-2}$
3,0	$9{,}000 \cdot 10^{-2}$	$7{,}045 \cdot 10^{-2}$	$4{,}000 \cdot 10^{-2}$	$2{,}233 \cdot 10^{-2}$	$1{,}230 \cdot 10^{-2}$	$1{,}036 \cdot 10^{-2}$	$7{,}992 \cdot 10^{-3}$
5,0	$3{,}190 \cdot 10^{-2}$	$2{,}495 \cdot 10^{-2}$	$1{,}414 \cdot 10^{-2}$	$7{,}857 \cdot 10^{-3}$	$4{,}306 \cdot 10^{-3}$	$3{,}625 \cdot 10^{-3}$	$2{,}803 \cdot 10^{-3}$
10	$7{,}924 \cdot 10^{-3}$	$6{,}197 \cdot 10^{-3}$	$3{,}511 \cdot 10^{-3}$	$1{,}947 \cdot 10^{-3}$	$1{,}054 \cdot 10^{-3}$	$8{,}807 \cdot 10^{-4}$	$6{,}695 \cdot 10^{-4}$

The γ activity of fission products, i. e. the rate of emission of γ radiation energy u(t), can be calculated for U^{235} and Pu^{239} at various moments in time following the explosion using the following formula [13]:

$$u(t) = A_0 t^{-\gamma_0} \text{ MeV/(sec·f)}. \quad (1.13)$$

The values of A_0 and γ_0 for various time intervals are presented in Table 1.3.

Table 1.3

VALUES OF COEFFICIENTS IN INTERPOLATION FORMULA (1.13) FOR CALCULATION OF γ ACTIVITY OF FRAGMENTS AT VARIOUS TIMES FOLLOWING EXPLOSION

Time Sectors for Which Formula is Applicable	Unit of Measurement of Time in Formula	A_0	γ_0
0.05 sec< t <1 sec	sec	0.4	0.27
1 sec < t <20 sec	"	0.4	0.72
20 sec < t < 10 min	"	0.95	1.01
10 min <t <10 hr	"	7.1	1.32
10 hr <t <100 hr	"	5.9	1.31
100 hr < t < 1000 hr	"	0.0276	0.89
10 hr < t < 100 hr	hr	$1.3 \cdot 10^{-4}$	1.31
100 hr <t< 1000 hr	"	$1.9 \cdot 10^{-5}$	0.89
10 min <t < 200 hr	sec	7.1	1.33
20 sec < t < 1000 hr	"	2	1.20

The short-lived γ radiation of the products of fission of U^{235} by thermal neutrons were studied in [14] from a few milliseconds to several seconds. Activities corresponding to decay times of 0.43 and 1.52 sec were detected.

Measurements performed by various authors with the fragments formed upon fission of uranium and plutonium by fast neutrons have shown that fragments with half-lives of less than one-tenth of one second are not present.

If we know u(t), we can calculate the energy radiated during the individual time intervals t_1-t_2:

$$W_{t_1 t_2} = \int_{t_1}^{t_2} u(t)\,dt \tag{1.14}$$

or, expressing u(t) by an exponential rule:

$$W_{t_1 t_2} = \frac{A_0}{\gamma_0 - 1}\left(\frac{1}{t_1^{\gamma_0 - 1}} - \frac{1}{t_2^{\gamma_0 - 1}}\right). \tag{1.15}$$

The energy radiated upon full decomposition of radioactive fragments is

$$W = \int_0^\infty u(t)\,dt = 8{,}4 \ \frac{\text{MeV}}{\text{f}} \ . \tag{1.16}$$

The energy of γ radiation at various moments in time following fission is presented on Figure 1.5.

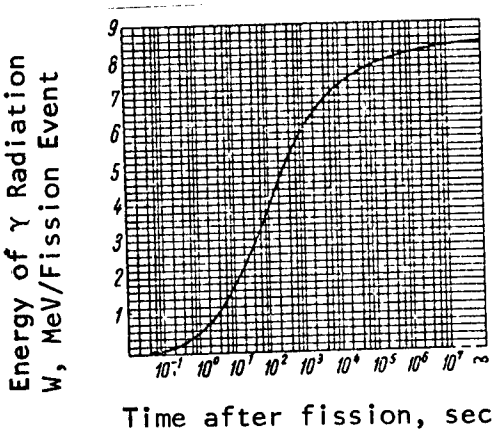

Figure 1.5. Quantity of Energy of γ Radiation of Fission Fragments at Various Moments in Time Following Fission

The energy spectrum of the γ quanta of fission products consists of a large number of lines, the relationship between which changes

with time. The mean energy of the spectrum becomes lower, but significant softening occurs only during the first hour after fission. This is illustrated by Figure 1.6, based on data from [15-19]. Figure 1.7 shows the γ radiation spectra of fragments constructed on the basis of data of [20] for various moments in time following fission. Since the volatile fission products are not of direct danger from the standpoint of formation of local radioactive fallout, the γ radiation which they cause is excluded from the total spectrum.

In order to solve certain problems, it is necessary to know how the relative activity of β and γ radiation of fragments changes with time [17]. Figure 1.6 shows the change in relative β and γ activity with time, constructed according to the data of [16]. The spectral distribution of β radiation of the mixture of fission products of U^{235} at various moments in time following an explosion [20] is shown on Figure 1.8.

The γ radiation of an atomic explosion is not determined solely by the activity of the fission fragments.

The reason for the development of short-period γ radiation during a nuclear explosion is the γ radiation developing upon interaction of neutrons with the nuclei of the medium surrounding the explosion. One of the processes causing the appearance of γ radiation is inelastic scattering of fast neutrons in the materials of the bomb, in the air and in the earth. The duration of existence of this radiation in the shell of the bomb does not exceed the time required for the shell to burst, i. e. about 10^{-5} sec. In addition to inelastic scattering, fast neutrons may enter into the reaction (n, p) or (n, α) with the emission of γ radiation, and the reaction (n, γ). The duration of this radiation corresponds approximately to the duration of radiation by inelastic scattering.

The delayed neutrons are captured by nitrogen in the air or the earth, forming secondary γ radiation. The time of luminescence of this radiation is determined by the diffusion of neutrons in the air. Therefore, the γ radiation arising upon capture of moderated neutrons lasts for considerably longer than the radiation resulting from fast neutrons.

The life time of neutrons in air (relative to the reaction N^{14} (n, p)C^{14} under normal atmospheric conditions) is about $60 \cdot 10^{-3}$ sec. Thus, 0.3 sec following the explosion, practically all neutrons have been captured and the capture γ radiation ceases to be emitted.

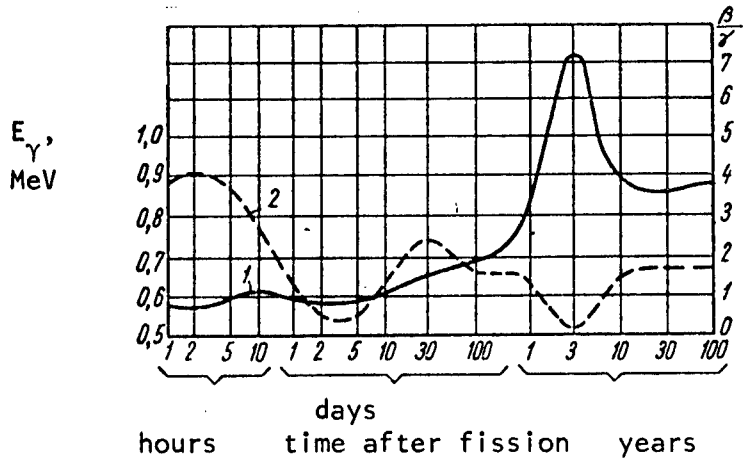

Figure 1.6. Change in Mean Energy of γ Quanta of Fragments of Fission of Pu^{239} (curve 2) and Ratio of Summary β Activity to Summary γ Activity (β/γ) of Fission Products (curve 1) as Functions of Time Following Fission

Although the life time of neutrons in the soil is brief, the air with its greater life time of neutrons may be a source of neutrons for capture in the soil. However, capture radiation in the soil is less significant in the formation of short-period radiation than capture radiation in the air. This results from the geometric factors determining the propagation of γ radiation in the soil, and the fact that the probability of capture of neutrons in the air is significantly higher than in the soil.

A significant portion of the neutrons formed in an explosion (90% for a shell permeability of 0.1) leaves the weapon with a mean energy of less than 1 KeV [4]. The mean distance traveled by neutrons in air to absorption is 210 m. The absorption of neutrons in air occurs primarily on nitrogen nuclei by two reactions:

$$N^{14}(n, p)C^{14} \quad (\sigma_{np} = 1{,}710^{-24}\ см^2);$$

$$N^{14}(n, \gamma)N^{15} \quad (\sigma_{n\gamma} = 0{,}1 \cdot 10^{-24}\ см^2).$$

In the reaction $N^{14}(n, p)C^{14}$ with slow neutrons, γ radiation is not observed; consequently, the primary source of γ radiation upon neutron capture in air is the reaction $N^{14}(n, \gamma)N^{15}$.

The life time of neutrons in air at normal atmospheric pressure, considering the total capture cross section, is 60 msec. Therefore, the neutron cloud at the center of the explosion, with a radius of about 250-300 m, will be a source of γ radiation for approximately 60 msec. The neutrons leaving the cloud in the process of moderation are also sources of γ radiation, but since there are very few such neutrons, their contribution to the short-period radiation is slight.

Since at the same time the neutrons leave the bomb a shock wave is formed with high density at its leading edge, the life time of the neutrons is significantly changed. The solution of the problem of a strong shock wave gives us the following approximation for the density of air ρ_ϕ at the leading edge of the shock wave [21]:

$$\frac{\rho_\phi}{\rho_0} = \frac{(\bar{\gamma}+1)p + (\bar{\gamma}-1)}{(\bar{\gamma}-1)p + (\bar{\gamma}+1)}, \tag{1.17}$$

where ρ_0 is the density of air under normal conditions; p is the pressure at the leading edge of the shock wave; $\bar{\gamma}$ = 1.4 for air at normal temperature. For a very strong wave ($p \to \infty$) where γ = 1.4, the maximum density of air in the shock front is 6. Since the air near the point of the blast is heated to very high temperatures, the value of γ ceases to be constant under these conditions. At temperatures around 10^4 degrees, a significant portion of the energy is attributable to oscillating levels, dissociation and ionization of molecules occur; therefore, the heat capacity of the air changes. Under these conditions, the value of $\bar{\gamma}$ may be 1.2. For $\bar{\gamma}$ = 1.2, the maximum density of air in the shock front may be 11 times greater than the density of undisturbed air.

Since the life time of a neutron in a medium is inversely proportional to its density, the minimum life time of a neutron in the shock wave decreases from 60 to 5.5 msec. However, we must consider that the total life time of a neutron t_1 is determined not only by the capture time t_c in the wave front, but also by the flight time t_{fl} in the cavity of low density:

$$t_1 = \chi t_3 + (1-\chi) t_{fl},$$

where (1 - χ) is the portion of neutrons reflected from the wave front into the cavity. Therefore, the minimum life time of a neutron in the leading edge of the shock wave exceeds 5.5 msec.

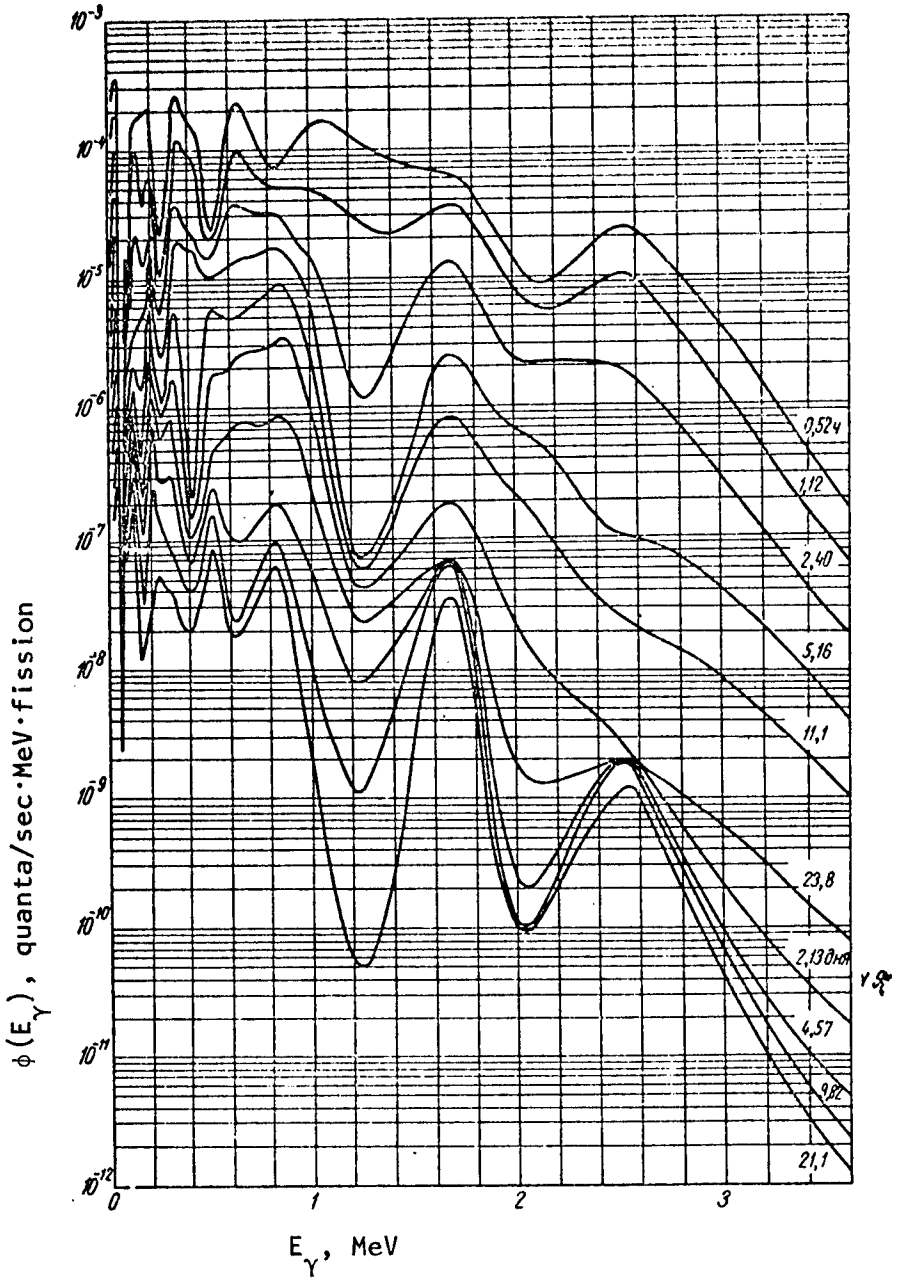

Figure 1.7. Spectral Distribution of γ Radiation of Fission Fragments at Various Moments in Time Following Fission

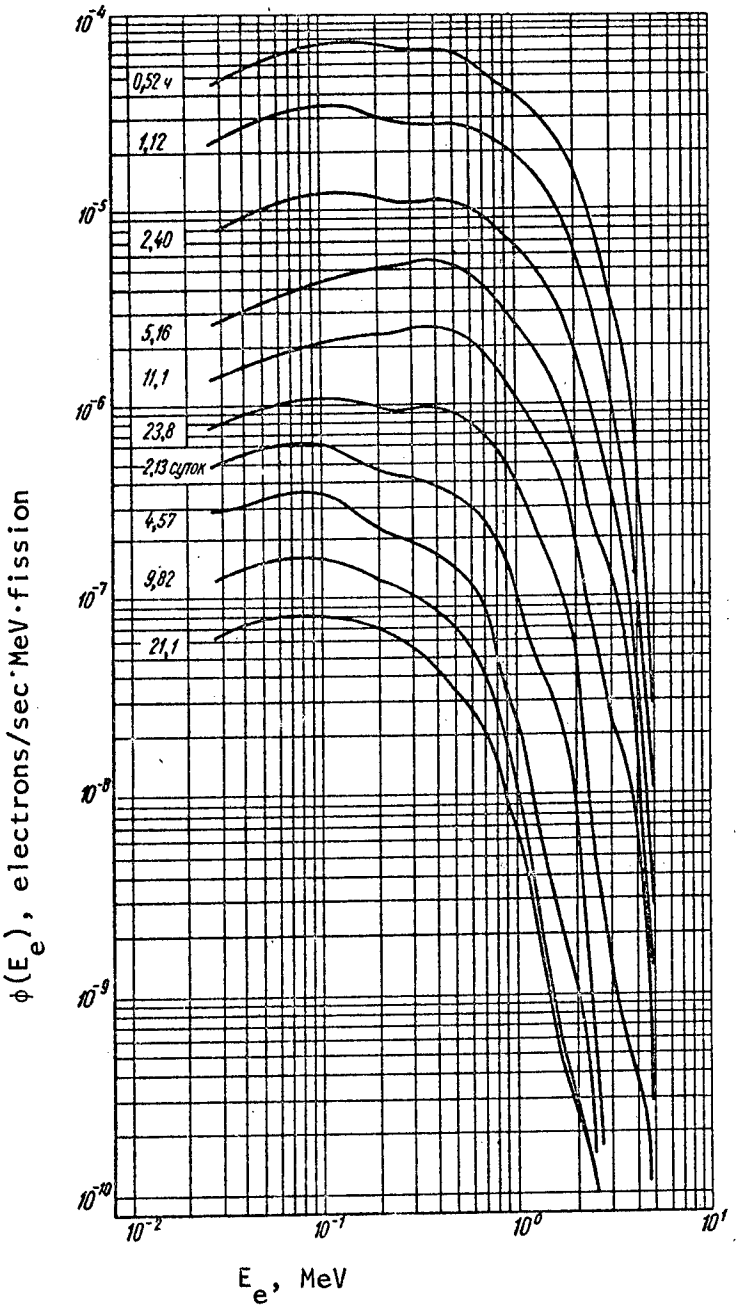

Figure 1.8. Spectral Distribution of β Radiation of Mixture of Fission Products of U^{235} at Various Moments in Time Following Explosion

Thus, if short-period γ radiation with periods of less than 5.5 msec exists, it cannot be explained as capture γ radiation. It results from the radiation of isomers formed upon interaction of fast neutrons with materials in the structure of the weapon. The short-period γ radiation from 5.5 to 20-30 msec may be partially caused by radiation of isomers and partially by capture of Maxwellian neutrons in the leading edge of the shock wave. The short-period γ radiation with a period of 30 msec or more results from capture of neutrons by nitrogen in the air.

The cross section of the reaction $N^{14}(n, \gamma)N^{15}$ is 17 times less than the cross section of the reaction $N^{14}(n, p)C^{14}$; therefore, only 6% of all neutrons will create short-period γ radiation.

According to the data of [22], each capture event liberates 10.82 MeV of γ quantum energy. Thus, for each neutron absorbed in the air, 0.64 MeV of γ radiation energy is radiated. Since each fission event emits 1.5 (for U^{235}) to 2 (for U^{239}) free neutrons, if all neutrons are absorbed by nitrogen in the air, the γ radiation liberated is 0.96-1.28 MeV/fission. This quantity is near the energy of γ radiation of fragments (1.8 MeV/fission) emitted in the first 10 sec (the mean time of application of γ radiation from the radioactive cloud to objects on the ground).

Since the time of capture radiation is less than the time of radiation of fragments, the dose rate of this short-period radiation will be significantly greater than the dose rate of the fragment γ radiation. At the initial moment, the intensity of capture γ radiation is about 21.4 MeV/(fission·sec), whereas the intensity of fragment γ radiation is 0.8 MeV/(fission·sec) [23]. Therefore, in the first moments following an atomic blast, the dose rate of capture γ radiation exceeds the dose rate of fragment γ radiation by over an order of magnitude. However, within a few tenths of a second, the primary contribution to the γ radiation is that of the fission fragments. Data on the spectrum of capture γ radiation are presented in [22].

Table 1.4 presents information on the energy and relative intensity of the capture radiation of nitrogen.

As we can see, the hardness of the capture γ radiation is considerably greater than the hardness of the fragment radiation. The mean energy of capture radiation is 6 MeV, of fragment radiation -- 2 MeV. As a result of capture of moderated neutrons, the upper layer of the earth (water) becomes itself a source of γ rays. Radiation from the earth occurs both at the moment of capture of neutrons, and during subsequent decay of artificially radioactive neuclei. The total yield

of energy of capture γ radiation per absorbed neutron for all elements except hydrogen is about 8 MeV. During capture of a thermal neutron by a hydrogen atom, γ radiation is liberated with an energy of 2.23 MeV.

Table 1.4

γ RADIATION SPECTRUM OF THE REACTION $N^{14}(n, \gamma)N^{15}$

Energy of γ Quantum, MeV	Relative Intensity, %	Energy of γ Quantum, MeV	Relative Intensity, %
4,48	18,3	7,36	4,9
5,29	30,5	8,28	2,4
5,55	2,44	9,16	0,6
6,32	1,22	10,82	6,1
7,16	0,6		

The radiation occurring upon capture of neutrons in soil is short-period radiation. The life time of neutrons in soil is about $0.5 \cdot 10^{-3}$ sec, i. e. significantly less than in air ($\approx 60 \cdot 10^{-3}$ sec). However, the air is the source which delivers neutrons to the ground for capture. Therefore, the time during which capture of neutrons in the soil may occur, with emission of γ radiation, is equal to the time of existence of neutrons in the air, i. e. about 0.3 sec.

Let us study the main characteristics of fragment γ radiation resulting from activation of the soil by the neutrons of a nuclear explosion.

According to the data of [4], only a small number of elements included in the composition of the soil play a significant role in the formation of γ-active isotopes. During the first few minutes following bombardment, one such element is Al^{28} ($T_{1/2}$ = 2.3 min). Its activity is almost one hundred times greater than the activity of all other isotopes. After a few hours have passed, the most significant activity is that of Na^{24} and Mn^{56}. Between 20 and 200 hours, the activity of the bombarded soil is almost completely determined by the activity of Na^{24}; therefore, during this interval, the effective period of decrease

of soil activity corresponds to the half life of Na^{24} (15 hours). After 200 hours have passed following the explosion, Fe^{56} remains active ($T_{1/2}$ = 47 days).

Later (t > 200 hr), the soil activity drops more slowly than calculations would indicate. This fact is apparently related to the presence of small quantities of dispersed elements in the earth. For example, cobalt, traces of which are always present in the earth, due to its large capture cross section and long half life (5.3 years), may significantly change the form of the curve for the interval of time during which short-period elements decay.

The residual γ radiation in the region of a blast may also result from fission fragments which fall to the ground from the radioactive cloud. The quantity of fragments which fall out on the ground is determined to a great extent by the conditions of the explosion and may differ significantly for blasts of the same power performed under different conditions: on the surface or in the air. Therefore, the degree of participation of fission fragments and activated soil in the creation of the dose of residual γ radiation may change significantly. With blasts in the air, when the quantity of fission fragments falling out of the radioactive cloud is not great, the activated soil is the primary source of residual radiation. When a blast is performed at low altitude over the ground, the residual radiation is primarily created by fission fragments.

The energy of γ radiation of fission fragments radiated between 10 seconds (the approximate time of completion of γ radiation of the radioactive cloud to objects on the ground) up to infinity is 6.6 MeV/fission (see Figure 1.5). For activated soil, this quantity is 0.48 MeV per neutron captured by the soil. If we base our calculations on the greatest possible γ radiation by the activated soil, i. e. the radiation produced by absorption of one-half of all neutrons in the soil, the energy radiated by the activated soil, ignoring self-absorption in the soil, is 0.48 MeV/fission when a plutonium bomb is exploded. Thus, even when a surface explosion occurs, the total quantity of energy radiated by the active soil is 14 times less than the energy of γ radiation of the fission fragments.

Direct comparison of the possible significance of fission fragments and activated soil in the creation of the dose of residual radiation is difficult due to the different spatial distribution of radiation from activated soil and fission fragments. Whereas the activity of the soil decreases with increasing distance from the point of the blast approximately according to the same rules as the decrease in neutron flux, the spatial distribution of fission fragments follows quite different regularities.

First of all, the spatial distribution of fission fragments is very asymmetrical and is determined by the direction of the wind which carries away the fission products. If the particles which fall out to the ground from the radioactive cloud form a thin layer of radioactive material, the soil is activated to a great depth -- some tens of centimeters. Therefore, a great portion of the γ radiation of the soil is absorbed in the soil itself. This decreases the significance of activated soil in the creation of residual γ radiation. The differing role of fragments and activated soil in the formation of residual radiation is also determined by the nature of the changes in intensity with time.

It follows from [24] that during the first 10 hours the activity of fission fragments decreases more rapidly than the activity of the soil. After 50 hours, the induced activity decreases more rapidly than the fragment activity. From 10 to about 50 hours, the rule of change of fission fragment activity and soil activity is approximately the same.

As we know, a significant portion of the fission fragments, even with surface blasts, falls out over tremendous areas [25]. If 1% of all fission fragments formed fall out over the region of the epicenter the residual radiation will be determined not by activated soil, but rather by fission fragments.

Far from the epicenter with surface blasts the residual radiation is determined by induced activity. With a surface blast of a pure hydrogen bomb, an order of magnitude more neutrons may be liberated per unit energy than when a fission bomb is exploded. Then we can expect that the energy of radiation of the activated earth will be on the same order of magnitude as the energy of radiation of fragments upon explosion of a fission bomb of the same power.

We note in conclusion that the residual activity formed upon capture of neutrons by the elements which compose the air is low in comparison to the activity of the fragments. For this reason, the products of activation of atmospheric air can be ignored in calculations.

BIBLIOGRAPHY

1. Bartholomev, G., Kinsey, B., *Phys. Rev.*, 93, 1434 (1954).

2. Ivanov, A. I., Rybkin, G. I., *Porazhayushcheye Deystviye Yadernogo Vzryva* [The Damaging Effects of a Nuclear Blast], Moscow, Voyenizdat Press, 1960.

3. Bonner, T. et al., *Phys. Rev.*, 101, 1514 (1956).

4. Yampol'skiy, P. A., *Neytrony Atomnogo Vzryva* [The Neutrons of an Atomic Blast], Moscow, Gosatomizdat Press, 1961.

5. Keepin, G. R. et al., *Phys. Rev.*, 107, 1044 (1957).

6. Gol'dshteyn, G., *Osnovy Zashchity Reaktorov* [Principles of Reactor Shielding], Moscow, Gosatomizdat Press, 1961.

7. Flerov, N. I., Talyzin, V. M., *Atomnaya Energiya*, Vol. 5, No.6, 1958.

8. Mayensheyn, F. et al., *Trudy Vtoroy Mezhdunarodnoy Konf. Po Mirnomu Ispol'z. Atomnoy Energii* [Works of Second International Conference on the Peaceful Uses of Atomic Energy], Geneva, 1958, Selected Reports of Foreign Scientists, Vol. 2, Moscow, Atomizdat Press, 1959, p. 297.

9. Kirbride, J., *Brit. Rep. NRDC-58, UKAE*, Febr. 13, 1955.

10. Protopopov, A. I., Shiryayev, B. N., *Zh. Eksperim. i Teor. Fiz*, Vol. 34, p. 331 (1958).

11. Protopopov, A. I., Shiryayev, B. N., *Zh. Eksperim. i Teor. Fiz*, Vol. 36, p. 954 (1959).

12. Lavrenchik, V. N., *Global'noye Vypadeniye Produktov Yadernykh Vzryvov* [Global Fallout of Nuclear Explosion Products], Moscow, Atomizdat Press, 1965.

13. Way, K., Wigner, E., *Phys. Rev.*, Vol.75, p. 1318 (1948).

14. Bralley, J., *Phys. Rev.*, Vol. 83, p. 5 (1951).

15. Leypunskiy, O. I. et al., *Atomnaya Energiya*, No. 3, p. 278 (1957), Vol 2

16. Bjornerstedt, R., *Arkiv fur fysik*, Vol. 16, p. 28 (1959).

17. Hunter, H., Ballow, N., *Nucleonics*, Vol. 9, No. 5, p. 2 (1955).

18. Seaborg, G., *Rev. Mod. Phys.*, Vol. 25, No. 2, p. 469 (1953).

19. Nesmeyanov, A. N. et al., *Polucheniye Radioaktivnykh Izotopov* [The Production of Radioactive Isotopes], Moscow, Goskhimizdat Press, 1954.

20. Nelms, A. T., Cooper, J. W., *Health Phys.*, p. 427 (1959).

21. Prode, H. J., *Appl. Phys.* , Vol. 26, p. 766 (1955).

22. Kinsey, B. B. et al., *Phys. Rev.*, Vol. 77, p. 723 (1950).

23. Way, K., Wigner, E., *Phys. Rev.*, Vol. 75, p. 1318 (1948).

24. Leypunskiy, O. I., *Gamma-Izlucheniye Atomnogo Vzryva* [The γ Radiation of an Atomic Explosion], Moscow, Atomizdat Press, 1959.

25. Kotkhari et al., *Yadernyye Vzryvy* [Nuclear Explosions], Moscow, Foreign Literature Press, 1958.

CHAPTER 2. THE FIELD OF NEUTRONS AND γ RADIATION OF A NUCLEAR BLAST

§ 1. Propagation of γ Radiation of a Nuclear Blast

At the moment of a blast, a near-point source of γ radiation appears in the form of the fission fragments, the activity of which $g(t)/(MeV/sec)$ and the spectrum $\Phi(E_\gamma)$ of which are known. The γ quanta emitted upon fission are ignored, since, as we have demonstrated, they are significantly attenuated by the material of the weapon. The γ radiation emitted by the fission fragments following evaporation of the shell of the weapon acts on objects on the ground for several tens of seconds, until the radioactive cloud rises to a considerable height. The propagation of γ radiation occurs through a practically infinite air medium (the influence of the ground will not as yet be analyzed).

Let us analyze briefly the case of propagation of γ radiation from a point source through a homogeneous infinite medium. Since this problem has spherical symmetry, the distribution of intensities and doses of γ radiation in space depends only on one spatial coordinate -- the distance from the source R.

The intensity of radiation of a point isotropic source I(R) decreases with increasing R due to increasing distance from the source, and also due to interactions with the medium. In correspondence with this, for a monoenergetic source it will be:

$$I(R) = \frac{g(t)}{4\pi R^2} B(E_{0\gamma}, R) e^{-\mu_0 R} \text{ MeV}/(\text{cm}^2 \cdot \text{sec}), \qquad (2.1)$$

where μ_0 is the attenuation factor of γ radiation in the air; $B(E_{0_\gamma}, R)$ is the factor of accummulation of intensity, equal to the ratio of total radiation intensity to the portion related only to direct (non-scattered) radiation. Expression (2.1) was written for the intensity of γ radiation; however, it can be extended to cover all effects related to the action of quanta.

The dose rate P for the case of monoenergetic radiation is related to the intensity I by the relationship

$$P = I \cdot 1{,}48 \cdot 10^{-5} \mu_e(E_{0\gamma}) \text{ r/sec}, \qquad (2.2)$$

where $\mu_e(E_{0\gamma})$ is the absorption factor of the energy of γ radiation in air.

In the case of non-monoenergetic radiation, expression (2.2) is written as

$$P = 1{,}48 \cdot 10^{-5} \int I(E_{0\gamma}) \mu_e(E_{0\gamma}) dE_\gamma \text{ r/sec}. \qquad (2.3)$$

As γ radiation propagates through matter, it becomes non-monoenergetic, even if a source of monoenergetic radiation with γ quantum energy $E_{0\gamma}$ is acting on the matter. In this case, $\mu_e(E_\gamma)$ is taken away from the integral sign:

$$P = 1{,}48 \cdot 10^{-5} \mu_e(E_\gamma) \int \frac{\mu_e(E_\gamma)}{\mu_e(E_{0\gamma})} I(E_{0\gamma}) dE_\gamma \text{ r/sec}. \qquad (2.4)$$

Since over a broad range of quantum energies μ_e depends little on E_γ, the factor of accummulation of dose power practically corresponds with the factor of accummulation of intensity; therefore

$$P(R) = 1{,}48 \cdot 10^{-5} \frac{g(t) \mu_e(E_{0\gamma}) B(E_{0\gamma}, R)}{4\pi R^2} e^{-\mu_0 R} \text{ r/sec}. \qquad (2.5)$$

Determination of the coefficient $B(E_{0\gamma}, R)$ is a problem in the theory of transfer of quanta or modeling experiments.

As a result of model experiments, the authors of [1] suggested the following dependence for dose rate

$$P(R) = \frac{1{,}48 \cdot 10^{-5} \mu_e(E_{0\gamma}) g(t) \bar{\alpha}}{4\pi R^2} e^{-R/l_{eff}} \text{ r/sec}, \qquad (2.6)$$

in which multiple scattering is considered by the dimensionless coefficient $\bar{\alpha}$ and the effective length of absorption of γ radiation energy under conditions of multiple scattering λ_{eff}.

Expression (2.6) is formally equivalent to expression (2.5), suggested in [2], but in place of the accummulation factor B, which changes greatly with distance, and the free path length $\lambda_0 = 1/\mu_0$, which is independent of distance, the quantities $\bar{\alpha}$ and λ_{eff}, which change slightly with distance, are used. In many cases, it is preferable to use formula (2.6). Table 2.1 shows the values of $\bar{\alpha}$ and λ_{eff} for air and two intervals of distances from the point isotropic source of γ radiation in the air [3].

In order to describe the dose rate of an atomic blast, we can express g(t) in formula (2.6) by the number of fission events and the activity of the fragments of one event u(t):

$$g(t) = 1{,}45 \cdot 10^{23} g u(t) \text{ MeV/sec.} \qquad (2.7)$$

The coefficients $\bar{\alpha}$, λ_{eff}, $\mu_e(E_\gamma)$ depend on the energy of the quanta emitted by the fragments. In correspondence with the data presented in § 3 of Chapter 1, we note that in the time interval of interest to us (several seconds following fission), the mean quantum energy is $\approx$ 2 MeV. Substituting the numerical value of coefficient α taken in Table 2.1 for this energy into formula (2.6), as well as the value of λ_{eff} (exp.) and expressing R in meters, we produce

$$P(t, R) = \frac{9{,}32 \cdot 10^3 q u(t)}{R^2} e^{-R/255} \text{ r/sec.} \qquad (2.8)$$

The source of fragment γ radiation following evaporation of the weapon is the radioactive cloud. Its diameter may reach some hundreds of meters. We must therefore determine the extent to which the nature of the propagation of γ quanta from this volumetric source will correspond with the case just studied of a point source in an infinite air medium.

For further analysis, let us make the following assumptions: the fission fragments are evenly distributed throughout the entire volume of the cloud; attenuation of radiation within the volume of the radioactive cloud occurs just as it occurs outside its volume.

Table 2.1

VALUES OF COEFFICIENTS $\bar{\alpha}$ AND λ_{eff} FOR CALCULATION OF DOSE RATE OF POINT SOURCE OF γ RADIATION IN AIR

E_γ, MeV	$\bar{\alpha}$		λ_{eff}, m	
	Interval of Distances, m		Interval of Distances, m	
	400-1000	1000-2000	400-1000	1000-2000
0,4	9,00	50,0	105	99
0,6	4,80	18,4	128	108
0,8	3,70	12,4	146	120
1,0	2,90	8,90	164	134
2,0	1,80	3,85	230	200
4,0	1,30	1,90	333	295
6,0	1,18	1,50	409	372
8,0	1,14	1,30	450	425
10,0	1,10	1,10	482	458

The power of the dose from a volumetric spherical γ source at any distance from the source can be calculated using the formula

$$P = \Gamma \int \frac{w(r) f(R'/\lambda)}{R'^2} dv \quad \text{r/sec}, \qquad (2.9)$$

where Γ is the γ constant of the source; w(r) is the specific activity of the γ source; $f(R'/\lambda)$ is the attenuation of the power in the medium as a result of absorption and scattering of the γ radiation. Integration is performed with respect to the volume of the source. Looking at Figure 2.1, we note:

$$dv = 2\pi y dr \frac{dx}{\sin\beta}; \quad \sin\beta = \frac{y}{r},$$

so that

$$dv = 2\pi r\, dr\, dx.$$

The power of the dose from a spherical layer of the source will be

$$\Delta P(R) = 2\pi\Gamma \int_{-r}^{+r} \frac{\omega(r)\, r f(R'/\lambda)}{R'^2}\, dr dx, \qquad (2.10)$$

where

$$R' = \sqrt{y^2 + (R-x)^2} = \sqrt{r^2 + R^2 - 2Rx}.$$

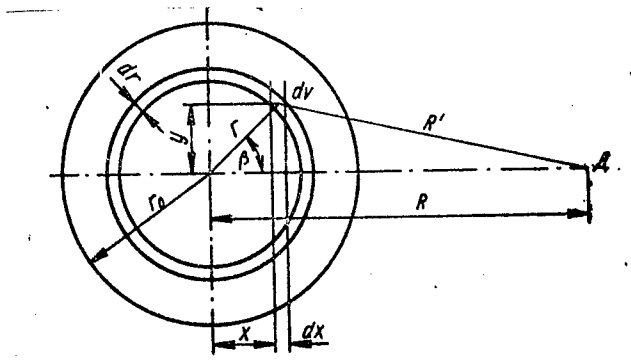

Figure 2.1. Geometry for Calculation of Dose of γ Radiation from Radioactive Cloud of Nuclear Explosion

After substituting this dependence into formula (2.9), we produce

$$\Delta P(R) = 2\pi\Gamma\omega(r)\, r dr \int_{-r}^{+r} \frac{f\left(\frac{R'}{\lambda}\right) dx}{r^2 + R^2 - 2Rx};$$

the power of the dose from the entire volume of a spherical source of radius r_0 will be

$$P = 2\pi\Gamma \int_0^{r_0} \omega(r)\, r dr \int_{-r}^{+r} \frac{f(R'/\lambda)\, dx}{r^2 + R^2 - 2Rx}. \qquad (2.11)$$

Since we are interested not in the absolute value of dose power from a spherical γ source, but rather only its ratio to the power of the dose from a point source of the same activity, which is

$$P_{т} = \frac{\Gamma Q f(R'/\lambda)}{R_0^2},$$

where

$$Q = 4\pi \int_0^{r_0} w(r)\, r^2 dr,$$

it will be

$$K_f = \frac{P}{P_{т}} = 0{,}5\, \frac{\int_0^{r_0} w(r)\, r dr \int_{-r}^{+r} \frac{f(R'/\lambda)\, dx}{r^2 + R^2 - 2Rx}}{\frac{f(R'/\lambda)}{R^2} \int_0^{r_0} w(r)\, r^2 dr}; \qquad (2.12)$$

since w(r) = const

$$K_f = \frac{\int_0^{r_0} r dr \int_{-r}^{+r} \frac{f(R'/\lambda)\, dx}{r^2 + R^2 - 2Rx}}{\frac{r_0^3 f(R'/\lambda)}{R^2}}. \qquad (2.13)$$

The results of calculations using this formula for various sizes of radioactive cloud and various distances from the point of measurement to the center of the source (in values of R/λ) are presented in Table 2.2.

We see from Table 2.2 that the dose power of fragment γ radiation from a spherical source with dimensions $r_0/\lambda \leq 2$ is equal to the dose power from a point source of the same activity, beginning at distances determined by the boundary of the source. We note that the

dimensions of the source of fragment γ radiation in all cases of practical importance are always less than $2r_0/\lambda$.

Table 2.2

RELATIONSHIP OF DOSE POWERS FROM SPHERICAL RADIOACTIVE CLOUD AND POINT SOURCE OF SAME ACTIVITY

Dimensions of Radioactive Cloud

$r_0/\lambda = 4$		$r_0/\lambda = 2$		$r_0/\lambda = 1$		$r_0/\lambda = 0,5$		$r_0/\lambda = 0,25$	
R/λ	K_f	R/λ	K_f	R/λ	K_f	R/λ	K_f	R/λ	K_f
6	1,8	3	1;0	2	1,0	1,0	1,0	0,5	1,0
4	2,6	2	1,2	1,0	1,0	0,5	1,0	0,25	1,0
3	1,3	1,5	0,8	0,75	0,83	0,37	0,82	0,188	0,8
2	0,4	1,0	0,4	0,5	0,43	0,25	0,46	0,125	0,45

Thus, using expression (2.8), we can find the dose power of fragment γ radiation at any distance from the center of the explosion. However, this solution plan for the problem is insufficient. The authors of [4] turned their attention to the fact that the absorption of γ radiation propagating from the center of an explosion should be sensitive to redistribution of air masses resulting from the passage of the shock wave. The shock wave forms a cavity in the air, in which there is no absorption of γ radiation. The size of the cavity increases with increasing explosion energy. Therefore, the dose of γ radiation at a given distance from the center of the explosion does not increase in proportion to the power as it increases, but rather more rapidly. The calculation of the transmission of γ radiation should take into consideration the actual distribution of air density created by the shock wave during the emission of the γ radiation. A plan for considering the influence of the shock wave was presented in [4].

Let us study the distribution of the density of air in the shock wave, which influences the propagation of γ radiation.

In a strong shock wave propagating from the center of an explosion, all the air is concentrated practically in a narrow edge around the leading edge of the wave and moves away from the center. Thus, inside the spherical shock wave front an area is created with low air density, i. e. a cavity.

After the shock wave has passed and the initial air pressure has been restored, the area with low air density remains. The entropy in the shock wave increases [5, 6], the air does not return to its initial state, and remains heated after passage of the shock wave and restoration of the initial pressure. In the area where the shock wave was strong (i. e. the pressure at the leading edge was significantly greater than atmospheric pressure), the residual heating is great and causes glowing of the air. The fireball formed after an atomic explosion is the "wake" of the passing shock wave. The pressure in the fireball is equal to atmospheric pressure, while the density is low as a result of the high temperature of the air. As an example, Figure 2.2 shows the distribution of air density across the leading edge of a shock wave 0.765 sec after the explosion of a nuclear weapon with a power of 300 Kt.

We can see from Figure 2.2 that 0.765 sec after the explosion at a distance of 600 m from the center $\rho_\phi/\rho_0 << 1$. The absorption of γ radiation in this area is negligible and it can be considered that there is a cavity inside the strong shock wave. The radius of the fireball r_{fb} determines the maximum distance over which the shock wave which has passed was still strong. As time passes and the radius of the shock front increases, the pressure in the leading edge of the shock wave decreases, the shock wave becomes weak, the air partially returns to the central areas and atmospheric pressure is restored everywhere with the exception of a slight peak at the shock wave. However, the temperature in the central area remains high, the air density remains low.

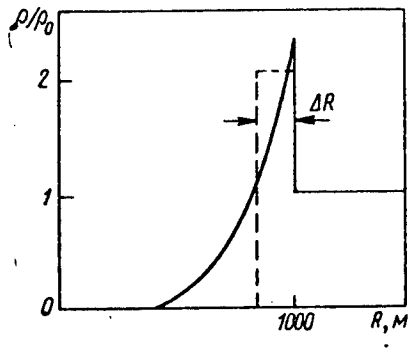

Figure 2.2. Distribution of Air Density in a Strong Shock Wave

Subsequently, the shock wave, propagating to an ever greater distance, is continually attenuated and degenerates to a sound wave. The shock wave phenomenon ends, but the air remains heated after it passes. Cooling of the air (and restoration of normal density) occurs by radiation and convection over an extended period of time, significantly greater than the time of emission of most of the γ radiation.

The γ radiation passes through the cavity practically without absorption, its flux attenuating within the cavity in inverse proportion to the square of the distance from the center, as is the case for propagation of γ radiation in a vacuum.

Consideration of the distribution of air density with a shock wave, which creates a heterogeneity in the medium surrounding the source, is performed by introducing the concept of the "optical thickness" for absorption of γ radiation. We know that if the absorption of radiation occurs exponentially, the intensity of the radiation which has traveled distance R in a homogeneous medium with length of absorption $\lambda(R)$ is determined by the so-called optical thickness

$$x_0 = \int_0^R \frac{dr}{\lambda}.$$

Correspondingly, the attenuation of radiation over path R is e^{-x_0}.

The absorption of γ radiation differs somewhat from exponential absorption due to the presence of repeated scattering. However, within a certain interval of distances it can be represented in exponential form. This gives us reason to extend the concept of "optical thickness" to the case of absorption of γ radiation in a heterogeneous medium and to consider that the attenuation of intensity due to absorption is

$$\exp(-x_0) = \exp\left[-\frac{1}{\lambda_{eff}(\rho_0)\rho_0}\int_0^R \rho dr\right], \qquad (2.14)$$

where ρ_0 and ρ are the air density before and after arrival of the shock wave.

In the undisturbed atmosphere, the optical thickness over path R is R/λ_{eff}. Suppose the radius of the leading edge of the strong shock

wave is R_ϕ. All air in the strong shock wave is practically concentrated in a layer of thickness ΔR at the leading edge of the shock wave, where for $\Delta R \ll R_\phi$ (see Figure 2.2), the optical thickness is

$$x_0 = \frac{1}{\lambda_{eff}(\rho_0)\,\rho_0}\int_0^R \rho dr = \frac{1}{\lambda_{eff}}\frac{\rho \Delta R}{\rho_0}. \qquad (2.15)$$

For approximate estimation, it is assumed that within the interval of ΔR the density ρ = const.

The value of the product $\Delta R(\rho/\rho_0)$ can be found from the condition that the mass of air at the edge of the shock wave near the surface with radius R_ϕ is equal to the mass of air which was formerly in the sphere of radius R_ϕ before the shock wave developed:

$$\rho 4\pi R_\phi^2 \Delta R = \rho_0 \frac{4}{3}\pi R_\phi^3;$$

$$\Delta R \frac{\rho}{\rho_0} = \frac{R_\phi}{3}.$$

Substituting this expression into formula (2.15), we find

$$x_0 = \frac{1}{3}\frac{R_\phi}{\lambda_{eff}}.$$

When there is no strong shock wave, the optical thickness is R/λ_{eff}. Thus, the redistribution of the mass of air in a strong shock wave causes the optical thickness along path R to decrease by two-thirds R_ϕ/λ_{eff}. Absorption of γ radiation within the shock wave occurs as if it contained a cavity of radius L:

$$L = R - \frac{\int \rho dR}{\rho_0}. \qquad (2.16)$$

In the case of a strong shock wave

$$L = \frac{2}{3}R_\phi. \qquad (2.17)$$

Absorption of γ radiation occurs outside the cavity in layer ΔR of dense air at the leading edge of the wave:

$$\Delta R = \frac{R_\Phi}{3}\frac{\rho_0}{\rho}. \tag{2.18}$$

Thus, at distance R from the center of the explosion (R > L), the optical thickness is $(R - L)/\lambda_{eff}$. The decrease in flux will be proportional to

$$\exp\left[-(R-L)/\lambda_{eff}\right],$$

whereas without the shock wave the intensity would be proportional to $\exp(-R/\lambda_{eff})$.

Thus, the strong shock wave causes the intensity of radiation to be determined by formula (2.10), in which the exponent contains R - L rather than R.

Coefficient $\bar{\alpha}$ remains practically unchanged in this case:

$$P(t, R) = \frac{1{,}48\cdot 10^{-5}\mu_c(E_{0\gamma})\,g(t)\,\bar{\alpha}}{4\pi R^2} e^{L/\lambda_{eff}} e^{-R/\lambda_{eff}}. \tag{2.19}$$

In the idealized case which we have studied, when the distribution of densities in the leading edge of the shock wave corresponds to that shown on Figure 2.2 by the dotted line, the radius of the cavity is equal to two-thirds the radius of the leading edge of the shock wave (2.17). With the actual distribution of densities in the shock wave, the effective radius of the cavity

$$L_{eff} < \frac{2}{3} R_\Phi.$$

By the effective radius of the cavity we shall mean the radius of an idealized cavity formed as a result of expulsion of air from the space around the source.

The effective radius of the cavity can be determined on the basis of the assumption that the density of the air at the leading edge of the shock wave can be described by the dependence [3]

$$\rho(l) = \rho_\Phi\left(\frac{l}{R_\Phi}\right)^n, \tag{2.20}$$

which is correct only for a strong shock wave. In this expression, l is the distance from the leading edge of the shock wave back toward the source.

The exponent n depends on the value of ρ_ϕ and is determined by calculating the quantity of air in the shock wave.

Before formation of the shock wave, the quantity of air contained in a volume of radius R_ϕ was $4/3(\pi R_\phi^3 \rho_0)$. Thus,

$$\frac{4}{3}\pi R_\phi^3 \rho_0 = 4\pi \int_0^{R_\phi} \rho(l)\, l^2\, dl. \tag{2.21}$$

Substituting expression (2.20) in the integral in place of $\rho(l)$, we find that

$$4\pi \frac{\rho_\phi}{R_\phi^n} \frac{R_\phi^{n+3}}{n+3} = \frac{4}{3}\pi \rho_0 R_\phi^3,$$

from which

$$n = 3\left(\frac{\rho_\phi}{\rho_0} - 1\right). \tag{2.22}$$

On the basis of these assumptions, we can calculate the actual optical thickness. Let us study two possible cases of placement of the source relative to the center of the explosion: 1) the detector is located within the shock wave ($R < R_\phi$); 2) the detector is located outside the shock wave ($R > R_\phi$).

In the first case

$$x_0 = \mu_{eff} \int_0^R \frac{\rho}{\rho_0} dR = \mu_{eff}\left(-R + R + \frac{1}{\rho_0}\int_0^R \rho dR\right) = \tag{2.23}$$

$$= \mu_{eff} R - \mu_{eff}\left(R - \int \frac{\rho}{\rho_0} dR\right) = \mu_{eff} R - \mu_{eff} L_{eff},$$

where

$$L_{eff} = R - \int_0^R \frac{\rho}{\rho_0} dR. \tag{2.24}$$

Substituting expression (2.20) for ρ in formula (2.24) and performing integration, we produce

$$L_{eff} = \dot{R}\left[1 - \frac{\frac{\rho_\Phi}{\rho_0}}{\frac{3\rho_\Phi}{\rho_0} - 2}\left(\frac{R}{R_\Phi}\right)^{3\left(\frac{\rho_\Phi}{\rho_0} - 1\right)}\right]. \tag{2.25}$$

Substituting formula (2.25) into expression (2.19), we produce

$$P(t, R) = \frac{1{,}48 \cdot 10^{-5}\, \mu_e (E_{0\gamma})\, g(t)\, \bar{\alpha}}{4\pi R^2}\, e^{\frac{L_{eff}}{\lambda_{eff}}}\, e^{-R/\lambda_{eff}}. \tag{2.26}$$

In the second case ($R > R_\Phi$), when where $R_1 > R_\Phi$, $\rho/\rho_0 = 1$,

$$\begin{aligned} x_0 &= \mu_{eff} \int_0^R \frac{\rho}{\rho_0}\, dR = \mu_{eff} \int_0^{R_\Phi} \frac{\rho}{\rho_0}\, dR + \mu_{eff} \int_{R_\Phi}^R dR = \\ &= -\mu_{eff} \int_0^{R_\Phi} \frac{\rho}{\rho_0}\, dR + \mu_{eff}[R - R_\Phi] = \mu_{eff} R - \\ &- \mu_{eff}\left(R_\Phi - \int_0^{R_\Phi} \frac{\rho}{\rho_0}\, dR\right) = \mu_{eff} R - \mu_{eff} L_{eff}, \end{aligned} \tag{2.27}$$

where

$$L_{eff} = R_\Phi - \int_0^{R_\Phi} \frac{\rho}{\rho_0}\, dR. \tag{2.27}$$

Substituting expression (2.20) into (2.27) and performing integration, we produce

$$L_{eff} = R_\Phi \frac{2\frac{\rho_\Phi}{\rho_0} - 2}{3\frac{\rho_\Phi}{\rho_0} - 2}. \tag{2.28}$$

Let us substitute formula (2.27) into expression (2.19); we produce a formula identical to expression (2.26), which covers both cases of placement of the detector relative to the shock wave. The difference lies in the expressions for L_{eff} of (2.24) and (2.27), which differ in that (2.24) includes R in place of R_ϕ.

Thus, the distribution of air density caused by the shock wave increases the dose power by exp ($\mu_{eff} L_{eff}$) times. The factor showing the number of times by which the dose power when there is a shock wave exceeds the dose power at the same moment in time but without a shock wave is called the dose power cavity factor K_p. In formula (2.26), the value of the cavity factor is approximated by the expression

$$K_p = e^{\mu_{eff} L_{eff}(t, q)}. \qquad (2.29)$$

Considering this, let us place K_p into the initial formula (2.8):

$$P(t, R) = \frac{9{,}32 \cdot 10^8 q u(t) K_p(t)}{4\pi R^2} e^{-R/255} \quad \text{r/sec}. \qquad (2.30)$$

The dependence of L_{eff} on t and q can be expressed using R_ϕ and ρ_ϕ/ρ_0, the values of which depend on the energy of the explosion and the time which has passed since the explosion. With a very strong shock wave, the following limiting expressions are produced for L_{eff}: 1) $L_{eff} = R$, when $R < R_\phi$ and, consequently, the effective radius of the cavity is independent of time; 2) $L_{eff} = \frac{2}{3} R_\phi$, when $R > R_\phi$.

The precise value of $L_{eff}(t)$ can be calculated on the basis of the expression

$$L_{eff}(t) = a(t) k \sqrt[3]{q}, \qquad (2.31)$$

where k = 100, and the dose power is expressed in kilotons. The dependence of a(t) for explosions of various powers is shown on Figure 2.3.

It should be noted that in determining the dimensions of the cavity we can use the rule of similarity of shock waves. If the values of $R_{\phi 1}$ and ρ_ϕ are known with explosion of a weapon of power q_1, the same

values of ρ_ϕ are produced when a weapon of power q_2 is exploded, but at a different moment in time t_2 and at a different distance, namely at moment

$$t_2 = t_1 \sqrt[3]{\frac{q_2}{q_1}}$$

and at distance

$$R_{\phi 2} = R_{\phi 1} \sqrt[3]{\frac{q_2}{q_1}}.$$

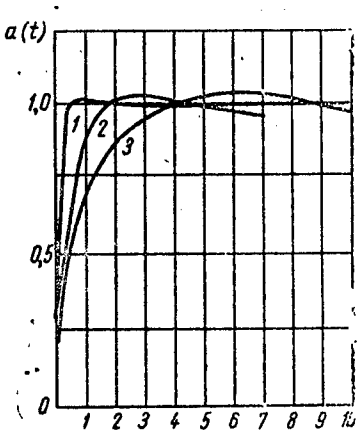

Figure 2.3. Size of Air Cavity as a Function of Time for Explosions of Various Powers: 20 Kt (curve 1); 200 Kt (curve 2); 2000 Kt (curve 3)

The values of R_ϕ and consequently of L_{eff} depend also on the conditions of the explosion. With a surface explosion, R_ϕ is greater than with an atmospheric explosion of the same power. This occurs due to the fact that with a surface explosion that portion of the explosive energy which would have been transmitted into the lower half space, i. e. half the explosive energy, remains in the upper half space, thus creating twice the energy density which would be created by an air blast. Therefore, the parameters of the shock wave with a surface blast are the same as would obtain with an air blast of twice the energy. In particular, in comparing air and surface explosions, the energy should be doubled for the surface explosion.

§ 2. Dose Power of γ Radiation With a Nuclear Explosion[1]

If there were no shock wave, the dose of fragment γ radiation from an atomic explosion would decrease monotonically with the passage of time, in proportion to the decreasing activity of fission fragments, and also as a result of the rise of the radioactive cloud. However, due to the formation and growth of the cavity, the absorption of γ radiation decreases with the passage of time, and after the shock wave passes the point of measurement, this point is inside the cavity, and the γ quanta are practically unattenuated. In other words, the dose rate of fragment radiation as a function of time is defined by the product of two factors: $u(t)e^{\mu_{eff}L_{eff}(t)}$, one of which (the activity of the fragments) decreases, while the other (the dose power cavity factor) at first increases due to the growth of the cavity, then decreases to unity as the disturbed atmosphere returns to its normal state.

Due to the simultaneous influence of these two factors, the dose power of fragment γ radiation passes through a minimum and a maximum.

Let us determine the dose power of capture γ radiation. The life time of neutrons in air with normal density, considering the total capture cross section, is τ = 60 msec. Therefore, the neutron cloud around the explosion (R ≃ 250-300 m) will be a source of γ radiation, the intensity of which is determined by the value of τ.

As concerns the dimensions of the source of capture γ radiation, calculations similar to those presented above for fragment γ radiation indicate that the factor, considering the influence of the finite dimensions of the cloud of Maxwellian neutrons on the formation of the dose of capture γ radiation during a nuclear explosion, can be written as follows:

---

[1]This book will not analyze capture γ radiation formed by absorption of neutrons by the earth, since its contribution at great distances and high altitudes of explosion is relatively slight. At slight distances from the explosion (several times the neutron mean free path length), capture γ radiation from the earth should be considered. It can be calculated in the same manner as the radiation scattered from the earth, using the "albedo" of capture γ radiation (see Engineering Compendium on Radiation Shielding, edited by Jaeger R. G. et al., Vol. 1, Springer-Verlag, Berlin-Heidelberg-New York, 1968, p. 33; Goryachev, I. V. et al., Report 56 at CEMA Symposium "Problems of Shielding From Penetrating Radiation of Reactors," Melekess, 21-26 April, 1969).

$$K_c = 0{,}5 \cdot \frac{\int_0^{r_0} e^{-r/\lambda_0} \frac{dr}{r} \int_{-r}^{+r} \frac{f(R'/\lambda)\,dx}{r^2 + R^2 - 2Rx}}{\frac{f(R'/\lambda)}{R^2} \lambda_0 (1 - e^{-r_0/\lambda_0})}. \qquad (2.32)$$

Factor K_c is equal to the ratio of dose power at distance R from the center of a volumetric source of radius R_s to the dose power at the same distance from a point source of equivalent activity.

This expression was produced by substituting the function $w(r) \approx e^{-r/\lambda_0}$, describing the spatial distribution of sources of capture γ radiation (λ_0 is the effective length of attenuation of neutrons in the cloud) into formula (2.12). Calculations of coefficient K_c using this expression have shown that the source of capture γ radiation can be considered a point source where $R'/\lambda \geq 0.1$, i. e. at practically all distances from the center of the explosion.

This indicates that we can determine the dose power of capture γ radiation by using formula (2.19). For capture γ radiation it will be as follows:

$$P(R) = \frac{1{,}48 \cdot 10^{-5} N q \varepsilon_\gamma \mu_e(E_{0\gamma}) \sigma_{n\gamma} e^{-\frac{t}{\tau}}}{\tau(\sigma_{n\gamma} + \sigma_{np})} \times \qquad (2.33)$$
$$\times \frac{\bar{\alpha}(1-a)\Delta(1-\zeta)}{4\pi R^2} e^{-\frac{R - L_{eff}(t)}{\lambda_{eff}}} \quad [\text{r/sec}],$$

where $N = 3 \cdot 10^{23}$ is the number of neutrons formed upon explosion of a weapon with a power of 1 Kt; q is the power of the explosion, Kt; ε_γ = 10.75 MeV is the energy liberated upon capture of one neutron by a nitrogen nucleus; a is the permeability of the shell; Δ is the portion of capture γ radiation resulting from the reaction of capture of neutrons by atmospheric nitrogen (according to [7], $\Delta = 0.9$); ζ is the share of neutrons from the cloud absorbed by the soil; with an air blast $\zeta = 0$, with a surface blast, $\zeta = 0.5$; $\sigma_{n\gamma} = 0.1 \cdot 10^{-24}$ cm^2 is the cross section of the reaction $N^{14}(n, \gamma)N^{15}$; $\sigma_{np} = 1.7 \cdot 10^{-24}$ cm^2 is the cross section of the reaction $N^{14}(n, p)C^{14}$.

At the initial moment of the explosion, the size of the cavity is not great. Since the dose power is defined at distances which are large in comparison with the dimensions of the area in which capture of Maxwellian neutrons occurs, we can assume without great error that

$$\cdot e^{-\frac{R-L_{eff}(t)}{\lambda_{eff}}} \approx e^{-\frac{R}{\lambda_{eff}}}.$$

If we substitute into equation (2.33) the numerical values of the quantities included in it, for an air blast ($\zeta = 0$) with a permeability of the shell of 0.1, the dose power will be

$$P(R, t) = \frac{5{,}4 \cdot 10^{9} q \bar{\alpha} e^{-R/\lambda_{eff}}}{R^2} e^{-\frac{t}{0{,}062}} \text{ r/sec.} \qquad (2.34)$$

If we consider the cavity effect, q in this equation must be replaced by $q^{1.05}$.

Figure 2.4 shows graphically the dependence of dose power on time which has passed since the moment of the explosion. The unit of power used is the dose power of fragment radiation at the first moment following the explosion.

The moment of the maximum of dose power depends on the distance and power of the explosion. At short distances, where the shock wave is strong, the maximum occurs earlier than at longer distances, namely occurring when the strong shock wave has passed the point of the detector.

At long distances, the power maximum may occur before passage of the shock wave through the point in question. As the power of the explosion increases, the maximum occurs later (ignoring short distances).

It should be noted that the ratio of ordinates of curves 2 and 3 on Figure 2.4 is equal to the dose power cavity factor K_p.

The dependences of dose power on time shown on Figure 2.4 were calculated without considering the rise of the cloud following the nuclear explosion, which causes an increase in distance from the source to the detector and, consequently, a decrease in L_{eff} which, in turn, should lead to a decrease in the maximum in the area of greater time since the moment of the explosion and more rapid decrease in P(t) than that shown on Figure 2.4.

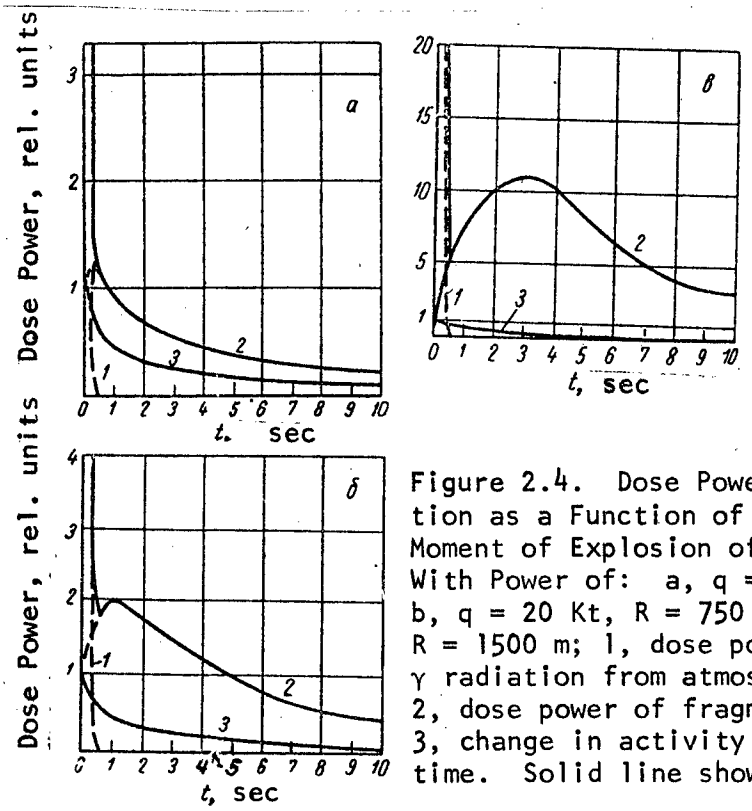

Figure 2.4. Dose Power of γ Radiation as a Function of Time Since Moment of Explosion of Nuclear Weapon With Power of: a, q = 2 Kt, R = 500 m; b, q = 20 Kt, R = 750 m; c, q = 20 Kt, R = 1500 m; 1, dose power of capture γ radiation from atmospheric nitrogen; 2, dose power of fragment γ radiation; 3, change in activity of fragments with time. Solid line shows total dose power.

Considering the rise of the radioactive cloud, the total dose power of γ radiation can be calculated using the formula

$$P(t, R) = \frac{5{,}12 \cdot 10^9 q u(t)\,\bar{\alpha}}{R^2} e^{-\frac{R - L_{eff}(t)}{\lambda_{eff}}} \left(\frac{R}{R_t}\right)^2 \cdot e^{-\frac{\Delta R}{\lambda_{eff}}} + \frac{5{,}4 \cdot 10^9 q^{1{,}05}\,\bar{\alpha}\, e^{-R/\lambda_{eff}}}{R^2} e^{-\frac{t}{0{,}062}}. \quad (2.35)$$

Here R_t is the distance from the center of the cloud at moment in time t; ΔR is the increment in the distance to the center of the cloud following its rise: $\Delta R = R_t - R$.

The distance to the center of the cloud at moment in time t can be found on the basis of the rise rate of the radioactive cloud, which was determined in [7]:

$$R_t = \sqrt{(R^2 - H^2) + (H + 16t^2)^2},$$

where H is the height of the explosion over the surface of the earth; R is the distance to the center of the explosion. It should be noted that although the prompt γ radiation amounts to only about 1% of the total dose of γ radiation of an atomic blast, still due to the extremely brief time of its application it can provide a sharp burst of γ radiation. It was noted above that the time of radiation of γ quanta during fission is approximately $(0.5\text{-}2.5)\cdot 10^{-9}$ sec, with 7.8 MeV liberated for each fission event. Considering the thousandfold attenuation in the materials of the weapon, the dose power of γ radiation still exceeds the dose power of fragment and capture γ radiation by several orders of magnitude.

§. 3. Calculation of γ Radiation Doses

If we know the dose rate of fragment γ radiation (2.19), we can calculate the integral dose at a given distance from the center of the blast:

$$D = \int_0^{t_{eff}} P dt = \frac{1{,}48\cdot 10^{-5}\,\mu_e(E_\gamma)\,\bar{\alpha}\,N e^{-R/\lambda_{eff}}}{4\pi R^2\cdot 10^4} \times \times \int_0^{t_{eff}} u(t)\, e^{\frac{L_{eff}(q,\,t)}{\lambda_{eff}}}\, dt, \tag{2.36}$$

where

$$Nu(t) = g(t) \text{ MeV/sec},$$

μ_e is the electron conversion factor; t_{eff} is the effective time during which the effect of γ radiation must be considered (due to radioactive decay of fragments and the rise of the cloud, the intensity of γ radiation drops rapidly), which is taken as 10 sec.

The integral included in expression (2.36) can be represented as

$$\int_0^{t_{eff}} u(t)\, e^{\frac{t_{eff}(q,\,t)}{t_{eff}}}\, dt \approx e^{\frac{\bar{L}(q)}{\lambda_{eff}}} \int_0^{t_{eff}} u(t)\, dt = e^{\frac{\bar{L}(q)}{\lambda_{eff}}} W, \tag{2.37}$$

where

$$W = \int_0^{10\,\text{sec}} u(t)\,dt = 2{,}05 \text{ MeV/fission}$$

Substituting the numerical values of coefficients into (2.36) and (2.37), we produce

$$D = \frac{2 \cdot 10^9 q e^{\bar{L}/\lambda_{eff}} e^{-R/\lambda_{eff}}}{R^2}. \tag{2.38}$$

An estimate of $\bar{L}$, the mean value of the cavity factor over the entire time of emission of quanta, can be made under the following assumptions: it is assumed that $\bar{L}$ is similar to the final radius of the fireball ($\bar{L} \approx r_{fb}$). This approximation is more precise, the less the time required for formation of the final dimensions of the cavity in comparison with the time of emission of γ quanta (since the expression with $\bar{L} \approx r_{fb}$ is eliminated from the integral with respect to time as a constant quantity), i. e. it is more precise, the less the power of the explosion.

This approximation is clearly inaccurate for high power explosions, since a large portion of the γ radiation is liberated before the moment when the fireball reaches its final size, i. e. with a high power explosion $\bar{L} < r_{fb}$.

The final radius of the fireball can be estimated on the basis of the energy which it contains. It follows from the theory presented in [5] that the energy of the heated air is about 50% of the energy of the explosion. Then

$$\frac{4}{3}\pi r_{fb}^3 \varepsilon = 0{,}5q;$$

$$\bar{L} \approx r_{fb} = \sqrt[3]{\frac{0{,}5q}{\frac{4}{3}\pi\varepsilon}}, \tag{2.39}$$

where ε is the energy per unit volume of the fireball.

If we ignore the increase in heat capacity with temperature and dissociation of air molecules, the energy of 1 g of air will be

$$\frac{5R(T - T_н)}{28{,}8} = 0{,}35(T - T_н) \text{ cal/g}.$$

Ignoring the value of T_H in comparison with T, we produce

$$\varepsilon = \rho_0 0{,}35T = \frac{\rho_0 T_0}{p_0}\frac{p_H}{T_H}0{,}35T = 1{,}23\cdot 10^{-1} p_H \text{ cal/cm}^3, \tag{2.40}$$

where p_H is the pressure of the air before the explosion; T_H and T are the temperatures of the air before and after the explosion; ρ_0, T_0 and p_0 are the density, temperature and pressure of the air under normal conditions.

Substituting the value of ε into formula (2.39), we produce

$$\bar{L} = 100\sqrt[3]{\frac{q}{p_H}}\ м. \tag{2.41}$$

Substituting expression (2.41) into formula (2.38), we can write

$$D = \frac{2\cdot 10^9 q\, e^{\frac{100}{\lambda_{eff}}\sqrt[3]{\frac{q}{p_H}}}\, e^{-R/\lambda_{eff}}}{R^2}. \tag{2.42}$$

For the case when p_H = 1 atm, T_H = 298° K, λ_{eff} is 255 m.

$$D = \frac{2\cdot 10^9 q\, e^{0{,}4\sqrt[3]{q}}\, e^{-R/255}}{R^2} = \frac{2\cdot 10^9 q\cdot 10^{0{,}174\sqrt[3]{q}}}{R^2} e^{-R/255} p. \tag{2.43}$$

In expressions (2.38), (2.42) and (2.43), the factor

$$\exp(\bar{L}/\lambda_{eff}) = \exp\left(\frac{100\sqrt[3]{q/p_H}}{\lambda_{eff}}\right),$$

which shows the number of times by which the dose is increased due to the effect of the shock wave, is specific. This factor is called the dose cavity factor K_d. In formula (2.43), the dose cavity factor is

$$K_d = e^{0{,}4\sqrt[3]{q}}. \tag{2.44}$$

Expression (2.43) is related to points lying outside the fireball, i. e. outside the cavity. Within the cavity, the absorption of γ radiation is zero and the dose changes in inverse proportion to the square of the distance from the center of the explosion.

The use of the quantity r_{fb} as the mean radius of the cavity $\overline{L}$ in calculations produces approximate results, suitable only for the explosion of low-power weapons.

In the case of high explosion power, we cannot expect satisfactory accuracy of calculation results using formula (2.43), since $\overline{L}$ is clearly less than r_{fb}. Furthermore, with increasing energy of the explosion, $\overline{L}$ should increase more slowly than $\simeq \sqrt[3]{q}$. With powerful explosions, the shock wave is strong throughout the time of emission of most of the γ radiation. According to the theory presented in [7], the radius of the leading edge of the strong shock wave at each moment in time is approximately proportional to $\sqrt[5]{q}$; therefore, it must be considered that actually $\overline{L}$ increases approximately as $\sqrt[5]{q}$.

Detailed analysis of the problem of doses leads to numerical values which can be described by various interpolation formulas. For example, the formula suggested in [3]:

$$D = 6{,}6 \cdot 10^8 q\, e^{0{,}925 \sqrt[5]{q} - 6{,}25 \cdot 10^{-5} q} \cdot \frac{e^{-R\rho_0/300}}{R^2} [p], \qquad (2.45)$$

is written in a form corresponding to the physical representation of the action of a shock wave.

We can also use a simpler expression:

$$D = 1{,}4 \cdot 10^9 q (1 + 0{,}2 q^{0{,}65}) \frac{e^{-R\rho_0/300}}{R^2} [p]. \qquad (2.46)$$

With a surface blast, the radius of the cavity is greater, corresponding to the radius of a cavity with an air blast of twice the power. Therefore, the dose with a surface blast is higher than with an air blast of a bomb of the same power:

$$D = 2{,}8 \cdot 10^9 q (1 + 0{,}3 q^{0{,}65}) \frac{e^{-R\rho_0/300}}{R^2} [p]. \qquad (2.47)$$

The doubled volume of the cavity with a surface blast in comparison to an air blast is retained only during the time of emission of γ radiation, since the hemispherical area of heated air separates from the ground and becomes spherical as time passes.

However, we can calculate the dose with a surface blast using formula (2.47) with sufficient approximate accuracy.

Figure 2.5 shows the values of doses at various distances from the epicentr of the explosion at Hiroshima [8]. From the figure we can see that there is a hard component in the γ radiation spectrum: the slope of the curve $\log DR^2 = f(R)$ decreases with increasing distance. In the 600-1600 m distance interval, $\lambda_{eff} = 282$ m, in the 2000-2600 m interval, $\lambda_{eff} = 393$ m. This last value of λ_{eff} corresponds to a mean γ radiation energy ≈ 6 MeV. The effect of capture γ radiation predominates over this sector.

The dose of the hard component, according to Figure 2.5, can be expressed by the empirical formula

$$D_h = \frac{5{,}5 \cdot 10^8 q\, e^{-R/393}}{R^2} [p]. \qquad (2.48)$$

Let us estimate the dose of the hard component, assuming that it is formed only by capture radiation.

The dose of capture γ radiation can be found by integrating expression (2.33) or (2.34) with respect to time

$$D_h = \frac{5{,}4 \cdot 10^9 q \bar{\alpha}\, e^{-R/\lambda_{eff}}}{R^2} \int_0^\infty e^{-t/0{,}062}\, dt\, [p]. \qquad (2.49)$$

Integrating, we produce

$$D_h = \frac{1{,}48 \cdot 10^{-5} N \varepsilon \bar{\alpha}\, \mu_e(E_{0\gamma})}{4\pi R^2 \cdot 10^4} e^{-R/\lambda_{eff}} [p]. \qquad (2.50)$$

Since the main portion of capture radiation should be radiated within 0.1 sec, when the radius of the shock wave is still small, the cavity factor is not considered. Substituting the values of quantities in (2.50):

$$N = 1.45 \cdot 1023\ q \text{ (for } \varepsilon = 1 \text{ MeV/fission}$$

$$\left.\begin{array}{l}\overline{\alpha} = 1{,}4 \\ \lambda_{eff} = 375\ м\end{array}\right\} 1000\ м < R < 2000\ м$$

$$\mu_c(E_{0\gamma}) = 1{,}9 \cdot 10^{-5}\ см^{-1} \text{ (for } E_{0_\gamma} = 6 \text{ MeV)},$$

we produce:

$$D_h = \frac{4{,}55 \cdot 10^8 q\, e^{-R/375}}{R^2}\ [p]. \tag{2.51}$$

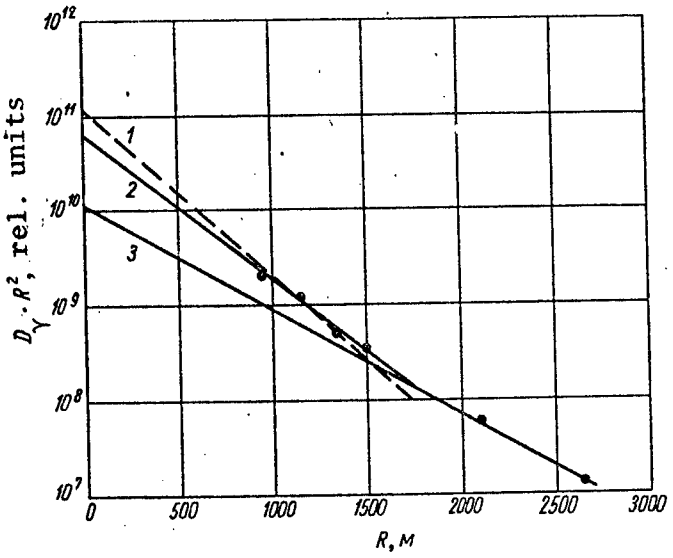

Figure 2.5. Spatial Distribution of Doses of γ Radiation During Explosion of Atomic Bomb at Hiroshima:

●, experimental data; 1, λ = 252 m; 2, λ = 282 m; 3, λ = 393 m

As we can see, the calculated estimate agrees satisfactorily with empirical formula (2.49). This confirms our assumption that the hard component of γ radiation observed in practice results from the capture of neutrons by nitrogen in the air.

The influence of the cavity on the dose of the hard component can be felt during strong explosions. It is always significantly less than the influence of the cavity on the dose of the fragment component,

first of all because the hard component is radiated over a short period of time, when the cavity is small, and secondly because the influence of the cavity decreases with increasing hardness of the radiation, i. e. with increasing λ_{eff}.

In the case of hydrogen bombs, the number of fragments is determined not by the entire energy of the explosion, but only by the portion involving the fission reaction, but the size of the cavity is determined by the entire energy of the explosion. Therefore, in the case of a thermonuclear explosion, the total power of the explosion is included only in the expression for the cavity factor.

In certain cases, there may be interest in the dependence of the accummulated γ radiation dose on time. Figure 2.6, based on data from [3], shows the rate of accummulation of the dose upon explosion of nuclear weapons of various powers.

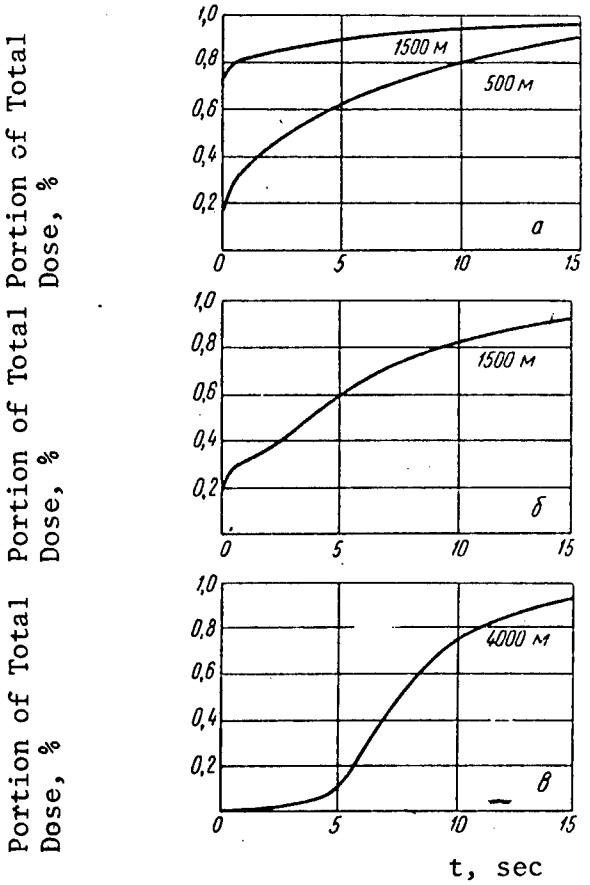

Figure 2.6. Rate of γ Radiation Dose Accummulation Upon Explosion of Nuclear Weapons With Powers of: a, q = 2 Kt; b, q = 200 Kt; c, q = 20,000 Kt.

We can see from the figure that the more powerful the explosion, the longer the dose continues to accummulate, since the cavity created by the shock wave continues to grow for a longer period of time.

The greater the distance, the more rapidly the dose accummulates, since the role of capture radiation increases.

§ 4. Spatial Distribution of Neutrons of Nuclear Explosion

The neutrons leaving the shell of the weapon interact with the nuclei of the surrounding medium: they are scattered, moderated and absorbed at various distances from the point of the explosion.

Let us first study the distribution of slow neutrons. The spatial distribution of slow neutrons is determined by the process of moderation and diffusion of neutrons in air. During the very first stage of the explosion, the temperature of the material of the bomb is about $10^{7°}$ K, corresponding to an energy of about 10^3 eV, to which energy level the neutrons are absorbed as they achieve thermal equilibrium with the material. The neutrons subsequently cool together with the material of the shell. A few microseconds after the explosion, the temperature of the shell can be estimated as some hundreds of thousands or millions of degrees. Therefore, considering the lower temperatures in the outer layers of the shell, it is probably correct to consider its temperature as approximately $5 \cdot 10^5$-$10^{6°}$ K as the neutrons fly outward, corresponding to a neutron energy of 50-100 eV. Thus, it can be considered that the energy of Maxwellian neutrons at the beginning of diffusion is some tens of electron volts.

One of the characteristics of air as a moderating medium is that the probability of absorption of low energy neutrons in air is high due to the high capture cross section of atmospheric nitrogen. Therefore, a neutron upon moderation has a high probability of being captured before it is moderated to thermal velocities. It can be considered approximately that a neutron in air is moderated on the average to an energy of about 0.2 eV and is captured at this energy by nitrogen [7].

Figure 2.7 shows the dependence of the flux of slow neutrons on the distance to the center of an explosion performed at high altitude, when the diffusion of neutrons occurs in air and the perturbing influence of the earth can be ignored [7]. As we can see from Figure 2.7, at distances less than 500 m, the flux of slow neutrons forming a cloud around the center of the explosion is determined primarily by neutrons leaving the shell as Maxwellian neutrons. At distances of greater than 500 m, the contribution of Maxwellian neutrons can be ignored. In this area the spatial distribution of slow neutrons is

determined by neutrons leaving the shell during the process of moderation, while at great distances the primary contribution is that of neutrons having high initial energies. This flux of slow neutrons $\Phi_T(R)$ at distances of greater than 500 m is described rather well by the exponential formula

$$\Phi_T(R) = C e^{-R/\lambda}, \tag{2.52}$$

where C is a constant, λ = 135 m is the relaxation length. This fact is determined by the fact that the value of $\Phi_T(R)$, as was shown in [7], is the sum of Gaussian distributions created by various sectors of the initial neutron spectrum. At distances of less than 400-500 m, the neutron flux is determined by Maxwellian neutrons alone, since in this range of distances the distribution is near Gaussian.

Therefore, with any value of permeability of the shell of the weapon, the curve characterizing the distribution of slow neutron flux for distances greater than 500 m will be approximately described by formula (2.52), with the single difference that constant C changes for a weapon of the same power. At short distances, the more or less rapid rise in neutron flux will be determined by the permeability of the shell.

If an explosion is performed at the surface of the ground or at a slight altitude over the ground, the ground may have a significant perturbing influence on the distribution of neutrons near its surface.

Figure 2.7 shows the distribution of the flux of slow neutrons in air at various distances from the center of a surface blast with a power of 20 Kt, calculated [7] considering the influence of the ground; the permeability of the shell is assumed equal to 0.1. As we can see, consideration of the influence of the ground in the solution of the problem of diffusion of neutrons in the air did not cause significant distortion of the distribution function of the slow neutron flux at distances R > 100 m. Near the point of the explosion at R < 100 m, the influence of the ground causes a significant increase in the flux of slow neutrons in comparison with diffusion in air. This is explained by the fact that the presence of the denser medium increases the concentration of slow neutrons, whereas in the air these neutrons would propagate to greater distances.

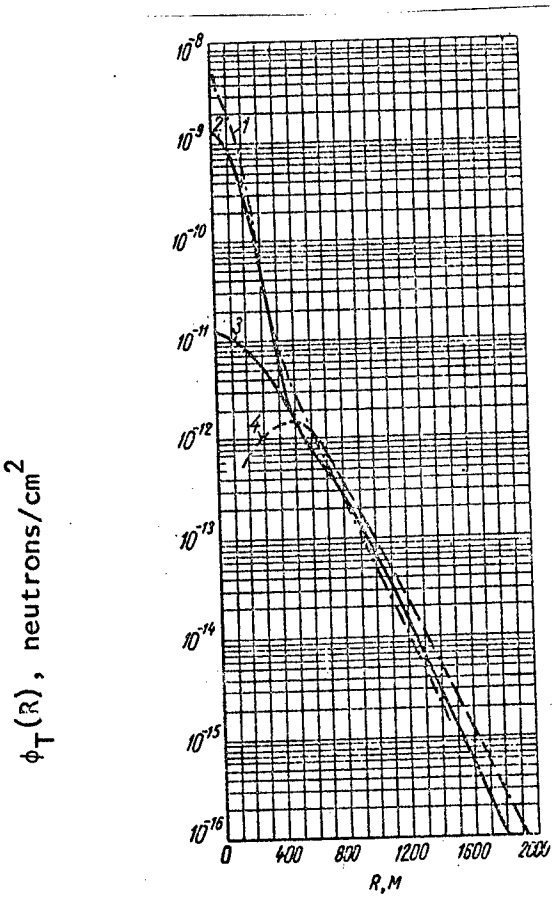

Figure 2.7. Spatial Distribution of Slow Neutrons With a Nuclear Explosion: 1, total flux of slow neutrons, explosion on surface of the earth; 2, total flux of slow neutrons, explosion in the air; 3, flux of slow neutrons generated by neutrons with energies over Maxwellian; 4, flux of slow neutrons generated by fast neutrons in thermonuclear explosion

At great distances, the earth acts as a neutron sink, as a result of which the flux of neutrons changes in comparison with the flux in an infinite air medium. At distances exceeding 150-200 m, the disturbing influence of the earth on the propagation of slow neutrons is slight, and therefore without great error we can use the results of calculation for an infinite air medium.

The numerical value of the preexponential term in formula (2.52) can be determined from Figure 2.7, which yields

$$\Phi_T(R) = 2{,}81 \cdot 10^{14} q a\, e^{-R/135} \text{ neutrons/cm}^2 (R > 500 \text{ m}), \qquad (2.53)$$

where a is the permeability factor of the shell.

The fact that formula (2.53) does not contain the term $1/R^2$ has no physical sense. It would be equally correct to use the term 1/R or $1/R^2$. Then the value of the attenuation distance would not be 135 m.

The flux of slow neutrons for distances less than 500 m can be represented by the formula

$$\Phi_T(R) = 3{,}74 \cdot 10^{14} q (1 - a)\, e^{-\frac{R}{3 \cdot 10^4}}. \qquad (2.54)$$

We should also discuss the problem of the spatial distribution of slow neutrons formed as a result of moderation and diffusion of delayed neutrons in the air. Figure 2.8 shows the distribution of slow (0.2 eV) neutrons, generated by delayed neutrons from a nuclear explosion with a maximum cavity radius of r_{fb} and considering the rise of the fireball. The data were produced by calculation [7] for an explosion of 1 Kt. In order to determine the flux of slow neutrons at a given distance from the explosion of a weapon of q Kt power, the value of $\Phi_T(R)$, determined from the graph of Figure 2.8 must be multiplied by the explosion power q, in correspondence with the calculated value of $\overline{L} = 100 \sqrt[3]{q}$ for the weapon in question.

Let us see what fluxes of slow delayed neutrons are possible with explosions of various powers. For example, for q = 400 Kt ($\overline{L}$ = 800 m) with a shell permeability of 0.1, at a range of 1000 m the flux of slow neutrons generated by prompt fission neutrons, in correspondence with equation (2.54), is $2.7 \cdot 10^{11}$ neutrons/cm^2. With this same power level of the explosion, the flux of slow delayed neutrons is also about $2.7 \cdot 10^{11}$ neutrons/cm^2. In other words, at q = 400 Kt and R = 1000 m, the share of slow delayed neutrons is half the total quantity of slow neutrons at this range. With increasing explosion power, the percentage of delayed neutrons may be even higher. As a result of the effect of the shock wave, the relative quantity of delayed neutrons increases, but not in proportion to the explosion power.

With a thermonuclear blast, most of the neutrons leaving the weapon have high energy. Still, at distances of over 600-700 m, these neutrons form a field of slow neutrons. Figure 2.7 (curve 4) shows the spatial distribution of the flux of slow neutrons (E_n < 0.625 eV) in an infinite air medium upon explosion of a thermonuclear weapon [9].

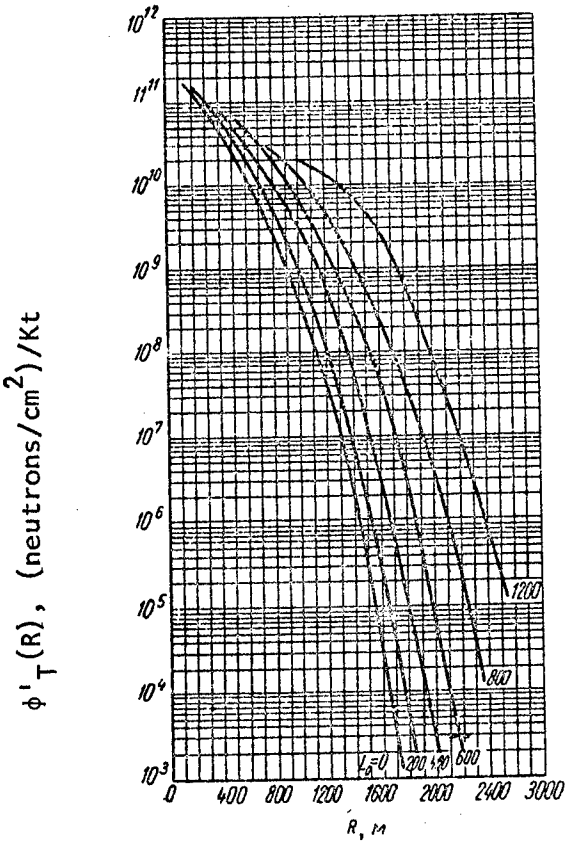

Figure 2.8. Dependence of Flux of Slow Neutrons Generated by Moderation of Delayed Neutrons in Air on Distance to Center of Explosion Considering Ascent of Cloud and Maximum Cavity Radius $L_0 = \overline{L}$.

The spectrum of neutrons of the source was assumed to consist 17% of fission neutrons with energies over 0.4 MeV and 83% of neutrons, evenly distributed in the interval from 12 to 16 MeV. The authors of this work believe that this spectrum of the source is characteristic for thermonuclear explosions, although the exclusion of neutrons with energies of below 0.4 MeV from the calculation results in a reduction in the number of slow neutrons in the near zone. We must note that the

spatial distribution of slow neutrons is insensitive to changes in the initial spectrum of neutrons over a rather broad range.

The neutrons leaving the shell of the weapon during the process of moderation have energies of from 100 eV to several MeV. Before the neutrons are moderated, they may travel a considerable distance in the air, the mean value of which is related to the energy of the neutrons leaving the shell. Thus, there are both slow and fast neutrons in the region of the blast.

Figure 2.9 shows the results of calculation of the spatial distribution of neutrons of point isotropic sources with various initial radiation spectra in an infinite air medium by the Monte Carlo method. The initial neutron energy used in the calculations correspond to the fission spectrum [10], to a source of monoenergetic neutrons with an energy of 14 MeV [10], and to the spectrum of neutrons from a thermonuclear blast [9]. In all cases, the results were normalized for a source with a power corresponding to one neutron/sec.

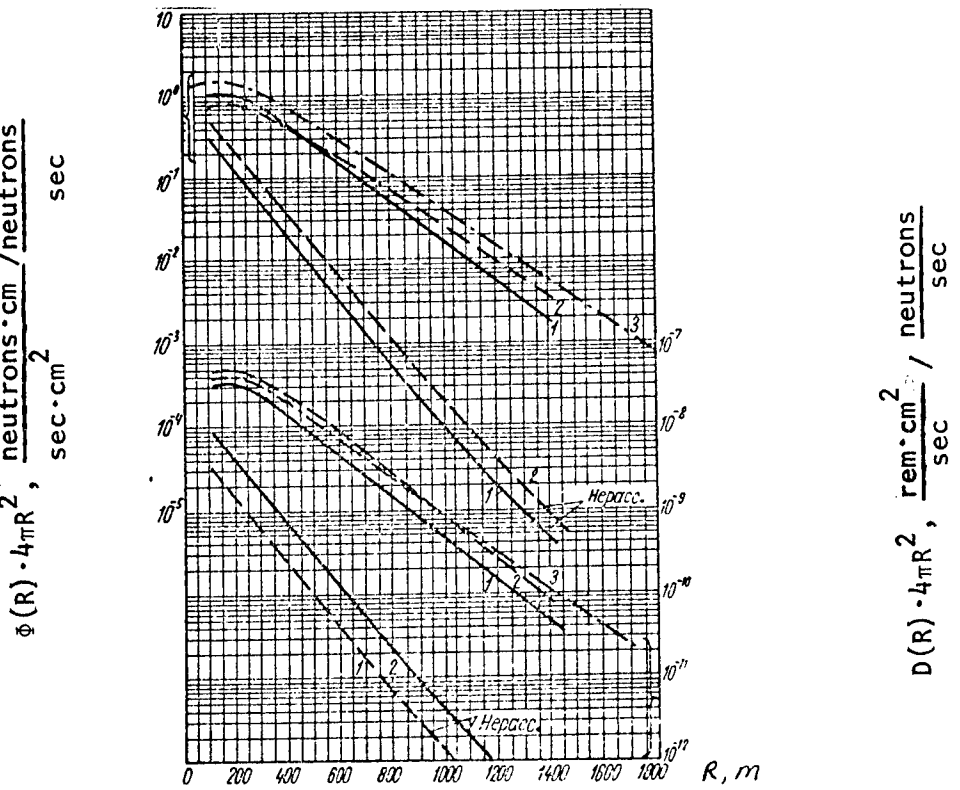

Figure 2.9. Spatial Distribution of Neutrons of Point Isotropic Source in Infinite Air Medium: 1, fission source. Flux and dose calculated for neutrons with $E_n \geq 0.1$ MeV; 2, source of neutrons with initial energy 14 MeV. Flux and dose calculated for neutrons with $E_n \geq 0.1$ MeV; 3, source of neutrons with spectrum modeling thermonuclear explosion. Flux and dose of neutrons calculated for neutrons with $E_n \geq 0.5$ MeV.

When there is a division boundary between two media -- earth and air -- its perturbing influence cannot be ignored. Detailed investigation of the influence of the earth on the spatial distribution of the dose or flux of neutrons during a nuclear blast was performed in [11]. The method of calculation suggested in this work consists of determining the influence of the earth on the distribution of the first collisions of neutrons with air nuclei near the source and last collisions near the detector. It is based on the assumption that the number of multipliscattered neutrons striking the detector from long distances is in the first approximation directly proportional to the number of first collisions of neutrons with nuclei of air near the source and last collisions near the detector.

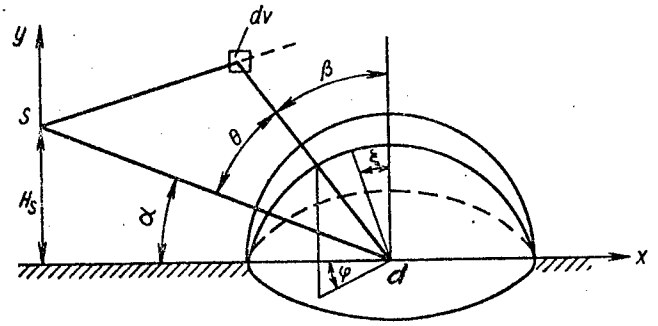

Figure 2.10. Geometry for Calculation of Distribution of Radiation With Air-Ground Division Boundary

Let us analyze a point isotropic source of neutrons of unit power, located at height H_s over the surface of the earth (Figure 2.10). The number of first scattering events which occur per unit volume of air dv will be

$$dN = \frac{\Sigma_s e^{-\Sigma_t \sqrt{x^2+y^2}}}{4\pi(x^2+y^2)}\,dv, \qquad (2.55)$$

where Σ_s is the macroscopic cross section of scattering of fast neutrons in air; Σ_t is the total cross section of the interaction of neutrons with air; $dv = x\,dx\,dy\,d\phi$.

For fast neutrons, it is justified to assume that $\Sigma_s = \Sigma_t$ [12]. Then the total number of first scattering collisions in the air near the source will be

$$N(H_s) = \frac{\Sigma_t}{2} \int_{-H_s}^{\infty} \int_{0}^{\infty} \frac{x e^{-\Sigma_t \sqrt{x^2 + y^2}}}{x^2 + y^2} dx\, dy. \qquad (2.56)$$

For an infinite air medium $N(H_s) = 1$. Thus, the value of $N(H_s)$ in the first approximation characterizes the portion of neutrons of the source which are scattered at least once in the air. Obviously, the best approximation is weighing of each first collision for the probability that the scattered neutron will have a later collision in the air.

If we assume that the first scattering event is isotropic in the laboratory system of coordinates, the probability that a neutron scattered once will not be absorbed by the earth is proportional to $N(H_s)$. Thus, the number of first collisions of neutrons in the air, weighed on the basis of their probability of undergoing further scattering, is determined as follows:

$$N'(H_s) = \frac{\Sigma_t}{2} \int_{-H_s}^{\infty} \int_{0}^{\infty} \frac{f(y)\, \rho\, e^{-\Sigma_t \sqrt{x^2 + y^2}}}{x^2 + y^2} dx dy, \qquad (2.57)$$

where $f(y) = N(H_s + y)$ is the weight function of centers of first collision.

In concluding formula (2.56), it was assumed that the earth is an absolutely black body. Actually, a portion of the neutrons which strike the earth without undergoing scattering in the air may be reflected back and, after further interactions, may strike the detector. The albedo of fast neutrons from the earth (see § 3 Chapter 4), depends on the incident angle, read from the normal as $\cos^{2/3} \beta$. If the integral albedo is equal to A_n^{π} for normal incidence, the total number of neutrons scattered from the earth will be

$$N_r(H_s) = \frac{A_n^{\pi}}{2} \int_{0}^{\infty} \frac{x H_s^{2/3} e^{-\Sigma_t \sqrt{x^2 + H_s^2}}}{(x^2 + H_s^2)^{4/3}} dx. \qquad (2.58)$$

Thus, the effective share of neutrons of the source experiencing single scattering near the source is expressed by the dependence

$$f(H_s) \quad N'(H_s) + N_r(H_s). \tag{2.59}$$

In order to estimate the influence of the earth near the detector, we assume that the centers of the last collisions are distributed evenly, and scattering is considered isotropic in the laboratory system of coordinates. The first assumption is rather obvious. Actually, the free path length of a neutron at distances of over 200 m from the source of fission, i. e. in the area where evenness of the spectrum of neutrons scattered in the air is observed, is about 72 m, while the effective length of attenuation of the flux is about 190 m. Thus, the density of neutrons does not change significantly in the area of the detector.

Although the assumption of isotropic scattering of neutrons is not usable for strict calculation of neutron transfer in an air medium, it should not have any significant influence on an estimation of the disturbing influence of the earth.

If the flux of primary neutrons near the source is considered the unit flux, the density of collisions at any point in the medium will be Σ_t. Thus, following the geometry of Figure 2.10, the flux of neutrons scattered in the air with an absolutely black surface of the earth at the point of the detector (at height H_d over the earth) will be

$$N(H_d) = \frac{\Sigma_t}{2} \int_{-H_d}^{\infty} \int_{0}^{\infty} \frac{x\, e^{-\Sigma_t \sqrt{x^2+y^2}}}{x^2+y^2}\, dx\, dy. \tag{2.60}$$

Since the reflection of neutrons from the earth has a significant influence on the effect at the detector only when it is located at a low altitude, let us assume that the neutrons scattered from the ground enter the detector without interacting with the nuclei of the air.

If A'_H is the share of neutrons reflected from the ground with isotropic distribution of incident neutrons (the flux of which in this case will be 1/2), with cosinusoidal distribution of neutrons reflected from the ground to the detector, they form the flux

$$N_r(H_d) = A'_H \int_0^{\infty} \frac{xH_d\, e^{-\Sigma_t \sqrt{x^2+H_d^2}}}{(x^2+H_d^2)^{3/2}}\, dx. \tag{2.61}$$

The sum of the two quantities $N(H_d)$ and $N_g(H_d)$ can be looked upon as the fraction $f(H_d)$ of the dose or flux observed in an infinite

air medium, which will be recorded by a detector located at height H_d over the earth:

$$f(H_d) = N(H_d) + N_g(H_d). \tag{2.62}$$

If D(R) is the dose (flux) of neutrons from the explosion at distance R from the center of a nuclear explosion in an infinite air medium, the dose with the source at height H_s and the detector at H_d over the surface of the earth can be expressed as

$$D(R, H_s, H) = D(R) f(H_s) f(H). \tag{2.63}$$

The factors $f(H_s)$ and $f(H_d)$ calculated on the basis of the discussions presented above are shown in Table 2.3. The calculation functions $f(H_s)$ and $f(H_d)$ presented in this table were checked experimentally with a suspended reactor. Good agreement was produced for source-detector distances of over 260 m [11].

Table 2.3

CORRECTION FACTORS $f(H_s)$ AND $f(H_d)$ FOR CONSIDERATION OF INFLUENCE OF THE EARTH ON SPATIAL DISTRIBUTION OF FAST NUCLEAR EXPLOSION NEUTRONS

H, м	$f(H_s)$			$f(H_d)$		
		Experimental			Experimental	
	Calculated	$R = 260$ м	$R = 350$ м	Calculated	$R = 260$ м	$R = 350$ м
0	0,434	—	—	0,697	—	—
10	—	—	—	0,720	0,714	0,828
15	0,612	0,586	—	0,840	0,841	0,858
29	0,715	0,717	0,701	—	—	—
35	0,746	0,755	0,746	0,913	0,884	0,932
44	—	—	—	0,931	0,931	0,931
53	0,806	0,806	0,806	—	—	—

Figure 2.11 shows the results of measurements [13] of the spatial distribution of the flux and dose of fast neutrons from a nuclear explosion. The experimental explosion was performed at an altitude of 215 m over the surface of the earth, while detectors were placed on the ground. As we can see from Figure 2.11, the spatial distribution of fast neutrons can be approximated with sufficient accuracy of an exponential dependence. The authors of [13] suggested that the dose of

neutrons of the nuclear explosion be calculated using the empirical formula

$$D(R) = \frac{4{,}42q \cdot 10^{10}}{R^2} e^{-\frac{\rho}{\rho_0}\frac{R}{184}} \text{ rad.} \qquad (2.64)$$

A similar expression can be used to calculate the flux of fast neutrons. For example, the neutron flux with $E_n > 0.75$ MeV can be calculated using the formula

$$\Phi(R) = \frac{1{,}05 \cdot 10^{19} q}{R^2} e^{-\frac{\rho}{\rho_0}\frac{R}{190}} \text{ neutrons/cm}^2. \qquad (2.65)$$

Although the number of delayed neutrons liberated upon fission is not great, the share of delayed neutrons acting at various distances from the center of the explosion may be comparable to the share of prompt fission neutrons. This results from the fact that as they are moderated in the shell, many of the fission neutrons reach the temperature of equilibrium with its atoms and into the air with an energy of about 1 KeV. As was shown above, these neutrons do not penetrate to distances of over 400 m. Therefore, at long distances, the neutron dose consists only of those fission neutrons which were not moderated to low energies upon passage through the shell.

In contrast to this, the delayed neutrons are liberated after the shell has flown apart. For example, for a shell with a permeability of 0.1, the share of delayed neutrons observed at distances of over 500 m should be greater than their initial share by approximately 10 times, i. e. should represent about 7% during fission of U^{235}.

The second factor facilitating the transmission of delayed neutrons over great distances is the presence of the cavity with low air density around the explosion center, the radius of which, as was demonstrated above, increases with increasing explosion energy. As the delayed neutrons pass through this cavity, they are almost unattenuated by the air, while the prompt neutrons propagate before formation of the cavity. Therefore, the presence of the cavity increases the share of delayed neutrons at great distances. The number of prompt and delayed neutrons formed is proportional to the power of the explosion; however, due to the formation of the cavity, the share of delayed neutrons at great distances will increase with increasing power of the explosion. Thus, with explosions of sufficient power, it may be that, in spite of the small share of formation of delayed neutrons, a significant portion of the total neutron dose results from these delayed neutrons.

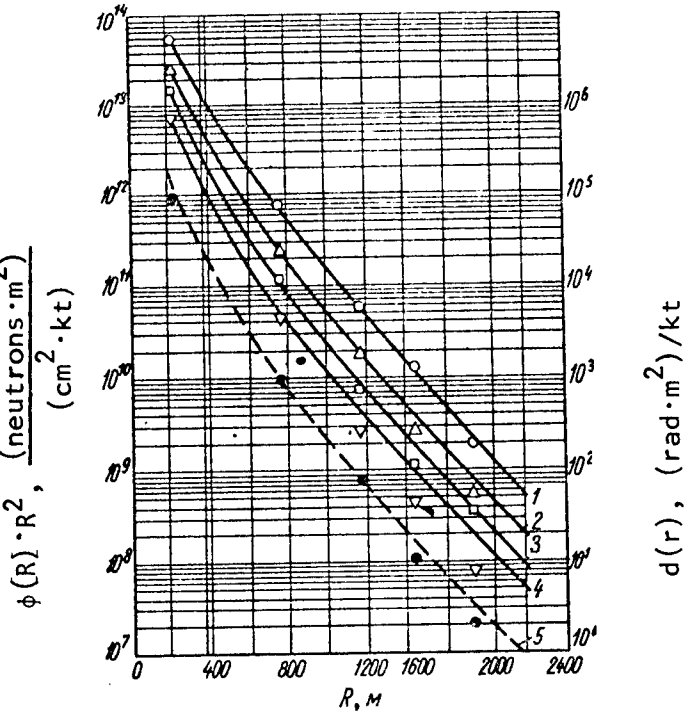

Figure 2.11. Fluxes of Neutrons Over Threshhold Value and Doses of Fast Neutrons as Functions of Distance to Center of Explosion: flux of neutrons $E_n > 5$ eV: curve 1, calculated; ●, experimental. Flux of neutrons $E_n > 0.75$ MeV: curve 2, calculated; Δ, experimental. Flux of neutrons $E_n > 1.5$ MeV: curve 3, calculated; □, experimental. Flux of neutrons $E_n > 2.5$ MeV: curve 4, calculated; ∇, experimental. Doses of fast neutrons: curve 5, calculated; o, experimental.

The total quantity of delayed neutrons recorded at a certain distance from the center of the explosion is determined by the number of neutrons formed, the effective size of the cavity and the rate of ascent of the cloud of fragments. Although the formation of the cavity increases the significance of delayed neutrons, the ascent of the cloud decreases their influence. Consequently, the number of delayed neutrons recorded for explosions of various powers will not be linearly related to the energy of the explosion, as is the case for fission neutrons.

The number of delayed neutrons radiated per unit time at time t following the explosion is expressed by the formula

$$N(t) = N_0 \sum_i \lambda_i a_i e^{-\lambda_i t}, \qquad (2.66)$$

where N_0 is the number of fission events; a_i is the total yield of delayed neutrons per fission event within the limits of the ith group; λ_i is the decay constant of neutrons in the ith group.

The values of the quantities included in this formula are presented in Table 1.1.

The total number of delayed neutrons liberated from the fragments formed in the explosion is

$$N_0 \sum_i a_i \int_0^\infty \lambda_i e^{-\lambda_i t} dt = N_0 \sum_i a_i. \qquad (2.67)$$

This quantity of neutrons is liberated in a few tens of seconds following the explosion.

Since the delayed neutrons form groups with various half life periods, the effective period increases with passing time. The resulting decay rule can be written as the formula

$$S(t) = A + B e^{-Ct} \text{ neutrons/(sec·fission)}, \qquad (2.68)$$

where t is the time following fission, sec.

The values of the coefficients included in this formula are:

	U^{235}	U^{238}	Pu^{239}
A	$8{,}4 \cdot 10^{-6}$	$1{,}15 \cdot 10^{-5}$	$3{,}87 \cdot 10^{-6}$
B	$7{,}31 \cdot 10^{-3}$	$3{,}08 \cdot 10^{-2}$	$2{,}62 \cdot 10^{-3}$
C	0,542	0,663	0,544

The power of the dose of delayed neutrons at moment in time t at distance R from the center of the explosion, considering the effect of the cavity and the ascent of the cloud, can be written as:

$$P_{n.3}(R, t) = \frac{3 \cdot 10^{23} q S(t) \eta(E_n) e^{-\frac{R - L(t)}{\lambda_{eff}}}}{4\pi R^2} \times \quad (2.69)$$

$$\times \left(\frac{R}{R'}\right)^2 e^{-\frac{\Delta R}{\lambda_{eff}}} \text{ rad/sec.}$$

Here $\eta(E_n)$ is the transition factor of the neutron flux to dose. It can be considered without great error that the energy of delayed neutrons, averaged over all groups, is 0.55 MeV. For neutrons of this energy, coefficient $\eta(E_n)$ is $2.15 \cdot 10^{-9}$ rad/(neutrons·cm^2) [14], λ_{eff} is the effective relaxation length of delayed neutrons in the air, which is about 157 m. The values of R' and ΔR are calculated as for γ quanta (see § 3 of this chapter).

The dependence of the size of the cavity $L_{eff}(t)$ on time for explosions of various powers is shown on Figure 2.3. As we can see from Figure 2.3, for explosions with the power of $\leq$ 2000 Kt at moment in time t = 2 sec the radius of the cavity is at least 80% of its final size. Since in this time only 20% of all delayed neutrons have been produced, for an explosion of between 1500 and 200 Kt yield, the radius of the cavity can be assumed constant over the entire time of action of the source of delayed neutrons. For precise calculation of the radius of the cavity, expression (2.31) should be used. However, it should be kept in mind that at high explosion powers, the value of k in this expression becomes less than 100, since a certain portion of the neutrons is emitted during the process of formation of the cavity. The total dose of delayed neutrons can be produced by integrating expression (2.69) with respect to time. Calculations show that with nuclear explosions with powers of up to 100 Kt, delayed neutrons can be ignored. For weapons with powers of 100 to 1000 Kt, the dose created by the delayed neutrons must be considered. With explosions of 1000 Kt and higher, at distances where the neutrons can be looked upon as a damaging factor, their dose is created primarily by the delayed neutrons.

§ 5. Spectral-Angular Distributions of Neutrons Scattered in the Air

The spectrum of the neutrons of a nuclear explosion in the air is determined by the form of the initial spectrum of the neutrons leaving the shell of the weapon, and the nuclear characteristics of the medium in which the propagation of the neutrons occurs. It was demonstrated above that the relative form of the spectrum of the neutrons

leaving the shell of the weapon during a nuclear explosion based on the principle of fission is almost independent of the design of the weapon.

It follows from experiments and calculation that, beginning at a certain distance R, the spectrum of the neutrons in the air changes relatively little. Thus, in [13] the behavior of individual energy groups of neutrons was studied as a function of distance R during explosion of a nuclear weapon. The results of the investigations are shown on Figure 2.11.

In [10], the integral neutron spectra by angles at various distances from the center of a nuclear explosion in the air were calculated by the Monte Carlo method. The nuclear explosion in this case was modeled by a point isotropic source of fission neutrons in an infinite air medium. The results produced in this work are shown on Figure 2.12. The nature of the energy distributions shown on the figure indicates th slight transformation of the spectrum of the neutrons from the nuclear explosion with increasing distance from its center.

This same figures shows for comparison data on the spectral distribution of nuclear explosion neutrons produced by direct measurement at 1180 m from the center of an experimental blast [13, 15] performed at the Nevada Test Site (USA). The experimental and calculated spectra for the distance of 1180 m were normalized for an energy of 1 MeV. As we can see, the relative course of the experimental and calculation curves correspond satisfactorily. This indicates that the presence of the earth-air division boundary has little influence on deformation of the spectrum of the nuclear explosion neutrons in comparison to the spectrum in an infinite air medium. The data shown on Figure 2.12 characterize the spectral distribution of fast neutrons of a nuclear explosion, the energy of which exceeds 0.1 MeV. As concerns slow and intermediate neutrons, we can gain an idea of their energy distribution from Figure 2.13, showing the results produced by the method of moments [16] for a point fission source in an infinite air medium.

A comparison with the fission spectrum gives us an idea of the degree of deformation of the spectrum of nuclear explosion neutrons scattered in air in comparison with the spectrum of neutrons produced by fission.

During a thermonuclear explosion, in addition to the fission neutrons, neutrons with an energy of 14 MeV are generated. During the process of inelastic scattering of these neutrons in the shell of the weapon, neutrons may be produced with a most probable energy of about 4 MeV. Figure 2.14 shows the spectra of neutrons scattered in the air, calculated [10] for point isotropic sources with initial neutron

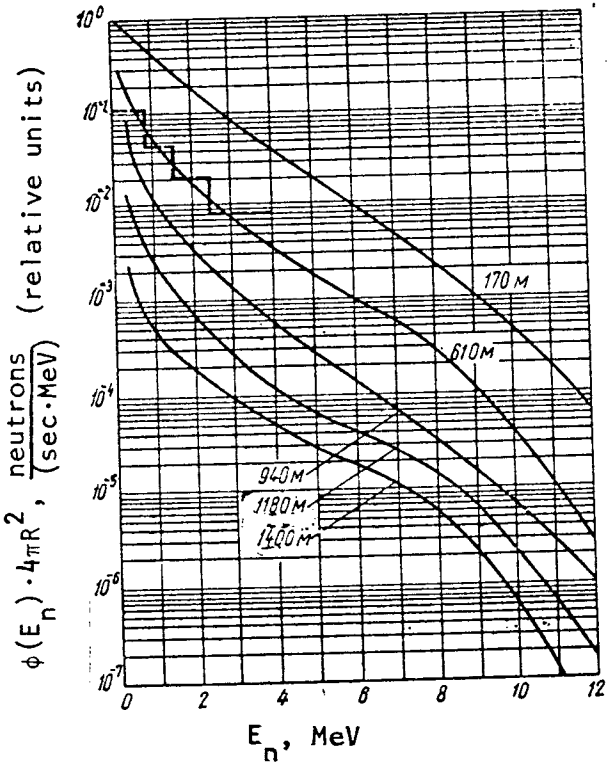

Figure 2.12. Spectra of Neutrons of Point Isotropic Fission Source in Infinite Air Medium at Various Distances From the Source

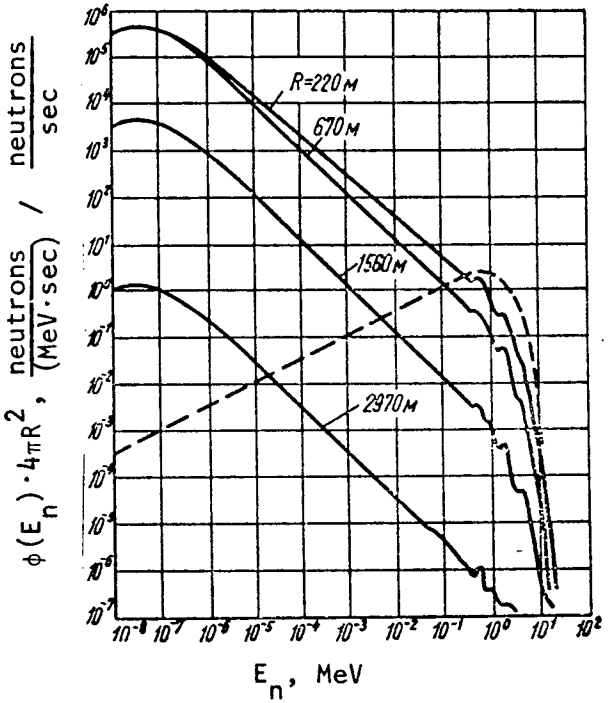

Figure 2.13. Nature of Spectral Distribution of Slow and Intermediate Neutrons of Nuclear Explosion. ------- Fission Spectrum

energies of 4 and 14 MeV. In each case, the power of the source was assumed equal to one neutron/sec.

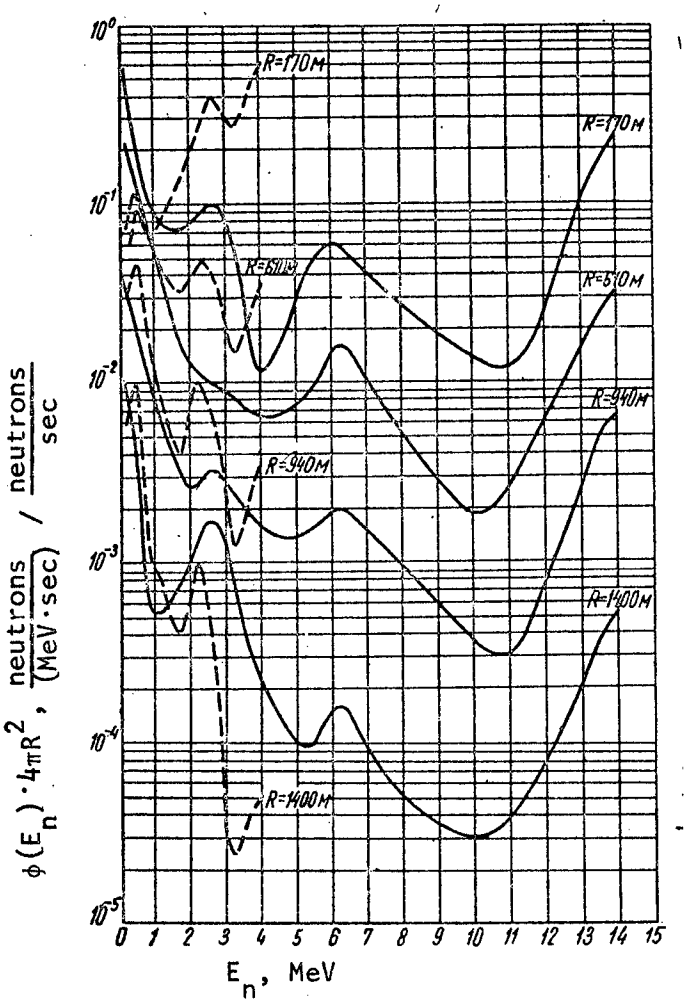

Figure 2.14. Spectra of Neutrons of Point Isotropic Sources With Initial Energies 4 MeV (- - - - -) and 14 MeV (————) in an Infinite Air Medium

In [9], the energy distributions of neutrons of a thermonuclear explosion with an initial spectrum consisting of fission neutrons (17%) and neutrons evenly distributed in the 12-16 MeV energy interval are calculated. The results produced in this work are shown on Figure 2.15. As we can see from this figure, with increasing distance to the center of a thermonuclear explosion, significant softening of the spectrum in the 10-16 MeV area occurs. However, below 8-9 MeV, the

integral spectrum of fast neutrons is deformed slightly. This same figure shows data relating to the slow and intermediate neutrons. They allow us to conclude that in the range of energies from 10^{-4} to 0.5 MeV, the spectral density of neutrons follows the rule $1/E_n^m$, where the exponent m is either equal to or slightly greater than unity, while the fluctuations of its value with increasing distance to the center of the nuclear blast are very slight.

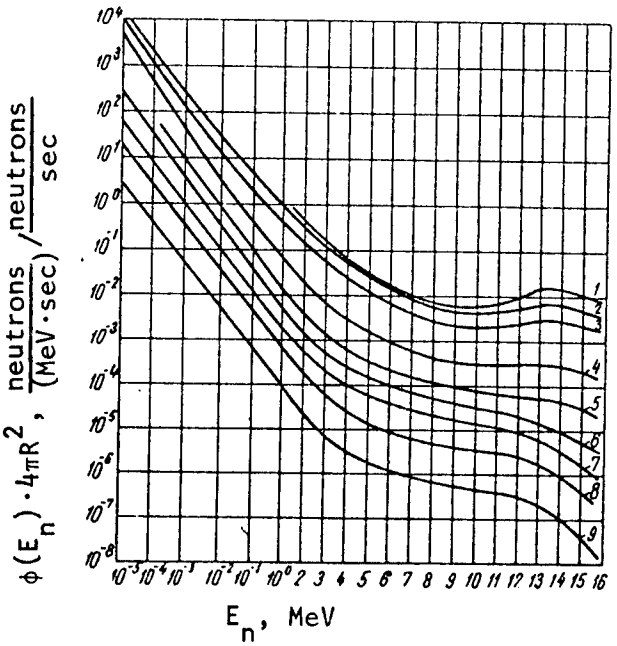

Figure 2.15. Spectra of Neutrons of Thermonuclear Explosion in Infinite Air Medium at Various Distances From the Point of the Explosion: 1, 64 m; 2, 214 m; 3, 385 m; 4, 810 m; 5, 1150 m; 6, 1330 m; 7, 1500 m; 8, 1670 m; 9, 2000 m

In addition to the spectral characteristics of radiation and their spatial distribution, the design of shielding from penetrating radiation of a nuclear explosion also requires a knowledge of the angular distribution of radiation scattered in the air. In analyzing the problem of the angular distribution of penetrating radiation produced by a nuclear blast, it is a common practice to base calculations on the concepts of the "polar angle" of scattering θ and the "angle of inclination" ξ of the scattered radiation. A diagram of the calculation of these angles is shown on Figure 2.10.

In [17], it is demonstrated on the basis of analysis of calculation data produced by the Monte Carlo method that the angular distribution function of neutron doses from a point isotropic fission source in an infinite air medium at distances at least exceeding the relaxation length can be described by the equation

(2.70)

where $F(\theta)$ is the field of the total dose of neutrons at a given point in space per unit solid angle from a direction characterized by the scattering angle θ. Thus, the following condition is observed:

(2.71)

This dependence agrees well, as we can see on Figure 2.16, with the experimental data of [13], in which the angular distributions of doses of neutrons at the surface of the earth were studied during experimental nuclear explosions in the air. The satisfactory agreement of the results of these works indicates the identical form of the angular distribution of neutrons of a nuclear explosion in an infinite air medium and near the earth-air division boundary.

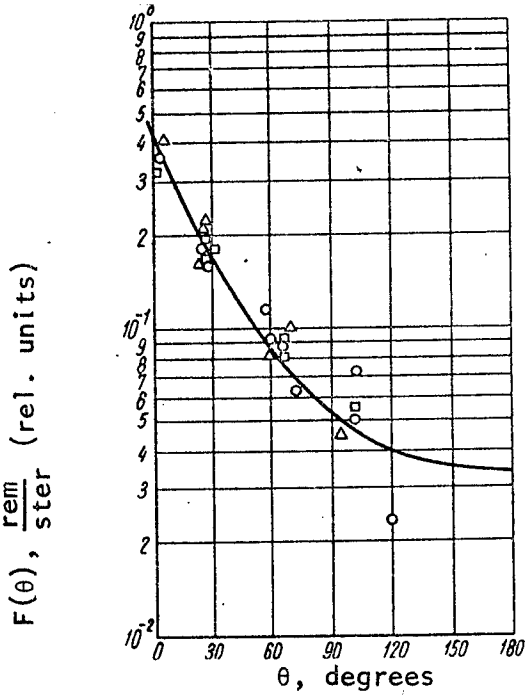

Figure 2.16. Angular Distribution Functions of Doses of Nuclear Explosion Neutrons Scattered in Air: ——; calculated [17]; experimental [13]: ○, R = 1240 m; △, R = 1450 m; □, R = 1660 m

It has been established in a number of works that the form of the angular distribution function of neutrons scattered in air does not change over a broad range of distances from the center of the explosion. This conclusion is illustrated on Figure 2.17, where the angular distributions of flux and dose of neutrons are shown at various distances from the center of a nuclear explosion [10]. As we can see, beginning at a distance of 165 m, the field of neutrons scattered in the air can be considered stable. Experimental confirmation of the equilibrium phenomena of the angular distributions of neutrons is presented by the data of Figure 2.16 [13], relating to various distances from the center of the explosion. It should also be noted that during measurement of angular distributions of neutrons scattered in the air [13], no dependence of the dose on angle of inclination ξ has been discovered for radiation striking a detector located on the surface of the earth and measuring radiation from the upper half space.

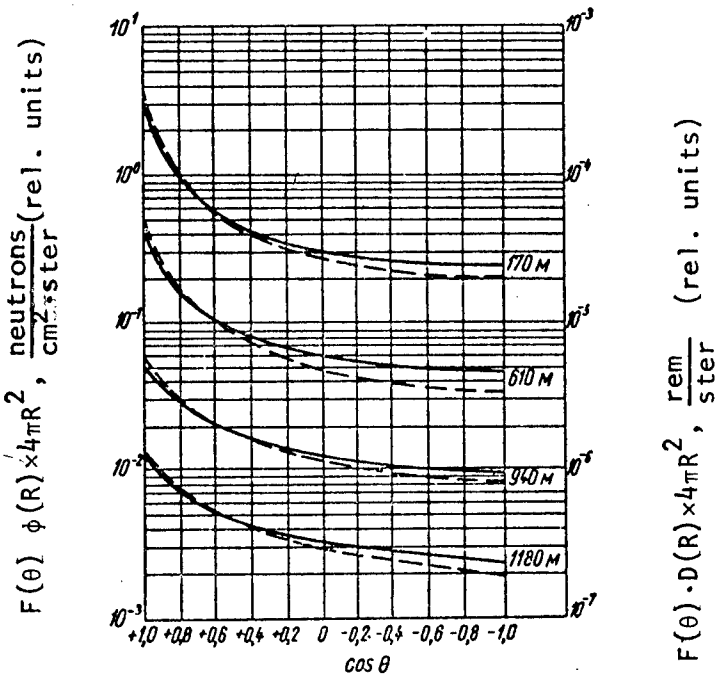

Figure 2.17. Angular Distributions of Flux (———) and Dose (-----) of Neutrons at Various Distances From Center of Nuclear Explosion

This indicates that the earth has no influence on the nature of the angular distribution of neutrons scattered in the air.

Although function $F(\theta)$ in an infinite air medium corresponds in form with the angular distribution function of neutrons near the earth-air division boundary when the detector records neutrons arriving only from the upper half space, the numerical values of the free term and the preexponential factor in equation (2.70) will be different). Obviously, when the source and detector are located on the surface of theearth, the values of these coefficients will be double the values produced according to equation (2.70) for an infinite air medium, if we consider the earth to be an absolutely black body. With other positions of the source relative to the detector and surface of the earth, characterized by the elevation angle of the explosion α between the direction of the source-detector line and the surface of the earth, these coefficients will have intermediate values. Therefore, we can write

$$F(\alpha, \theta) = K_\alpha (0{,}033 + 0{,}4045\, e^{-0{,}0334\theta}), \tag{2.72}$$

where K_α is a coefficient which is dependent on angle α.

Let us first study the hypothetical case of an absolutely black surface of the earth. Integration of equation (2.72) with respect to the upper half space can be performed as follows:

$$2K_\alpha \left[\pi \int_0^\alpha \sin\theta\, (0{,}033 + 0{,}4045\, e^{-0{,}0334\theta})\, d\theta + \right. \tag{2.73}$$

$$\left. + \int_\alpha^{\pi-\alpha} \sin\theta \left(\pi - \arccos \frac{\operatorname{tg}\alpha}{\operatorname{tg}\theta} \right) (0{,}033 + 0{,}4045\, e^{-0{,}0334\theta})\, d\theta \right].$$

The angular distribution function of this integral should be equal to unity by definition. From this, it is easy to find the value of coefficients K_α for any angles α.

The influence of reflection of neutrons from the surface of the earth can be considered by using the results of [18, 19], which show (see § 3, Chapter 4) that the integral dose albedo in concepts of the flux of neutrons from the source of fission in the air from the surface of the earth is described by the expression

$$A^{\Pi}_{n,\gamma}(\beta) = 0{,}435 \frac{\Sigma_g - \Sigma_H}{\Sigma_g} \cos^{3/2}\beta, \tag{2.74}$$

where Σ_g and Σ_H are the total macroscopic neutron cross sections of the ground and hydrogen contained in the ground; β is the angle of

incidence of neutrons on the surface of the earth, measured from the normal (see Figure 2.10).

Since a portion of the integral dose in the detector located near the surface of the earth is created by neutrons reflected from the earth, the values of coefficients K_α in equation (2.72) will be different than with an absolutely black medium. They can be found by solving the equation

$$\int_{2\pi} [1 + A^n_{n,d}(\beta)] K_\alpha (0{,}033 + 0{,}4045\, e^{-0{,}03345\theta})\, d\Omega = 1, \qquad (2.75)$$

the integration of which is performed with respect to the upper half space.

If we know the integral value of $A^n_{nd}(\alpha)$, the albedo of neutrons from the nuclear explosion with a fixed elevation of the explosion α (§ 6, Chapter 2), coefficient K_α can be calculated using the formula

$$K_\alpha^{-1} = 2 [1 + A^n_{n,д}(\alpha)] \int_0^{\pi/2} \int_0^{\pi} \{0{,}033 + 0{,}4045 \times$$
$$\times \exp [-0{,}03345 \arccos (\sin\beta \cos\varphi \cos\alpha + \cos\beta \sin\alpha)]\} \sin\beta d\beta d\varphi. \qquad (2.76)$$

The values of coefficients K_α for soils of varying moisture contents, characterizing their contents of hydrogen, and for water calcualted according to this equation are presented on Figure 2.18 [20].

Thus, the dose of neutrons arriving per unit solid angle from the upper half space from directions with low angle θ can be calculated using formula (2.72) considering coefficient K_α.

The form of the angular distribution of neutrons from a thermonuclear explosion is similar to that of a fission weapon. This is easy to see by comparing the data of Table 2.4, relating to a thermonuclear explosion [9], to the angular distribution functions of neutrons from a nuclear explosion shown on Figure 2.17. In both cases, the angular distributions of neutron flux are normalized per unit value of $\cos\theta$ (divided by $\Delta \cos\theta$), Thus, by dividing the quantities in Table 2.4 and Figure 2.17 by 2π, we produce the value of the angular distributions per unit solid angle. The results shown on Figure 2.17 relate to a flux of neutrons with energies $E_n \geq 0.2$ MeV, in Table 2.4 -- $E_n \geq 0.5$ MeV.

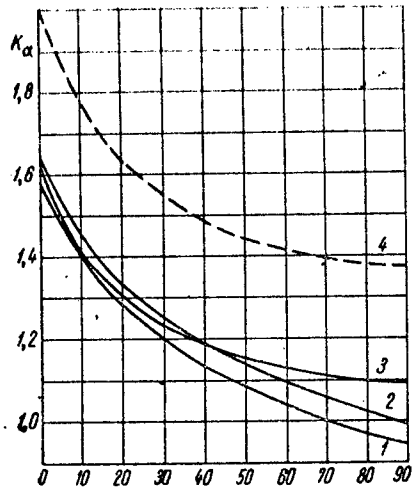

Figure 2.18. Coefficient $\overline{K}_\alpha$ of Neutrons for an Absolutely Black Surface of the Earth (curve 4) and K_α for Scattering Media as Functions of α: 1, dry soil, composition: hydrogen 1.24%, oxygen 52.38%, aluminum 7.85%, silicon 38.53% by weight; 2, moist soil, composition: hydrogen 2.54%, oxygen 57.36%, aluminum 7.08%, silicon 38.32%; 3, water

As concerns slow neutrons, their angular distribution is near isotropic.

In [10], the energy distribution of scattered neutrons arriving at the detector from various directions was also studied. Table 2.5 shows the spectral-angular distributions of neutrons from a nuclear explosion scattered in the air, calculated for a range of 595 m [10]. These data indicate that the energy distribution of neutrons scattered in the air is independent of angle θ. The angular spectra correspond in form to the integral spectrum of the neutrons of a nuclear explosion (see Figure 2.12). Experimental studies during nuclear tests [13] have confirmed this conclusion.

Table 2.5

SPECTRAL-ANGULAR DISTRIBUTION OF NEUTRONS SCATTERED IN AIR AT 595 m FROM CENTER OF NUCLEAR EXPLOSION $\Phi(\Delta E_n, \Delta\Omega)\ 4\pi R^2$ neutrons/(cm^2·sec)

Angular Interval $\Delta\cos\vartheta$	Distance From Center of Blast, m					
	216	390	820	1510	2200	2900
0,9÷1,0	0,3642(+1	0,1579(+1	0,1717	0,3612(—2	0,5253(—4	0,1299(—5
0,8÷0,9	0,1202(+1	0,7939	0,1036	0,2148(—2	0,3067(—4	0,2598(—5
0,7÷0,8	0,9998	0,6731	0,8110(—1	0,1584(—2	0,1127(—3	0,4454(—6
0,6÷0,7	0,6072	0,5184	0,7549(—1	0,3046(—2	0,2398(—4	0,2419(—6
0,5÷0,6	0,5692	0,4234	0,8293(—1	0,1398(—2	0,2615(—4	0,4170(—6
0,4÷0,5	0,4297	0,2667	0,5071(—1	0,1282(—2	0,2235(—4	0,1962(—6
0,3÷0,4	0,4983	0,2799	0,3183(—1	0,8358(—3	0,9168(—5	0,2128(—6
0,2÷0,3	0,4884	0,3364	0,3157(—1	0,1019(—2	0,1289(—4	0,4334(—6
0,1÷0,2	0,4558	0,1639	0,4031(—1	0,1084(—2	0,8637(—5	0,7243(—7
0,0÷0,1	0,4425	0,2090	0,3333(—1	0,2754(—2	0,1436(—4	0,1503(—6
—0,1÷0,0	0,3289	0,2073	0,2908(—1	0,8158(—3	0,2561(—4	0,2491(—6
—0,2÷—0,1	0,3181	0,3018	0,4266(—1	0,8150(—3	0,8686(—5	0,9854(—7
—0,3÷—0,2	0,3520	0,2018	0,1924(—1	0,6357(—3	0,2723(—4	0,2767(—7
—0,4÷—0,3	0,2564	0,2583	0,2573(—1	0,4344(—3	0,6524(—5	0,3358(—6
—0,5÷—0,4	0,2317	0,1757	0,3080(—1	0,3832(—3	0,9053(—5	0,3247(—6
—0,6÷—0,5	0,2417	0,2325	0,2283(—1	0,8716(—3	0,8145(—5	0,1460(—5
—0,7÷—0,6	0,3491	0,1849	0,2440(—1	0,1781(—2	0,2068(—4	0,3572(—7
—0,8÷—0,7	0,2912	0,1557	0,2465(—1	0,7969(—3	0,8351(—4	0,7314(—7
—0,9÷—0,8	0,2267	0,1338	0,2093(—1	0,6330(—3	0,1330(—4	0,3973(—6
—1,0÷—0,9	0,2659	0,1148	0,2437(—1	0,6638(—3	0,2510(—5	0,1691(—7

Note. Read 0.1781 (-2 = 0.001781.

Table 2.4

ANGULAR DISTRIBUTION OF FLUX OF FAST NEUTRONS $4\pi R^2\Phi(R)F(\theta)$ AT VARIOUS DISTANCES FROM THE CENTER OF A THERMONUCLEAR EXPLOSION IN AN INFINITE AIR MEDIUM [2π NEUTRONS·cm^2/(cm^2·ster)]

$\Delta\theta$, degrees	Energy Interval, MeV (ΔE_n)								$\Phi(\Delta\theta)$ neutrons/(cm^2·sec)
	0,2—0,4	0,4—0,6	0,6—0,75	0,75—1,5	1,5—2,5	2,5—4,0	4,0—6,0	6,0—10,0	
0—10	0,5367 (—3	0,3560 (—3	0,3476 (—3	0,1670 (—2	1,1698 (—2	0,1034 (—2	0,8729 (—3	0,3587(—3	0,6874 (—2
10—20	0,1874 (—2	0,1726 (—2	0,1969 (—2	0,3400 (—2	0,2720 (—2	0,1302 (—2	0,6097 (—3	0,1596(—3	0,1376 (—1
20—30	0,3308 (—2	0,1334 (—2	0,1250 (—2	0,2801 (—2	0,2028 (—2	0,1304 (—2	0,2365 (—3	0,1613(—3	0,1242 (—1
30—40	0,3037 (—2	0,3604 (—2	0,2405 (—2	0,4013 (—2	0,1615 (—2	0,9497 (—3	0,5298 (—3	0,1457(—3	0,1630 (—1
40—50	0,4235 (—2	0,2370 (—2	0,1655 (—2	0,5123 (—2	0,2119 (—2	0,1210 (—2	0,3704 (—3	0,2390(—4	0,1711 (—1
50—60	0,4373 (—2	0,2046 (—2	0,1202 (—2	0,4189 (—2	0,1590 (—2	0,5791 (—3	0,1127 (—3	0,1811(—6	0,1409 (—1
60—70	0,4758 (—2	0,1350 (—2	0,9089 (—3	0,2249 (—2	0,2798 (—2	0,7583 (—3	0,2563 (—3	0,3613(—5	0,1308 (—1
70—80	0,3201 (—2	0,1586 (—2	0,8902 (—3	0,1942 (—2	0,2085 (—2	0,7110 (—3	0,8636 (—4	0,7166(—6	0,1050 (—1
80—90	0,2446 (—2	0,1391 (—2	0,5031 (—2	0,2255 (—2	0,1166 (—2	0,3474 (—5	0,1380 (—4	0,9743(—5	0,1212 (—1
90—100	0,1287 (—2	0,1759 (—2	0,6692 (—3	0,2355 (—3	0,5286 (—3	0,1883 (—4	0,6281 (—4	0,4281(—4	0,4604 (—2
100—110	0,2909 (—2	0,3459 (—2	0,7072 (—3	0,1576 (—2	0,7057 (—3	0,1113 (—2	0,1050 (—3	0,1187(—4	0,1059 (—1
110—120	0,4504 (—2	0,1235 (—2	0,1019 (—2	0,2061 (—2	0,7133 (—3	0,7306 (—4	0,4394 (—4	0,1431(—4	0,9762 (—2
120—130	0,1731 (—2	0,1507 (—2	0,2960 (—3	0,8492 (—3	0,8902 (—3	0,9344 (—4	0,2557 (—6		0,5367 (—2
130—140	0,2507 (—2	0,6497 (—3	0,4714 (—3	0,1403 (—2	0,6619 (—3	0,8435 (—4	0,3786 (—5		0,5781 (—2
140—150	0,2633 (—2	0,6037 (—3	0,3513 (—3	0,6394 (—3	0,4395 (—3	0,4525 (—4	0,1466 (—4		0,4727 (—2
150—160	0,8194 (—3	0,4932 (—3	0,3027 (—3	0,1108 (—2	0,3045 (—3	0,1405 (—3	0,3192 (—12		0,3168)—2
160—170	0,5457 (—3	0,4603 (—3	0,4318 (—3	0,9272 (—3	0,1474 (—3	0,1007 (—7	0,5437 (—17		0,2512 (—2
170—180	0,1018 (—2	0,1096 (—3	0,9362 (—4	0,5999 (—3	0,3533 (—4	0,5295 (—5			0,1862 (—2
$\Phi(\Delta E_n)$, neutrons/(cm^2·sec)	0,4562 (—1	0,2604 (—1	0,2000 (—1	0,3704 (—1	0,2224 (—1	0,9425 (—3	0,3319 (—2	0,9325(—3	0,1646 (—0

§ 6. Reflection of Neutrons From the Earth During a Nuclear Blast in the Air

In addition to the neutrons scattered in the air and acting on surface structures from the upper half space, during a nuclear blast the phenomenon of reflection of neutrons from the surface of the earth is observed. These neutrons also make a contribution to the dose of penetrating radiation within structures which rise over the surface of the earth. We analyze below the characteristics of neutrons scattered from the earth during a nuclear blast in the air.

Based on known dependence (2.74), the values of the integral dose albedo of neutrons from a nuclear blast

$$A^{n}_{n,\,d}(\alpha) = 2\int_0^{\pi/2}\int_0^{\pi} 0{,}87\,\frac{\Sigma_g - \nu_H}{\Sigma_g}\cos^{4/3}\beta\sin\beta\,\overline{K}_\alpha\,\{0{,}033 + 0{,}4045\exp[-0{,}03345\arccos(\sin\beta\cos\varphi\cos\alpha + \cos\beta\sin\alpha)]\}\,d\beta d\varphi. \tag{2.77}$$

In this expression, we use the coefficient $\overline{K}_\alpha$, calculated using formula (2.73) for an absolutely black earth (Figure 2.18).

Similar calculations can be made for the case of reflection of neutrons of the atomic blast from water, if we use the expression describing the albedo for water [19, 21]:

$$A^{n}_{n,\,d}(\alpha) = 2\int_0^{\pi/2}\int_0^{\pi} \sin\beta\,[0{,}22\cos\beta + 0{,}30\,(1-\cos\beta)]\,\overline{K}_\alpha \times \{0{,}033 + 0{,}4045\exp[-0{,}03345\arccos(\sin\beta\cos\varphi\cos\alpha + \cos\beta\sin\alpha)]\}\,d\beta d\varphi. \tag{2.78}$$

The dependence of the total albedo of nuclear blast neutrons from soil and water for various angles α is illustrated on Figure 2.19.

In § 5 of Chapter 2, we have studied the problem of the angular distributions of nuclear blast neutrons arriving at the detector from the upper half space.

As concerns the angular distribution of neutrons arriving at the detector from the lower half space, in the case when the detector is located directly at the surface of the earth, this distribution is determined entirely by neutrons reflected from the ground, the distribution of the flux of which, as has been established [18, 22], is isotropic. If the detector is located at some height over the ground,

the neutrons reflected from the surface of the earth in the direction of the detector will be attenuated in the layer of air next to the earth. On the other hand, neutrons entering the layer of air near the ground may be scattered in the direction of the detector and recorded by it as coming from the earth.

The contribution of these two phenomena to the distribution of neutrons propagating from the direction of the earth can be calculated if we know the integral albedo $A^{\pi}_{n,\,d}(\alpha)$ and the spatial distribution of neutrons of the atomic blast.

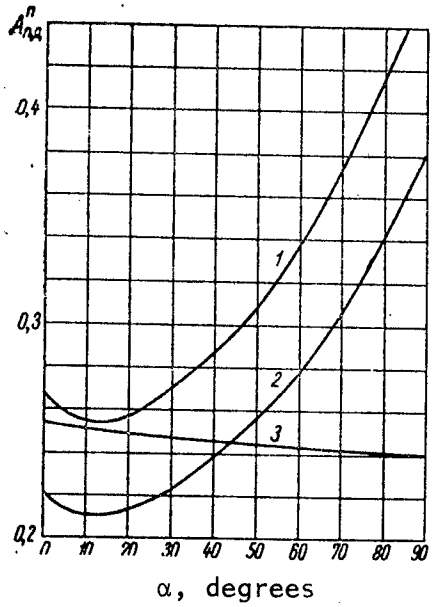

Figure 2.19. Integral Albedo of Nuclear Blast Neutrons for Water (Curve 3) and Soil. Composition of soil and symbols correspond to Figure 2.18.

Let us analyze the solution of this problem in the geometry shown on Figure 2.20. The source of fission neutrons, with power Q neutrons/sec, is located at height H_s and at distance R, which is greater than the relaxation length of neutrons in air, from detector d, located at height H_d over the surface of the earth. The position of the source relative to the detector is fixed by angle α

The total flux of neutrons at point B is

$$\Phi_B = f_S(H_S) f_d(H_B) \frac{Q}{4\pi l^2} e^{-\frac{l}{\lambda}}, \qquad (2.79)$$

where

$$H_B = H_d - x\cos\beta; \quad l^2 = R^2 + x^2 - Rx\cos\theta.$$

The number of fission events per element of volume

$$dN = \Phi_B \Sigma_S dv = \Phi_B \Sigma_S x^2 dx d\omega, \qquad (2.80)$$

where Σ_s is the macroscopic cross section of scattering of neutrons in air; $d\omega$ is the solid angle subtended at point d by an elementary area ds.

If we assume that the scattering of fission neutrons in the air is isotropic in the laboratory system of coordinates, the neutrons scattered in an element of volume dv around point B will create at the detector d the flux:

$$d\Phi'_d = \frac{\Phi_B \Sigma_S x^2 d\omega dx}{4\pi x^2} e^{-\Sigma_t x}, \qquad (2.81)$$

where Σ_t is the total macroscopic cross section of the interaction of neutrons with atoms in the air.

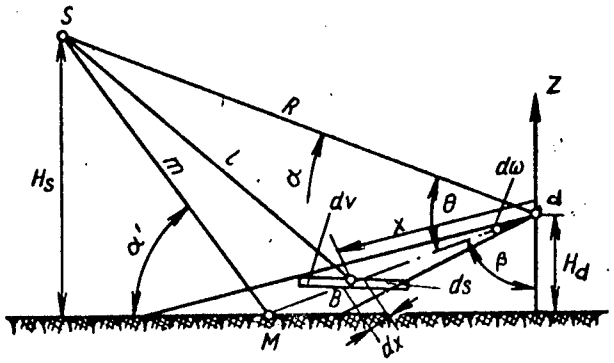

Figure 2.20. Analysis of Angular Distributions of Neutrons Propagating From the Direction of the Earth

The flux per unit solid angle is

$$\frac{d\Phi'_d}{d\omega} = \frac{\Phi_R \Sigma_S}{4\pi} e^{-\Sigma_t x} dx. \qquad (2.82)$$

Substituting (2.79) into this expression and integrating along beam dm, we produce

$$\frac{d\Phi'_d}{d\omega} = Q \int_0^{H/\cos\beta} \frac{\Sigma_S e^{-l/\lambda} f_s(H_S) f_d(H_B)}{16\pi^2 l^2} e^{-\Sigma_t x} dx. \qquad (2.83)$$

The total flux of neutrons at point d will be

$$\Phi_d = f_S(H_S) f_d(H_d) \frac{Q}{4\pi R^2} e^{-\frac{R}{\lambda}}. \qquad (2.84)$$

Therefore, the flux of neutrons arriving at point d per unit body angle from the direction characterized by angle β, and created by neutrons scattered in the layer of air near the ground in relationship to the total flux of neutrons at point d can be written as:

$$\frac{d\Phi'_d}{d\omega} = \frac{R^2 \Sigma_S}{4\pi} \int_0^{H_d/\cos\beta} \frac{e^{-l/\lambda}}{l^2} \frac{e^{-\Sigma_t x}}{e^{-R/\lambda}} \frac{f_d(H_d - x\cos\beta)}{f_d(H_d)}. \qquad (2.85)$$

Let us now study the reflection of neutrons from the earth at point M. The total flux at point M is

$$\Phi_M = f_S(H_S) f_d(0) \frac{S}{4\pi m^2} e^{-\frac{m}{\lambda}}. \qquad (2.86)$$

If the integral albedo of neutrons at point M is $A^{\pi}_{nh}(\alpha')$, the flux of neutrons reflected at point M will be

$$\Phi''_M = \frac{A^{\pi}_{nd}(\alpha') \Phi_M}{1 + A^{\pi}_{n\pi_\gamma}}, \qquad (2.87)$$

where

$$m^2 = R^2 + \left(\frac{H_d}{\cos\beta}\right)^2 + \frac{RH_d}{\cos\beta}\cos 0.$$

With isotropic distribution of neutrons reflected from the ground in any direction per unit solid angle the reflection is

$$\frac{d\Phi^*_M}{d\omega} = \frac{\Phi^*_M}{2\pi}. \qquad (2.88)$$

Considering the attenuation of reflected neutrons as they propagate from point M in the direction toward detector d and relating the flux of reflected neutrons arriving from this direction to the total flux at point d, we can write

$$\frac{d\Phi_{cd}^{*}}{d\omega} = \frac{A_{nh}^{n}(\alpha')\,R^{2}}{2\pi\,[1 + A_{nh}^{n}(\alpha')]}\,\frac{e^{-\frac{m}{\lambda}}\,f_{cd}(0)}{m^{2}f_{cd}(H_{cd})}\,\frac{e^{-\Sigma_{t}\frac{H_{cd}}{\cos\beta}}}{e^{-\frac{R}{\lambda}}}. \qquad (2.89)$$

The total flux of neutrons at point d arriving from the direction of the earth per unit body angle from the direction with polar angle β and azimuth angle ϕ is determined by the sum of expressions (2.85) and (2.89). In this case, $\cos\theta = \sin\beta\cos\phi\cos\gamma + \cos\beta\sin\gamma$.

Since the spectrum of neutrons of the source of fission is very slightly transformed as the neutrons propagate through the air and are reflected from the ground, all of the discussions presented above remain correct for the dose of neutrons as well. Thus, we can calculate the angular distribution function of neutron doses arriving at a detector placed at a certain height from the direction of the earth.

Figure 2.21 shows the results of calculation of the angular distributions of neutron doses arriving from the lower half space at a detector placed at various heights over the surface of the earth at a distance from 800 m from the center of the explosion with an elevation angle of the explosion $\alpha = 20°$. As we can see, the angular intensity of neutrons arriving at the detector from the direction of the earth depends little on angle β, with the exception of directions near horizontal, where it increases significantly. The angular distributions of these neutrons show rather precise axial symmetry, which is rather clearly demonstrated by Figure 2.22. The maximum divergence in the values of angular intensities at angles β near horizontal is 20° for angles $\phi = 0$ and $\phi = 180°$ and with the height of the detector over the surface of the earth $H_d = 2$ m. This divergence increases to 35% for $H_d = 20$ m. With lower values of angle β, it amounts to a few percent.

The data on Figure 2.21 also indicate that the relative form of angular distributions of neutrons depend little on the height of the detector over the surface of the earth. Only for heights beginning at 20 m does the course of the dependence of angular intensity begin to change for directions horizontal. However, this deformation is slight and can be ignored in practical calculations of the shielding of surface structures.

It is interesting to analyze the composition of neutron radiation arriving at the detector from the direction of the earth by components.

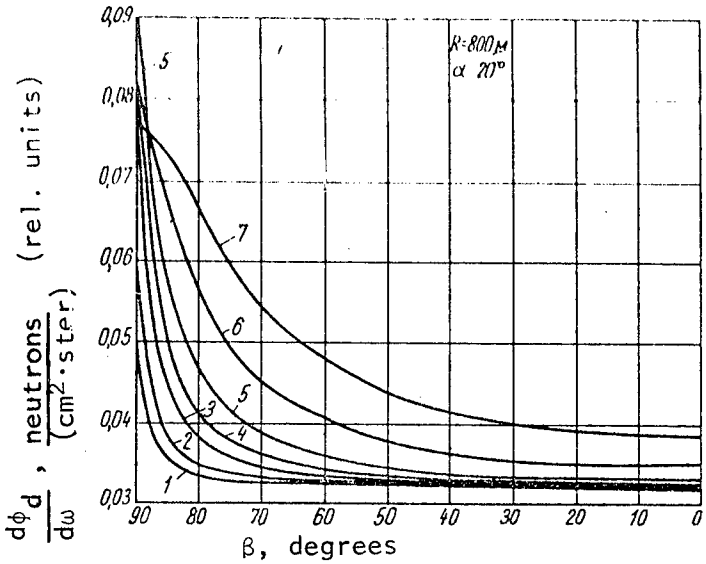

Figure 2.21. Angular Distributions of Neutrons Arriving From the Direction of the Earth at a Detector Located at Height H_d, equal to: 1, 0.5 m; 2, 1.0 m; 3, 2.0 m, 4, 3.0 m; 5, 5.0 m; 6, 10 m; 7, 20 m. Data relate to azimuthal direction determined by angle $\phi = 0$, read from projection of source-detector line on surface of the earth.

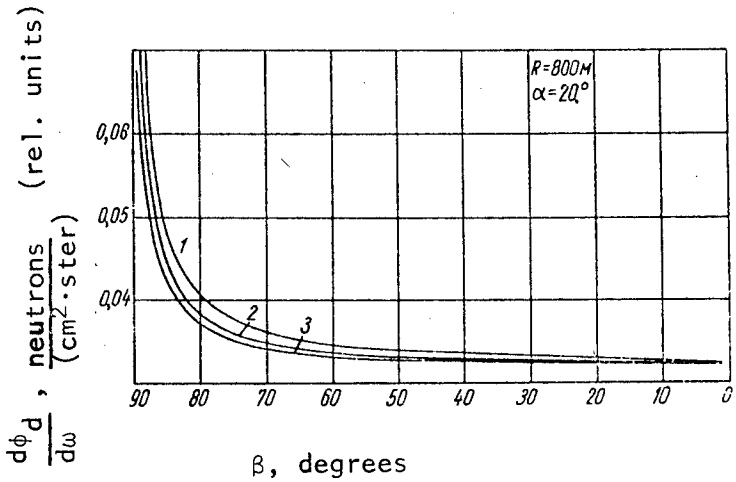

Figure 2.22. Angular Distribution Functions of Neutrons for Various Azimuthal Directions: 1, $\phi = 0°$, 2, $\phi = 90°$, 3, $\phi = 180°$

Figure 2.23 shows the contribution of neutrons reflected from the ground and scattered in the air, arriving at the detector from various directions depending on the position of the detector over the surface of the earth. As we can see from this figure, for low detector altitudes (up to 0.5 m) over the surface of the ground, the flux of neutrons arriving at the detector from directions near horizontal is approximately evenly divided between neutrons reflected from the earth and scattered in the near-earth layer of air. With increasing height H_d, the component of neutrons scattered in the air begins to predominate. Nevertheless, as was shown on Figure 2.22, the form of the angular distributions of the summary dose of neutrons resulting from superposition of the dependences of the distribution of reflected and scattered neutrons remains practically unchanged for all heights H_d studied.

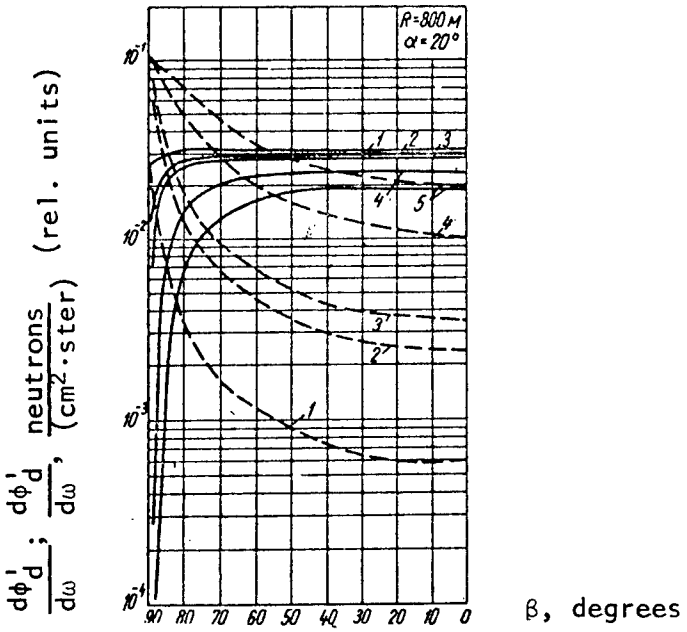

Figure 2.23. Contribution of Neutrons Reflected From the Ground (solid lines) and Scattered in the Near-Surface Layer of air (dotted lines) to Total Dose of Neutrons Arriving at Detector From Direction of Ground With Azimuthal Angle $\phi = 0°$. Data relate to various positions of detector over the surface: 1, H_d = 0.5 m; 2, H_d = 1.0 m; 3, H_d = 2.0 m; 4, H_d = 10 m; 5, H_d = 20 m.

The functions of differential distributions of neutron doses produced allowed us to calculate the dependence of the total dose of neutrons arriving at a detector from the direction of the ground on the height of the detector over the surface of the ground. This dependence, produced by integrating the angular distribution functions with respect to the lower half space, is shown on Figure 2.24. As we can see, the share of neutrons striking the detector from the direction of the ground increases with increasing height of the detector over the surface of the ground.

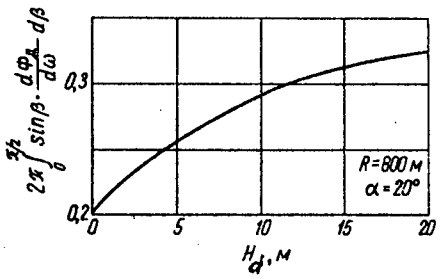

Figure 2.24. Total Dose of Neutrons Arriving at Detector From the Direction of the Ground as a Function of Height of Detector Over Surface of Ground

It should be noted that the differential and integral characteristics of neutrons propagating from the direction of the earth depend very little on the distance to the center of the explosion. The maximum divergence was 5-10%. Therefore, the divergence can be ignored in practical calculations.

The results produced allow us to consider the contribution of neutrons propagating from the direction of the earth correctly in calculating the shielding of surface structures from the radiation of nuclear explosions.

§ 7. Spectral-Angular Distribution of Initial γ Radiation in a Nuclear Blast

As is the case for neutrons, when a certain disance from the source is reached (1-2 times the free path length of unscattered radiation), quasi-equilibrium is observed in the angular and energy distributions of γ quanta scattered in the air. This conclusion is confirmed by the results of [10], in which the energy and angular characteristics of γ radiation of an atomic explosion in the air were calculated by the Monte Carlo method.

Figure 2.25 shows the spectra of individual components of the γ radiation of a nuclear explosion, calculated for a range of 1240 m from the center of the blast. It should be kept in mind that in the calculations performed in [10], attenuation of the prompt γ radiation in the shell of the weapon was not considered, and the influence of the shock wave on the propagation of fragment γ radiation was not analyzed. Therefore, the spectra of the individual components shown on Figure 2.25 should be considered independently. Their share in the integral flux of γ quanta may be different than that indicated by Figure 2.25.

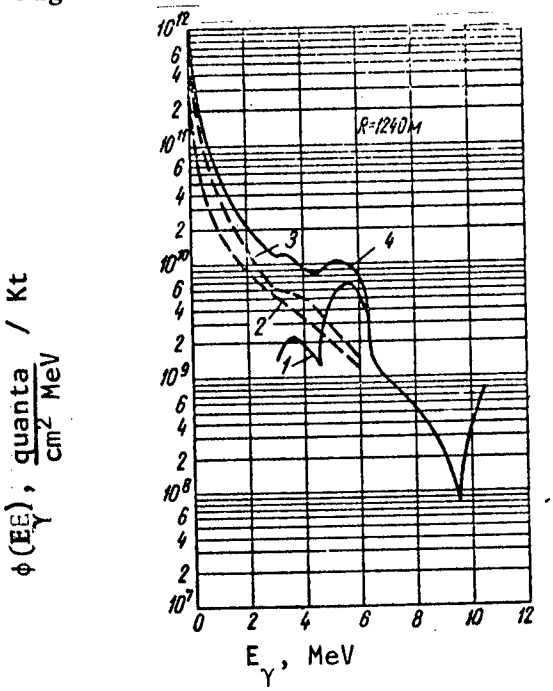

Figure 2.25. Spectra of γ Radiation of Point Isotropic Fission Source in Infinite Air Medium: 1, capture γ radiation; 2, γ quanta of fission fragments; 3, prompt fission γ radiation; 4, total flux of γ radiation

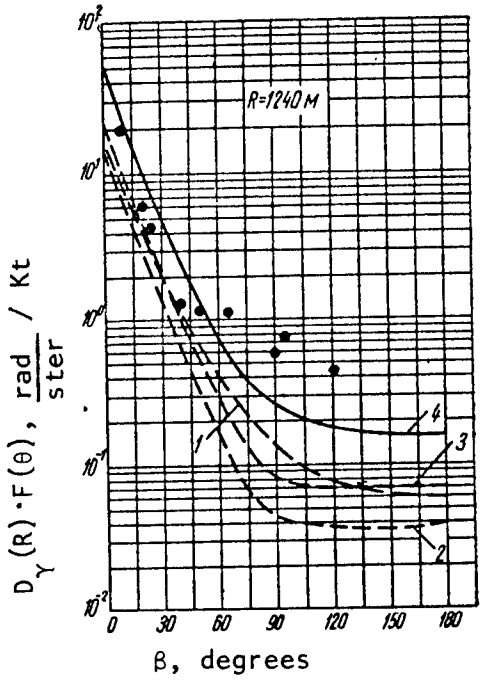

Figure 2.26. Angular Distributions of Doses of γ Radiation of Nuclear Explosion: 1, capture radiation; 2, fragment γ radiation; 3, prompt fission γ radiation; 4, total dose of γ rays. o, measured during actual tests

The fact of establishment of equilibrium of the angular distribution of γ radiation during nuclear blasts in the air has been confirmed by experimental data produced in [13]. These measurements also establish that the nature of the angular distribution of γ radiation is almost independent of the type of nuclear weapon and its power.

Figure 2.26 shows the dependences of the angular distributions of prompt (attenuation in the shell of the weapon ignored), fragment and capture γ radiation produced in [10], as well as the total dose of γ radiation during a nuclear blast. Here also we see the experimental points borrowed from [13].

As we can see from Figure 2.26, the coincidence of calculated and experimental data on angular distribution of γ radiation dose is rather good for scattering angles $\theta < 60°$. The divergence at larger angles, which is generally insignificant in relation to the integral dose, can be explained by failure to consider the scattering of γ radiation from the walls of the collimator and by the presence of capture γ radiation from the structural materials of the experimental installation. The divergence resulting from scattering on the walls of the collimator should increase with increasing collimator aperture, which was experimentally observed.

The angular intensity function of fragment γ quanta scattered in the air produced in [10] can be described by the dependence

$$F_f(\theta) = K_\alpha^f [0{,}0092 + 3{,}22 \exp(-0{,}08\theta)]. \tag{2.90}$$

The angular distributions of capture γ radiation dose follow the equation

$$F_c(\theta) = K_\alpha^c [0{,}008 + 2{,}11 \exp(-0{,}065\theta)]. \tag{2.91}$$

In these expressions, function $F(\theta)$ characterizes the share of the total dose of scattered radiation of a given component arriving per unit body angle from the direction determined by scattering angle θ, counted from the line connecting the source and detector.

K_α is a normalizing factor which depends on angle α between the surface of the earth and the direction toward the center of the blast, as well as the reflecting properties of the soil. It can be calculated:

$$K_\alpha = \frac{\overline{K}_\alpha}{1 + A_{\gamma d}^n(\alpha)}, \tag{2.92}$$

where $\overline{K}_\alpha$ is the normalizing factor calculated for a hypothetical absolutely black surface of the earth, not reflecting the γ radiation

which strikes it; $A^{\pi}_{\gamma d}(\alpha)$ is the integral albedo of the γ rays from the soil for a given elevation angle of the explosion α.

With an absolutely black surface of the earth, coefficient $\overline{K}_{\alpha}$ can be calculated by the expression

$$(\overline{K}^{f}_{\alpha})^{-1} = 2\left\{\pi\int_{0}^{\alpha}\sin\theta\,[0{,}0092 + 3{,}22\exp(-0{,}08\theta)]\,d\theta + \right.$$
$$\left. + \int_{\alpha}^{\pi-\alpha}\sin\theta\left(\pi - \arccos\frac{\operatorname{tg}\alpha}{\operatorname{tg}\theta}\right)[0{,}0092 + 3{,}22\exp(-0{,}080)]\,d\theta\right\}. \qquad (2.93)$$

for fragment γ radiation and

$$(\overline{K}^{c}_{\alpha})^{-1} = 2\left\{\pi\int_{0}^{\alpha}\sin\theta\,[0{,}008 + 2{,}11\exp(-0{,}065\theta)]\,d\theta + \right.$$
$$\left. + \int_{\alpha}^{\pi-\alpha}\sin\theta\left(\pi - \arccos\frac{\operatorname{tg}\alpha}{\operatorname{tg}\theta}\right)[0{,}008 + 2{,}11\exp(-0{,}065\theta)]\,d\theta\right\} \qquad (2.94)$$

for capture γ radiation.

The results of calculation of coefficients $\overline{K}_{\alpha}$ using these expressions are presented on Figure 2.27.

The main portion of the capture γ radiation is radiated in 0.1 sec, and the influence of the capture γ radiation is practically ended by 0.3 sec after the explosion.

During this time, the cloud practically does not rise. Therefore, the source of capture γ radiation, like the source of neutrons, can be considered nonmoving.

The change in dose power of fragment γ radiation with time is determined by the decrease in activity of the fission fragments, as well as the influence of the ascent of the cloud and the effect of formation of the cavity as the shock wave passes through the atmosphere:

$$P_f(t) \sim u(t)\,K_p(t)\,K_{\text{н}}(t). \qquad (2.95)$$

The cavity factor for the dose power is

$$K_p(t) = e^{\mu_{eff} L_{eff}(t,\,q)}. \qquad (2.96)$$

where $L_{eff}(t, q)$ is the effective radius of the cavity at a given moment

in time after explosion of a weapon with a power of q Kt. $K_H(t)$ is a coefficient considering the influence of ascent of the cloud on the dose power at the given moment in time:

$$K_H(t) = e^{-\mu_{eff}\Delta R}\left(\frac{R}{R_t}\right)^2, \tag{2.97}$$

where R is the distance to the point of the explosion; R_t is the distance to the center of the cloud at moment in time t; ΔR is the change in the distance to the center of the cloud with time: $\Delta R = R_t - R$.

Naturally, when the source of fragment γ radiation is considered to move, the value of coefficient K_α^f will not remain constant during the time of accummulation of the dose of fragment γ radiation.

If the calculation of the scattering angles θ is performed for a moving polar axis corresponding with the direction to the center of the rising cloud of the atomic blast, the effective value of coefficient K_α^f over the entire time of application of fragment γ radiation in the region of the atomic blast is determined from the expression

$$K^l_{\alpha\,eff} = \frac{\int_0^{t_{eff}} K^l_\alpha(t)\, u(t)\, K_p(t)\, K_H(t)\, dt}{\int_0^{t_{eff}} u(t)\, K_p(t)\, K_H(t)\, dt}. \tag{2.98}$$

Here $K_\alpha^f(t)$ is the value of coefficient K_α^f at each given moment in time, determined by the change in the elevation angle of the center of the cloud with time $\alpha(t)$.

Integration is performed up to that moment in time t_{eff} when, as a result of radioactive decay of fragments and ascent of the cloud, the intensity of γ radiation drops to a value which, from the standpoint of accummulation of total dose, can be ignored. Usually t_{eff} can be considered equal to 10-15 sec.

However, it is inconvenient to read angles relative to a moving axis, since usually the initial conditions in the calculations are limited by values of angles α and θ read from the vector direction to the center of the explosion, and in order to determine the dose of fragment γ radiation arriving from any given direction fixed by the value of the

initial scattering angle θ, it would be necessary to trace the change of scattering angle with time $\theta(t)$ relative to the moving center of the cloud by changing the elevation angle of the center of the cloud $\alpha(t)$ and the related coefficient $K_{\alpha}^{f}(t)$, as well as the change in the quantities $u(t)$, $K_p(t)$ and $K_H(t)$. In this case, the dose of γ radiation per unit solid angle can be determined in relative units using the following formula

$$D(0, \varphi) \sim \frac{\int_0^t K_{\alpha}^{f}(t)\left[0{,}0092 + 3{,}22\, e^{-0{,}080\,(t)}\right] u(t) K_p(t) K_H(t)\, dt}{\int_0^t u(t) K_p(t) K_H(t)\, dt}, \qquad (2.99)$$

where

$$\theta(t) \quad \arccos\left[\sin\left(\operatorname{arc\,tg}\frac{H + 16t^2}{\sqrt{R^2 - H^2}} - \alpha\right)\sin\theta\cos\varphi + \right.$$
$$\left. + \cos\left(\operatorname{arc\,tg}\frac{H + 16t^2}{\sqrt{R^2 - H^2}} - \alpha\right)\cos\theta\right]. \qquad (2.100)$$

Obviously, the use of this expression involves extremely cumbersome calculations for practical purposes. Still, when precise calculation is required, this formula should be used.

For practical purposes in calculations related to the angular distributions of fragment γ radiation in air, it is recommended to consider that the source of fragment γ radiation remains nonmoving throughout its entire time of action and is located at a certain effective height corresponding to the height where the radioactive cloud is located at the moment of radiation of half of the total dose of γ radiation of the explosion.

In contrast to neutrons, the energy distribution of γ radiation of a nuclear explosion is significantly transformed with changing angle θ. As the scattering angle θ increases, the spectrum of γ quanta softens. This follows from the results of calculation of the distribution of γ radiation of an atomic explosion in the atmosphere, performed by the Monte Carlo method [12]. Tables 2.6 and 2.7, composed on the basis of the results of this work, show the spectral-angular distributions of scattered γ quanta. The quantities presented in the tables characterized the distribution of γ ray doses scattered per unit body angle within the limits of a given interval of angles θ by energy groups.

The angular quantities are the ratio

$$\Xi(\theta, E_\gamma) = \frac{\int_{\Delta\theta}\int_{\Delta E_\gamma} F(\theta, E_\gamma)\sin\theta d\theta dE_\gamma}{\int_{\Delta\theta} F(\theta)\sin\theta d\theta}, \qquad (2.101)$$

where $F(\theta, E_\gamma)$ is the spectral-angular distribution function of the γ quanta scattered in the air, characterizing the dose of scattered γ radiation in the interval of energies from E_γ to $E_\gamma + dE_\gamma$, arriving in a unit body angle from the direction defined by the scattering angle θ.

As we can see from the tables, significant softening of the scattered γ quanta is observed in the range of angles θ from 0 to 90°. With a further increase in angle θ, deformation of the spectrum is practically not observed.

The value of the spectral-angular characteristics of the γ radiation scattered in air allows us to estimate the influence of the phenomenon of reflection from the earth on the value of coefficient $\overline{K}_\alpha$. Considering the reflection of γ radiation from the earth, it can be calculated on the basis of equation (2.92).

The integral albedo of γ radiation with a nuclear explosion can be calculated using the expression

$$A^{\pi}_{\gamma E}(\alpha) = \overline{K}_\alpha \int_{E_\gamma} \int_0^{\pi/2} \int_0^{\pi} \sin\beta F(\theta)\,\Xi(0, E_\gamma)\,A^{\pi}_{\gamma E}(\beta, E_\gamma)\,dE_\gamma)d\beta d\varphi, \qquad (2.102)$$

where $A^{\pi}_{\gamma E}(\beta, E_\gamma)$ is the albedo for the energy of γ radiation with initial energy E_γ, striking the surface of the earth at angle β. According to [23], it is

$$A^{\pi}_{\gamma E}(\beta, E_\gamma) = 3{,}2\,\frac{1}{E_\gamma}\,\frac{1}{\cos\beta}\,\frac{\rho_g}{Z^3}. \qquad (2.103)$$

Here ρ_g is the density of the ground ($\simeq$ 1.7 g/cm^3), while its effective atomic number $Z \simeq 13$.

Table 2.6

ENERGY COMPOSITION OF DOSE OF SCATTERED FRAGMENT γ RADIATION $\Xi_f(\theta, E_\gamma)$
(% DOSE IN GIVEN ANGULAR INTERVAL)

$\Delta\theta$, degrees	Interval of Energies ΔE_γ, MeV									
	0.1–0.2	0.2–0.3	0.3–0.5	0.5–0.75	0.75–1.0	1–1.5	1.5–2	2–3	3–4	4–6
0–10	0.76	0,53	0,23	0,67	2,23	4,7	12,50	12,93	37,45	28,0
10–20	0.97	0,69	1,53	2,85	3,92	8,55	16,52	40,25	17,3	7,42
20–30	1,41	1,19	4,66	4,28	6,24	28,84	21,0	28,55	3,83	
30–40	3,25	2,24	13,43	15,66	11,11	38,65	13,93	1,73		
40–50	12,45	8,11	9,78	13,5	18,6	36,0	0,56			
50–60	9,55	9,33	14,31	22,91	36,27	7,63				
60–70	17,52	14,0	17,03	47,67	1,53	2,25				
70–80	23,80	38,89	21,62	15,69						
80–90	46,65	18,37	31,69	3,28						
90–100	59,75	5,15	35,1							
100–110	43,36	14,67	42,97							
110–120	51,13	23,83	25,04							
120–130	45,14	34,64	20,22							
130–140	48,9	40,78	10,32							
140–150	56,86	37,49	5,65							
150–160	50,87	43,5	5,63							
160–170	46,06	52,84	1,1							
170–180	55,3	44,7								

Table 2.7

ENERGY COMPOSITION OF DOSE OF SCATTERED CAPTURE γ RADIATION $\Xi_c(\theta, E_\gamma)$

(% DOSE IN GIVEN ANGULAR INTERVAL)

$\Delta\theta$, degs	Interval of Energies ΔE_γ, MeV											
	0,1—0,2	0,2—0,3	0,3—0,5	0,5—0,75	0,75—1,0	1—1,5	1,5—2	2—3	3—4	4—6	6—8	8—10
0—10	0,05	—	0,03	0,16	0,29	0,31	0,98	4,27	13,53	68,6	3,13	8,65
10—20	0,33	0,25	0,37	0,79	1,58	3,05	6,83	27,33	25,96	22,46	8,36	2,69
20—30	0,94	0,82	0,89	1,72	2,34	17,61	22,75	39,31	13,62			
30—40	4,25	5,58	2,88	6,63	12,95	33,29	25,93	8,49				
40—50	6,34	5,96	6,23	9,18	17,63	46,73	7,63					
50—60	7,38	4,94	6,94	11,06	46,47	23,21						
60—70	11,08	6,60	11,83	38,42	9,34	22,73						
70—80	14,06	9,68	27,74	48,52								
80—90	30,79	30,99	16,58	21,64								
90—100	33,20	4,15	62,65									
100—110	29,87	31,19	38,94									
110—120	45,05	15,55	39,4									
120—130	58,20	31,73	10,07									
130—140	29,64	38,39	31,97									
140—150	47,60	51,54	0,86									
150—160	43,75	55,07	1,18									
160—170	44,18	55,36	0,46									
170—180	62,18	37,82										

In expression (2.102), angle θ as a function of angular distribution $F(\theta)$ is calculated using the expression

$$\theta = \arccos(\sin\beta\cos\varphi\cos\alpha + \cos\beta\sin\alpha).$$

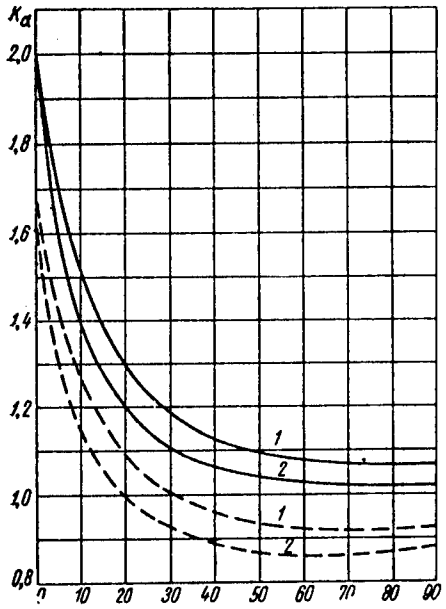

α, degrees

Figure 2.27.

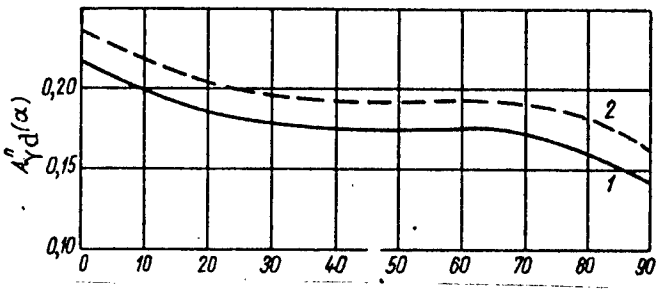

α, degrees

Figure 2.28. Integral Albedo of γ Radiation of Nuclear Explosion for Soil: 1, for capture γ radiation; 2, for fragment γ radiation

The results of calculation of the integral albedo of γ radiation of a nuclear explosion are presented on Figure 2.28, while the corresponding values of coefficients K_α are shown by the dotted line on Figure 2.27.

Bibliography

1. Leypunskiy, O. I. et al., *Atomnaya Energiya*, Vol. 2, P. 278 (1957).

2. Fano, V., *Nucleonics*, Vol. 11, No. 8, p. 55 (1953).

3. Leypunskiy, O. I., *Gamma-Izlucheniye Atomnogo Vzryva* [The Gamma Radiation of an Atomic Explosion], Moscow, Atomizdat Press, 1959.

4. Leypunskiy, O. I., *Atomnaya Energiya*, Vol. 6, p. 49 (1959).

5. Sedov, L. I., *Metody Podobiya i Razmernostey v Mekhanike* [Methods of Similarity and Dimensionalities in Mechanics], Moscow, Gostekhizdat Press, 1954.

6. Taylor, G., *Proc. Roy. Soc.*, Vol. 201, p. 168 (1950).

7. Yampol'skiy, P. A., *Neytrony Atomnogo Vzryva* [The Neutrons of an Atomic Explosion], Moscow, Atomizdat Press, 1961.

8. Lewis, E. B., *Science*, Vol. 125, p. 965 (1957).

9. Karcher, R. H., *Nucl. Sci. Engng.*, Vol. 27, p. 367 (1967).

10. Wells, M. B., *NRDL-OCDM. Shielding Symposium Proc., R and L.*, Vol. 110, p. 308 (1960).

11. French, R. L., *Nucl. Sci. Engng.*, Vol. 19, No. 2, p. 151 (1964).

12. ***Reactor Handbook, v. 111, part B, Shielding, 233 Interscience, New York*** (1962).

13. Ritchie, R., Hurst, G., *Health Phys.*, Vol. 1, No. 4, p. 390 (1959).

14. Snyder, W., Neufeld, J., *Brit. Radiol.*, Vol. 28, p. 331 (1950).

15. *Deystviye Yadernogo Oruzhiya* [The Effects of a Nuclear Explosion], Translated from the English, Moscow, Voyenizdat Press, 1963.

16. Spielberg, D., *NRDL-OCDM. Shielding Symposium Proc., R and L.*, No. 110, p. 416 (1960)

17. French, R., *Health Phys.*, Vol. 8, p. 299 (1962).

18. French R., Wells, M., *Nucl. Sci. Engng.*, Vol. 19, p. 441 (1964).

19. Goryachev, I. V., Trykov, L. A., Kukhtevich, V. I., *Atomnaya Energiya*, Vol. 21, No. 4, p. 246 (1966).

20. Goryachev, I. V., *Atomnaya Energiya*, Vol. 19, No. 4, p. 396 (1965).

21. Goryachev, I. V., Kukhtevich, V. I., Trykov, L. A., *Byulleten' Informatsionnogo Tsentra Po Yadernym Dannym* [Bulletin of Information Center for Nuclear Data], No. 3, Atomizdat Press, 1966, p. 522

22. Goryachev, I. V., Kukhtevich, V. I., Trykov, L. A., *Voprosy Dozimetrii i Zashchity Ot Izlucheniy* [Problems of Dosimetry and Protection From Radiation -- Collection of Works], No. 6, Moscow, Atomizdat Press, 1967, p. 13.

23. Bulatov, B. P., Garusov, Ye. A., *Atomnaya Energiya*, Vol. 5, No. 6, p. 631 (1958).

CHAPTER 3. RADIATION OF RADIOACTIVE FALLOUT

§ 1. Types of Radioactive Fallout

The residual radiation following a nuclear explosion results from three factors: fission fragments, induced activity and the remains of the nuclear charge.

As concerns the relationship between induced and fragment activity, this problem was discussed in considerable detail in Chapter 1. We will note only that with high altitude air bursts, the yield of activation products is low, since only a small fraction of the neutrons reaches the surface of the earth below the epicenter of the blast. The radioactive contamination resulting from matter with induced activity will in this case cover only a small region, where other damaging factors of the blast are more important -- the shock wave and the light radiation. However, even with a surface blast, for which a comparatively high yield of activation products is observed, fragments are predominant in the radioactive contamination of the surface of the earth by products of the blast.

In addition to this, particles of the portion of the charge which is not yet undergone fission: uranium or plutonium, settle to the earth. The isotopes of these elements which undergo fission emit α particles, as well as a certain number of low energy γ quanta. The half life of U^{235} is $7 \cdot 10^8$ years, of Pu^{239} -- $24.3 \cdot 10^3$ years. Due to the slow decay of these isotopes, their radioactivity is negligible in comparison with the activity of fission fragments.

Due to the low penetrating capacity of α particles (they are almost completely absorbed in a layer of air 2.5-5 cm thick), plutonium is dangerous only if it enters the organism.

Thus, of all products of a nuclear explosion, the fission fragments are the main products determining the radiation danger in the region of fallout of these products from the cloud.

The danger for radioactive contamination of the terrain is represented by a surface blast of a nuclear weapon. During air blasts, the radioactive isotopes condense primarily on particles of the material of the weapon and represent no significant danger, since due to their small size the particles precipitate slowly and are scattered over a great area. With surface explosions, large quantities of earth are caught up in the fireball and form particles, onto which the radioactive isotopes precipitate.

The particles of earth captured during the nuclear explosion and entering the central portion of the fireball at temperatures amounting to several millions of degrees, evaporate; the particles entering the area with lower temperature melt. A large quantity of crushed earth is caught up by the ascending air stream, drawn up into the cloud and mixed in it. As the particles of evaporated and melted earth cool, they condense and are formed into drop-shaped or spherical particles, which frequently adhere to the unmelted particles of earth.

The formation of the radioactive wake begins immediately after the explosion of a nuclear weapon, when the earth drawn up into the atomic cloud begins to fall back onto the surface. The rate of fallout and the location of the point where particles return to the earth in relation to the point of the explosion depend on the size of the particles and the wind speed. The atomic cloud is moved by the wind, and the precipitating particles form a trail behind it.

All radioactive fallout can be divided into three main types [1, 2].

1. Local -- with large particles (up to 50 μ). These particles fall out during the first 10-20 hours following the explosion over a territory up to 400-500 km from the center of the explosion. It has been established [3] that about 80-90% of the radioactive material formed during a surface blast falls out in the form of local fallout.

2. Continental fallout consists of fine particles which enter the upper layers of the troposphere. The precipitation of these particles is slower due to their small diameter (5 μ and less). They continue to fall out onto the earth for 2-3 weeks following a blast. During this time, the cloud covers a great distance over the earth's surface. Most of the short-lived radioactive isotopes in continental fallout decay before reaching the ground.

3. Global fallout consists of fine particles (less than 1 μ) carried into the stratosphere. These particles fall out very slowly.

They continue to precipitate onto the surface of the earth over a period of time which has been estimated variously as from one half year to 5-7 years.

Special cases arise when radioactive clouds mix with rain or snow clouds. In these situations, the rain drops or snow flakes capture the radioactive particles and accelerate fallout. It is assumed [4] that the effectiveness of capture of radioactive particles by raindrops and snowflakes is the same.

When rain acts on an explosion cloud, local areas of increased contamination may be produced. For example, as calculations and observations performed in the USA in 1955 showed, about 29% of all particles with diameters of 10 μ are washed out by rain with an intensity of 1 mm/hr in 15 minutes.

In the following, we will analyze the phenomena accompanying local fallout.

§ 2. Formation of the Field of γ Radiation Over a Sector of Radioactive Contamination

The radioactive particles precipitating from a nuclear cloud settle onto the surface of the earth. The surface radioactive contamination of the terrain thus formed exists for a relatively short time. Gradually, over the course of the next few weeks, various processes cause the radioactive products to begin to penetrate into the depth of the soil either together with their carrier particles or as a result of being washed from the surface of these particles, or as a result of breakdown of the particles. Volumetric contamination of the upper layer of soil then develops to a depth of several centimeters. According to the data of [5], 80-95% of all activity is contained in the top layer (5-6 cm).

Objects located on the contaminated surface of the earth are acted upon by β and γ radiation from the fission fragments. The main problem of protection from radioactive fallout consists of shielding from γ radiation, which is the most penetrating and biologically dangerous type produced.

Let us study first a simplified model of an area of radioactive contamination, evenly covered with radioactive particles. Any surface distribution of γ activity can be considered to consist of individual point isotropic sources and the dose power over the ground can be calculated as the sum of the doses from these sources.

For a point isotropic source of γ radiation in an infinite air medium, the dose power at a point separated from it by a distance of R(m) can be found using the expression

$$P_i(R) = 5{,}09 \frac{\mu_{ai} u_i}{4\pi R^2} B_i(R) e^{-\mu_i R} [p/u], \quad [r/hr], \tag{3.1}$$

where μ_i is the linear coefficient of absorption of the dose of γ radiation of the sourse with initial energy of E_i; μ_{ai} is the coefficient of absorption of the energy of γ radiation in the air, cm^{-1}; u_i is the activity of the source, MeV/sec; B_i is the dose accummulation factor in the air, which, according to the results of [6], can be calculated using the equation

$$B_i(R) = [1 + 1{,}09e^{-0{,}155E_i}(\mu_i R) + 1{,}73e^{-2{,}311E_i}(\mu_i R)^2] \times \times \exp[(-0{,}085)\exp[-3{,}0E_i(\mu_i R)]]. \tag{3.2}$$

Another expression which approximates the dose accummulation factor B_i (R) with good accuracy in the 0.5-2.0 MeV energy interval is the following formula, suggested in [7]:

$$B_i(R) = 1 + \mu_i R + \frac{(\mu_i R)^2}{7E_i^{2,4}}. \tag{3.3}$$

The presence of the division boundary prevents the accummulation factors calculated for homogeneous infinite media from being applied directly; corrections must be introduced to the calculation formulas, considering the influence of the heterogeneity of the medium. The influence of the underlying surface is generally considered by the correction factor Δ_π, defined as the ratio of power of the dose from a source located at the earth-air boundary to the power of the dose from a source located in a homogeneous air medium. The value of this factor depends on the atomic number z and density of the underlying medium, as well as the energy of the γ radiation from the source, the height of the detector over the surface of the ground and its distance from the source.

It was demonstrated in [8] that if heterogeneous media are similar in atomic number, as can be considered in the case of air and soil, the correction factor can be calculated using the expression

$$\Delta_\pi = \frac{1 + \frac{1}{2}[B_i'(\mu_i' R) - 1]}{B_i'(\mu_i' R)} + \frac{e^{-\mu_i' R}[B_i'(\mu_i' R) - 1]}{2e^{-\mu_i' R} B_i'(\mu_1' R)}, \tag{3.4}$$

where B_i', B_i'' are the accummulation factors for infinite air and soil homogeneous media respectively.

Let us analyze some particular cases. Near the source, when R is low, it is $\mu_i' R \simeq 0$, $e^{-\mu_i' R} = 1$ and $B_i' (\mu_i' R) = 1$,

$$\Delta_H = 1 + \frac{1}{2} e^{-\mu_i'' R} [B_i'' (\mu_i'' R) - 1]. \tag{3.5}$$

As you can see, at very close distances to the source $\Delta_H > 1$, i. e. the power in the detector is greater than for a homogeneous medium, due to the contribution of back scattering from the underlying surface.

If R is great, i. e. $e^{-\mu_i'' R} \to 0$,

$$\Delta_H = \frac{1 + \frac{1}{2} [B_i' (\mu_i' R) - 1]}{B_i' (\mu_i' R)}. \tag{3.6}$$

This expression demonstrates that for great distances the dose power at the detector is less than for the corresponding distances in an infinite medium. We note that expression (3.6) is applicable for source-detector distances greater than 0.5 m.

The power of the dose at the point of observation over a flat isotropic source is determined by integrating the contributions from elementary sources dP located on the plane over the entire surface of the plane:

$$dP_i (R) = 5{,}09 \frac{\mu_{ai} a_i}{4\pi R^2} B_i (R) e^{-\mu_i R} ds. \tag{3.7}$$

If we use expression (3.3) for the dose accummulation factor, assuming $ds = 2\pi R dR$ (Figure 3.1) and performing integration from H to R_0, we produce an expression for the dose power $P(H, R_0)$ from an area with radius $r_0 = \sqrt{R_0^2} = H^2$ at the point of observation, located over the center of this area at height H:

$$P(H, R_0) = 5{,}09 \frac{\mu_{ai} u_i}{2} [E_1(\mu_i H) - E_1(\mu_i \sqrt{r_0^2 + H^2}) + \\ + \frac{e^{-\mu_i H}}{7E_i^{2,4}}(1 + 7E_i^{2,4} + \mu_i H) - \frac{e^{-\mu_i \sqrt{r_0^2 + H^2}}}{7E_i^{2,4}}(1 + \\ + 7E_i^{2,4} + \mu_i \sqrt{r_0^2 + H^2})]. \qquad (3.8)$$

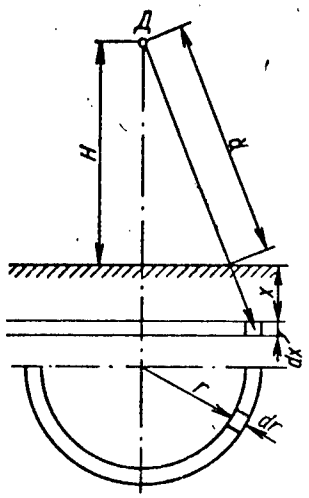

Figure 3.1. Plan of Calculation of Dose Power Over Radioactively Contaminated Sector

For an area of infinite radius ($r_0 = \infty$)

$$P(H) = 5{,}09 \frac{\mu_{ai} u_i}{2} \left[E_1(\mu_i H) + \frac{e^{-\mu_i H}}{7E_i^{2,4}}(1 + 7E_i^{2,4} + \mu_i H) \right]. \qquad (3.9)$$

Here $E_1(x) = E_i(-x)$ is the integral exponential function. When it is necessary to consider the influence of the underlying surface, expression (3.4) must be multiplied by correcting factor Δ_H.

Formulas (3.8) and (3.9) allow us to determine the share contributed by an area with any radius r to the total dose power from an area with infinite radius. Table 3.1 shows the results of calculation of the

radius of sectors determining 50, 75 and 90% of the total dose at the point of measurement over an infinite contaminated sector for three different γ quantum energies. The calculations were performed considering the earth-air division boundary.

Table 3.1

RADII OF SECTORS (IN METERS) DETERMINING 50, 75 AND 90% OF THE TOTAL DOSE OF RADIATION AT A POINT OVER A CONTAMINATED SECTOR OF INFINITE EXTENT

H, M	$E_i = 0{,}41$ MeV			$E_i = 1{,}25$ MeV			$E_i = 2{,}8$ MeV		
	50%	75%	90%	50%	75%	90%	50%	75%	90%
1	6	40	122	6	42	130	7	50	140
10	8	86	170	38	92	180	45	115	200
50	12	60	258	98	173	280	112	205	300

As we can see from the table, at low height over the earth, the dose of γ radiation is primarily determined by sources located not over 100-150 m from the point of measurement. The γ activity of more remote sources creates only a low percentage of the total dose.

We note that the radii of areas making an identical contribution to the total dose power at the point of observation depends only slightly on the primary energy of the γ radiation.

As we have noted, radioactive contamination of an area causes contamination of the upper soil layer. The individual point sources of γ radiation in this case are distributed through this layer of soil. In order to calculate the dose power over the surface of a γ-active soil layer, we must consider the absorption of radiation in this layer.

Let us analyze the case of volumetric contamination with an activity decreasing with depth exponentially

$$u_V(x) = u_V(0)\, e^{-mx}, \tag{3.10}$$

where $u_V(0)$ is the volumetric activity of the surface layer; m is a constant quantity characterizing the rate of decrease of concentration with depth.

As was demonstrated in [9], this type of source if formed several weeks following fallout of the radioactive products onto terrain as a result of their penetration into the soil. The value of m may reach 0.3-6.0 cm^2/g for various soils and times following fallout of the radioactive precipitate.

The same type of volumetric contamination is observed upon activation of the earth by the neutrons of a nuclear explosion.

The dose power in the air over an infinitely large sector of contamination with a distribution of γ activity through the upper layer is

$$P_V(H) = 5{,}09\frac{u_V(0)\mu_{al}}{2m}\left\{E_1(\mu_i H) - e^{(B-1)\mu_i H}E_i(B\mu_i H) + \right.$$
$$\left. + \frac{B-1}{B}e^{-\mu_i H}\left[1 + \frac{1}{7E_i^{2,4}}\left(1 + \mu_i H + \frac{1}{B}\right)\right]\right\}, \qquad (3.11)$$

where $B = 1 + m/\mu_i$.

It is similarly easy to produce a formula for a sector of limited size. It should be noted that the effective radius of action of a volumetric source is considerably less than the effective radius of action of a surface source. For example, at a height of 1 m over the surface of the earth, 90% of the total dose of γ radiation is collected from an area limited by a radius of 15-20 m, while at a height of 25 m it is collected from an area with a radius of 100 m.

The form of the contaminated territory (radioactive wake) varies widely and depends primarily on the weather conditions -- speed and direction of the wind at various altitudes reached by the cloud. The actual gradience of the density of surface contamination are such [10] that within the areas providing practically complete collection of the dose at the point of observation over the contaminated surface, the density of contamination can be considered constant with high reliability.

§ 3. Angular and Energy Distributions of γ Radiation Over a Contaminated Surface

The structure of the γ field over a radioactively contaminated surface is determined first of all by the radioactive decay of the

explosion products and the related change in the energy composition of the γ quanta emitted and, secondly, by the nature of interaction of the γ radiation of radioactive decay with the air and the soil.

Works [11, 12] present the results of calculation of the differential spectra of γ radiation over an infinite plane, evenly covered with fission products of various ages.

Table 3.2 shows the results of calculation of the spectral and angular distributions of γ radiation of fission products with ages from 1.12 hours to 9.82 days over an ideally flat plane of infinite size. These same tables contain information on the angular distributions of the total flux and dose of γ quanta, as well as the integral spectra of γ radiation [12].

The data of Table 3.2, which relate to fluxes of γ quanta, are expressed in units of quanta/($cm^2 \cdot sec$), while the dose is expressed in rad/hr. All results are normalized for the surface activity corresponding to one U^{235} fission event per 1 cm^2 of surface of the earth. It must be noted that the fluxes of quanta shown in Table 3.2 are integral for the energy and angular intervals indicated. In order to make the transition to differential characteristics of the angular [quanta/($cm^2 \cdot$ sec·ster)] and energy [quanta/($cm^2 \cdot$sec·MeV)] distributions, the quantities presented must be divided by the solid angles corresponding to the angular intervals and the energy intervals.

Analysis of the angular distributions of the dose of γ quanta corresponding to fission products of various ages indicates that the angular dose distribution function of γ quanta from fission products is insensitive to transformations of the γ radiation spectra of the fission products within limits of 1 hour to 10 days after the explosion. This is understandable if we consider that below the horizon the primary contribution to the dose over the contaminated area is that of unscattered radiation of sources located on the surface of the earth. The attenuation of unscattered radiation in the air is insensitive to changes of energy within the limits of the transformation of the γ radiation spectra of fission products. The dose power of γ quanta arriving from the upper half space over the surface of the earth, i. e. scattered in the air, is only 7-8% of the total dose power. The dose power of scattered radiation (in the air and in the ground) amounts to a total of about 15% of the complete dose power of γ quanta of fission products over the contaminated sector.

Data on the angular distributions of dose power of γ radiation at various heights over a flat isotropic source with an age of fission

Table 3.2

ANGULAR ENERGY DISTRIBUTIONS OF γ QUANTA AT 1 M ALTITUDE OVER INFINITE FLAT CONTAMINATION SECTOR, $\phi(\Delta\beta, \Delta E_\gamma)$ $\frac{\text{quanta}}{(\text{cm}^2 \cdot \text{sec})}$ / fissions/cm^2)

β, degrees	Quantum Energy, MeV										$\Phi(\Delta\beta)$, $\frac{\text{quanta}}{(\text{cm}^2 \cdot \text{sec})}$	$D(\Delta\beta)$, rad/hr
	0.060	0.100	0.180	0.300	0.500	0.750	1.000	1.500	2.500	3.500		
Time After Explosion 1.12 hr												
170	1,197 (−8	6,957 (−8	1,436 (−7	2,001 (−7	1,826 (−7	1,292 (−7	8,266 (−8	1,088 (−7	1,294 (−7	3,230 (−8	1,090 (−6	1,276 (−12
160	3,747 (−8	2,666 (−7	5,847 (−7	5,958 (−7	5,617 (−7	4,074 (−7	2,528 (−7	3,313 (−7	3,958 (−7	9,886 (−8	3,533 (−6	3,928 (−12
150	6,088 (−8	4,508 (−7	9,597 (−7	9,404 (−7	1,179 (−7	8,124 (−7	4,399 (−7	5,763 (−7	6,888 (−7	1,720 (−7	6,280 (−6	7,026 (−12
140	7,707 (−8	6,490 (−7	1,306 (−6	1,306 (−6	1,297 (−7	2,141 (−6	6,602 (−7	8,653 (−7	1,034 (−6	2,583 (−7	8,625 (−6	1,010 (−11
130	5,569 (−8	5,783 (−7	1,581 (−6	1,736 (−6	1,933 (−6	1,688 (−6	1,002 (−6	1,236 (−6	1,477 (−6	3,691 (−7	1,166 (−5	1,448 (−11
120	1,440 (−7	9,620 (−7	1,883 (−6	2,085 (−6	2,649 (−6	2,250 (−6	1,467 (−6	1,782 (−6	2,126 (−6	5,279 (−7	1,588 (−5	2,029 (−11
110	1,218 (−7	1,190 (−6	2,772 (−6	3,098 (−6	4,607 (−6	3,750 (−6	2,219 (−6	2,886 (−6	3,216 (−6	7,957 (−7	2,466 (−5	3,186 (−11
100	1,610 (−7	1,237 (−6	3,552 (−6	4,166 (−6	7,653 (−6	6,759 (−6	3,992 (−6	5,056 (−6	5,676 (−6	1,412 (−6	3,966 (−5	5,518 (−11
90	6,056 (−7	1,839 (−6	7,867 (−6	9,381 (−6	2,235 (−5	2,254 (−5	1,444 (−5	2,031 (−5	2,526 (−5	6,930 (−6	1,315 (−4	2,151 (−10
80	5,782 (−7	2,966 (−6	4,098 (−6	3,683 (−6	2,612 (−6	1,356 (−6	9,790 (−7	1,900 (−6	2,135 (−7	1,523 (−7	1,854 (−5	1,286 (−11
70	8,910 (−7	2,023 (−6	2,969 (−6	3,315 (−6	1,550 (−6	9,615 (−7	2,285 (−8	1,558 (−7	4,801 (−8		1,194 (−5	5,036 (−12
60	7,181 (−7	2,917 (−6	2,859 (−6	2,023 (−6	8,139 (−7	1,466 (−7	1,882 (−7				9,665 (−6	3,065 (−12
50	1,111 (−6	2,026 (−6	2,106 (−6	1,011 (−6	8,660 (−7	1,309 (−7					7,250 (−6	2,095 (−12
40	1,675 (−6	1,852 (−6	1,532 (−6	1,418 (−6	1,206 (−7	1,191 (−8					6,609 (−6	1,472 (−12
30	4,815 (−7	1,012 (−6	7,471 (−7	6,642 (−7	1,562 (−7	1,535 (−8					3,077 (−6	7,360 (−13
20	7,483 (−7	1,643 (−6	1,022 (−6	5,073 (−7	7,799 (−8	2,623 (−9					4,091 (−6	8,079 (−13
10	3,425 (−7	7,226 (−7	3,820 (−7	2,899 (−7	2,216 (−9	1,929 (−9					1,741 (−6	3,390 (−13
0	1,455 (−7	8,012 (−7	1,892 (−7	2,822 (−8	1,413 (−8	8,526 (−10					1,179 (−6	2,038 (−13
$\Phi(\Delta E_\gamma)$, $\frac{\text{quanta}}{(\text{cm}^2 \cdot \text{sec})}$	7,967 (−6	2,321 (−5	3,655 (−5	3,655 (−5	4,863 (−5	4,210 (−5	2,575 (−5	3,521 (−5	4,027 (−5	1,075 (−5	3,070 (−4	3,859 (−10
Time AFter Explosion 9.8 days												
170	1,620 (−11	1,489 (−10	3,096 (−10	3,040 (−10	1,687 (−10	1,285 (−10	1,426(−10	2,281(−11	1,721(−10	7,897(−12	1,421 (−9	1,256 (−15
160	6,460 (−11	5,456 (−10	1,116 (−9	9,013 (−10	5,062 (−10	3,960 (−10	4,361(−10	6,981(−11	5,264(−10	2,416(−11	4,586 (−9	3,857 (−15
150	1,045 (−10	8,992 (−10	1,810 (−9	1,545 (−9	1,255 (−9	8,536 (−10	7,588(−10	1,214(−10	9,161(−10	2,204(−11	8,306 (−9	7,082 (−15
140	1,263 (−10	1,264 (−9	2,634 (−9	2,136 (−9	1,161 (−9	1,141 (−9	1,139(−9	1,823(−10	1,375(−9	6,314(−11	1,122 (−8	9,911 (−15
130	1,099 (−10	1,249 (−9	3,413 (−9	3,049 (−9	1,700 (−9	1,641 (−9	1,686(−9	2,604(−10	1,965(−9	9,022(−11	1,517 (−8	1,413 (−14
120	2,234 (−10	1,802 (−9	4,364 (−9	3,841 (−9	2,452 (−9	2,266 (−9	2,399(−9	3,761(−10	2,810(−9	1,290(−10	2,066 (−8	1,979 (−14
110	2,388 (−10	2,334 (−9	6,494 (−9	5,990 (−9	4,282 (−9	3,750 (−9	3,643(−9	7,961(−10	4,234(−9	1,915(−10	3,196 (−8	3,116 (−14
100	3,171 (−10	3,129 (−9	9,108 (−9	8,994 (−9	7,061(−9	6,755 (−9	6,403(−9	1,441(−9	7,487(−9	3,450(−10	5,101 (−8	5,370 (−14
90	8,265 (−10	5,701 (−9	2,485 (−8	2,496 (−8	2,103(−8	2,271 (−8	2,448(−8	4,952(−9	3,285(−8	1,694(−9	1,611 (−7	2,017 (−13
80	9,653 (−10	5,199 (−9	5,871 (−9	4,493 (−9	2,936 (−9	1,705 (−9	1,078(−9	9,673(−10	4,210(−11	3,722(−11	2,329 (−8	1,192 (−14
70	1,523 (−9	3,122 (−9	4,015 (−9	4,053 (−9	1,920 (−9	1,132 (−9	3,691(−11	1,193(−10	1,174(−11		1,593 (−8	6,089 (−15
60	1,571 (−9	3,853 (−9	4,564 (−9	2,035 (−9	9,550 (−10	1,597 (−10	2,094(−10				1,334 (−8	3,819 (−15

(Table 3.2)

β, degrees	Quantum Energy, MeV										$\Phi(\Delta\beta)$, quanta/cm²·sec	$D(\Delta\beta)$, rad/hr
	0,060	0,100	0,180	0,300	0,500	0,750	1,100	1,500	2,500	3,500		
50	1,566(—9	4,112(—9	3,161(—9	1,118(—9	8,788(—10	7,124(—11					1,091(—8	2,611(—1
40	2,901(—9	3,615(—9	1,966(—9	1,540(—9	1,307(—10	6,377(—12					1,016(—8	2,007(—1
30	8,611(—10	1,818(—9	1,129(—9	6,997(—10	2,270(—10	5,161(—12					4-740(—9	1,014(—1
20	1,367(—9	2,762(—9	1,817(—9	6,997(—10	1,086(—10	1,555(—12					6,757(—9	1,247(—1
10	9,560(—10	8,895(—10	8,102(—10	3,333(—10	5,369(—13	7,026(—13					2,990(—9	5,408(—1
0	1,596(—10	8,243(—10	1,521(—10	2,876(—11	2,275(—11	9,661(—13					1,188(—9	2,044(—1
$\Phi(\Delta E_\gamma)$, quanta/cm²·sec	1,390(—8	4,327(—8	7,759(—8	6,672(—8	4,681(—8	4,273(—8	4,242(—8	9,309(—9	5,241(—8	2,627(—9	3,978(—7	3,721(—1

1. Energy of γ quanta correspond to upper boundary of energy interval. For example, quantities in column under figure 0.500 are values of γ quanta fluxes in the 0.300-0.500 MeV interval.

2. First column corresponds to energy interval 0.04-0.060 MeV.

3. Values of angle β indicated correspond to lower boundary of angular interval. For example, quantities in row opposite 170 correspond to γ quanta in angular interval β = 170-180°.

4. Read 1.197 (-2 = 0.01197.

products of 1.12 hours are presented in [13]. Figure 3.2 shows the angular distribution functions of dose $F(\beta)$ for an ideal flat fallout source, normalized to the dose at an altitude of 1 m over the ground, so that

$$2\pi \int_0^{\pi} F(\beta) \sin \beta d\beta = \frac{D(H)}{D(H=1)}. \qquad (3.12)$$

The angular distribution functions corresponding to a height of 1 m over the surface of the ground can be described with sufficient accuracy by the empirical expression

$$F(\beta) = \begin{cases} 0{,}0122 + 0{,}0484e^{-9\cos^2\beta} & 0^\circ \leqslant \beta < 90^\circ \\ 0{,}04 + 1{,}3e^{10\cos\beta} & 90^\circ \leqslant \beta \leqslant 180^\circ. \end{cases} \qquad (3.13)$$

As a result of the influence of irregularities of the underlying surface, the angular distributions of dose power over an actual sector of contamination should differ from the angular distributions of γ radiation over an ideal flat source. It should be expected here that the form of the spectrum of scattered radiation will change comparatively slightly due to the significant contribution of multiply scattered quanta. The intensity of unscattered quanta changes strongly. For this reason we can expect that the angular distributions of dose power of γ radiation might undergo significant change in the area of angles β near 90°.

Figure 3.3 shows experimental data on the angular distributions of of dose power at 1 m over a contaminated area with various types of relief: over the flat bottom of a dry lake (curve 3) and an area of dry steppe (curve 4) [14], as well as over a very level virgin grassy area (curve 2) [15]. The experimental distributions produced in these cases correspond in the first case to the "effective" height of measurements (with an ideally flat surface) of 6 m, in the second case -- 12 m, in the third case -- 3 m. This same figure shows for comparison the angular dependence of dose power at a height of 1 m with no microrelief (curve 1). As was assumed, the angular distribution is distorted with values of angle β near 90°.

The angular spectra of γ quanta over a radioactively charged area with an age of fission products of 9 days were measured in [16]. The results of these measurements are shown on Figure 3.4.

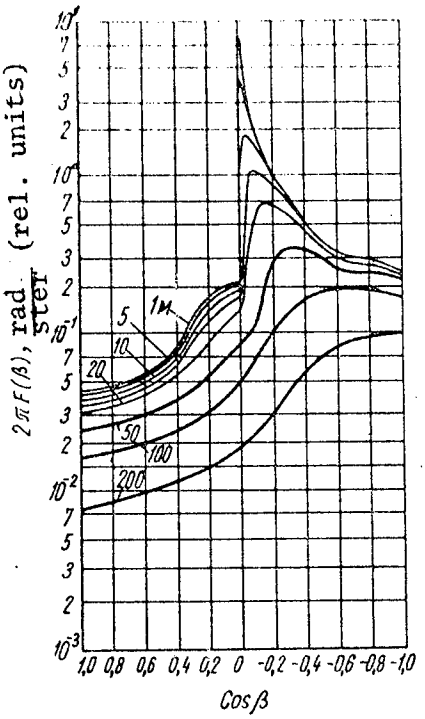

Figure 3.2. Angular Distributions of Dose Power of γ Quanta for Ideal Flat Source of Radioactive Fallout Various Heights Over the Ground

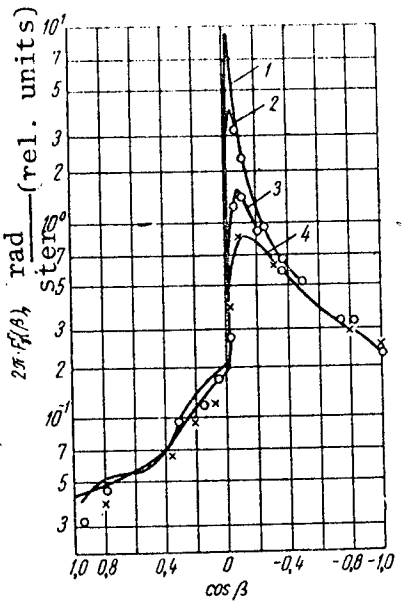

Figure 3.3. Angular Distribution of Dose Power at 1 m Over Contaminated Surface.

Bibliography

1. Libby, W. F., *Science*, Vol. 123, p. 3199 (1956).

2. Wilckens, F., *Saldatund Technik*, Vol. 2, No. 6, p. 292 (1959).

3. Lushkova, N. P. (Editor), *Yadernyye Vzryvy* [Nuclear Explosions], Moscow, Foreign Literature Press, 1958.

4. Fedorov, Ye. K., (Editor), *Meteorologiya i Atomnaya Energiya* [Meterology and Atomic Energy], Moscow, Foreign Literature Press, 1959.

5. Lapp, R. E., *Bull. ATomic Scientists*, Vol. 15, No. 5, p. 181 (1959).

6. Bunney, L. R., *Sam D. Health Phys.*, Vol. 13, No. 9, p. 1033 (1967).

7. Holland, Materials of International Conference on Peaceful Uses of Atomic Energy, Geneva, 1955, Vol. 13, Moscow, Foreign Literature Press, 1958, p. 339.

8. Kimel', L. R., *Voprosy Fiziki Zashchity Reaktorov* [Problems of the Physics of Reactor Shielding], No. 1, Moscow, Atomizdat Press, 1963, p. 217.

9. Izrael', Yu. A., Stukin, Ye. D., *Gamma-Izlucheniye Radioaktivnykh Vypadeniy* [The Gamma Radiation of Radioactive Fallout], Moscow, Atomizdat Press, 1967.

10. Petrov, R. V. et al., *Zashchita Ot Radioaktivnykh Osadkov* [Protection from Radioactive Fallout], Moscow, Medgiz Press, 1963.

11. Devries, T. W., *Trans of the ANS.*, Vol. 7, p. 320 (1964).

12. French, R. L., *Health Phys.*, Vol. 11, No. 5, p. 369 (1965).

13. Spenser, L. V., *Zashchita Ot Gamma Izlucheniya Radioaktivnykh Vypadeniy* [Protection From the Gamma Radiation of Radioactive Fallout], Moscow, Atomizdat Press, 1965.

14. Huddleston, C. M., et al., *Health Phys.*, Vol. 11, No. 6, p. 537 (1965).

15. Izrael', Yu. A., *Atomnaya Energiya*, Vol. 17, No. 2, p. 137 (1964).

16. Frank, A. L., *Health Phys.*, Vol. 12, p. 1715 (1966).

Figure 3.4. Spectral-Angular Distributions of γ Quanta at 1 m Over Terrain Contaminated With 9 day old Nuclear Fission Products

CHAPTER 4. PENETRATION OF NEUTRONS THROUGH SHIELDING

§1. Attenuation of Unscattered Neutrons

As we know, the flux of unscattered neutrons beyond shielding resulting from a flat monoenergetic source with energy E_n is determined by the expression

$$\Phi_{n,\,u}(E_n,\ \delta) = \Phi\ (E_n)\, e^{-\Sigma_t(E_n)\delta'}, \tag{4.1}$$

where $\Phi(E_n)$ is the flux of neutrons without the shielding; δ' is the thickness of the material of the shielding, measured in the direction of movement of the neutrons of the initial beam; $\Sigma_t(E_n)$ is the total macroscopic cross section of interaction of neutrons for energy E_n.

For a continuous spectrum, expression (4.1) becomes

$$\Phi_{n,\,u}(E, \delta) = \int_{E_n} \Phi(E_n)\, e^{-\Sigma_t(E_n)\delta'} dE_n. \tag{4.2}$$

The penetration of the dose of unscattered neutrons through the barrier is described similarly:

$$D_{nu}(E_n,\ \delta) = \int_{E_n} \Phi(E_n)\eta\ (E_n)\, e^{-\Sigma_t(E_n)\delta'}\, dE_n. \tag{4.3}$$

Here $\eta(E_n)$ is the transfer factor from the flux of neutrons to the dose.

Thus, the dose of unscattered neutrons beyond the shielding barrier is determined by the product of the dose of neutrons without the shield times a certain factor $K_{n,\,u}(E_n,\ \delta)$, which will be referred

to in the following as the dose penetration coefficient (or factor) of unscattered neutrons:

$$K'_{nu}(E_n, \delta) \quad \frac{\int_{E_n} \Phi(E_n)\,\eta(E_n)\,e^{-\Sigma_t(E_n)\delta'}\,dE_n}{\int_{E_n} \Phi(E_n)\,\eta(E_n)\,dE_n}. \qquad (4.4)$$

However, expressions (4.3) and (4.4) are correct only if $\Sigma_t(E_n)$ is a smooth function or if all resonances in the cross section are defined. For the dependence $\Sigma_t(E_n)$ with a strongly expressed resonant structure located beyond the limits of resolution of the research apparatus, infiltration of neutrons along the minima in the cross section is observed. As a result of this, the effective value of the cross section decreases, i. e. neutrons are attenuated less than is indicated by the total cross section [1].

Measurements performed in [2, 3] have shown that infiltrtion does not appear significantly with all resonant structures. It is significant only when there are frequent and deep resonances. This sort of course of the total cross section of neutrons with energies corresponds to elements with ordinal numbers Z > 15-20 and in the energy area E_n < 1.5-2 MeV. In a mixture of elements, the minima and maxima in the cross sections of individual components will partially overlap, as a result of which the effect of infiltration decreases.

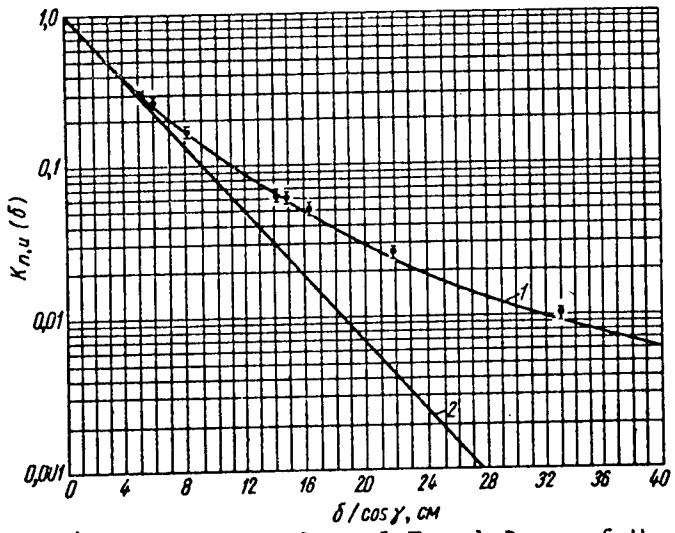

Figure 4.1. Penetration of Total Dose of Unscattered Neutrons in Reactor Spectrum as a Function of Thickness of Iron Shield: 1, 0, experimental data; 2, calculated data

One of the most characteristic elements in which the effect of infiltration appears clearly is iron. Figure 4.1 shows the experimentally measured dependence of the transmission factor of the dose of unscattered neutrons on thickness of iron shield [4, 5]. Measurements were performed with a reactor, the spectrum of which was quite similar in form to the energy distribution of neutrons from a nuclear explosion, scattered in air. For comparison, this same figure shows the calculated attenuation based on total cross sections, borrowed from [6]. For the spectrum of the nuclear explosion, the effective unscattered neutron dose transmission factor for iron can be found from the empirical expression

$$K_{n.u}(\delta) = e^{-0.247\delta'}[1 + 3\cdot 10^{-3}(\delta')^{3,24}]. \qquad (4.5)$$

It should be kept in mind that the "slant" thickness δ' of the screen is $\delta/\cos\gamma$, where γ is the angle of incidence of the initial beam at the surface of the shield, read from the normal; δ is the thickness of the shield measured in the normal cross section.

Table 4.1

TRANSMISSION FACTORS OF UNSCATTERED MONOENERGETIC NEUTRONS $K_{n,u}(E_n, \delta)$ FOR IRON

E_n, MeV	Iron Thickness, cm						
	5	7	10	15	22	31	38
0,1	0,240	0,155	0,091	0,045	0,0224	0,0115	0,0076
0,2	0,296	0,200	0,126	0,066	0,0324	0,0167	0,0117
0,3	0,30	0,20	0,127	0,067	0,0338	0,0173	0,0115
0,4	0,18	0,107	0,050	0,018	0,0050	0,00152	0,00071
0,5	0,40	0,30	0,195	0,102	0,045	0,0181	0,0103
0,6	0,37	0,263	0,167	0,087	0,0406	0,02	0,0115
0,7	0,253	0,162	0,093	0,043	0,017	0,0068	0,0036
0,8	0,316	0,214	0,126	0,060	0,0252	0,0098	0,0053
0,9	0,38	0,275	0,17	0,083	0,035	0,014	0,0076
1,0	0,38	0,27	0,165	0,079	0,0315	0,012	0,0063
1,2	0,34	0,234	0,132	0,059	0,022	0,0079	0,0038
1,4	0,31	0,2	0,11	0,044	0,0138	0,0039	0,00165
1,6	0,30	0,195	0,103	0,039	0,0117	0,00296	0,00115
1,8	0,29	0,19	0,094	0,0324	0,0087	0,002	0,00071
2,0	0,288	0,178	0,086	0,0262	0,0063	0,0012	0,00039

If it is required to calculate the transmission factor for the dose of unscattered neutrons through an iron shield for any other spectrum, the data of Table 4.1 can be used, showing the results of measurements of the transmission factors of monoenergetic neutrons for iron.

§ 2. Transmission of Scattered Neutrons Through Shield Barriers

The field of neutrons of a nuclear explosion in air can be represented as a set of flat, singly directed beams, oriented in space in correspondence with the angular distribution function. Therefore, in order to design a shield for the neutrons of a nuclear explosion, we must first of all obtain information on the penetration of neutrons of a flat, singly directed beam with various incidence angles at the surface of the screen.

A number of works have been dedicated to investigation of the problem of the attenuation of neutrons by flat shields of various materials. In [7, 8], the attenuation of the total dose of a broad, singly directed beam of monoenergetic neutrons with normal and inclined incidence at barriers of various materials was studied. According to the data of [7], the transmission factor for the total dose of monoenergetic neutrons can be represented by the relationship

$$K_{n,\,t}(E_n,\,\gamma,\,\delta) = \zeta(\gamma,\,E_n)\,e^{-\frac{\delta}{\lambda(\gamma,\,E_n)}}. \tag{4.6}$$

The values of the preexponential factor $\zeta(\gamma, E_n)$ and the relaxation lengths $\lambda(\gamma, E_n)$ of the total dose of neutrons, taken from [7], are presented in Tables 4.2 and 4.3.

As analysis of the data of these tables indicates, the angular dependence of the preexponential factors $\zeta(\gamma, E_n)$ for iron and polyethylene can be represented with an error of not over 30% by the simple relationship

$$\zeta(\gamma,\,E_n) = \zeta(\gamma = 0,\,E_n)\cos\gamma, \tag{4.7}$$

which is correct for measured thickness of layers throughout the entire investigated interval of energies.

Table 4.2

RELAXATION LENGTH $\lambda(\gamma, E_n)$ AND FACTOR $\zeta(\gamma, E_n)$ FOR CALCULATION OF NEUTRON DOSE TOTAL TRANSMISSION FACTOR FOR IRON

γ, Degrees	ζ		λ, cm	ζ		λ, cm
	Experimental	Calculated	Experimental	Experimental	Calculated	Experimental
	$E_n = 3$ MeV			$E_n = 0,83$ MeV		
0	1,00±0,03	1,0	14,2∓0,3	1,00±0,05	1,0	19,0±0,4
26	1,00±0,03	0,90	8,4∓0,2	0,88±0,06	0,90	18,0±0,3
38	0,93±0,04	0,79	7,4∓0,3	—	0,79	—
47	—	0,68	—	0,85±0,06	0,68	9,3±0,5
56	—	0,56	—	0,73±0,04	0,56	7,3±0,4
62	0,47±0,03	0,47	5,1∓0,3	—	0,47	—
	$E_n = 0,22$ MeV			$E_n = 0,024$ MeV		
0	1,00±0,05	—	19,0±0,3	0,83±0,03	0,83	27±1
26	0,88±0,05	—	18,0±0,3	—	0,75	—
38	—	—	—	—	0,66	—
47	0,80±0,04	—	9,3±0,5	0,75±0,05	0,56	11,0±0,5
56	0,69±0,04	—	7,3±0,4	—	0,47	—
62	—	—	—	—	0,39	—

The angular dependence of the relaxation length of the dose of neutrons with initial energies of 3 and 0.83 MeV for polyethylene can be expressed with an error of not over 8% using a similar relationship:

$$\lambda(\gamma, E_n) = \lambda(\gamma = 0, \quad E_n)\cos\gamma, \tag{4.8}$$

correct for approximately $2 \leq \delta \leq 10$ cm.

In the area of polyethylene thicknesses $\approx 10 \leq \delta \leq 30$-40 cm for monoenergetic neutrons with energies of 0.8-3 MeV, the relaxation length should depend on angle γ significantly more weakly than following the rule of the cone. This is confirmed by data on the penetration of neutrons with energies of 0.22 MeV and 24 KeV through layers of polyethylene. With thickness of $1\text{-}2 \leq \delta \leq 6\text{-}10$ cm for E_n = 0.22 MeV, the

Table 4.3

RELAXATION LENGTH $\lambda(\gamma, E_n)$ AND COEFFICIENT $\zeta(\gamma, E_n)$ FOR CALCULATION OF NEUTRON DOSE TOTAL TRANSMISSION FACTOR FOR POLYETHYLENE

Degrees γ	ζ		λ, cm		ζ		λ, cm	
	Experimental	Calculated	Experimental	Calculated	Experimental	Calculated	Experimental	Calculated
	$E_n = 3$ MeV				$E_n = 0,83$ MeV			
0	1,30±0,04	1,30	6,4±0,2	6,4	1,10±0,04	1,10	3,4±0,1	3,4
26	1,25±0,04	1,17	6,3±0,2	5,8	1,10±0,06	0,90	3,15±0,07	3,06
38	1,17±0,05	1,03	5,2±0,3	5,1	—	0,87	—	2,7
47	—	0,88	—	4,4	1,00±0,05	0,75	2,3±0,07	2,3
56	—	0,73	—	3,6	0,83±0,05	0,62	2,0±0,1	1,9
62	0,85±0,04	0,61	2,9±0,15	3,0	—	0,52	—	1,6
	$E_n = 0,22$ MeV				$E_n = 0,024$ MeV			
0	1,1±0,04	1,1	—	2,3±0,05	1,33±0,06	1,33	2,0±0,1	—
26	1,1±0,1	0,99	—	2,2±0,12	—	1,2	—	—
38	—	0,87	—	—	—	1,05	—	—
47	0,78±0,08	0,75	—	1,9±0,1	0,89±0,05	0,91	2,0±0,15	—
56	0,49±0,05	0,62	—	1,8±0,1	—	0,74	—	—
62	—	0,52	—	—	—	0,62	—	—

relaxation length depends very little on angle γ. For E_n = 24 KeV with thicknesses over 4 cm the relaxation length of the dose is independent of angle γ. With polyethylene thicknesses over 30-40 cm, the relaxation length of the dose apparently should not depend on angle γ throughout the entire range of energies studied.

Table 4.4

EXPERIMENTAL VALUES OF λ(cm) AND ζ FOR WATER AND POLYETHYLENE
$\gamma = 0°$

Energy of Neutrons, MeV	Polyethylene		Water	
	λ	ζ	λ	ζ
15	18,4±0,4	1,18±0,02	18,4±0,4	1,10±0,03
3	6,4±0,2	1,30±0,04	7,6±0,15	1,20±0,04
0,83	3,4±0,1	1,10±0,04	3,40±0,07	1,00±0,05
0,22	2,30±0,05	1,10±0,04	2,61±0,07	1,00±0,05
0,24	2,00±0,10	1,33±0,06	—	—

As neutrons propagate through iron, the dependence of $\lambda(\gamma, E_n)$ on angle γ is expressed more sharply than the law of the cone.

Table 4.4 presents for comparison data relating to the transmission of neutrons through water and polyethylene (ρ = 0.93 g/cm^3) with normal incidence of neutrons with initial energies from 0.024 to 15 MeV on the surface of the shield [8].

Particularly valuable are the results of measurement of the transmission factors of the total dose of neutrons of a nuclear reactor through protective shielding, since the spectrum of these neutrons is quite similar to the spectrum of nuclear explosion neutrons scattered in air. Table 4.5 shows the transmission factors for various thicknesses of iron, concrete and polyethylene, measured using the neutrons of a reactor with normal and inclined incidence of the beam on the surface of the shield.

The important characteristics of the field of neutrons passing through the shielding are their angular and energy distributions. A large number of works published up to the present time has been

dedicated to the study of the angular distributions of scattered neutrons with normal incidence to the barrier. In [9], a report is presented on a study of the angular distributions of the dose of reactor neutrons beyond layers of polyethylene and lead. The angular distributions of doses of fast neutrons beyond shielding of polyethylene of various thicknesses with normal incidence of the beam of neutrons with reactor spectrum are presented. In [10], a study is described of the spectral and angular distribution of fast reactor neutrons beyond a shield of polyethylene 23 cm thick under conditions of normal incidence of the beam to the screen.

The angular characteristics of neutrons scattered by shielding were studied in the greatest detail in [26]. The energy and angular characteristics of reactor neutrons beyond shielding made of iron, concrete and polyethylene were studied experimentally. The experimental results of this work confirm the calculations performed for the same conditions by the Monte Carlo method and in the $2P_7$ approximation using the R.O.Z. program [11].

As was shown in [12, 13], the angular distributions of the dose of fast neutrons in relative units with normal incidence to the barrier with a thickness of at least 1-2 free path lengths can be described by the dependence

$$f(\psi) = \frac{1+\frac{1}{\psi_0^2}}{2\pi\left(1-\frac{e^{-\frac{\pi}{2}\psi_0}}{\psi_0}\right)} e^{-\frac{\psi}{\psi_0}}. \qquad (4.9)$$

This function characterizes the share of the dose of scattered neutrons leaving the protective barrier per unit solid angle in the direction characterized by polar angle ψ, read from the normal to the surface of the shield. Thus, the form of the field of scattered neutrons is determined only by empirical constant ψ_0, called the characteristic angle. Table 4.6 shows values of characteristic angles for various materials. In multilayered shields, the angular distribution of neutrons is determined by the last layer (next to the detector), if its thickness is over 1-2 λ.

In order to find the dose of neutrons propagating beyond a barrier in the direction of angle ψ, expression (4.9) must be multiplied by the total dose of scattered neutrons on the surface of the barrier, which is equal to

$$D_{n,\,s}(\delta) = D_{n,\,0}[K_{n,\,t}(\delta) - K_{n,\,u}(\delta)] = D_{n,\,0}K_{n,\,u}[B_n(\delta) - 1], \qquad (4.10)$$

Table 4.5

TOTAL NEUTRON DOSE PENETRATION FACTOR $K_{nt}(\lambda, \delta)$ FOR REACTOR SPECTRUM AND VARIOUS SHIELDING MATERIALS

γ, degrees	Thickness of Concrete, cm			Thickness of Iron, cm				Thickness of Polyethylene, cm			
	5	15	25	4	8	14	20	4	8	16	29
0	0,771	0,382	0,133	0,822	0,539	0,341	0,216	0,567	0,240	0,0600	0,890 (—2
10	0,750	0,364	0,128	0,810	0,530	0,335	0,209	0,560	0,227	0,0547	0,781 (—2
20	0,736	0,341	0,117	0,781	0,512	0,320	0,195	0,542	0,212	0,0462	0,620 (—2
30	0,702	0,306	0,101	0,740	0,473	0,283	0,174	0,509	0,191	0,0364	0,457 (—2
40	0,634	0,150	0,0792	0,673	0,420	0,240	0,144	0,438	0,152	0,0253	0,298 (—2
50	0,543	0,181	0,0546	0,588	0,340	0,184	0,111	0,320	0,108	0,0158	0,162 (—2
60	0,398	0,110	0,0320	0,420	0,237	0,126	0,076	0,211	0,0638	0,761 (—2	0,629 (—3
70	0,246	0,0509	0,0148	0,236	0,131	0,0723	0,0452	0,106	0,0300	0,290 (—2	0,160 (—3
80	0,105	0,151 (—2	0,440 (—2	0,0930	0,0504	0,0311	0,0194	0,0350	0,920 (—2	0,683 (—2	0,683 (—3

Note. Read 0.440(-2 = 0.00440.)

where $K_{n,\,t}$ and $K_{n,\,u}$ are the total dose transmission factors for neutrons for the barrier and the doses of neutrons in the unscattered component respectively; $D_{n,\,0}$ is the dose of neutrons without the barrier; $B_n(\delta)$ is the neutron accummulation factor beyond a barrier of thickness δ.

Table 4.6

VALUES OF CHARACTERISTIC ANGLE ψ_0 FOR NORMAL INCIDENCE OF REACTOR NEUTRONS TO PROTECTIVE BARRIERS

Shield Material	Density, g/cm³	Thicknesses Studied, cm	Threshold of Recording of Neutrons, MeV	ψ_0, Degs	Reference
Water	1,0	15; 45	0.7	30	[12]
Polyethylene	0,89	7,5; 15; 23; 38	Total Dose	30	[14]
»	0,93	3,5; 9,5	0,2	30	[4]
Concrete	2,16	25	Total Dose	45	[4]
Iron	7,8	5; 10; 14	» »	50	[4]

Table 4.7 shows several values of neutron dose accummulation factors with normal incidence beyond various shields.

Table 4.7

VALUE OF DOSE TRANSMISSION FACTOR FOR UNSCATTERED REACTOR NEUTRONS $K_{n,u}$ AND ACCUMMULATION FACTOR $B_n(\delta)$ WITH NORMAL INCIDENCE

Material	Parameter	Thickness of Protective Shielding, cm						
		5	10	15	20	30	40	50
Iron	$B_n(\delta)$	2,6	4,6	7,7	11	17,2	22	26
	$K_{n,\,u}(\delta)$	0,31	0,13	0,065	0,033	0,13	0,0057	0,0026
Concrete	$B_n(\delta)$	1,5	2,3	3,2	4	6,5	10,8	17
	$K_{n,\,u}(\delta)$	0,48	0,24	0,12	0,06	0,0146	0,004	0,0012
Polyethylene ($\rho = 0{,}93$ g/cm³)	$B_n(\delta)$	3	5,8	9,7	16	34,5	70	130
	$K_{n,\,u}(\delta)$	0,12	0,017	0,004	0,0012	0,000135	0,000021	0,0000040

Table 4.8

ANGULAR DEPENDENCE OF SCATTERED NEUTRON DOSE POWER BEYOND SHIELDS OF IRON AND POLYETHYLANE -- $f(\gamma, \psi, \tau)$, $ster^{-1}$ (rel. units)

γ, degrees	τ, degrees	ψ, degrees 0	10	20	30	50	70
			Iron — 5 *см*				
0	0		0,183		0,110	0,088	0,079
30	0	0,102				0,140	0,108
	180				0,077	0,07	0,062
50	0	0,069			0,084		0,097
	180				0,060	0,056	0,052
70	0	0,052			0,075	0,101	
	180				0,049	0,039	0,043
			Iron — 14 *см*				
0	0		0,148		0,089	0,057	0,057
	0	0,069				0,069	0,060
30	180				0,052	0,044	0,039
	0	0,051			0,051		0,041
50	180				0,038	0,034	0,031
	0	0,030			0,024	0,025	
70	180				0,024	0,021	0,019
			Polyethylene — 9,5 *см*				
0	0		0,032		0,020	0,010	0,004
30	0	0,018				0,014	0,006
	180			0,008		0,003	0,001
	0	0,008			0,012		0,003
50	180				0,003		

Very few data on the angular distributions of neutrons with inclined incidence of the initial beam to the barrier can be found in the literature.

In Table 4.8, based on [26], we present the angular distributions of the doses of neutrons beyond iron and polyethylene shields with various angles of incidence γ of a flat, unidirectional beam of reactor neutrons.

The energy distributions of neutrons as functions of angles of incidence γ and scattering angle ψ have certain common regularities for

barriers of various materials. With increasing angles γ and ψ, the neutron spectra soften. The greatest softening in the low energy area of the spectrum is characteristic for hydrogen-containing media. With large angles γ and ψ (over 50°) practically 90-95% of all neutrons fall in the area of energies below 0.5 MeV (contribution to dose at least 70-80%). For shields of concrete and iron, these estimates are true for the energy area $E_n < 1$ MeV.

The spectra of neutrons with energies below 0.2 MeV in these media can be described by a dependence of the form $\Phi(E_n) \simeq E_n^{-l}$, where l varies from 0.7 to 1.1. The low energy portion of the spectrum is important for calculation of the dose of secondary γ radiation produced by neutron capture.

§ 3. Reflection of Neutrons From Barriers

No unified terminology has been established for description of the characteristics of neutrons reflected from barriers; therefore, it is expedient first to introduce definitions and symbols. The differential albedo (angular distribution of back scattering of radiation) is a function of the initial radiation energy E, angle of incidence γ, polar angle ψ and azimuthal angle τ of reflection. Angles γ and ψ are counted from the normal to the surface. The differential albedo will be represented by the letter a. The first left subscript indicates the type of radiation (n = neutrons, γ = γ radiation), while the second subscript indicates the albedo of the number of particles (little h) or dose (d). The superscripts determine the quantities in which the incident (first) and reflected (second) radiation are expressed. The current density (or simply current) will be represented by T, the flux density (or flux) by π. For example, the differential dose albedo for neutrons for an incident current and reflected flux is written as $a_{n,d}^{t,\pi}(E, \gamma, \psi, \tau)$. If the incident and reflected radiation (both) are expressed in current or flux terms, the second (identical) superscript is omitted. The differential current and flux albedos are related by the formula

$$a^n(E, \gamma, \psi, \tau) = a^T(E, \gamma, \psi, \tau)\frac{\cos\gamma}{\cos\psi}; \qquad (4.11)$$

integration of the differential albedo with respect to angles produces the integral albedo

$$A(E, \gamma) = \int_0^{2\pi} d\tau \int_0^{\pi/2} a(E, \gamma, \psi, \tau)\sin\psi d\psi. \qquad (4.12)$$

The integral albedo is given the same indexes as the differential albedo. We present below a brief review of works dedicated to study of the reflection of neutrons, and certain results which may be useful in calculations.

Among the first works on the determination of albedo is experimental work [15]. It presents data on the measurement of the integral numerical albedo $A_{n,\ h}$ of monoenergetic neutrons from paraffin and water with normal and inclined incidence of neutrons to the surface of the reflector. The range of neutron energies studied in the initial beam was from the energy of thermal neutrons to 5 MeV.

It has been found that the reflection factor of neutrons from hydrogen-containing material decreases with increasing energy. The range of incidence angles of the neutron beam studied (counted from the normal) was from 0 to 75°. The angular dependence of the albedo on incidence angle γ for all energy values studied can be expressed by the relationship

$$1 - A^{\text{п}}_{n,h}(\gamma) = [1 - A^{\text{п}}_{n,h}(\gamma = 0)] \cos\gamma. \qquad (4.13)$$

Work [16] was dedicated to the determination of the empirical regularities for description of the characteristics of the field of neutrons reflected from iron, concrete and earth on the basis of Monte Carlo calculations [17].

It was found in this work that the differential "dose" albedo of neutrons from concrete, iron and earth of various compositions (various water contents) can be described by the empirical expression

$$a^{\text{п, т}}_{n,d}(E, \gamma, \psi) = a^{\text{п}}_{n,d}(E, \gamma = 0, \psi = 0)\cos^{2/3}\gamma\cos\psi \ \text{ster}^{-1}, \qquad (4.14)$$

where $a^{\text{т}}_{n,\ d}$ is the differential dose albedo with normal incidence and reflection of the flat beam of neutrons (the tabular value, depending on initial energy E and type of scattering material).

It is demonstrated in this work that for neutrons with the fission spectrum and for the spectrum leaving the shield, the angular albedo for all materials studied can be expressed by the formula

$$a^{\text{пт}}_{n,d}(E, \gamma, \psi) = \frac{1}{\pi}\frac{0{,}435\,(\Sigma_t - \Sigma_{\text{H}})}{\Sigma_{\text{т}}}\cos^{2/3}\gamma\cos\psi, \qquad (4.15)$$

where Σ_t is the total macroscopic cross section of all elements included in the composition of the scattering material, weighted with respect to to the neutron spectrum; Σ_H is the macroscopic cross section of hydrogen contained in the material, weighted for the neutron spectrum.

Expression (4.15) describes the differential albedo of neutrons for all materials studied except water. For the integral dose albedo of fast neutrons from water with normal incidence, [16] suggests the dependence

$$A^{\Pi}_{n,d}(E, \gamma = 0) = \frac{0{,}435\,(\Sigma_t - \Sigma_H)}{\Sigma_t}. \tag{4.16}$$

In [18], the Monte Carlo method was used to calculate the integral values of numerical (in terms of "current") and dose (in terms of "flux") albedos of monoenergetic neutrons and neutrons with the fission spectrum with inclined incidence to reflectors of various thicknesses, and the energetic distributions of the reflected neutrons are presented.

In [19], a broad range of information is presented on determination of the characteristics of the neutron field reflected from concrete. These characteristics were calculated by the Monte Carlo method and measured experimentally (in terms of "current"). The calculations were performed for initial energies of neutrons E from 0.2 to 8 MeV and angles of incidence of the unidirectional beam γ = 0, 45, 60, 75 and 85°. The experimental data agreed well with the calculated data.

In [20], an attempt was made to produce a semi-empirical expression, using a number of assumptions concerning the nature of the interaction of neutrons with the scattering nuclei. A four-parameter semi-empirical formula is presented in this work for the differential dose albedo for iron, aluminum, dry earth, earth with 50% moisture content, earth with 100% moisture content and concrete. This formula is written in terms of neutron "current" and covers the area of energies from 0.1 to 14 MeV.

The formula produced has the following form:

$$a^{\tau}_{n,d}(E, \gamma, \psi, \tau) = E_1(E)\cos\psi + \frac{E_2(E) + E_3(E)\cos\psi_s}{1 + E_4(E)\dfrac{\cos\gamma}{\cos\psi}} \quad [\text{ster}^{-1}], \tag{4.17}$$

where ψ_s is the total scattering angle, determined from the expression

$$\cos\psi_s = \sin\gamma\sin\psi\cos\tau - \cos\gamma\cos\psi, \tag{4.18}$$

Table 4.9

ENERGY DEPENDENCE OF PARAMETERS FOR FOUR-PARAMETER FORMULA OF DIFFERENTIAL DOSE ALBEDO FOR FAST NEUTRONS

Parameters	Reflector Material Index	E_n, MeV							
		0,1	0,25	0,5	1,0	2,0	3,0	5,0	14,0
$E_1(E)$	1	0,1401	0,1385	0,1817	0,0797	0,0904	0,1147	0,0756	0,0657
	2	0,1528	0,1491	0,1523	0,0940	0,1287	0,1020	0,0689	0,0584
	3	0,0706	0,0710	0,0834	0,0727	0,0691	0,0810	0,0442	0,0288
	4	0,0648	0,0687	0,0813	0,0583	0,0547	0,0617	0,0431	0,0269
	5	0,0746	0,0820	0,0659	0,0505	0,0641	0,0389	0,0311	0,0187
	6	0,0673	0,0661	0,0693	0,0477	0,0488	0,0407	0,0218	0,0287
$E_2(E)$	1	0,0776	0,0672	0,0796	0,0643	0,0863	0,0858	9,0710	0,0575
	2	0,0488	0,0874	0,0649	0,1008	0,0966	0,1129	0,1017	0,0770
	3	0,0819	0,0628	0,0703	0,0676	0,0921	0,0991	0,1214	0,0697
	4	0,0711	0,0727	0,0793	0,0740	0,0971	0,0836	0,0787	0,0812
	5	0,0561	0,0514	0,0982	0,0838	0,0972	0,1154	0,1132	0,0788
	6	0,0615	0,0556	0,1051	0,0633	0,1259	0,1010	0,1042	0,0567
$E_3(E)$	1	0,0093	—0,0095	0,0684	—0,0067	—0,0118	0,0140	0,0293	0,0195
	2	—0,0014	0,0329	0,0112	—0,0381	—0,0101	—0,0122	0,0172	0,0147
	3	0,0406	0,0278	0,0585	—0,0228	0,0189	0,0546	0,0047	0,0235
	4	0,0343	0,0292	0,0611	—0,0166	—0,0016	0,0154	0,0177	0,0444
	5	0,0517	0,0294	0,0671	—0,0295	0,0149	0,0133	0,0289	0,0240
	6	0,0555	0,0345	0,0964	—0,0118	0,0393	0,0297	0,0212	0,0408
$E_4(E)$	1	1,1654	1,0115	2,5708	0,9052	0,8566	1,2569	0,9325	1,9877
	2	0,4868	2,9778	1,2733	1,4044	1,2834	1,4061	1,9476	2,6300
	3	1,5033	0,6753	0,8982	0,6403	1,0692	2,3264	2,6435	1,6450
	4	1,166	1,1058	1,2315	0,5448	1,1314	1,4523	1,3720	1,8531
	5	1,0278	1,2818	1,3826	0,7913	1,4744	1,5615	1,8382	1,6692
	6	1,4170	1,2275	2,5801	0,6001	2,0462	1,7238	1,7486	1,4914

Note: 1, iron; 2, aluminum; 3, concrete; 4, dry earth; 5, earth with 50% relative moisture content; 6, earth with 100% relative moisture content

in which τ is the azimuthal angle of reflected radiation, counted from the projection of the direction of the incident beam on the surface of the reflector.

The values of parameters $E_1(E)$, $E_2(E)$, $E_3(E)$ and $E_4(E)$ are presented in Table 4.9.

It is indicated in [20] that the results calculated by the four-parameter formula agree well with the data produced by the Monte Carlo method [17].

Works [21-24, 26] present the results of studies performed for determination of the characteristics of the field of reflected neutrons, performed experimentally for the reactor spectrum (water, earth, iron) by a calculation method in the $2P_7$ approximation (for the same conditions and media) and using the Monte Carlo method [21] for water and various groups of incident neutrons ΔE. Figure 4.2 shows the dependence $a^{\pi}_{n,d}(\gamma, \psi, \tau)$ and $a^{\pi}_{n,h}(\gamma, \psi, \tau)$ for water, earth and iron for the spectrum of neutrons leaving a reactor [23].

We can see from Table 4.2 that the flux albedo is always greater than the corresponding value of dose power and that this difference increases with improvement of the moderating properties of the medium. The angular distributions of flux density of reflected neutrons are similar to the isotropic distributions for materials with high atomic number and sharply anisotropic for light shielding materials such as water and polyethylene. As we can see from the figure, even for an iron shield, total isotropy is not observed, and therefore the empirical dependence (4.14) suggested by the authors of [16], in which the angular distribution of dose power of reflected neutrons is assumed proportional to cos ψ must be looked upon as approximate.

In the case of a light reflector (water, polyethylene), the angular distributions of flux and dose power of reflected neutrons depend significantly on the azimuthal angle τ, whereas for earth and iron this dependence is slight.

The difference in the behavior of the angular distributions of flux and dose power for various materials can be easily explained, keeping in mind the angular distribution of neutrons upon scattering (in an elementary event) and the absorption cross section.

The dependence of the integral dose albedo $A^{\pi}_{n,d}(\gamma)$ on incidence angle of a flat, infinite beam of neutrons with the reactor spectrum to

barriers of iron, earth and water is shown on Figure 4.3 [22]. We can see from Figure 4.3 that the albedo for iron and earth acts similarly, whereas for water the course of the dependence differs significantly from the other cases since as angle γ increases in the case of water the energy of the neutrons scattered at slight angles ψ increases significantly. The effect of the influence of hydrogen at high values of γ is noted in the case of earth as well. As we can see from Figure 4.3, the agreement of experimental and calculated (Monte Carlo method) data is quite satisfactory.

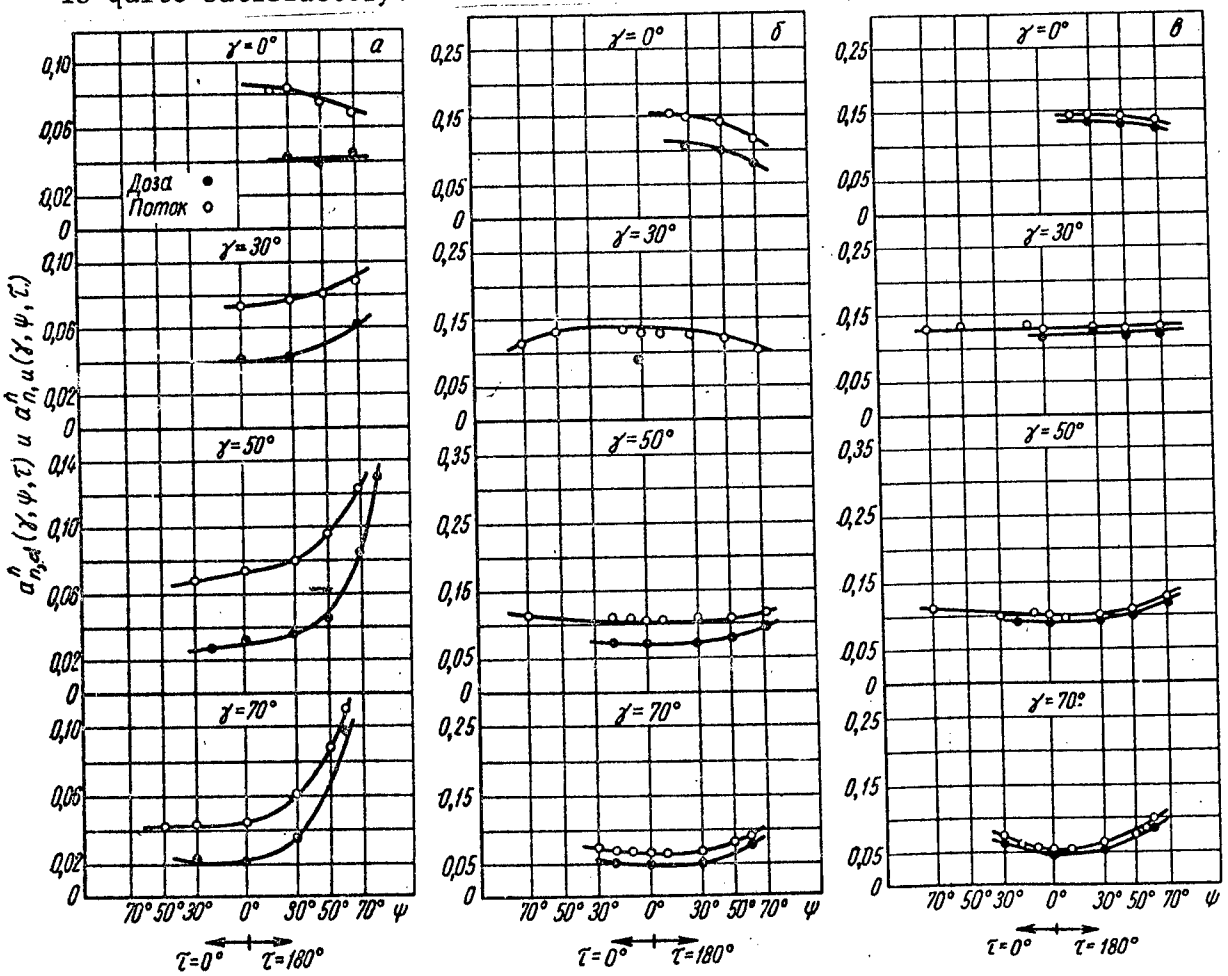

Figure 4.2. Angular Distributions of Dose and Flux of Neutrons, Reflected From Water, Earth and Iron With Various Incidence Angles of a Beam With Reactor Spectrum to the Surface: a, 10 cm water; b, 30 cm earth; c, 19 cm iron.

Analysis of the results illustrated by Figure 4.3 shows that the integral dose albedo for iron and earth is described well by an empirical dependence [see formula (4.14)].

The dependence $A^{\pi}_{n,d}(\gamma)$ for water and polyethylene [26] can be described by the following empirical relationship:

$$A^{\pi}_{n,d}(\gamma) = A^{\pi}_{n,d}(\gamma = 0)\cos\gamma + 0{,}3(1 - \cos\gamma). \tag{4.19}$$

This expression is correct with $\gamma < 70°$, the accuracy of the empirical expressions presented being no worse than about 10%, which is quite satisfactory for practical purposes.

Analysis of the experimental and calculation data (Monte Carlo method) indicates that for a medium such as water, the value of $A^{\pi}_{n,d}$ depends little on the form of the incident neutron spectrum. Thus, for the neutron spectrum of a Po-Be source ($E_{av} \approx 4$ MeV), as for the spectrum of reactor neutrons ($E_{av} \approx 0.65$ MeV) and for the softened neutron spectrum from a Po-Be source ($E_{av} \approx 2$ MeV), $A^{\pi}_{n,d}$ ($\gamma = 0$) = 0.18 (with a threshold for recording of reflected neutrons ≈ 1 KeV).

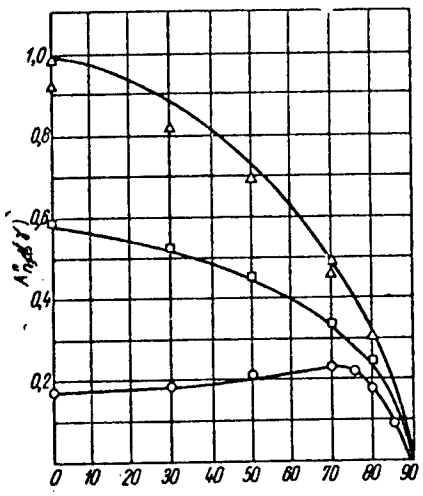

Figure 4.3. Dependence of Integral Dose Albedo on Angle of Incidence of Flat, Unidirectional Beam of Neutrons With Reactor Spectrum to Barriers of Iron (Δ), Earth (□), and Water (0). ———, Data produced by Monte Carlo calculation.

Table 4.10

DIFFERENTIAL DOSE ALBEDO $a^{\pi}_{n,d}(\Delta E, \nu, \psi)\cdot 10^{-3}$, rem·ster^{-1}

ΔE_n, MeV	ν, degrees	$\psi = 0°$	$\psi = 30°$			$\psi = 45°$			$\psi = 60°$		
		—	$\tau = 0°$	$\tau = 90°$	$\tau = 180°$	$\tau = 0°$	$\tau = 90°$	$\tau = 180°$	$\tau = 0°$	$\tau = 90°$	$\tau = 180°$
0,4—0,8	0	16,0			14,8			13,2			10,3
	45	21,9	25,9	21,9	18,9	27,8	20,5	15,8	28,8	16,8	12,2
	60	25,3	34,0	25,5	20,4	42,3	24,4	17,7	60,7	20,6	13,9
	75	29,9	51,6	30,1	22,8	93,0	29,5	20,0	125,7	26,6	16,4
	85	29,4	79,9	29,8	21,9	142,6	30,0	19,7	193,0	29,0	16,9
0,8—1,4	0	37,9			31,1			23,9			15,7
	45	37,4	32,0	33,5	40,0	29,7	28,4	36,3	28,2	21,1	27,6
	60	35,3	35,8	32,8	39,3	42,0	29,4	38,4	60,0	23,8	32,2
	75	35,9	50,3	34,8	40,6	88,0	33,1	42,4	128,0	31,0	39,9
	85	31,3	79,0	32,2	37,7	136,0	32,4	42,3	209,0	30,7	44,5
1,4—2,5	0	25,1			22,0			18,1			12,6
	45	31,5	31,7	28,1	28,0	30,6	24,1	23,3	29,1	18,0	16,6
	60	34,0	39,5	31,8	30,6	47,3	28,7	26,7	66,0	22,7	20,5
	75	39,2	59,2	37,1	34,5	104,0	34,4	31,6	158,0	28,8	26,2
	85	37,5	96,8	37,0	33,0	186,0	36,8	31,5	246,0	33,8	28,2
2,5—4	0	39,5			33,6			27,3			19,1
	45	44,2	42,1	41,4	42,3	40,3	35,2	37,0	36,2	26,4	27,9
	60	48,7	51,5	45,5	46,0	59,5	40,4	41,4	85,0	30,0	32,6
	75	51,5	74,3	49,5	48,4	130,0	46,5	45,5	174,0	39,1	38,8
	85	44,4	113,0	44,4	43,8	201,0	43,8	43,6	251,0	40,4	41,1
4—5	0	33,3			29,6			26,2			18,5
	45	45,4	46,3	42,3	40,2	44,1	37,4	34,1	40,1	28,8	24,6
	60	49,7	58,6	48,3	40,9	66,7	43,7	34,8	83,0	35,0	26,4
	75	56,1	79,4	55,2	47,4	132,0	52,3	42,6	167,0	45,0	35,4
	85	51,5	124,0	51,3	44,0	187,0	50,3	39,8	247,0	46,1	33,2

The value of $A^{\pi}_{n,d}$ with a recording threshold E ≈ 0.2 MeV, although it differs slightly for spectra of neutrons of various "hardnesses," is still very low: from 0.14 for the spectrum of the Po-Be source to 0.125 for the reactor spectrum. For a water (polyethylene) reflector, the contribution of neutrons with energies E < 0.2 MeV to the dose is quite significant (about 30%), and cannot be ignored. For such media as iron, concrete, earth, the contribution of neutrons with energies E < 0.2 MeV to the total dose is slight (not over 10%).

Since the differential albedo for water is not described by simple approximation expressions Table 4.10 presents numerical data from [21].

Investigations of the dependence of integral albedo $A^{\pi}_{n,d}(\gamma)$ on thickness of barriers of iron, aluminum, concrete, graphite, etc. performed on the basis of the results of [18, 22], have shown that it can be expressed by the following empirical relationship:

$$A^{\pi}_{n,d}(\gamma, \delta) = A^{\pi}_{n,d}(\gamma = 0)\cos^{3/4}\gamma\left(1 - e^{-\frac{0,14}{\cos\gamma}}\right). \qquad (4.20)$$

In conclusion we note that the form of the energy distributions of neutrons reflected from barriers (for example, see [25]) differs little from the distributions beyond the protective shields with comparable scattering angles.

Bibliography

1. Nikolayev, M. N., Filippov, V. V., *Nucl. Energy*, Vol. 18, p. 471 (1964).

2. Kukhtevich, V. I. et al., *Atomnaya Energiya*, Vol. 23, p. 191 (1967).

3. Clifford, C. E. et al., *Nucl. Sci. and Engng.*, Vol. 27, p. 299 (1967).

4. Kukhtevich, V. I. et al., *Report 47 at CEMA Symposium "The Problem of Shielding From the Penetrating Radiation of Reactors,"* Melekess, 21-26 April 1969.

5. Kukhtevich, V. I. et al., *Byulleten' Informatsionnogo Tsentra Po Yadernyn Dannym*, No. 4, Moscow, Atomizdat Press, 1967, p. 534.

6. Hughes, D. J., Harvey, J. A., *Neutron Sections, USAEC Report BNL-325* (1955).

7. Miroshnikov, G. V., *Atomnaya Energiya*, Vol. 18, No. 5, p. 529 (1965).

8. Miroshnikov, G. V., *Ibid*, p. 532.

9. Beissner, R. E., *Western J. T. ANS Transactions*, Vol. 5, No. 2, p. 402 (1962).

10. Mooney, L. G., *JREE Transactions*, Vol. 5, p. 10 (1963).

11. Germogenova, T. A., *Voprosy Fiziki Zashchity Reaktorov* [Problems of the Physics of Reactor Shielding -- Collection of Works], No. 2, Moscow, Atomizdat Press, 1966, p. 22.

12. Begtyarev, S. F. et al., *Byulleten' Informatsionnogo Tsentra Po Yadernyn Dannym*, 1966, p. 533.

13. Begtyarev, S. F. et al., *Atomnaya Energiya*, Vol. 21, p. 392 (1966).

14. Henry, R. L., *ANS Transactions*, Vol. 7, p. 40 (1964).

15. Kochin, A. M. et al., *Atomnaya Energiya*, Vol. 7, No. 4, p. 81 (1959).

16. French,,R. L., Weces, M. B., *Nucl. Sci. Engng.*, Vol. 19, p. 441 (1964).

17. Allen, F. J. et al., *Neutron Reflection and Flux Versus Depth for Iron, BRL-1199* (1963).

18. Leimdorfer, M., *FOA-4, Rapport, A 4365-411*, Stockholm,Marz (1964)

19. Maerker, K. E., Muckenthaler, F.J.,*Nucl. Sci. Engng.*, Vol. 22, p. 455 (1965).

20. Taik, J. Song.,*ANS Transactions*, Vol. 10, No. 2, p. 727 (1967).

21. Gudkova, L. Ya., Zolotukhin, V. G., *Atomnaya Energiya*, Vol. 21, p. 122 (1967).

22. Trykov, L. A. et al., *Atomnaya Energiya*, Vol. 21, p. 246 (1966).

23. Goryachev, I. V. et al., *Informatsionnogo Tsentra Po Yadernyn Dannym*, 1966, p. 522.

24. Kukhtevich, V. I. et al., *Voprosy Dozimetrii i Zashchity Ot Izlucheniya* [Problems of Dosimetry and Protection From Radiation], No. 6, Moscow, Atomizdat Press, 1967, p. 13.

25. Goryachev, I. V. et al., *Laderna Energie*, Vol. 8, No. 13, p. 281 (1967).

26. Goryachev, I. V., *Voprosy Fiziki Zashchity Reaktorov* [Problems of the Physics of Reactor Shielding -- Collection of Works], 1959, pp. 97; 128; 144.

CHAPTER 5. PENETRATION OF γ AND β RADIATION THROUGH SHIELDING

§ 1. Attenuation of Unscattered γ Radiation

The transmission factor of unscattered monochromatic γ radiation is calculated using expressions similar to formula (4.1), in which the total macroscopic cross section of the interaction of γ radiation with the medium is usually referred to as the linear attenuation factor and represented by $\mu(E_\gamma)$.

The thickness of the absorber can be conveniently expressed in units of mass (g/cm^2). Correspondingly, μ is frequently expressed in square centimeters per gram (cm^2/g) and referred to as the mass absorption factor, represented as μ/ρ. The mass absorption factor of chemically complex materials or mixtures consists of the sum of the mass absorption factors of the component elements, taken with their statistical weight, proportional to the content of each element.

The total attenuation factors for γ quanta in materials are complex functions of energy E_γ. At the present time, they have been determined with a mean accuracy of about 1% and presented in the form of tables or graphs in many works (for example, in [1]. However, in certain cases, particularly when calculations are performed by computer, expressions are required for the attenuation factors, written in an analytic form. A parabolic approximation for the total mass attenuation factor was suggested in [2]:

$$\frac{\mu(E_\gamma)}{\rho} = c_0 + c_1\varepsilon + c_2\varepsilon^2, \tag{5.1}$$

where ε is the wave length of a γ quantum in Comptom units; $\varepsilon = E_\gamma(\text{MeV})/0.511$.

Formula (5.1) can be written in a form more convenient for practical calculations

$$\frac{\mu(E_\gamma)}{\rho} = b_0 + \frac{b_1}{E_\gamma} + \frac{b_2}{E_\gamma^2}, \qquad (5.2)$$

the coefficients b and c being related by the formulas: $b_0 = c_0$; $b_1 = 0.511\ c_1$; $b_2 = 0.261\ c_2$.

Table 5.1 presents the coefficients of the parabolic approximation for various materials. The maximum relative error of approximation using these coefficients, according to estimates of the authors of [2], will not exceed 4% in the 0.03-0.08 MeV energy range, 3% in the 0.08-0.03 MeV range and 5% in the 0.3-10 MeV range.

Approximate expressions with this level of accuracy should be used carefully, since when calculations with low error are required they are suitable only for low values of attenuation. For example, with an accuracy of 5% and an attenuation of the primary beam by a factor of 10, the error in calculating the attenuation factor of the unscattered radiation is 10%, while when the attenuation is by a factor of 1000 the error may reach 60%.

For complex chemical compounds not included in Table 5.1, the mass attenuation factors can be calculated based on the known dependences $\mu_i(E_\gamma)/\rho_i$ of the individual elements using the expression

$$\frac{\mu(E_\gamma)}{\rho} = \sum \frac{\mu_i}{\rho_i} a_i, \qquad (5.3)$$

where a_i is the weight share of the ith element in the mixture or chemical compound.

If the shielding surface is struck by nonmonochromatic γ radiation, the attenuation of the unscattered component does not follow the simple exponential rule due to the filtration of hard γ quanta. In this case the attenuation factor of the unscattered component can be found by integration with respect to the entire spectrum $\Phi(E_\gamma)$ of the initial γ radiation similarly to expression (4.2).

Table 5.1

COEFFICIENT OF PARABOLIC APPROXIMATION, $\times 10^{-3}$

Element, Material	$E_\gamma = 0{,}03 \div 0{,}08$ MeV			$E_\gamma = 0{,}08 \div 0{,}3$ MeV			$E_\gamma = 0{,}3 \div 10$ MeV		
	b_0	b_1	b_2	b_0	b_1	b_2	b_0	b_1	b_2
Carbon	135	2,07	0,201	71,5	23,3	—1,56	14,9	113	—37,7
Oxygen	174	—8,65	1,04	75,4	21,1	—1,20	16,3	108	—34,5
Sodium	246	—33,0	3,24	70,4	20,2	—0,808	17,2	99,3	—30,7
Magnesium	319	—53,5	4,95	76,1	18,4	—0,381	18,3	100	—30,4
Aluminum	353	—65,3	6,10	69,8	20,3	—0,430	18,4	96,9	—29,1
Silicon	411	—83,2	7,92	73,9	19,5	—0,0400	19,7	98,2	—28,9
Potassium	866	—227	21,4	86,4	4,75	4,12	22,0	86,9	—22,8
Calcium	999	—269	25,6	90,3	2,14	5,34	23,1	87,8	—22,6
Iron	1730	—512	51,2	103	—21,7	13,8	24,8	72,1	—14,4
Copper	2110	—646	66,6	118	—40,4	20,1	25,9	65,1	—9,85
Water	182	—6,27	0,891	75,4	28,5	—2,0	17,0	124	—40,5
Sand	289	—44,6	4,32	67,2	26,6	—1,34	17,8	104	—32,1
Concrete	365	—68,2	6,59	67,9	24,2	—0,739	18,2	103	—31,6

§ 2. Penetration of Scattered γ Radiation Through Shielding

The concept of the transmission factor $K_{\gamma s}$ for the dose of scattered radiation of a flat unidirectional beam, the ratio of the integral dose of scattered radiation reaching the internal surface of the barrier to the total dose of γ quanta striking its outer surface, is introduced in order to characterize the attenuation of scattered γ radiation in the barrier.

In [3], the Monte Carlo method was used to calculate the transmission factors for scattered radiation for barriers of concrete and iron (3.7-60.0 g/cm^2 thickness) upon incidence of a flat, unidirectional beam to the surface of the barrier at various angles. Table 5.2 shows the results relating to transmission of the energy of scattered γ radiation by concrete shields with various incident γ radiation energies. It is remarkable that for low barrier thicknesses, the maximum intensity of transmitted scattered radiation is observed at high angles of incidence of the primary γ radiation. The data of these same tables can be used to calculate the energy factor of accummulation with inclined incidence of γ radiation:

$$B_E(E_\gamma, \delta, \gamma) = e^{-\mu(E_\gamma)\delta\left(\frac{1}{\cos\gamma}-1\right)} + K_{\gamma s}(E_\gamma, \delta, \gamma)\, e^{\mu(E_\gamma)\delta}. \qquad (5.4)$$

In [4], the dose factors of accummulation of γ radiation with initial energies from 0.2 to 10 MeV are calculated for inclined incidence of a broad unidirectional beam to concrete barriers (Table 5.3).

If the accummulation factor $B(E_\gamma, \delta, \gamma)$ is known for a given barrier, the transmission factor for scattered γ radiation can be calculated using the expression

$$K_{\gamma s}(E_\gamma, \delta, \gamma) = [B(E_\gamma, \delta, \gamma) - 1]\, e^{-\mu(E_\gamma)\frac{\delta}{\cos\gamma}}. \qquad (5.5)$$

For a complex spectrum of initial γ radiation

$$K_{\gamma s}(\delta, \gamma) = \int_{E_\gamma} \Phi(E_\gamma)\,[B(E_\gamma, \delta, \gamma) - 1]\, e^{-\mu(E_\gamma)\frac{\delta}{\cos\gamma}}\, dE_\gamma. \qquad (5.6)$$

Broad information on the transmission of scattered γ radiation by screens of iron was produced in [5], in which calculations were performed by the Monte Carlo method. The energy groups of initial γ

Table 5.2

TRANSMISSION FACTORS OF SCATTERED γ RADIATION ENERGY FOR CONCRETE BARRIERS

cos γ	Barrier Thickness, g/cm²				
	3,75	7,5	15	30	60
Initial Energy 0.35 MeV					
0	0,1960	0,1250	0,0617	0,0126	0,0004
0,25	0,2480	0,2210	0,1190	0,0254	0,0011
0,50	0,1990	0,2290	0,1660	0,0471	0,0028
0,75	0,1640	0,2170	0,1980	0,0786	0,0073
1,00	0,1410	0,2020	0,2040	0,1980	0,0162
Initial Energy 0,66 MeV					
0	0,1725	0,1150	0,0631	0,0170	0,0006
0,25	0,2050	0,1990	0,1260	0,0391	0,0034
0,50	0,1590	0,2040	0,1780	0,0728	0,0086
0,75	0,1340	0,1900	0,2030	0,1130	0,0161
1,00	0,1150	0,1730	0,2030	0,1490	0,0325
Initial Energy 1.25 MeV					
0	0,1460	0,1080	0,0534	0,0177	0,0011
0,25	0,1570	0,1870	0,1280	0,0450	0,0039
0,50	0,1150	0,1690	0,1700	0,0895	0,0159
0,75	0,0891	0,1510	0,1880	0,1300	0,0341
1,00	0,0716	0,1370	0,1820	0,1570	0,0604
Initial Energy Corresponding to Spectrum of γ Radiation of U^{235} Fission Products 1.12 Hours After Explosion					
0	0,1520	0,1000	0,0505	0,0145	0,0018
0,25	0,1580	0,1770	0,1200	0,0460	0,0049
0,50	0,1170	0,1640	0,1630	0,0905	0,0157
0,75	0,0925	0,1520	0,1680	0,1270	0,0386
1,00	0,0809	0,1360	0,1690	0,1430	0,0667
Initial Energy Corresponding to Spectrum of γ Radiation of U^{235} Fission Products 23.8 hours After Explosion					
0	0,1660	0,1140	0,0555	0,0152	0,0015
0,25	0,1870	0,1970	0,1240	0,0365	0,0042
0,50	0,1450	0,1870	0,1680	0,0765	0,0108
0,75	0,1150	0,1800	0,1850	0,1110	0,0246
1,00	0,0991	0,1640	0,1880	0,1440	0,0417

radiation were selected considering the convenience of application of these data for calculation of the attenuation of γ radiation of a nuclear explosion. The spectral intensity of γ quanta was considered constant within the limits of each energy group. The results of calculation of the transmission factors for scattered γ radiation are presented in Table 5.4.

In [6, 7], an empirical formula is presented for calculation of the accummulation factors from a flat isotropic source for a heterogeneous shield with any number of layers of various materials in the 1-7 MeV γ radiation energy range:

$$B_{het} = \sum_{n=1}^{N} B_n\left(\sum_{i=1}^{n} \mu_i \delta_i\right) - \sum_{n=2}^{N} B_n\left(\sum_{i=1}^{n-1} \mu_i \delta_i\right), \qquad (5.7)$$

where N is the total number of shielding layers; B_n is the accummulation factor of the homogeneous material of the i-th layer (the count of layers is performed from the source inward), taken with the corresponding thickness $\sum_{i=i}^{n} \mu_i \delta_i$ in free path lengths.

Formula (5.7) was checked experimentally with a large number of combinations in the barrier geometry for a point isotropic and flat isotropic source of γ radiation. In both cases, the formula gave good correspondence. This allows us to assume that it will be correct for a flat unidirectional beam of initial γ radiation as well.

[Pages 126-129 of source missing]

Table 5.3

DOSE ACCUMMULATION FACTORS FOR CONCRETE

cos γ	For μδ				cos γ	For μδ			
	0,5	1,0	2,0	4,0		0,5	1,0	2,0	4,0
	$E_\gamma = 0{,}2$ MeV					$E_\gamma = 4{,}0$ MeV			
1,0	1,59	2,15	3,54	6,95	1,0	1,28	1,54	2,12	3,25
0,75	1,67	2,34	4,18	11,1	0,75	1,34	1,70	2,48	4,13
0,50	1,72	2,79	7,43	66,3	0,50	1,46	1,99	3,52	0,78
0,25	2,16	6,37	106	—	0,25	1,74	3,29	17,0	—
0,10	8,76	—	—	—	0,10	4,92	—	—	—
	$E_\gamma = 0{,}5$ MeV					$E_\gamma = 6{,}0$ MeV			
1,0	1,62	2,23	3,73	8,10	1,0	1,08	1,46	1,89	2,63
0,75	1,68	2,39	4,51	13,4	0,75	1,31	1,59	2,17	3,22
0,50	1,80	2,78	8,00	64,6	0,50	1,41	1,84	2,66	4,93
0,25	2,16	6,50	104	—	0,25	1,64	2,70	12,2	—
1,0	9,06	—	—	—	0,10	3,99	—	—	—
	$E_\gamma = 1{,}0$ MeV					$E_\gamma = 10{,}0$ MeV			
1,0	1,45	1,88	2,90	5,78	1,0	1,16	1,32	1,61	2,07
0,75	1,49	2,04	3,49	8,94	0,75	1,20	1,41	1,82	2,81
0,50	1,65	2,42	5,70	38,5	0,50	1,28	1,56	2,18	5,25
0,25	1,88	4,96	62,2	—	0,25	1,48	2,28	9,03	—
0,10	6,98	—	—	—	0,10	3,20	—	—	—
	$E_\gamma = 2{,}0$ MeV								
1,0	1,38	1,73	2,52	4,29					
0,75	1,47	1,91	2,95	6,38					
0,50	1,55	2,22	4,65	17,1					
0,25	1,82	4,24	39,0	—					
0,10	6,02	—	—	—					

Table 5.4

DOSE TRANSMISSION FACTORS OF SCATTERED γ RADIATION FOR IRON SHIELDS

γ, Degrees	Shield Thickness, cm					
	2,0	5,0	10	14	19	25
			$E_\gamma = 0,1 \div 0,2$ MeV			
0	0,119 (—2	0,759 (—4	0,321 (—5	0,221 (—6	0,904 (—8	0,236 (—9
30	0,823 (—3	0,392 (—4	0,110 (—5	0,609 (—7	0,160 (—8	—
50	0,445 (—3	0,431 (—4	0,402 (—6	0,457 (—9	—	—
75	0,623 (—4	0,877 (—6	0,120 (—8	—	—	—
			$E_\gamma = 0,2 - 0,3$ MeV			
0	0,649 (—2	0,585 (—3	0,185 (—4	0,822 (—6	0,454 (—7	0,161 (—8
30	0,288 (—2	0,321 (—3	0,630 (—5	0,311 (—6	0,136 (—6	0,337 (—9
50	0,187 (—2	0,110 (—3	0,806 (—6	0,132 (—7	0,162 (—9	—
75	0,314 (—3	0,104 (—4	0,585 (—7	0,940 (—9	—	—
			$E_\gamma = 0,3 - 0,5$ MeV			
0	0,762 (—2	0,223 (—2	0,947 (—4	0,520 (—5	0,162 (—6	0,364 (—8
30	0,622 (—2	0,138 (—2	0,606 (—4	0,403 (—5	0,150 (—6	0,318 (—8
50	0,463 (—2	0,587 (—3	0,922 (—5	0,347 (—6	0,634 (—8	0,834 (—10
75	0,957 (—3	0,642 (—4	0,157 (—5	0,681 (—7	0,124 (—8	—
			$E_\gamma = 0,5 - 0,75$ MeV			
0	0,109 (—1	0,492 (—2	0,458 (—3	0,604 (—3	0,730 (—5	0,590 (—6
30	0,110 (—1	0,355 (—2	0,309 (—3	0,390 (—4	0,301 (—5	0,164 (—6
50	0,742 (—2	0,171 (—2	0,120 (—3	0,148 (—4	0,118 (—5	0,493 (—7
75	0,208 (—2	0,175 (—3	0,320 (—5	0,204 (—6	0,870 (—8	0,162 (—9
			$E_\gamma = 0,75 - 1,0$ MeV			
0	0,132 (—1	0,775 (—2	0,132 (—2	0,274 (—3	0,316 (—4	0,910 (—5
30	0,135 (—1	0,630 (—2	0,718 (—3	0,170 (—3	0,180 (—4	0,147 (—5
50	0,101 (—1	0,340 (—2	0,317 (—3	0,423 (—4	0,511 (—5	0,272 (—6
75	0,292 (—2	0,376 (—3	0,344 (—4	0,214 (—5	0,122 (—6	0,402 (—8
			$E_\gamma = 1,0 - 1,5$ MeV			
0	0,175 (—1	0,117 (—1	0,383 (—2	0,107 (—2	0,163 (—3	0,293 (—4
30	0,175 (—1	0,103 (—1	0,194 (—2	0,499 (—3	0,622 (—4	0,553 (—5
50	0,151 (—1	0,560 (—2	0,105 (—2	0,204 (—3	0,294 (—4	0,244 (—5
75	0,462 (—2	0,721 (—3	0,351 (—2	0,209 (—5	0,135 (—6	0,381 (—8

We can see from Table 5.5 that characteristic angle ψ_0 has a tendency to decrease with increasing energy of primary γ quanta and increasing atomic number Z of the scattering medium.

Information on the angular characteristics of scattered γ radiation with inclined incidence of the initial beam to the surface of the barrier is quite sparse. As a rule, the periodical literature presents only individual examples of results. In [15], the angular distributions of doses of scattered Co^{60} γ radiation were investigated with inclined incidence to shields of iron and aluminum. Figure 5.1 shows the nature of the azimuthal dependence of the angular distribution function of γ quanta scattered on iron.

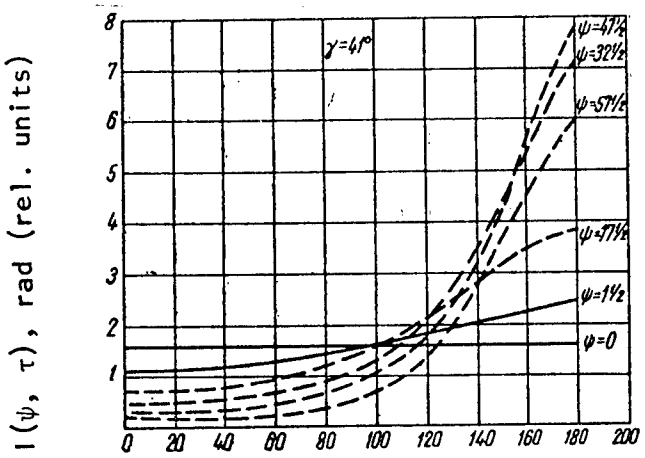

Figure 5.1. Angular Distributions of Co^{60} γ Radiation Dose With Inclined Incidence to Barrier of Iron 2 cm Thick

In [10, 12], it is demonstrated on the basis of experimental studies that the angular distributions of the dose of γ quanta scattered on a shield, as well as the differential and integral spectra are determined by the last layer of the shield if its thickness is over 1-2 free path lengths. The relative values of γ radiation doses depend on the order and are determined by the accummulation factors of the heterogeneous mixtures.

§ 3. Reflection of γ Quanta From Protective Shielding

The integral energy albedo of γ quanta in the range of energies of primary radiation 0.3 MeV < E_γ < 2.0 MeV is inversely proportional to the energy E_γ and the square of the atomic number of the scattering material Z. With increasing density of the material ρ and angle of incidence of the beam for a given Z, the energy albedo increases. The empirical dependence of the energy albedo on E_γ, Z, ρ and γ, according to [16], is

$$A^{\text{п}}_{\gamma E}(E_\gamma, \gamma) = 3{,}2\frac{1}{E_\gamma}\frac{1}{\cos\gamma}\frac{\rho}{Z^2} \qquad (5.12)$$

where 6 < Z < 50 and γ < 80°; and

$$A^{\text{п}}_{\gamma E}(E_\gamma, \gamma) = 3{,}2\frac{1}{E_\gamma}\frac{1}{\cos^2\gamma}\frac{\rho}{Z^2} \qquad (5.13)$$

where Z > 50 and γ < 80°.

In the area of energies of γ quanta of primary radiation 2.0 < E_γ < 10 MeV, according to [17, 18], the dependence of the energy albedo on E_γ is retained, while the dependence on atomic number Z of the scattering material is weaker due to the increasing influence of secondary annihilation radiation. With energy of primary γ quanta E_γ < 0.3 MeV, due to the strong photoelectric absorption, the energy albedo of γ quanta decreases with decreasing E_γ and increasing Z of the scattering material (Figure 5.2) [19].

The dose albedo of γ quanta differs somewhat from the energy albedo. Table 5.6 presents several values of dose and energy albedo for concrete.

The dependences (5.12) and (5.13) presented characterize the albedo of γ radiation for scattering materials of semi-infinite thickness. With a thin reflector layer, the albedo does not reach its maximum value. Experiments [20] have shown that the dependence of γ quantum albedo on thickness of the scattering material δ with normal incidence of the primary radiation is described for materials with Z ≤ 26 by the empirical expression

$$A^{\text{п}}_{\gamma d}(\delta) = A^{\text{п}}_{\gamma d}(\infty)\left[1 - e^{-2\rho(E_\gamma)^{\delta}}\right], \qquad (5.14)$$

where $A^{\pi}_{\gamma d}(\infty)$ is the albedo for a semi-infinite scattering material. For heavy materials (lead) this dependence is

$$A^{\pi}_{\gamma d}(\delta) = A^{\pi}_{\gamma d}(\infty)\,[1 - e^{-8\mu(E_\gamma)\delta}]. \qquad (5.15)$$

Table 5.6

DOSE AND ENERGY ALBEDO OF γ QUANTA FOR CONCRETE

γ, Degrees	Albedo	Energy of γ Quanta E_γ, MeV			
		0,2	0,5	1,0	2,0
0	$A^{\pi}_{\gamma, E}(\gamma, E_\gamma)$	0,154	0,085	0,041	0,017
	$A^{\pi}_{\gamma, д}(\gamma, E_\gamma)$	0,138	0,074	0,040	0,020
30	$A^{\pi}_{\gamma, E}(\gamma, E_\gamma)$	0,170	0,097	0,051	0,021
	$A^{\pi}_{\gamma, д}(\gamma, E_\gamma)$	0,148	0,083	0,045	0,023
60	$A^{\pi}_{\gamma, E}(\gamma, E_\gamma)$	0,242	0,160	0,098	0,048
	$A^{\pi}_{\gamma, д}(\gamma, E_\gamma)$	0,220	0,146	0,099	0,055
~90	$A^{\pi}_{\gamma, E}(\gamma, E_\gamma)$	0,500	0,413	0,348	0,266
	$A^{\pi}_{\gamma, д}(\gamma, E_\gamma)$	0,470	0,395	0,355	0,303

With thicknesses equal to approximately two mean free path lengths, the scattering material can be considered semi-infinite from the standpoint of back scattering of γ radiation.

The spectra of the reflected radiation are significantly softer than the primary γ quanta. As an example, Figure 5.3 shows the distribution of Co^{60} γ quanta reflected from concrete by energies for cases of normal and inclined incidence of primary γ radiation to the concrete. As we can see, the spectrum of the reflected radiation in all cases has

a maximum at 0.16-0.30 MeV, regardless of the angle of incidence of the primary radiation. With inclined incidence of the γ radiation to the barrier surface, the spectrum of the reflected radiation becomes harder. This is natural, since in this case the γ quanta may return through the surface of the absorber after being scattered at lower angles and, consequently, changing their energy less than in reflection of the normal incident radiation.

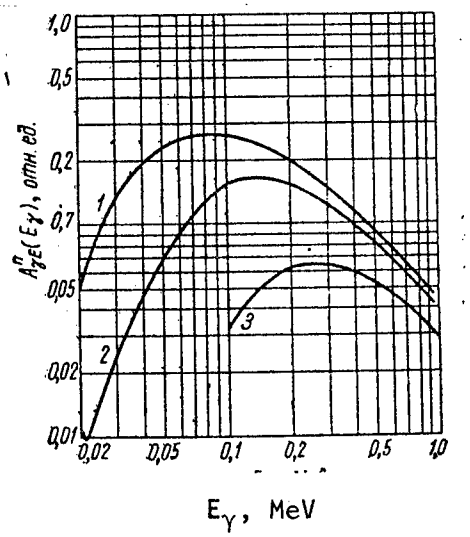

Figure 5.2.

The nature of the angular dependence of back scattered radiation is determined by the competition of two processes: on the one hand, the probability of scattering and hardness of γ quanta increase with decreasing scattering angles; on the other hand, the path traveled by the scattered radiation in the material increases, consequently increasing the probability of absorption, which is greater, the greater the Z of the scattering material. Therefore, the angular distribution of intensities of scattered γ radiation is anisotropic.

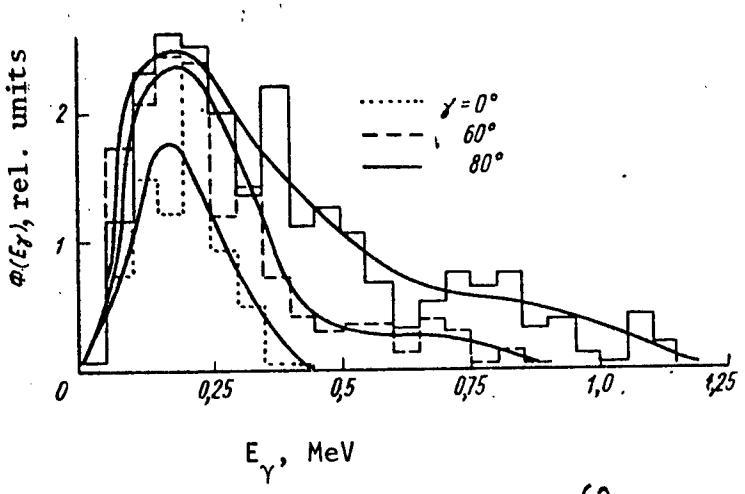

Figure 5.3. Distribution of Co^{60} γ Quanta Reflected From Concrete by Energies for Cases of Normal and Inclined Incidence of Primary Radiation to Concrete

The differential albedo of the dose of γ radiation, describing the relative value of the dose of γ quanta scattered per unit solid angle in the direction characterized by reflection angle ψ is determined by the following semi-empirical formula, suggested in [21]:

$$a_{\gamma d}^{\text{пт}}(E_\gamma, \gamma, \psi, \tau) = \frac{C\Upsilon(\psi_s)\,10^{26} + C'}{1 + \cos\gamma \sec\psi}, \qquad (5.16)$$

where $\Gamma(\psi_s)$ is the differential cross section of Comptom scattering per electron; C and C' are empirical constants, depending only on the energy of the incident radiation E_γ and the composition of the reflector. The scattering angle ψ_s is determined from expression (4.18). Expression (5.16) describes the differential albedo in concepts of current. For transition to flux quantities, it must be divided by cos ψ.

Based on expression (5.16), we can also calculate the integral albedo:

$$A_{\gamma d}^{\text{пт}}(E_\gamma, \gamma) = C\left\{\int_0^1 \frac{d(\cos\gamma)}{1 + \cos\gamma \sec\psi} \int_0^{2\pi} \Upsilon(\psi_s)\,10^{26} d\tau\right\} + C'\left\{\left[1 - \cos\gamma \ln\frac{1 + \cos\gamma}{\cos\gamma}\right]\right\}. \qquad (5.17)$$

The values of empirical constants C and C' produced for various materials in [22] are presented on Table 5.7.

Table 5.7

PARAMETERS C AND C' FOR CALCULATION OF DIFFERENTIAL DOSE ALBEDO USING SEMI-EMPIRICAL FORMULA (5.16)

Scattering Material	E_γ, MeV	C	C'
Water	0,2	−0,0187±0,0027	0,1327±0,0054
	0,662	0,0309±0,0047	0,0253±0,0034
	1,00	0,0470±0,0053	0,0151±0,0025
	2,50	0,0995±0,0068	0,0058±0,0010
	6,13	0,1861±0,0107	0,0035±0,0005
Concrete	0,2	0,0023±0,0038	0,0737±0,0065
	0,662	0,0347±0,0050	0,0197±0,0035
	1,00	0,0503±0,0056	0,0118±0,0025
	2,50	0,0999±0,0078	0,0051±0,0011
	6,13	0,1717±0,0103	0,0048±0,0005
Iron	0,2	0,0272±0,0033	0,0100±0,0062
	0,662	0,0430±0,0045	0,0063±0,0030
	1,00	0,0555±0,0049	0,0045±0,0021
	2,50	0,1009±0,0073	0,0044±0,0010
	6,13	0,1447±0,0101	0,0077±0,0006
Lead	0,2	0,0044±0,0002	0,0050±0,0004
	0,662	0,0308±0,0015	0,0100±0,0007
	1,00	0,0452±0,0013	0,0083±0,0004
	2,50	0,0882±0,0014	0,0001±0,0002
	6,13	0,1126±0,0048	0,0063±0,0002

In [22], the analytic dependences of constants C and C' on incident radiation energy are suggested for calculation of the differential albedo of concrete:

$$C = \exp[-2{,}92 + 0{,}681 \ln E_\gamma + 0{,}0111 (\ln E_\gamma)^2 - 0{,}0413 (\ln E_\gamma)^3];$$

$$C' = \exp[-5{,}89 + 0{,}275 (E_\gamma - 3{,}25)^2] \text{ where } 0{,}1 \leqslant E_\gamma \leqslant 1{,}0 \text{ MeV}; \quad (5.18)$$

$$C' = \exp[-4{,}86 + 0{,}36 (E_\gamma - 2{,}0)^2] \text{ where } 1{,}0 < E_\gamma \leqslant 2 \text{ MeV};$$

$$C' = \exp[-4{,}83 - 0{,}013 E_\gamma] \text{ where } 2{,}0 < E_\gamma \leqslant 10 \text{ MeV}. \quad (5.19)$$

134

§ 4. Attenuation of β Radiation in Protective Shielding

For thick shielding with mass thickness $\delta > 1\text{-}2$ g/cm^2, in which an electron is fully decelerated, the total energy of the Bremstrahlung radiation generated is proportional to the first power of the atomic number of the absorbing material Z [23]

$$\widehat{C}(E_e, Z) = 5{,}77 \cdot 10^{-4} Z E_e^2 \text{ MeV/electron}, \qquad (5.20)$$

where E_e is the energy of monoenergetic electrons.

The dose of Bremstrahlung at the internal surface of the shield can be calculated using the equation

$$D_{тр} = \int_{E_\gamma} K_{тр}(E_\gamma)\, \eta_{тр}(E_\gamma)\, \Delta N_{тр}(E_\gamma)\, E_\gamma dE_\gamma, \qquad (5.21)$$

where $\Delta N_{tp}(E_\gamma)$ is the number of Bremstrahlung quanta with energies in the interval from E_γ to $E_\gamma + dE_\gamma$, emitted by the source per unit time per unit area; $\eta_{tp}(E_\gamma)$ is the transfer factor from flux to dose power; it is equal to $1.6 \cdot 10^{-8}\ \mu_a(E_\gamma)$, where $\mu_a(E_\gamma)$ is the electron conversion factor for biological tissue (cm^2/g); $K_{tp}(E_\gamma)$ is the Bremstrahlung radiation attenuation factor of the shield material.

For electrons with energy E_e, the Bremstrahlung radiation spectrum

$$N_{тр}(E_\gamma) = I(E_e)\, \Phi_{тр}(E_\gamma)\, \widehat{C}(E_e, Z), \qquad (5.22)$$

where $I(E_e)$ is the current of electrons with energy E_e through the surface of the screen, related to each unit energy interval; $F_{tp}(E_\gamma)$ is the relative contribution of Bremstrahlung radiation of the various spectral components.

The spectral distribution of Bremstrahlung radiation with complete deceleration of the electrons, roughtly speaking, is independent of the atomic number of the absorber and the electron energy. It is demonstrated in [20], that the energy radiated per unit interval of energies is expressed approximately by the formula

$$\Phi_{\text{тр}}(E_\gamma) = \text{const}\left[4\left(1 - \frac{E_\gamma}{E_e}\right) - 3\frac{E_\gamma}{E_e}\ln\left(\frac{E_e}{E_\gamma}\right)\right]. \qquad (5.23)$$

Table 5.8 presents the relative contributions of various spectral components of Bremstrahlung radiation calculated according to this formula.

Table 5.8

RELATIVE CONTRIBUTIONS OF VARIOUS SPECTRAL COMPONENTS OF BREMSTRAHLUNG

E_γ/E_e	$\Phi_{\text{тр}}(E_\gamma)$, %	E_γ/E_e	$\Phi_{\text{тр}}(E_\gamma)$, %
0—0,1	26,9	0,5—0,6	6,5
0,1—0,2	20,5	0,6—0,7	4,5
0,2—0,3	15,8	0,7—0,8	2,8
0,3—0,4	12,1	0,8—0,9	1,5
0,4—0,5	9,0	0,9—1,0	0,4

The final expression for Bremstrahlung radiation dose power considering attenuation in the shield will be:

$$D_{\text{тр}} = 1{,}8\cdot 10^{-8}\int_{E_e} I(E_e)\,\widehat{C}(E_e, Z)\,dE_e \int_{E_\gamma} K_{\text{тр}}(E_\gamma)\times \times \mu_a(E_\gamma)\,\Phi_{\text{тр}}(E_\gamma)\,dE_\gamma. \qquad (5.24)$$

The attenuatio of Bremstrahlung radiation by the shield material can be considered if we assume that the radiation formed in an elementary deceleration event is sufficiently isotropic. With a shield thickness of δ, the attenuation factor for Bremstrahlung radiation can be calculated using the expression

$$K_{\text{тр}}(E_\gamma) = B_{\text{тр}}(E_\gamma, \delta)\,Ei[-\mu(E_\gamma)\delta], \qquad (5.25)$$

where the function Ei is the integral exponent

$$Ei(x) = \int_x^\infty \frac{e^{-y}\,dy}{y}.$$

The Bremstrahlung γ radiation dose accummulation factors $B_{tp}(E_\gamma)\delta)$ can be produced on the basis of the data of [24, 25].

In [26], based on analysis of Monte Carlo method calculations of the transmission of electrons with energies of 0.4-10 MeV through various materials, a formula is suggested for calculation of the attenuation factor of electrons with normal incidence to the screen:

$$K_e(E_e, \bar{\delta}, Z) = \exp\left[-\left(\frac{0{,}634E_e Z^{-0,23}}{\bar{\delta}^{0,848}}\right)^{-7(Z-3{,}25)^{-0,24}}\right], \qquad (5.26)$$

where E_e is the energy of the incident electrons, MeV; $\bar{\delta}$ is the mass thickness of the shield, g/cm^2.

The thickness of the absorbed dose of penetrating electrons with initial spectrum $\Phi(E_e)$ can be calculated from the expression

$$D_e = 0{,}8\cdot 10^{-8}\int_{E_e} \Phi(E_e)\frac{E_e}{\lambda(E_e)}K_e(E_e, \delta, Z)\times \times dE_e \frac{\text{mrad}}{\text{hr}} \Big/ \frac{\text{electrons}}{\text{cm}^2\cdot\text{sec}} \qquad (5.27)$$

where $\lambda(E_e)$ is the path of an electron with energy E_e in biological tissue, g/cm^2. The value of the paths of electrons can be produced using formula [25]

$$\lambda(E_e) = (0{,}542E_e - 0{,}133)\ \text{g/cm}^2. \qquad (5.28)$$

It should be noted on the whole that with a shielding thickness $\bar{\delta} \leq 1.0$ g/cm^2, the majority of the total dose of β radiation is created by electrons penetrating through the shield. With a shield thickness $\bar{\delta} > 1\text{-}2$ g/cm^2, the dose is determined entirely by Bremstrahlung.

§ 5. Yield of Secondary γ Radiation From the Shield

As they pass through the shield and interact with the nuclei of elements in the composition of the shield, neutrons generate secondary γ radiation. The formation of secondary γ radiation primarily results from the reaction of radiation capture of neutrons. Secondary γ radiation in some cases makes a significant contribution to the total dose beyond the shielding.

In order to calculate the dose of secondary γ radiation beyond the shielding, it is necessary to know the spectral composition of the capture γ radiation, its total production and its angular distribution.

The spectral composition of prompt γ quanta with radiation capture of thermal neutrons has been well studied, and the primary results were collected in [27]. The yield of capture γ radiation from the protective barrier is determined primarily by the distribution of sources of capture γ radiation through the volume of the barrier. The distribution of sources of capture γ radiation in the absorbing layer corresponds to the spatial distribution of thermal neutrons in the shield and neutrons moderated to thermal velocities.

The rate of absorption of neutrons per unit volume can be written as

$$\Sigma_a \Phi_{th}, \tag{5.29}$$

where Σ_a is the macroscopic cross section of absorption of thermal neutrons; Φ_{th} is the flux of thermal neutrons.

The distribution of the flux of thermal neutrons in the barrier can be found by solving the diffusion equation

$$\frac{d^2\Phi_{th}(x)}{dx^2} - \frac{\Phi_{th}(x)}{L^2} + \frac{S(x)}{D} = 0, \tag{5.30}$$

where S(x) is the density of generation of thermal neutrons in the shield barrier itself; L is the diffusion length of thermal neutrons in the shielding medium; D is the coefficient of diffusion of thermal neutrons.

If generation of thermal neutrons does not occur in the barrier and the only source of these neutrons is the external field of thermal neutrons diffusing inward, the solution of the diffusion equation is as follows:

$$\Phi_{th}(x) = I_{th}(0)\frac{L}{D}\frac{\operatorname{sh}\frac{\delta + 2D - x}{L}}{\operatorname{ch}\frac{\delta + 2D}{L}}, \tag{5.31}$$

where $I_{th}(0)$ is the current of thermal neutrons striking the surface of the shield. Actually, the formation of thermal neutrons in the protective shield always occurs. A portion of the fast neutrons, being moderated, goes over into the group of thermal neutrons, which may be captured by nuclei of the media and thus become sources of capture γ radiation.

In order to solve the diffusion equation in this case it is convenient to use the two-group theory in the form in which it is used for calculation of the fluxes of thermal and fast neutrons in reactor design. In the case of neutrons of moderate energies, the theory is quite sufficient, but for neutrons having high energy and penetrating to greater distances, the theory produces significant error.

The solution in the two-group approximation is

$$\Phi_{th}(0) = \frac{I_f(0)}{\left(\frac{L_s}{L}\right)^2 - 1}\left(\frac{L_s \operatorname{sh}\frac{\delta+2D-x}{L_s}}{D \operatorname{ch}\frac{\delta+2D}{L_s}} - \frac{L}{D}\frac{\operatorname{sh}\frac{\delta+2D-x}{L}}{\operatorname{ch}\frac{\delta+2D}{L}}\right) + \tag{5.32}$$

$$+ I_{th}(0)\frac{L}{D}\frac{\operatorname{sh}\frac{\delta+2D-x}{L}}{\operatorname{ch}\frac{\delta+2D}{L}}.$$

where L_s is the length of moderation.

The nature of the distribution of sources of capture γ quanta in the shield medium corresponds with the distribution of thermal neutrons in the medium. The number of γ quanta produced in a unit volume about point N is proportional to $\Phi(x)\Sigma_a$.

Thus, in order to determine the yield of capture γ quanta, we must find the flux of capture γ quanta at the surface of the shield generated at various depths in the barrier.

Let us study an infinitely thin flat isotropic source of γ quanta located at depth 8 in a plate with a thickness of δ (Figure 5.4).

Let us determine the flux Φ_γ -- the number of γ quanta which are not scattered -- at point A.

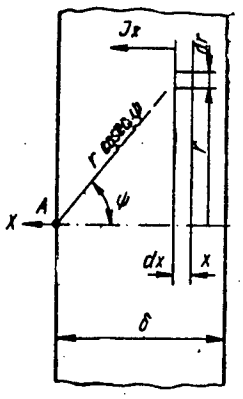

Figure 5.4. Calculation of Yield of Capture γ Radiation From Shielding

We represent by r the distance from a certain point in the plane of the source to the x-axis, passing through point A perpendicular to the plane of the source. The number of photons leaving each unit area of the source per unit time is equal to I_x. If these photons are radiated isotropically, their flux at point A will be

$$d\Phi_\gamma = I_x e^{-\mu(E_\gamma)\delta \sec\psi} \frac{dr}{r \operatorname{cosec}^2 \psi}. \tag{5.33}$$

The flux of photons Φ_γ at point A from the entire plane of the source will be:

$$\Phi_\gamma = I_x \int_{\mu\delta}^{\infty} e^{-y} \frac{dy}{y} = -I_x Ei(-\mu\delta), \tag{5.34}$$

where -Ei (-z) = $\int_z^\infty e^{-y} \frac{dy}{y}$ is the integral exponent.

In order to consider scattered photons, we must introduce the accummulation factor B, i. e.

$$\Phi_\gamma = -I_x BEi(-\mu\delta). \tag{5.35}$$

Let us now determine the value of current dI of γ quanta at point B from point sources located in the circle r, r + dr:

$$dI = I_x = e^{-\mu\delta \sec\psi} \frac{dr}{r \operatorname{cosec}^2 \psi} \cos\psi. \tag{5.36}$$

The total current of γ quanta at point A from the entire flat source will be

$$I = I_x [e^{-\mu\delta} + \mu\delta Ei(-\mu\delta)]. \tag{5.37}$$

If the thermal neutrons are captured during the process of diffusion through the plate shown on Figure 5.4, we can use equation (5.31), where there are no fast neutrons, to determine the rate of capture of thermal neutrons per unit area in a layer of thickness dx:

$$\Sigma_a I_{th}(0) \frac{L}{D} \frac{\operatorname{sh} \frac{\delta + 2D - x}{L}}{\operatorname{ch} \frac{\delta + 2D}{L}} dx. \tag{5.38}$$

With sufficiently large values of $\frac{\delta+2D}{L}$, this expression is simplified:

$$\eta_\gamma \frac{I_{th}(0)}{L} e^{-x/L} dx, \tag{5.39}$$

where η_γ is the yield of γ quanta per captured neutron.

This formula gives us the number of capture γ quanta arising in a layer of thickness dx per unit surface area.

In layer dx, the currents of γ quanta in direction x and in the opposite direction are equal; therefore,

$$I_x = \frac{1}{2} \frac{I_{th}(0)}{L} e^{-x/L} dx. \tag{5.40}$$

Let us now determine the total current of all capture γ quanta generated in a flat screen of thickness δ. For this, in expression (5.37) we substitute the value of I_x from formula (5.40). A convenient approximation is produced if coefficient μ is replaced by the linear γ quantum energy absorption factor μ_E and at the same time B is assumed

equal to 1. Then we produce the following expression for the resulting current of γ quanta formed in layer dx:

$$\frac{1}{2}\varepsilon_\gamma \frac{I_{th}(0)}{L} e^{-x/L}\left[e^{-\mu_E x} + \mu_E x\, Ei(-\mu_E x)\right] dx,$$

and from all capture γ quanta generated in the barrier and leaving its surface in the direction of the neutron source,

$$I_c = I_{th}(0)\frac{\varepsilon_\gamma}{2L}\int_0^\delta e^{-x/L}\left[e^{-\mu_E x} + \mu_E x Ei(-\mu_E x)\right] dx = \tag{5.41}$$

$$= I_{th}(0)\frac{\varepsilon_\gamma}{2L}\left\{-\left[\frac{e^{-(1/L+\mu_E)x}}{\frac{1}{L}+\mu_E}\right]_0^\delta + \mu_E\int_0^\delta e^{-x/L}\, xEi(-\mu_E x)\, dx\right\},$$

where ε_γ is the total energy of γ radiation generated upon capture of one neutron, equal to the product of the yield η_γ times the mean energy of capture γ quanta.

Integrating this expression [28], we produce

$$I_c = I_{th}(0)\frac{E_\gamma}{2}\mu_E L\left\{\frac{1}{\mu_E L}\left[1 - e^{-(1+\mu_E L)\delta/L}\right] - \left(\frac{\delta}{L}+1\right)\times\right.$$
$$\left.\times e^{-\delta/L} Ei\left(-\mu_E L\frac{\delta}{L}\right) + Ei\left[-(1+\mu_E L)\frac{\delta}{L}\right] - \ln\frac{1+\mu_E L}{\mu_E L}\right\} = \tag{5.42}$$
$$= I_{th}(0) K_c.$$

Calculation of the flux through the surface opposite to the surface struck by the neutrons is performed similarly:

$$I_c' = I_{th}(0)\frac{\varepsilon_\gamma}{2L}\int_0^\delta e^{-x/L}\left\{e^{-\mu_E(\delta-x)} + \mu_E(\delta-x) Ei\left[-\mu_E(\delta-x)\right]\right\} dx =$$

$$= I_{th}(0)\frac{\varepsilon_\gamma}{2L}\left\{-\frac{e^{-\mu_E\delta}}{\frac{1}{L}-\mu_E}\left[e^{-(1/L-\mu_E)x}\right]_0^\delta + \mu_E e^{-\delta/L}\int_0^\delta e^{\delta-x/L}(\delta-x)\times\right. \tag{5.43}$$
$$\left.\times Ei\left[-\mu_E(\delta-x]\, d(\delta-x)\right\}.\right.$$

After integration [28] we produce the function K_c', characterizing the yield of energy of capture γ quanta generated per incident thermal neutron on the opposite surface of the shield

$$I_c' = I_{th}(0)\,\varepsilon_\gamma \frac{\mu_E L}{2} e^{-\delta/L}\left\{\frac{1}{\mu_E L}\left[e^{(1-\mu_E L)\,\delta/L} - 1\right] + \right.$$
$$\left. + \overline{Ei}\left[(1-\mu_E L)\frac{\delta}{L}\right] - \ln\frac{1-\mu_E L}{\mu_E L}\right\} = I_{th}(0) K_c', \qquad (5.44)$$

where

$$\overline{Ei}(z) = \int_{-\infty}^{z} \frac{e^y}{y}\,dy.$$

If $(1 - \mu_E L)$ is negative, we must replace the expression

$$\overline{Ei}\,\mu_E\left[(1-\mu_E L)\frac{\delta}{L}\right] - \ln\frac{1-\mu_E L}{\mu_E L}$$

with another expression

$$Ei\left[-(-\mu_E L - 1)\frac{\delta}{L}\right] - \ln\frac{\mu_E L - 1}{\mu_E L}. \qquad (5.45)$$

In designing shielding, we must consider also the capture γ radiation formed upon capture of moderated fast neutrons. To do this, in place of expression (5.39) we use the first portion of formula (5.32) which, with sufficiently high values of $\delta + 2D/L_s$ and $\delta + 2D/L$, will be:

$$\frac{\frac{I_f(0)}{L_s}\left(\frac{L_s}{L}\right)^2}{\left(\frac{L_s}{L}\right)^2 - 1} \cdot e^{-x/L_s} - \frac{\frac{I_f(0)}{L}}{\left(\frac{L_s}{L}\right)^2 - 1} e^{-x/L}. \qquad (5.46)$$

This expression must be introduced to formula (5.44).

In order to simplify calculation, we can replace L with L_s in (5.44) [28]:

$$\overline{I}'_{cf} = I_f(0)\,\varepsilon_\gamma \frac{\mu_E L_s}{2} e^{-\delta/L_s}\left\{\frac{1}{\mu_E L_s}\left[e^{(1-\mu_E L_s)} - 1\right] + \right.$$
$$+\left(\frac{\delta}{L} - 1\right)e^{\delta/L_s}\,Ei\left(-\mu_E L_s \frac{\delta}{L_s}\right) + \overline{Ei}\left[(1-\mu_E L_s)\frac{\delta}{L_s}\right] - \qquad (5.47)$$
$$\left. - \ln\frac{1-\mu_E L_s}{\mu_E L_s}\right\} = I_f(0)\,\overline{K}'_{cf}.$$

According to expression (5.46), the value of $\overline{K}_{cf}'$ produced must be multiplied by

$$\frac{\left(\frac{L_s}{L}\right)^2}{\left(\frac{L_s}{L}\right)^2 - 1},$$

and the value of K_c', corresponding to the same conditions, by

$$\frac{1}{\left(\frac{L_s}{L}\right)^2 - 1}$$

then we subtract the second product from the first product:

$$K'_{cf} = \overline{K}'_{cf}\frac{\left(\frac{L_s}{L}\right)^2}{\left(\frac{L_s}{L}\right)^2 - 1} - K'_c\frac{1}{\left(\frac{L_s}{L}\right)^2 - 1}. \qquad (5.48)$$

Similarly, we can find the yield of capture γ radiation energy on the side of the source:

$$K_{cf} = \overline{K}_{cf}\frac{\left(\frac{L_s}{L}\right)^2}{\left(\frac{L_s}{L}\right)^2 - 1} - K_c\frac{1}{\left(\frac{L_s}{L}\right)^2 - 1}. \qquad (5.49)$$

These functions characterize the yield of capture γ radiation on the surface of the shield resulting from moderated neutrons.

Table 5.9 shows constants for calculation of the yield of capture γ radiation from certain materials.

Table 5.9

CONSTANTS FOR CALCULATION OF YIELD OF CAPTURE γ RADIATION

Material	L, см	D, см	Σ_a, см	L_s, см	n_γ, Quanta/Neutrons	n_γ av, MeV	μ_E, $см^{-1}$
Water	2,9	0,14	0,017	5,6	1,0	2,23	9,0241
Iron	1,5	0,461	0,205	16,0	1,1	6,4	0,177
Concrete	4,85	0,342	0,0146	8,65	1,0	6,0	0,048

The results of calculation of the yield of capture γ radiation from shield barriers of various compositions and thickness are presented on Figure 5.5.

One important characteristic of secondary γ radiation is its angular distribution. If the protective shield is represented as a barrier of infinite area and thickness δ, the angular distributions of the capture γ radiation leaving the barrier will be independent of the azimuthal angle and the points near which they are studied.

Since the distribution function of neutron capture density can be expressed by an exponential dependence, simple calculations allow us to produce the angular distribution function of capture γ radiation energy flux generated by thermal neutrons diffusing from without:

$$f'_c(\psi) = \frac{I_{th}(0)}{I'_c(\delta)} \varepsilon_\gamma \frac{\cos\psi}{4\pi} \frac{e^{-\frac{\mu_E \delta}{\cos\psi}} - e^{-\frac{\delta}{L}}}{\cos\psi - \mu_E L}; \tag{5.50}$$

$$f_c(\psi) = \frac{I_{th}(0)}{I_c(\delta)} \varepsilon_\gamma \frac{\cos\psi}{4\pi} \frac{1 - e^{-\frac{\delta}{\cos\psi}\left(\mu_E + \frac{\cos\psi}{L}\right)}}{L\mu_E + \cos\psi}. \tag{5.51}$$

The angular distribution functions of capture γ radiation energy flux resulting from moderated fast neutrons can be represented as

$$f'_{cf}(\psi) = \frac{I_f(0)\,\varepsilon_\gamma}{I'_{cf}\left[\left(\frac{L_s}{L}\right)^2 - 1\right]} \frac{\cos\psi}{4\pi}\left[\left(\frac{L_s}{L}\right)^2 \frac{e^{-\frac{\mu_E \delta}{\cos\psi}} - e^{-\frac{\delta}{L_s}}}{\cos\psi - \mu_E L_s} - \frac{e^{-\frac{\mu_E \delta}{\cos\psi}} - e^{-\frac{\delta}{L}}}{\cos\psi - \mu_E L}\right]; \tag{5.52}$$

$$f_{cf}(\psi) = \frac{I_f(0)\,\varepsilon_\gamma}{I_{cf}\left[\left(\frac{L_s}{L}\right)^2 - 1\right]} \frac{\cos\psi}{4\pi}\left[\left(\frac{L_s}{L}\right)^2 \times \right.$$

$$\left. - \frac{1 - e^{-\frac{\delta}{\cos\psi}\left(\mu_E - \frac{\cos\psi}{L_s}\right)}}{L_s\,\mu_E - \cos\psi} - \frac{1 - e^{-\frac{\delta}{\cos\psi}\left(\mu_E - \frac{\cos\psi}{L}\right)}}{L\mu_E + \cos\psi}\right]. \tag{5.53}$$

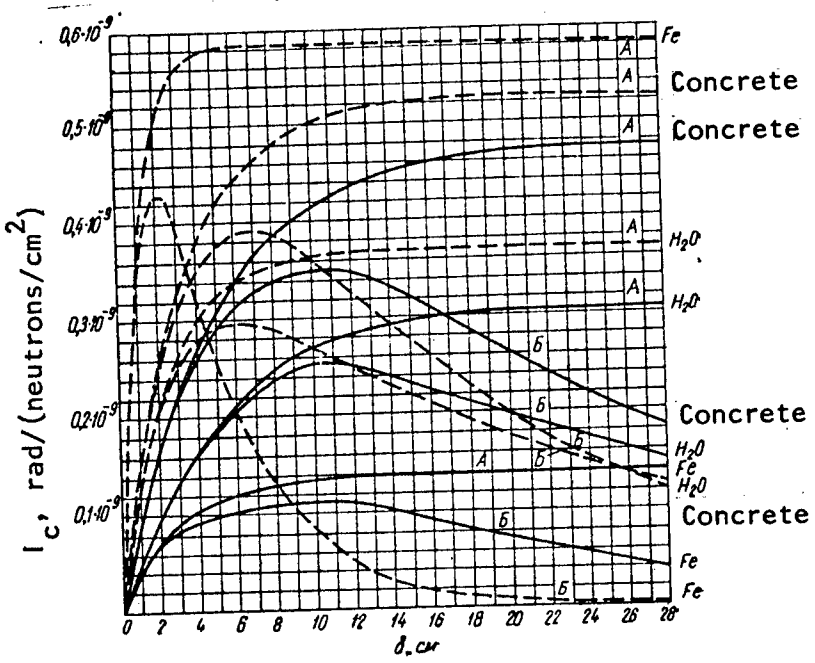

Figure 5.5. Functions of Yield of Secondary γ Radiation From Protective Barrier: A, on side of source (K); B, on opposite side (K'); ———, due to capture of fast neutrons moderated in barrier (K_{cf}); -----, due to capture of thermal neutrons striking barrier from without (K_c)

These functions characterize the portion of the total energy (dose) of capture γ radiation on the surface of the barrier leaving per unit solid angle in the direction defined by angle γ, which is counted from the normal to the surface of the barrier.

Bibliography

1. Leypunskiy, O. I. et al., *Rasprostraneniye Gamma-Kvantov v Veshchestve* [Propagation of Gamma Quanta in Matter], Moscow, Fizmatgiz Press, 1960.

2. Marenkov, O. S., Derzhimanov, R. S., *Atomnaya Energiya*, Vol. 18, No. 5, p. 520 (1965).

3. Raso, D., *Health Phys.*, Vol. 5, p. 126 (1961).

4. Raso, D., *Trans. of the ANS*, Vol. 5, No. 1, p. 218 (1962).

5. Goryachev, I. V. et al., *Atomnaya Energiya*, Vol. 26, No 6, p. 542 (1969).

6. Broder, D. L., *Voprosy Fiziki Zashchity Reaktorov* [Problems of the Physics of Reactor Shielding -- Collection of Works], No. 1, 1963, p. 198.

7. Kayurin, Yu. P., Shalin, B. A., *Voprosy Fiziki Zashchity Reaktorov* [Problems of Physics of Reactor Shielding -- Collection of Works], Vol. 2, 1966, p. 160.

8. Stolyarova, Ye. L. et al., *Pribory i Metody Analiza Izlucheniy* [Instruments and Methods for Analysis of Radiation -- Collection of Works], No. 3, Moscow, Gosatomizdat Press, 1962, p. 15.

9. Larichev, A. V., *Atomnaya Energiya*, Vol. 11, No. 5, p. 443 (1961).

10. Larichev, A. V., Klimanova, L. F., *Pribory i Metody Analiza Izlucheniy* [Instruments and Methods for Analysis of Radiation -- Collection of Works], 1962, p. 37.

11. Shirkin, L. M., *Atomnaya Energiya*, Vol. 19, p. 394 (1965).

12. Larichev, A. V., *Voprosy Fiziki Zashchity Reaktorov* [Problems of Physics of Reactor Shielding -- Collection of Works], 1963, p. 214.

13. Hubbel, J. et al., *Phys. Rev.*, Vol. 108, p. 1361 (1957).

14. Larichev, A. V., Mitin, V. I., *Voprosy Dozimetrii i Zashchity Ot Izlucheniy* [Problems of Dosimetry and Shielding From Radiation -- Collection of Works], No. 2, Moscow, Atomizdat Press, 1963, p. 47.

15. Dahlstrom, T. S., Thompson, W. E., *Trans. of the ANS*, Vol. 5, (1962).

16. Bulatov, B. P., Garusov, Ye. A., *Atomnaya Energiya*, Vol. 5, p. 631 (1958).

17. Perkins, J. E., *Appl. Phys.*, Vol. 26, p. 655 (1955).

18. Leimdorfer, M., *Nucl. Sci. Engng.*, Vol. 17, pg. 345, 357 (1963).

19. Johns, H. E. et al., *Brit. J. Radiol.*, Vol. 27, p. 32 (1953).

20. Bulatov, B. P., Leypunskiy, O. I., *Atomnaya Energiya*, Vol. 7, p. 551 (1959).

21. Raso, D. L., *Nucl. Sci. Engng.*, Vol. 17, p. 411 (1963).

22. Chilton, A. B., Davisson, C. M., *Trans. of the ANS*, Vol. 8, No. 2, p. 656 (1965).

23. Wyard, S. J., *Nucleonics*, Vol. 13, No. 7, p. 44 (1955).

24. Larichev, A. V., Listin, V. I., *Voprosy Dozimetrii i Zashchity Ot Izlucheniy* [Problems of Dosimetry and Shielding From Radiation -- Collection of Works], 1962, p. 55.

25. Golub, V. V., Panchenko, A. M., *Atomnaya Energiya*, Vol. 24, No. 1, p. 71 (1968).

26. Mar, B. W., *Trans. of the ANS*, Vol. 7, No. 2, p. 322 (1964).

27. Groshev, L. V. et al., *Atlas Spektrov γ-Luchey Radiatsionnogo Zakhvata Teplovykh Neytronov* [Atlas of Spectra of γ-Rays From Radiation Capture of Thermal Neutrons], Moscow, Atomizdat Press, 1958.

28. Golubev, B. P., *Dozimetriya i Zashchita Ot Ioniziruyushchikh Izlucheniy* [Dosimetry and Shielding From Ionizing Radiation], Moscow-Leningrad, Gosenergoizdat Press, 1963.

CHAPTER 6. DESIGN OF SHIELDING OF SURFACE STRUCTURES FROM THE RADIATION OF A NUCLEAR EXPLOSION

§ 1. General Form of Angular Distribution Functions of Doses of Neutrons and γ Radiation During a Nuclear Explosion

The angular energy distribution functions of neutrons and γ radiation from a nuclear explosion presented in Chapter 2 describe the field of radiation near the surface of the earth when the position of the center is known. However, the specific position of the center of an explosion is always unknown.

If the distribution of probability densities of appearance of centers of explosions in the azimuthal direction around a position to be designed is considered even, corresponding to the rule of circular scattering of shells relative to an aiming point, the characteristics of the shielding properties of a structure can be determined as the mean result produced for various azimuthal positions of the epicenter of the explosion around the object being designed. This approach greatly increases the volume of calculation in determining the protective properties of a structure. A significant reduction of the required volume of calculation can be achieved if we do not use the expressions relating to a fixed explosion center as the angular distribution functions, but rather use certain general functions considering the equal probability of appearnace of an explosion at various azimuthal positions [1].

For neutrons, this function can be calculated as follows:

$$F_n(\Omega, \beta) = \frac{1}{\pi}\int_0^{\pi} \{0{,}033 + 0{,}4045\exp[-0{,}03345\arccos \times (\sin\beta\cos\varphi\cos\alpha + \cos\beta\cos\alpha)]\}\, d\varphi \ \text{ster}^{-1}. \quad (6.1)$$

the results of calculation of this generalized angular distribution function for neutrons of a nuclear explosion, based on expression (6.1) are

shown on Figure 6.1. This function describes the share of the total dose of neutrons arriving at a detector per unit solid angle from the direction determined by angle β, which is read from the normal to the surface of the earth.

The angular distribution functions of doses of fragment γ radiation are calculated similarly:

$$F_f(\Omega, \beta) = \frac{1}{\pi} \int_0^{\pi} \{0{,}0092 + 3{,}22 \exp[-0{,}08 \arccos(\sin\beta \times \cos\varphi \cos\alpha + \cos\beta \sin\alpha)]\}\, d\varphi \tag{6.2}$$

as are the functions for capture γ radiation

$$F_c(\Omega, \beta) = \frac{1}{\pi} \int_0^{\pi} \{0{,}008 + 2{,}11 \exp[-0{,}065 \arccos(\sin\beta \times \cos\varphi \cos\alpha + \cos\beta \sin\alpha)]\}\, d\varphi. \tag{6.3}$$

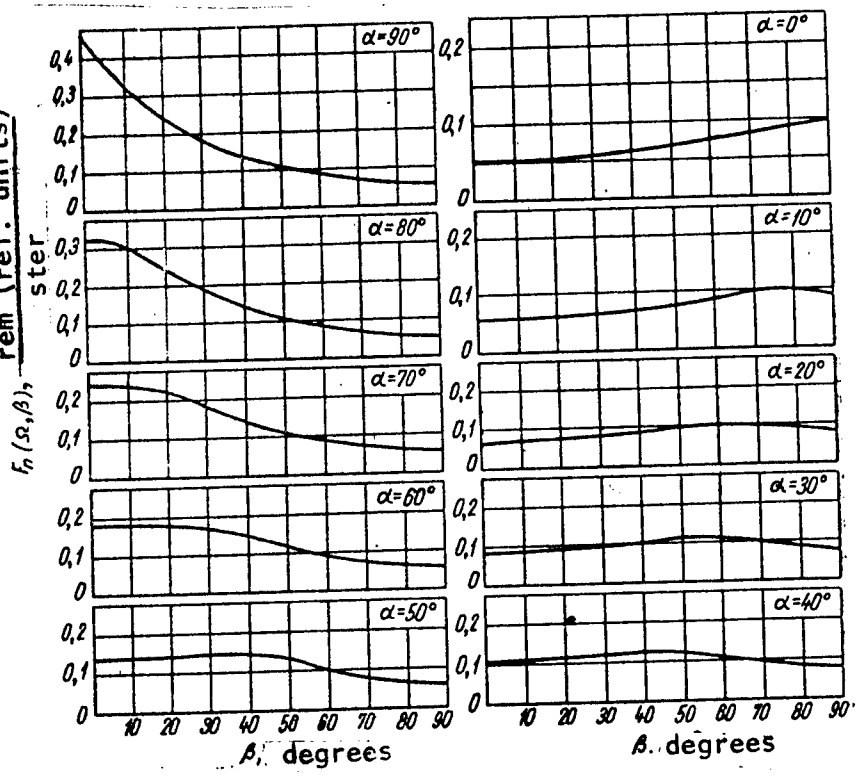

Figure 6.1. Generalized Angular Distribution Functions of Doses of Nuclear Explosion Neutrons $F_n(\Omega, \beta)$

The results of calculations of the generalized angular distribution functions of the γ radiation of a nuclear explosion scattered in the air are shown on Figure 6.2. When the data of Figure 6.2 are used in practical calculations for the design of shielding, the quantities $F(\Omega, \beta)$ must be multiplied by the corresponding values of coefficients K_α, calculated in correspondence with the design elevation angle of the explosion α (symbols for angles shown on Figure 2.10).

The generalized angular distribution functions of doses of γ radiation from a nuclear explosion can be conveniently used to estimate the penetration of radiation through spaces in structures, when the γ quanta scattered in the air can act directly on the people in the structure without undergoing the attenuating effects of the walls and roof. These data are insufficient to design closed shielding or sectors covered with various shields, since the spectral characteristics of the radiation change significantly as a function of angle β.

The data presented in Chapter 2 on the spectral and angular distributions of γ quanta scattered in the air following a nuclear explosion allow us to calculate the generalized characteristics of the spectral-angular distributions of the γ radiation. These calculations were performed using the equation

$$F_f(\Omega, \beta, E_\gamma) = \frac{1}{\pi} \int_0^\pi \Xi'_f(0, E_\gamma) [0{,}0092 + 3{,}22 \exp(-0{,}080)] \, d\varphi \qquad (6.4)$$

for fragment γ radiation and

$$F_c(\Omega, \beta, E_\gamma) = \frac{1}{\pi} \int_0^\pi \Xi'_c(\theta, E_\gamma) [0{,}008 + 2{,}11 \exp(-0{,}065\theta)] \, d\varphi \qquad (6.5)$$

for capture γ radiation.

In these expressions $\theta = \arccos(\sin\beta \cos\phi \cos\alpha + \cos\beta \sin\alpha)$. The value of these functions calculated for various energy intervals ΔE_γ, angles β and α are presented in Tables 6.1 and 6.2. When performing calculations using equations (6.4) and (6.5), the functions $\Xi(\theta, E_\gamma)$ were selected from Tables 2.6 and 2.7 in correspondence with the expression

$$\Xi'(0, E_\gamma) = \frac{\Xi(\theta, E_\gamma)}{100}, \qquad (6.6)$$

keeping in mind the assumption that the spectral distribution of the doses

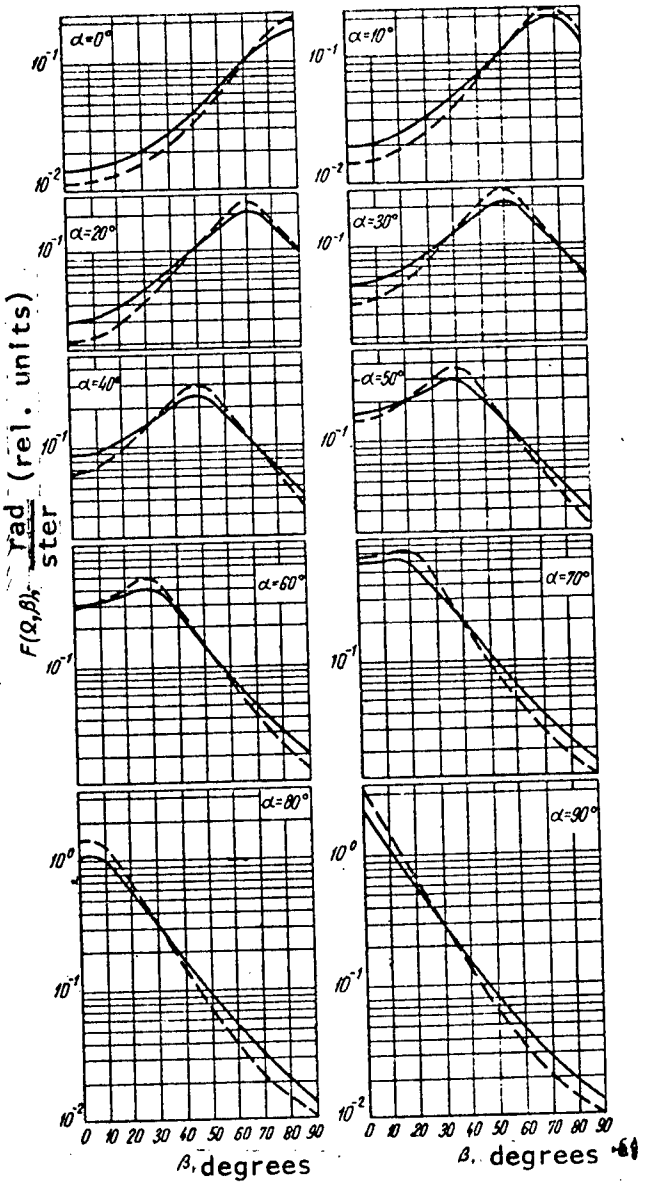

Figure 6.2. Generalized Angular Distribution Function of γ Quantum Doses: ———, for fragment γ radiation $F_f(\Omega, \beta)$; - - - - -, for capture γ radiation $F_c(\Omega, \beta)$

shown in Tables 2.6 and 2.7 for angular intervals $\Delta\theta$ remain unchanged with all angles θ within the limits of the interval $\Delta\theta$ in question.

Thus, the functions $F(\Omega, \beta, E_\gamma)$ produced characterize the portion of the total dose of scattered radiation of this component in the energy interval ΔE_γ arriving per unit solid angle from the direction determined by angle β, under the condition that the distribution function of probability densities of explosion centers in the azimuthal direction relative to the design position is constant. These results represent exhaustive information on radiation acting on structures from the upper half space over the surface of the earth following a nuclear explosion.

As concerns radiation scattered from the ground, no additional calculations are necessary with respect for neutrons, since the angular distribution function of the dose of neutrons reflected from the ground is isotropic. The angular distribution of neutrons incident to the surface of structures from the earth from any direction depends only on angle β, read from the normal to the surface of the earth.

The angular distribution of the dose of initial γ radiation reflected from the earth does not have azimuthal symmetry. However, the use of the assumption of evenness of distribution of the probability of appearance of explosion centers in the azimuthal direction around the calculated position makes it possible to produce a generalized distribution function of γ quantum reflected from the earth, in which the angular dose power depends only on one parameter -- angle β.

The differential albedo of γ quanta of a nuclear explosion can be calculated using the formula

$$a^{\pi}_{\gamma, d} = 2 \sum_{E_\gamma} \int_0^{\pi/2} \int_0^{\pi} \overline{K}_\alpha F(\Omega, \beta, E_\gamma)\, a^{\pi\tau}_{\gamma, d}(E_\gamma, \psi_s) \sin\beta\, d\beta\, d\varphi, \qquad (6.7)$$

where $a^{\pi t}_{\gamma, d}(E_\gamma, \psi_s)$ is the differential albedo for a broad parallel beam of γ quanta for earth described by formula (5.16).

The total scattering angle ψ_s of reflected radiation is calculated using the equation

$$\cos\psi_s = \sin\beta \sin\psi \cos\varphi - \cos\beta \cos\psi, \qquad (6.8)$$

where ψ is the exit angle of the reflected radiation, read from the normal to the surface of the earth. The remaining angles have values corresponding to Figure 2.10.

Table 6.1

SPECTRAL-ANGULAR DISTRIBUTION OF FRAGMENT γ RADIATION

$F_f(\Omega, \beta, E_\gamma)$, $\frac{\text{rad}}{\text{ster}}$ (rel. units)

degrees	Energy Interval ΔE_γ, MeV									
	0,1—0,2	0,2—0,3	0,3—0,5	0,5—0,75	0,75—1	1—1,5	1,5—2	2—3	3—4	4—6
					$\alpha=0°$					
0	0,00693	0,597 (—3	0,00407	—	—	—	—	—	—	—
10	0,00623	0,00155	0,00399	0,228 (—3	—	—	—	—	—	—
20	0,00487	0,00343	0,00404	0,00104	—	—	—	—	—	—
30	0,00506	0,00308	0,00387	0,00403	0,175 (—3	0,182 (—3	—	—	—	—
40	0,00491	0,00338	0,00429	0,00439	0,00438	0,001079	0,177 (—5	—	—	—
50	0,00627	0,00453	0,00484	0,00560	0,00572	0,00780	0,198 (—3	0,112 (—4	—	—
60	0,00594	0,00392	0,00799	0,00861	0,00701	0,0169	0,00514	0,72 (—3	0,53 (—4	—
70	0,00553	0,00409	0,00753	0,00732	0,00786	0,02679	0,01582	0,1879	0,00255	0,113 (—3
80	0,00589	0,00443	0,00703	0,00828	0,00929	0,02427	0,02564	0,0513	0,01951	0,00778
90	0,00632	0,00455	0,00617	0,00742	0,00978	0,02449	0,03094	0,4578	0,05717	0,03898
					$\alpha=10°$					
0	0,00679	0,00267	0,00461	0,477 (—3	—	—	—	—	—	—
10	0,00521	0,00460	0,00401	0,00158	—	—	—	—	—	—
20	0,00561	0,00294	0,00427	0,00508	0,207 (—3	0,229 (—3	—	—	—	—
30	0,00502	0,00321	0,00505	0,00503	0,00507	0,00123	0,18 (—5	—	—	—
40	0,00672	0,00408	0,00539	0,00460	0,00630	0,00862	0,21 (—3	0,112 (—4	—	—
50	0,00584	0,00390	0,00866	0,00908	0,00749	0,01821	0,00557	0,753 (—3	0,53 (—4	—
60	0,00586	0,00406	0,00818	0,00821	0,00835	0,02813	0,01630	0,01972	0,00274	0,113 (—3
70	0,00608	0,00432	0,00721	0,00878	0,00949	0,2497	0,02625	0,05287	0,02046	0,00837
80	0,00641	0,00451	0,00632	0,00745	0,00973	0,02519	0,03177	0,04777	0,05819	0,3918
90	0,00587	0,00442	0,00694	0,00817	0,00917	0,02420	0,03536	0,05128	0,01981	0,00811

$\alpha=20°$

0	0,005022	0,00821	0,00456	0,00331	—	—	—	—	—	—
10	0,00460	0,00537	0,00432	0,00802	0,272 (—3	0,32 (—3	—	—	—	—
20	0,00525	0,00420	0,00527	0,00663	0,00623	0,00150	0,18 (—5	—	—	—
30	0,00720	0,00439	0,00601	0,00677	0,00775	0,00972	0,23 (—3	0,112 (—4	—	—
40	0,00615	0,00380	0,00985	0,01050	0,00863	0,02073	0,00626	0,84 (—3	0,53 (—4	—
50	0,00612	0,00390	0,00941	0,00883	0,00949	0,3071	0,01747	0,02164	0,00290	0,11 (—3
60	0,00588	0,00399	0,00813	0,00949	0,01065	0,02685	0,02781	0,05645	0,02173	0,00893
70	0,00674	0,00465	0,00710	0,00815	0,01072	0,0260	0,03343	0,04872	0,06069	0,04137
80	0,00609	0,00431	0,00721	0,00878	0,00949	0,02497	0,02625	0,05287	0,02046	0,00837
90	0,00554	0,00408	0,00753	0,00732	0,00786	0,02679	0,01582	0,01879	0,00255	0,11 (—3

$\alpha=40°$

0	0,00848	0,00553	0,00666	0,0092	0,01336	0,02454	0,38 (—3	—	—	—
10	0,00870	0,00643	0,00856	0,01257	0,01890	0,02050	0,377 (—3	0,112 (—4	—	—
20	0,00671	0,00512	0,01336	0,01891	0,01437	0,03257	0,00961	0,00126	0,53 (—4	—
30	0,00512	0,00556	0,01145	0,01345	0,01331	0,04325	0,02479	0,02957	0,00404	0,113 (—3
40	0,00694	0,00491	0,01041	0,01290	0,01371	0,03528	0,03606	0,07299	0,02802	0,01153
50	0,00721	0,00454	0,00922	0,01051	0,01346	0,03262	0,04171	0,06029	0,07439	0,05055
60	0,00634	0,00402	0,00915	0,01033	0,01130	0,03019	0,03122	0,06316	0,02382	0,0099
70	0,00614	0,00391	0,00951	0,00888	0,00956	0,03156	0,01761	0,02142	0,00268	—
80	0,584	0,00390	0,00866	0,00908	0,00749	0,01821	0,00556	0,75 (—3	0,53 (—4	—
90	0,00627	0,00453	0,00484	0,0050	0,00572	0,0078	0,198 (—3	0,112 (—4	—	—

$\alpha=90°$

0	0,02453	0,01710	0,00742	0,02162	0,07197	0,15169	0,40342	0,4173	0,01209	0,90367
10	0,01106	0,00772	0,00335	0,00975	0,03247	0,06843	0,18199	0,18825	0,54525	0,40767
20	0,00639	0,00455	0,01015	0,01879	0,02584	0,05636	0,10890	0,26534	0,11405	0,04891
30	0,00425	0,00358	0,01404	0,01289	0,01880	0,08688	0,06326	0,0860	0,01154	—
40	0,00456	0,00314	0,01886	0,02199	0,01560	0,05427	0,01956	0,002429	—	—
50	0,00848	0,00553	0,006666	0,0092	0,01336	0,02454	0,38 (—3	—	—	—
60	0,00625	0,00500	0,00608	0,01701	0,54 (—3	0,803 (—3	—	—	—	—
70	0,00502	0,00821	0,00456	0,00331	—	—	—	—	—	—
80	0,00679	0,00267	0,00461	0,477 (—3	—	—	—	—	—	—
90	0,00693	0,60 (—3	0,00407	—	—	—	—	—	—	—

Table 6.2

SPECTRAL-ANGULAR DISTRIBUTION OF CAPTURE γ RADIATION $F_c(\Omega, \beta, E_\gamma)$ $\frac{rad}{ster}$ (rel. units)

β, degrees	Energy Interval ΔE_γ, MeV											
	0,1—0,2	0,2—0,3	0,3—0,5	0,5—0,75	0,75—1	1—1,5	1,5—2	2—3	3—4	4—6	6—8	8—10
						$\alpha=0°$						
0	0,518(—4	0,584(—3	0,00882	—	—	—	—	—	—	—	—	—
10	0,00285	0,00308	0,00502	0,00196	—	—	—	—	—	—	—	—
20	0,00330	0,00299	0,00521	0,00488	—	—	—	—	—	—	—	—
30	0,00385	0,00263	0,00398	0,00616	0,00112	0,00251	—	—	—	—	—	—
40	0,00425	0,00299	0,00418	0,00469	0,00787	0,00486	0,33 (—4	—	—	—	—	—
50	0,00482	0,00381	0,00440	0,00538	0,00760	0,01881	0,00205	0,647(—4	—	—	—	—
60	0,00513	0,00498	0,00389	0,00595	0,00897	0,0209	0,01085	0,00338	0,97 (—4	—	—	—
70	0,00435	0,00407	0,00324	0,00493	0,00602	0,02257	0,01823	0,0246	0,00833	0,151(—3	0,113(—3	0,726(—4
80	0,00429	0,00398	0,00327	0,00473	0,00686	0,0180	0,01501	0,0353	0,02576	0,01919	0,00698	0,00225
90	0,00425	0,00378	0,00302	0,00452	0,00620	0,0163	0,01195	0,0264	0,02634	0,0700	0,00633	0,00878
						$\alpha=10°$						
0	0,00605	0,00608	0,00325	0,00425	—	—	—	—	—	—	—	—
10	0,00429	0,00378	0,00492	0,00778	—	—	—	—	—	—	—	—
20	0,00300	0,00239	0,00377	0,00762	0,00139	0,00319	—	—	—	—	—	—
30	0,00385	0,00314	0,00478	0,00567	0,00887	0,00559	0,33 (—4	—	—	—	—	—
40	0,00471	0,00360	0,00471	0,00573	0,00844	0,02077	0,00232	0,647(—4	—	—	—	—
50	0,00542	0,00494	0,00471	0,00644	0,00979	0,02295	0,0115	0,00355	0,97 (—4	—	—	—
60	0,00452	0,00382	0,00413	0,00552	0,00756	0,02381	0,01911	0,02597	0,00866	0,151(—3	0,11 (—3	0,72 (—4
80	0,00401	0,00362	0,00292	0,00454	0,00649	0,01621	0,01253	0,02671	0,0268	0,07128	0,00661	0,00392
90	0,00427	0,00397	0,00325	0,00469	0,00679	0,01786	0,01566	0,03482	0,02565	0,01936	0,00702	0,00241

β, degrees	Energy Interval ΔE_γ, MeV											
	0,1—0,2	0,2—0,3	0,3—0,5	0,5—0,75	0,75—1	1—1,5	1,5—2	2—3	3—4	4—6	6—8	8—10
					$\alpha=20^\circ$							
0	0,00426	0,00293	0,00840	0,01469	—	—	—	—	—	—	—	—
10	0,0040	0,00257	0,00576	0,01358	0,00196	0,00457	—	—	—	—	—	—
20	0,00470	0,00368	0,00457	0,00827	0,01123	0,00682	0,33 (—4	—	—	—	—	—
30	0,00411	0,00357	0,00633	0,00738	0,01029	0,02429	0,00255	0,65 (—4	—	—	—	—
40	0,00509	0,00525	0,00554	0,0077	0,01129	0,02570	0,01303	0,00407	0,97 (—4	—	—	—
50	0,00457	0,00402	0,00460	0,00618	0,00855	0,02601	0,02108	0,0284	0,00953	0,15 (—3	0,113(—3	0,73 (—4
60	0,00423	0,00363	0,00420	0,00541	0,00789	0,01967	0,01746	0,0384	0,0283	0,02129	0,00770	0,0026
70	0,00426	0,00348	0,00367	0,00494	0,00697	0,01698	0,01349	0,0285	0,0287	0,0742	0,00703	0,00929
80	0,00438	0,00367	0,00359	0,00501	0,00747	0,01842	0,01624	0,0358	0,0266	0,01996	0,00727	0,00243
90	0,00435	0,00407	0,00323	0,00493	0,00682	0,02257	0,01823	0,0246	0,00833	0,15 (—3	0,113(—3	0,726(—4
					$\alpha=40^\circ$							
0	0,0057	0,00535	0,00559	0,00824	0,01583	0,0604	0,00712	—	—	—	—	—
10	0,00645	0,00542	0,00623	0,00947	0,02666	0,0503	0,00513	0,65 (—4	—	—	—	—
20	0,00672	0,00664	0,00585	0,01299	0,02010	0,0431	0,0803	0,00621	0,97 (—4	—	—	—
30	0,00504	0,00449	0,00546	0,01076	0,01181	0,0378	0,0293	0,03952	0,01315	0,151 (—3	0,113 (—3	0,73 (—4
40	0,00504	0,00467	0,00463	0,00891	0,01095	0,0266	0,0228	0,04954	0,03654	0,02738	0,00995	0,00343

β,	Energy Interval ΔE_x, MeV											
	0,1—0,2	0,2—0,3	0,3—0,5	0,5—0,75	0,75—1	1—1,5	1,5—2	2—3	3—4	4—6	6—8	8—10
50	0,00363	0,00343	0,00530	0,00690	0,00851	0,0223	0,0176	0,03511	0,03528	0,09102	0,00861	0,01131
60	0,00404	0,00377	0,00497	0,0061	0,00821	0,0224	0,0197	0,04255	0,03184	0,02333	0,00893	0,00283
70	0,00458	0,00404	0,00461	0,00620	0,00857	0,0261	0,0212	0,02846	0,00931	—	—	—
80	0,00542	0,00494	0,00471	0,00644	0,00979	0,0229	0,0115	0,00355	0,97 (4	—	—	—
90	0,00482	0,00381	0,00440	0,00538	0,0076	0,0188	0,00205	0,65 (—4	—	—	—	—
						$\alpha=90°$						
0	0,00106	—	0,63(—3	0,00339	0,00614	0,00656	0,0207	0,09038	0,2864	1,45203	0,6625	0,18309
10	0,555(—3	—	0,33(—3	0,00177	0,00322	0,00344	0,01087	0,04737	0,15011	0,7611	0,03473	0,09597
20	0,001924	0,00146	0,00216	0,00460	0,00921	0,01778	0,03982	0,15933	0,15134	0,1309	0,04874	0,01568
30	0,002896	0,00253	0,00274	0,0053	0,00721	0,00543	0,0701	0,12113	0,04197	—	—	—
40	0,00699	0,00919	0,00476	0,01092	0,0213	0,0548	0,0427	0,01398	—	—	—	—
50	0,00569	0,00935	0,00559	0,00824	0,0158	0,0604	0,00712	—	—	—	—	—
60	0,00562	0,00335	0,005997	0,01948	0,00473	0,0115	—	—	—	—	—	—
70	0,00426	0,00293	0,00840	0,01470	—	—	—	—	—	—	—	—
80	0,00604	0,00608	0,00325	0,00425	—	—	—	—	—	—	—	—
90	0,52(—4	0,58(—3	0,00882	—	—	—	—	—	—	—	—	—

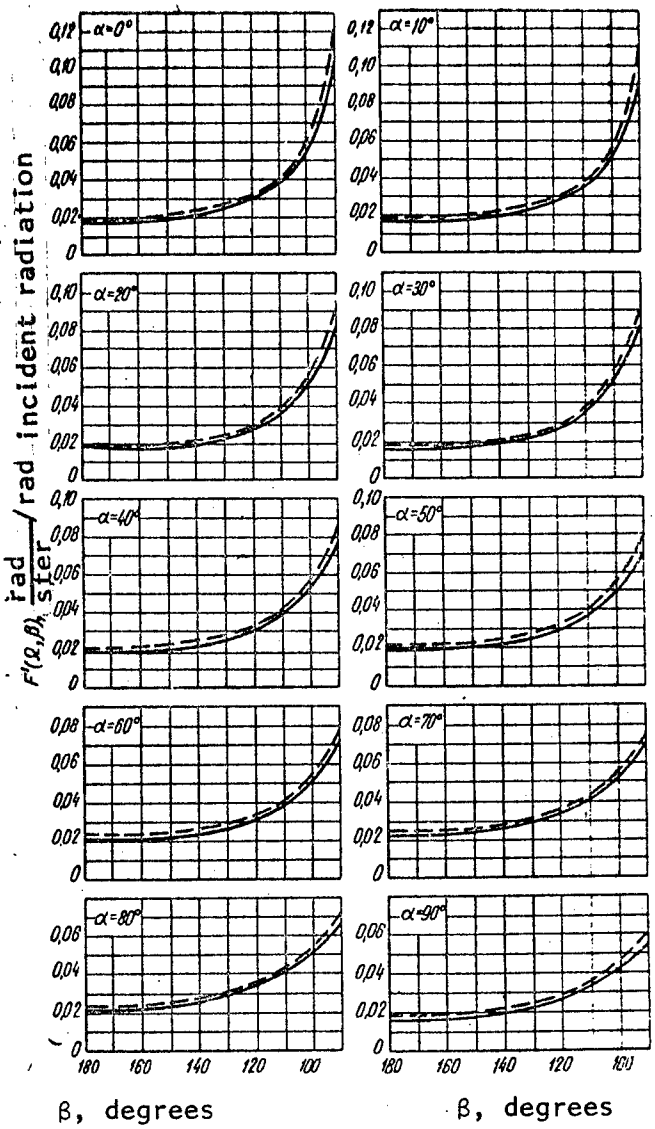

Figure 6.3. Generalized Angular Distribution Functions of Doses of γ Radiation Scattered From the Earth: ————, for fragment γ radiation $F'_f(\Omega, \beta)$; -----, for capture γ radiation $F'_c(\Omega, \beta)$.

The results of calculation of the generalized characteristics of the angular distributions of γ radiation scattered from the earth are shown on Figure 6.3.

§ 2. Method of Design of Shielding for Surface Structures

The radiation of a nuclear explosion and radioactive fallout, scattered in the air, strikes the walls of structures rising over the surface of the ground or buried below the surface, penetrates through them and acts on the people inside the structures.

Let us study the general nature of this effect in greater detail using the example of a simple protective structure shown on Figure 6.4. If the integral dose in the open terrain of any type of nuclear explosion radiation is D_0, in correspondence with the form of the function and spectral-angular distributions of the radiation in the air, the dose generated at the surface of the wall by the radiation arriving from direction $\bar{\Omega}$ with energy E will be $D_0F(\bar{\Omega}, E)$. With an angle of incidence to the surface of the wall of γ, the total dose of this type of radiation at point A on the internal surface of the wall will be

$$D_{At} = D_0 \int_{2\pi} \int_{E} F(\Omega, E) K_t(\delta, \gamma, E) d\Omega dE, \qquad (6.9)$$

where $K_t(\delta, \gamma, E)$ is the transmission factor for the total dose of the parallel beam of radiation striking the surface of the wall at angle γ with initial energy E, and integration is performed with respect to the entire spectrum of bombarding particles and all directions in the half space over the outer surface of the wall.

If we ignore boundary effects at points of contact between the wall and other elements of the structure due to the slight contribution of these effects to the total illuminated surface, we can consider that this value of total dose D_{At} will be characteristic for all points on the internal surface of the flat wall.

Dose D_{At} is formed by the scattered and unscattered radiation leaving the wall, so that

$$D_{At} = D_{As} + D_{Au}, \qquad (6.10)$$

where D_{As} and D_{Au} are the doses of scattered and unscattered components of radiation at point A.

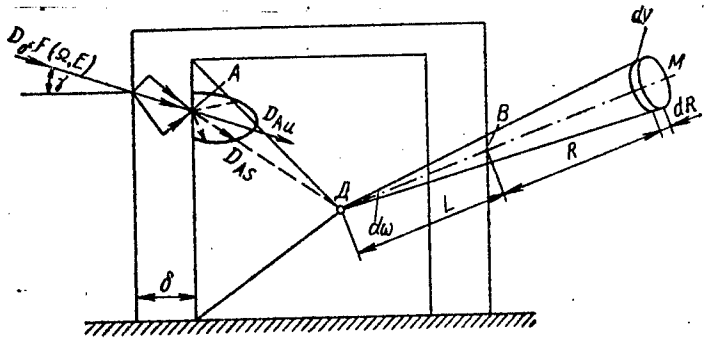

Figure 6.4. Analysis of Method of Calculating Shielding for Surface Structures.

The dose of the scattered component at point A on the internal surface of the wall can be calculated from the equation

$$D_{As} = D_0 \int_{2\pi} \int_{E} F(\Omega, E) K_s(\delta, \gamma, E)\, d\Omega dE, \qquad (6.11)$$

where $K_s(\delta, \gamma, E)$ is the transmission factor of the dose of the scattered component of radiation, striking the surface of the wall at angle γ with initial energy E.

The dose of unscattered radiation at a detector located on the inner surface of the wall will be

$$D_{Au} = D_0 \int_{2\pi} \int_{E} F(\Omega, E) K_u(\delta, \gamma, E)\, d\Omega dE, \qquad (6.12)$$

where $K_u(\delta, \gamma, E)$ is the dose transmission factor for unscattered radiation in a parallel beam, if

$$D_{As} = D_0 \Gamma(\delta); \qquad (6.13)$$

$$D_{Au} = D_0 \Lambda(\delta), \qquad (6.14)$$

where $\Gamma(\delta)$ and $\Lambda(\delta)$ are the generalized transmission factors, called the barrier factors.

If the detector is moved from point A to point D, located at a certain distance from the inner surface of the wall, the dose at the detector is changed [2, 3]. The attenuation resulting from movement of the detector away from the wall will be referred to as geometric attenuation. Geometric attenuation can be looked upon as the effect of the finite extent of the source. Actually, the wall acts as a secondary source, and if this source were infinite in size, there would be no difference between positions of the detector A and D, since in both cases the detector would collect radiation from a 2π space. Geometric attenuation occurs because the wall is finite in size and as the detector is moved from A to D, the solid angle in which radiation is collected is reduced.

Thus, the change in the dose at point D from the scattered component can be calculated by introducing the so-called geometric radiation attenuation factor G

$$D_{ds} = D_{As} G_{ds}. \tag{6.15}$$

If the angular distribution function of the dose of scattered radiation leaving the barrier is known, the geometric factor is determined by integrating the angular distribution function $f(\bar{\omega})$ within limits of solid angle ω_d, subtended by the wall in question or an element of the wall at point D:

$$G_{ds} = \int_{\omega_d} f(\omega)\, d\omega. \tag{6.16}$$

In the simplest case, when the scattered radiation leaving the barrier is distributed isotropically, expression (6.16) is simplified:

$$G_{ds} = \frac{\omega_d}{2\pi}, \tag{6.17}$$

and the dose of scattered radiation at point D can be calculated as

$$D_{ds} = D_{As} \frac{\omega_d}{2\pi}. \tag{6.18}$$

This expression shows that the dose of scattered radiation at the detector at some distance from the wall decreases in comparison with the dose of scattered radiation at the surface of the wall, in inverse proportion to the square of the distance to the wall.

The assumption of isotropy of radiation scattered in shields of a structure and radiating within it is basic to the method of calculation used. Although consideration of the angular distribution of radiation by the scattered component represents no difficulty in principle and equation (6.16) can be rather simply realized when the problem is solved by electronic computer, the lack in many cases of exhaustive information on angular distributions of radiation, particularly with inclined incidence to the surface of the barrier, hinders consideration of the angular characteristics. However, the assumption of isotropy of the scattered radiation should not lead to any significant errors.

As concerns the contribution of the unscattered component, its dose at point D is determined in correspondence with the expression

$$D_{du} = D_0 \int_{\omega_d} \int_E F(\Omega, E) K_u(\delta, \gamma, E) d\Omega dE, \qquad (6.19)$$

Integration in which is performed within limits of the solid angle subtended by the wall or wall element being studied at the point of placement of the detector. Physically, this corresponds to the fact that the particles of the unscattered component do not change the direction of their initial movement upon penetration through the barrier and therefore that portion of the radiation of the nuclear explosion which strikes the surface of the wall, moving in directions passing by point d, cannot act on the detector located at this point. However, since the particles of the unscattered component do not interact with the materials of the wall, the wall cannot be looked upon as a secondary source. Therefore, in contrast to the scattered radiation, the unscattered radiation does not undergo geometric attenuation upon movement from the surface of the wall to the detector. Actually, the sources of those particles which strike the detector without interacting with the material of the wall are the centers of the last scattering events in the atmosphere. The degree of geometric attenuation of the dose of unscattered radiation propagating from the wall to the detector depends on the relationship between distances from the scattering center to the wall and from the wall to the detector.

If a particle has undergone scattering in the direction of the detector at distance R from the wall and, without interacting with the material of the wall, strikes the detector, located at distance L from it, the factor of geometric attenuation is $R^2/(R + L)^2$. Let us estimate the value which may be reached by this factor under actual conditions. Let us assume for simplicity that the density of scattering centers in the air surrounding the structure is identical throughout and that the

number of particles scattered per unit volume about point M is N. In an element volume dv, this will amount to

$$Ndv = NR^2 d\omega dR.$$

Their flux at point B per unit solid angle is

$$\frac{NR^2 d\omega dR}{4\pi R^2 d\omega} e^{-R/\lambda} = \frac{Ne^{-R/\lambda}\, dR}{4\pi}.$$

Integrating with respect to ray BM, we produce

$$\Phi_B = \frac{N}{4\pi} \int_0^\infty e^{-\frac{R}{\lambda}} dR = \frac{N\lambda}{4\pi}. \tag{6.20}$$

At point D this amounts to

$$\Phi_d = \frac{N}{4\pi} \int_0^\infty \frac{R^2 e^{-R/\lambda}}{(R+L)^2} dR. \tag{6.21}$$

The geometric factor determining the attenuation of the unscattered component upon propagation from the wall to a detector located at distance L from it is

$$G_{du} = \frac{\Phi_d}{\Phi_B} = \frac{1}{\lambda} \int_0^\infty \frac{R^2 e^{-R/\lambda}}{(R+L)^2} dR. \tag{6.22}$$

Calculations performed using this equation show that the geometric factor is 0.994 for a distance L = 1 m from the wall; 0.986 for L = 2 m; 0.958 for L = 5 m; 0.922 for L = 10 m.

Thus, for practical purposes in the design of shielding of surface structures, geometric attenuation of the dose of the unscattered component can be ignored. The total dose at point D within the structure is determined by adding the contribution from the individual walls and the structural elements

$$D_d = \Sigma (D_{ds} + D_{du}). \tag{6.23}$$

In some cases in order to estimate the protective properties of structures, we can use a simplified calculation method. According to this method, the contribution of any given structural element to the total dose at point D is calculated using the formula

$$\tilde{D}_d = D_A G_{d,s} = (D_{As} + D_{Au}) G_{d,s}. \tag{6.24}$$

It is not difficult to see that in expression (6.24), the unscattered radiation component reaching the internal surface of the wall is given the same geometric attenuation as the scattered component. This causes a reduction in the dose at point D in comparison to the actual dose by

$$\Delta D_d = D_{du} - D_{Au} G_{ds} = D_0 \left[\int_{\omega_d} \int_E F(\bar{\Omega}, E) K_u(\delta, \gamma, E) \, d\Omega dE - \right.$$
$$\left. - G_{ds} \int_{2\pi} \int_E F(\bar{\Omega}, E) K_u(\delta, \gamma, E) \, d\Omega dE. \right. \tag{6.25}$$

Thus, the results of calculations performed using the two methods outlined above are interrelated by the relationship

$$D_d = \tilde{D}_d - \Delta D_d. \tag{6.26}$$

In many cases, however, the value of correction ΔD_d is insignificant and expression (6.24) can be used for approximate design of shielding.

§ 3. Calculation of Barrier and Geometric Factors in Attenuation of Radiation

The value of the barrier factor depends on the material and thickness of the shield δ, its position in space and the spectral angular distribution of the radiation scattered in the air.

If the position of the wall of a structure is fixed by angle θ (see Figure 6.5), calculated between the normal to its outer surface and the normal to the earth (top downward), the barrier factor of transmission of the total neutron dose is calculated using the expression

$$\Lambda_{n,t}(\delta, \vartheta, \alpha) = 2 \int_0^{\pi/2} \int_0^{\pi} \sin \gamma K_{nt}(\delta, \gamma) F_n(\Omega, \beta) \, d\gamma d\tau, \tag{6.27}$$

where $\beta = \arccos(\sin\gamma\cos\tau\sin\vartheta + \cos\gamma\cos\vartheta)$.

The barrier transmission factor for the unscattered component of neutron dose is defined as

$$\Lambda_{nu}(\delta, \vartheta, \alpha) = 2\int_0^{\pi/2}\int_0^{\pi} \sin\gamma K_{nu}(\delta, \gamma) F_n(\Omega, \beta)\, d\gamma\, d\tau. \qquad (6.28)$$

Then the barrier transmission factor for the scattered component of neutrons is

$$\Lambda_{ns}(\delta, \vartheta, \alpha) = \Lambda_{nt}(\delta, \vartheta, \alpha) - \Lambda_{nu}(\delta, \vartheta). \qquad (6.29)$$

The results of calculation of the barrier transmission factors for the total neutron dose and the scattered component of neutrons are presented in Appendix 1 (Table a. 1 and Table a. 2.).

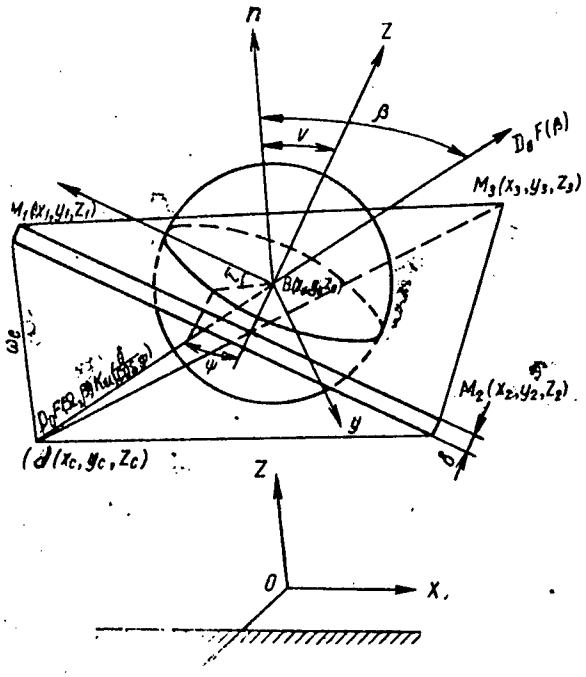

Figure 6.5. Geometry of General Design of Shielding of a Structure

The barrier transmission factor for the total dose of fragment γ radiation is calculated using the equation

$$\Lambda^f_{\gamma t}(\delta, \vartheta) = 2 \sum_{E_\gamma} \int_0^{\pi/2} \int_0^{\pi} \sin \gamma F_f(\Omega, \beta, E_\gamma)\ K^f_{\gamma t}(\delta, \gamma, E_\gamma)\, d\gamma d\tau. \qquad (6.30)$$

Addition is performed over the entire spectrum of γ quanta scattered in the air.

Similarly, the barrier transmission factor of the unscattered component of γ quanta is calculated by

$$\Lambda^f_{\gamma u}(\delta, \vartheta) = 2 \sum_{E_\gamma} \int_0^{\pi/2} \int_0^{\pi} \sin \gamma F_c(\Omega, \beta, E_\gamma)\, e^{-\mu(E_\gamma) \frac{\delta}{\cos \gamma}}\, d\gamma d\tau. \qquad (6.31)$$

The barrier transmission factor for the scattered component is

$$\Lambda^f_{\gamma s}(t, \vartheta) = \Lambda^f_{\gamma t}(\delta, \vartheta) - \Lambda^f_{\gamma t}(\delta, \vartheta). \qquad (6.32)$$

The results of calculation of the barrier transmission factors for the total dose of γ quanta and the dose of scattered fragment γ radiation are presented in Appendix 2 (Tables a. 3 and a. 4).

Using expressions similar to (6.30) and (6.31), the barrier transmission factors for the total dose of capture γ radiation in the air $\Lambda^c_{\gamma t}(\delta, \theta, \alpha)$ γ radiation from radioactive fallout $\Lambda_{\gamma t}(\delta, \theta)$ and the corresponding factors for the unscattered component $\Lambda^c_{\gamma u}(\delta, \theta, \alpha)$ and $\Lambda^r_{\gamma u}(\delta, \theta, t)$ were calculated. The factors $\Lambda^c_{\gamma t}(\delta, \theta, \alpha)$ and $\Lambda^c_{\gamma s}(\delta, \theta, \alpha)$ are presented in Appendix 3 (Tables a. 5 and a. 6), while $\Lambda^r_{\gamma t}(\delta, \theta, t)$ and $\Lambda^r_{\gamma s}(\delta, \theta)$ are presented in Appendix 4 (Tables a. 7. and a. 8).

The barrier transmission factors for capture γ radiation formed in the materials of the shielding structure were determined using the expression

$$\Lambda^3_\gamma(\delta, \vartheta, \alpha) = 2K'_{cf}(\delta) \int_0^{\pi/2} \int_0^{\pi} \sin \gamma \cos \gamma F(\beta)\, d\gamma d\tau = \\ = \Lambda^3_{\gamma i}(\delta)\, \Lambda^3_{\gamma j}(\vartheta, \alpha). \qquad (6.33)$$

Factors $\Lambda^3_{\gamma i}(\delta)$ and $\Lambda^3_{\gamma j}$ (θ, α) are presented in Table 5 (Tables a. 9 and a. 10).

As concerns calculation of the geometric attenution factors of radiation within the shielding structure, with the assumption made of isotropy of the distribution of the scattered radiation leaving the barrier it is reduced, as follows from expression (6.17), to calculation of the solid angles subtended by the structural elements in question at the point of observation.

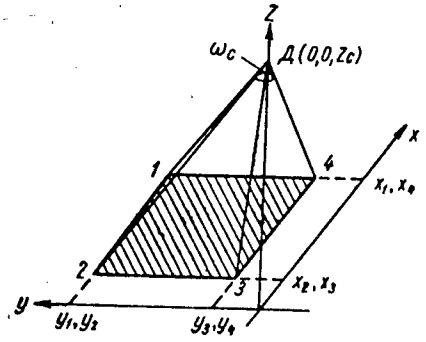

Figure 6.6. Position of Coordinate System Describing Rectangular Radiating Surface

In many cases of practical importance, the elements of the structure are rectangular (walls, ceilings) or can be represented as a sum of rectangular elements. Calculation of the solid angles in this case is rather simple [4].

If we use the geometry of Figure 6.6, on which the coordinate origin is selected in the plane of the rectangular element in question beneath the location of the detector, the distance from the detector to the plane of the rectangle is represented by z_c, and the coordinates of the four angles of the rectangle are represented by x_i, y_i $(i = 1, 2, 3, 4)$, then if the coordinate system is selected so that its axes are parallel to the sides of the rectangle and the numeration of the angles is performed clockwise, the solid angle subtended by the rectangle in question at point D will be

$$\omega_d = \left| q'_1 \tau_0(\varepsilon_1, \eta_1) - q'_2 \tau_0(\varepsilon_2, \eta_2) + q'_3 \tau_0(\varepsilon_3, \eta_3) - q'_4 \tau_0(\varepsilon_4, \eta_4) \right| \text{ ster}, \qquad (6.34)$$

where

$$\tau_0(\varepsilon_i, \eta_i) = \operatorname{arctg} \frac{\varepsilon_i}{\eta_i \sqrt{\varepsilon_i^2 + \eta_i^2 + 1}}; \tag{6.35}$$

$$\varepsilon_i = \left| \frac{y_i}{x_i} \right|; \quad \eta_i = \left| \frac{z_c}{x_i} \right|; \quad q_i' = \frac{y_i}{\varepsilon_i x_i}. \tag{6.36}$$

In more complex cases, when the form of the structure cannot be represented by flat rectangular elements, the method described below must be used to calculate the solid angles.

If the protective shield has a complex shape, it can be represented as a set of triangular elements of arbitrary form. The solid angle subtended at any point by a triangular element oriented arbitrarily in space is relatively easy to calculate.

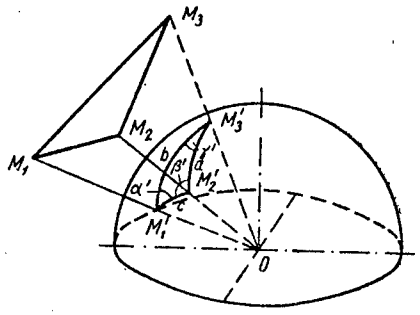

Figure 6.7. Calculation of Solid Angle of Element of Triangular Shape

Suppose O M_1 M_2 M_3 is a triangular solid angle fixed in coordinate system Oxyz by points M_i (x_i, y_i, z_i) of each side and point O (x_0, y_0, z_0) (Figure 6.7).

If we construct a sphere of unit radius with its center at point O, it is not difficult to see that the value of quantity ω, the solid angle, is exactly equal to the value of the area of the surface of the spherical triangle formed by the trace of each edge on the surface of the sphere:

$$S_{\Delta M_1' M_2' M_3'} = \underline{\omega} = (\alpha' + \beta' + \gamma' - \pi), \tag{6.37}$$

where α', β' and γ' are the angles at point $\Delta M'_1 M'_2 M'_3$, equal to:

$$\alpha' = 2 \arcsin \sqrt{\frac{\sin(n-b)\sin(h-c)}{\sin b \sin c}}; \quad (6.38)$$

$$\beta' = 2 \arcsin \sqrt{\frac{\sin(n-a)\sin(h-c)}{\sin a \sin c}}; \quad (6.39)$$

$$\gamma' = 2 \arcsin \sqrt{\frac{\sin(n-a)\sin(h-b)}{\sin a \sin b}}. \quad (6.40)$$

The values of a, b and c determine the lengths of the sides of this triangle and are calculated according to the relationships of the scalar product of the vectors M_1, M_2 and M_3, constructed on the faces of the solid angle:

$$a = \arccos \frac{(M_2 M_3)}{\| M_2 \| \| M_3 \|}; \quad (6.41)$$

$$b = \arccos \frac{(M_1 M_3)}{\| M_1 \| \| M_3 \|}; \quad (6.42)$$

$$c = \arccos \frac{(M_1 M_2)}{\| M_1 \| \| M_2 \|}. \quad (6.43)$$

$$2h = a + b + c. \quad (6.44)$$

§ 4. Sequence of Design of Shielding From the Radiation of Nuclear Explosions

The calculation of the shielding ability of a surface structure[1] against the radiation of nuclear explosions is reduced to arbitrary subdivision of the surfaces of the structure into individual elements, determination of the position of these elements in space, determination of the barrier transmission factors for these elements and the geometric attenuation factors relative to a selected design position within the structure, with subsequent addition of radiation doses created at the detector by the individual structural elements.

---

[1]The calculation plan for subterrainean structures differs only in that there is only one surface in this case.

Let us first study a simple method of estimating the shielding of a surface structure, the use of which does not require computer equipment. This method is recommended to be used when the surface of the structure to be calculated can be represented as a set of a small number of flat rectangular shields. The edges of these elements are selected so that the thickness of the shield of homogeneous material within each is identical.

The position of each of the rectangular shields in this type of structure is determined by the value of angle θ between the normal to the surface of the earth and the external normal of the element (see Figure 6.5).

In correspondence with this angle and the known shield thickness δ, the appendices of this book can be used to find the barrier transmission factors for the total dose of neutrons and γ radiation from a nuclear explosion.

After this, the geometric attenuation factor is calculated for each element of the structure and the selected design points within the structure. The geometric factor is calculated using expression (6.17). The solid angle subtended by the rectangular element at the detection point is determined using equation (6.34).

The contribution of each element to the total transmission factor for the structure at the design point is calculated using the expression

$$\Pi_i = \Lambda_i G_{d,s}. \tag{6.45}$$

The total transmission factor of the structure for the dose of each type of radiation is determined by adding the values for each structural element. In order to produce the transmission factor for all types of radiation existing in a nuclear explosion, the total transmission factors for the individual types of radiation must be added in correspondence to their relative share of the total dose of nuclear radiation on the open terrain.

If a shielding structure has a complex shape and complex shield structure, analysis of the shielding properties may require dividing the entire surface into a large number of elements. In particular, this necessity arises when the form of the structure is curved. In this case, the dimensions of the elements must be selected so that the thickness of the shield does not change significantly within the limits

of an element, and the surface can be considered flat. The mathematical operations involved in calculating this type of shielding are simple to perform if the elements are triangles of arbitrary shape. The position of each triangular element can be fixed by the coordinates of its points on the external surface $M_1(x_1, y_1, z_1)$, $M_2(x_2, y_2, z_2)$, $M_3(x_3, y_3, z_3)$, calculated in the main system of coordinates XYZ, coupled to the structure being calculated. This main system of coordinates will be selected in the remainder of this book such that the positive direction of the Z axis forms a perpendicular to the surface of the earth. The thickness of the shielding can be fixed by the mean thickness δ of a shield within the limits of each of the geometric elements selected, measured in the normal cross section.

Thus, the first stage in calculation consists of preparation of a system of initial data concerning the geometry of the shielding structure, which includes the set of coordinates of points selected on the external surface of the structure and the thickness of the shielding materials at these points. Preparation of this type of initial information for a structure of any configuration represents no great difficulties.

The second stage in calculation consists of determination for each element of the angle θ read between the normal to the element and the normal to the surface of the earth.

The normal to the element will be considered the unit vector n, perpendicular to its external surface (Figure 6.7). We note also that in the system of coordinates which we are using, the normal to the surface of the earth corresponds in its direction to the axis OZ. Thus, angle θ between the normal to the element and the normal to the surface of the earth is the angle between the normal to the element and the OZ axis.

The vector of the normal to the element is found as the vector product of two noncolinear vectors, lying in the plane of the surface of the element. These vectors can be the vectors $M_1 M_2$ and $M_1 M_3$, constructed on the sides of the triangle defining the element (see Figure 6.5).

The vectors M_1M_2 and M_1M_3 can be defined as follows:

$$\begin{aligned} \mathbf{M_1M_2} &= |(x_2 - x_1);\ (y_2 - y_1);\ (z_2 - z_1)|; \\ \mathbf{M_1M_3} &= |(x_3 - x_1);\ (y_3 - y_1);\ (z_3 - z_1)|. \end{aligned} \tag{6.46}$$

The resulting vector product will be the vector N:

$$\mathbf{N} = [\mathbf{M_1M_2};\ \mathbf{M_1M_3}] = \begin{vmatrix} \mathbf{i} & \mathbf{j} & \mathbf{k} \\ (x_2 - x_1) & (y_2 - y_1) & (z_2 - z_1) \\ (x_3 - x_1) & (y_3 - y_1) & (z_3 - z_1) \end{vmatrix} = \tag{6.47}$$

$$= \begin{vmatrix} (y_2 - y_1)(z_3 - z_1) - (y_3 - y_1)(z_2 - z_1) \\ (x_2 - x_1)(z_3 - z_1) - (x_3 - x_1)(z_2 - z_1) \\ (x_2 - x_1)(y_3 - y_1) - (y_2 - y_1)(x_3 - x_1) \end{vmatrix} = \begin{vmatrix} x_N \\ y_N \\ z_N \end{vmatrix}$$

In order that the direction of vector N might correspond to the direction of the vector of the normal to the element n, the numeration of points M_1, M_2 and M_3 should be selected counterclockwise as seen from the end of vector n.

Thus,

$$\vartheta = \arccos \frac{z_N}{\sqrt{x_N^2 + y_N^2 + z_N^2}}. \tag{6.48}$$

The third stage in the calculation consists of calculating the doses of the scattered radiation component of each type from the structural element. In correspondence with the known thickness of the shielding material δ of the element and the angle θ calculated for it, the barrier transmission factors of the doses of the scattered component of neutrons and γ radiation from the nuclear explosion are determined from the appendices.

Then, calculation of the geometric attenuation factor is performed for each structural element and the selected design points within the structure, fixed by the coordinates D, x_d, y_d, z_d). The geometric factor is calculated using expression (6.17). The solid angle subtended by the triangular element $M_1M_2M_3$ at the point of detection D is determined in correspondence with equation (6.37). We should note only that the vectors M_1, M_2 and M_3 used in calculation of the solid angle are the vectors, the origins of which are located at point D (x_d, y_d, z_d), the ends at points $M_1(x_1, y_1, z_1)$, $M_2(x_2, y_2, z_2)$ and $M_3(x_3, y_3, z_3)$ respectively, i. e.

$$\begin{aligned}\mathbf{M}_1 &= |(x_1 - x_c);\ (y_1 - y_c);\ (z_1 - z_c)|;\\ \mathbf{M}_2 &= |(x_2 - x_c);\ (y_2 - y_c);\ (z_2 - z_c)|;\\ \mathbf{M}_3 &= |(x_3 - x_c);\ (y_3 - y_c);\ (z_3 - z_c)|.\end{aligned} \tag{6.49}$$

The contribution of each element to the total transmission factor of the scattered component at the point in question is calculated using the expression

$$\Pi_s = \Lambda_s G_{ds}. \tag{6.50}$$

The total transmission factor of the structure for the scattered component of the dose of each type of radiation is determined by adding the values of Π_s for all structural elements.

The fourth stage is the calculation of angle β between the lines connecting the point to the center of the element and the normal to the surface of the earth.

The coordinates x_B, y_B, z_B of the center of gravity of the triangular element, fixed by the coordinates of points $M_1(x_1, y_1, z_1)$, $M_2(x_2, y_2, z_2)$ and $M_3(x_3, y_3, z_3)$ are calculated using the equations

$$\left.\begin{aligned} x_B &= \frac{x_{23} - x_1}{y_{23} - y_1} y_B + \frac{x_1 y_{23} - y_1 x_{23}}{y_{23} - y_1};\\ y_B &= \frac{(y_{12} - y_3)(x_1 y_{23} - y_1 x_{23}) + (y_{23} - y_1)(y_3 x_{12} - x_1 y_{12})}{(x_{12} - x_3)(y_{23} - y_1) - (y_{12} - y_3)(x_{23} - x_1)};\\ z_B &= z_1 + \frac{x_B - x_1}{x_{23} - x_1}(z_{23} - z_1), \end{aligned}\right\} \tag{6.51}$$

where

$$x_{12} = \frac{x_2 - x_1}{2} + x_1;\quad y_{12} = \frac{y_2 - y_1}{2} + y_1;\quad z_{12} = \frac{z_2 - z_1}{2} + z_1;$$
$$x_{23} = \frac{x_3 - x_2}{2} + x_2;\quad y_{23} = \frac{y_3 - y_2}{2} + y_2;\quad z_{23} = \frac{z_3 - z_2}{2} + z_2.$$

The unit vector corresponding in direction to the direction from point $D(x_d, y_d, z_d)$ to the center of element $B(x_B, y_B, z_B)$ is the vector

$$\mathbf{B} = |(x_B - x_d);\ (y_B - y_d);\ (z_B - z_d). \tag{6.52}$$

Therefore, the desired angle β is

$$\beta = \arccos \frac{z_B - z_A}{\sqrt{(x_B - x_A)^2 + (y_B - y_A)^2 + (z_B - z_A)^2}}. \qquad (6.53)$$

The fifth stage in the calculation consists of calculation of angle ψ between the line connecting the point to the center of the element and the normal to the element.

Angle ψ is defined as the angle between vectors B and n and is calculated using the formula

$$\psi = \arccos \frac{(\mathbf{nB})}{\| \mathbf{n} \| \| \mathbf{B} \|} = \arccos \frac{(\mathbf{nB})}{\| \mathbf{N} \| \| \mathbf{B} \|}. \qquad (6.54)$$

The coordinates of vectors B and n are calculated using formulas (6.52) and (6.47) respectively.

Thus,

$$\psi = \frac{x_N (x_B - x_A) + y_N (y_B - y_A) + z_N (z_B - z_A)}{\sqrt{(x_B - x_A)^2 + (y_B - y_A)^2 + (z_B - z_A)^2}\sqrt{z_N^2 + y_N^2 + z_N^2}}. \qquad (6.55)$$

During the sixth stage, the dose of the unscattered component of neutrons at the point of detection is calculated. In correspondence with the angle β calculated for the element, using the data of § 1 of Chapter 6, the values of the generalized angular distribution functions of radiation scattered in the air or reflected from the earth $F(\Omega, \beta)$ are found. The contribution of each element to the total transmission factor of the unscattered component of each type of radiation at the point in question is

$$\Pi_u(\delta, \beta, \psi) = F(\Omega, \beta)\, \omega_A K_u(\delta, \psi), \qquad (6.56)$$

where $K_u(\delta, \psi)$ is the transmission factor for the dose of the unscattered component of radiation by a shield of thickness δ with a beam incident angle to its surface $\gamma = \psi$.

In the case of γ radiation, addition is performed for the entire spectrum of energies:

$$\Pi_{\gamma, u}(\delta, \beta, \psi) = \sum_{E_\gamma} F(\Omega, \beta, E_\gamma)\, \omega\, K_{\gamma u}(\delta, \psi, E_\gamma). \qquad (6.57)$$

The total transmission factor of the structure for the unscattered component of each type of radiation is determined by addition of the values of Π_u^* for all structural elements. The transmission factor of the structure for the total dose of radiation of each type is equal to the sum of the transmission factors for the scattered and unscattered components:

$$\Pi_t = \Pi_s + \Pi_u. \qquad (6.58)$$

In order to produce the transmission factor for all types of radiation acting during a nuclear explosion, the total transmission factors for the individual types of radiation must be added in correspondence to their relative shares in the total dose of nuclear radiation on the open terrain.

This method of calculation considers the presence in the structure of windows and open doorways. For these elements with 0 shielding thickness, the transmission factor of the scattered component of radiation is zero, the transmission factor for the unscattered component is one. Therefore, using the method which we have outlined it is possible to calculate the radiation situation at windows and openings.

§ 5. Estimate of Radiation Dose Repeatedly Scattered Within a Structure

The radiation from a nuclear explosion which passes through the shielding may undergo repeated reflection from the walls of the structure, thus increasing the dose recorded at any point within the structure. An estimation of the degree of increase of the dose within a structure due to reflection can be performed using the example of a room of spherical shape.

If for simplicity we assume that the angular distribution of radiation leaving the walls of the spherical room is isotropic, and the total transmission factor for the walls of the structure is identical everywhere and equal to K_t, the transmission factor for radiation for the entire structure for any point within the room is $\Pi_t = 2K_t$.

Due to the symmetry of the problem, the angular distribution of radiation striking the surface of the wall at any point on the wall is isotropic. If the albedo of radiation from the material of the walls of

the room is $A_d^{\pi}(\gamma)$, where γ is the angle of incidence of the radiation to the surface of the wall, the dose of singly reflected radiation at the point of observation is

$$D' = K_t \int_0^{\pi/2} \sin\gamma\, A_d^{\pi}(\gamma)\, d\gamma. \tag{6.59}$$

For neutrons in the case of concrete or iron walls

$$\begin{aligned} D_n' &= K_t A_{nd}^{\pi}(\gamma = 0) \int_0^{\pi/2} \sin\gamma \cos^{2/3}\gamma d\gamma = \\ &= 0{,}6 K_t A_{nd}^{\pi}(\gamma = 0), \end{aligned} \tag{6.60}$$

where $A_{nd}^{\pi}(\gamma = 0)$ is the albedo with normal incidence on the surface of the wall, about 0.9 for iron and 0.6 for concrete.

Since as been shown in Chapter 4 the distribution of reflected neutrons is isotropic, and their spectrum is slightly deformed in comparison to the spectrum of the incident neutrons to the barrier, the geometric conditions of repeated reflection will correspond precisely with the conditions of first reflection. Therefore, the dose recorded due to multiple reflection at any point M within the structure will be

$$D_n^{M} = K_t \frac{0{,}6 A_{nd}^{\pi}(\gamma = 0)}{1 - 0{,}6\, A_{nd}^{\pi}(\gamma = 0)}. \tag{6.61}$$

In the case of a concrete structure, $D_n^m = 0.563\ K_t$, for iron walls $D_n^m = 1.175 \cdot K_t$. Recalling that the transmission factor for radiation of the structure for any point within the structure is $\Pi = 2\ K_t$, we can conclude that in order to consider the contribution of multiply reflected neutrons within a concrete structure the total transmission factor for neutrons Π_t should be multiplied by 1.28. For structures with iron shielding, this correcting factor is about 1.585. In other words, the increase in the dose due to multiple reflection within a concrete structure is about 28%, within an iron structure about 58.5%. For polyethylene (water), this contribution is about 8-10%.

In the case of γ radiation, the yield of singly reflected radiation D_γ' is $D_\gamma = A_{\gamma d}^{\pi} K_t$, i. e. 0.073 K_t for water, 0.069 K_t for concrete

and 0.066 K_t for iron based on the mean γ radiation energy [3].

It was established in Chapter 5, with the exception of cases of incidence of γ radiation at very high inclination, the cosinusoidal dependence is very satisfactory as an approximation of the angular distribution of radiation scattered back from a barrier. As concerns the spectral distribution of reflected γ radiation, most γ quanta undergoing single or multiple reflection have energies in the intervals 0.1-0.5 MeV (see Figure 5.3). We can see from Figure 5.2 that in this energy interval the albedo of the γ radiation does not change significantly at all and can be assumed equal to 0.065 for iron, 0.160 for concrete and 0.25 for water with normal incidence.

The contribution of the second reflection of γ quanta from the walls is

$$D'_\gamma = 2\pi D'_\gamma \int_0^{\pi/2} A^{\pi}_{\gamma d} \sin\gamma\cos\gamma d\gamma = D'_\gamma A^{\pi}_{\gamma d}, \qquad (6.62)$$

$A^{\pi}_{\gamma d}$ is the albedo of γ radiation from the wall with an energy of 0.1-0.5 MeV and normal incidence.

The dose recorded due to multiple reflection at any point within the structure will be

$$D^{M}_\gamma = D'_\gamma + D'_\gamma \frac{A^{\pi}_{\gamma d}}{1 - A^{\pi}_{\gamma d}}. \qquad (6.63)$$

For concrete, this expression is 0.082, for iron 0.0707 and for water 0.0985. Thus, in order to consider the contribution of multiply reflected γ quanta from the walls within a concrete structure, the total transmission factor for γ quanta should be multiplied by about 1.041, within an iron structure -- by about 1.0304 and within a structure having a shield of water or polyethylene -- about 1.050. In other words, the contribution of multiply reflected γ quanta does not exceed 5% and can generally be ignored.

Bibliography

1. Goryachev, I. V., Godovanik, B. K., *Atomnaya Energiya*, Vol. 25, p. 49 (1968).

2. Kazanskiy, Yu. A. et al., *Byulleten' Informatsionnogo Tsentra Po Yadernym Dannym* [Bulletin of Information Center for Nuclear Data], No. 2, Moscow, Atomizdat Press, 1965, p. 305.

3. Degtyarev, S. F. et al., *Atomnaya Energiya*, Vol. 21, p. 395 (1966).

4. Spenser, L. V., *Zashchita Ot γ-Izlucheniya Radioaktivnykh Vypadeniy* [Shielding From the γ Radiation of Radioactive Fallout], Moscow, Atomizdat Press, 1965.

5. Leypunskiy, O. I., *Rasprostraneniye γ-Kvantov v Veshchestve* [The Propagation of γ Quanta in Matter], Moscow, Fizmatgiz Press, 1960.

APPENDIX 1

Table a. 1

BARRIER TRANSMISSION FACTORS OF TOTAL DOSE OF NEUTRONS FROM NUCLEAR EXPLOSION $\Lambda_{nt}(\delta, \theta, \alpha)$ FOR VARIOUS MATERIALS

α, Degrees	θ, degrees									
	0	20	40	60	80	100	120	140	160	180
	Iron, δ=16 *см* ($\times 10^{-4}$)									
0	0941	1038	1080	1084	0989	0781	0666	0432	0322	0253
10	0911	0925	0956	0958	0911	0800	0627	0448	0360	0235
20	0883	0876	0904	0897	0857	0688	0597	0442	0378	1234
30	0879	0875	0831	0792	0677	0619	0456	0403	0319	0272
40	0885	0874	0809	0709	0587	0465	0373	0312	0278	0278
50	0897	0876	0811	0701	0593	0456	0411	0335	0318	0295
60	0917	0880	0804	0678	0576	0454	0413	0352	0344	0313
70	0931	0868	0786	0659	0560	0450	0425	0375	0374	0341
80	0873	0845	0752	0632	0547	0447	0441	0395	0400	0363
90	0820	0830	0738	0623	0538	0442	0468	0414	0421	0387
	Iron, δ=20 *см* ($\times 10^{-4}$)									
0	0624	0617	0603	0593	0529	0413	0320	0241	0183	0173
10	0622	0616	0599	0570	0512	0400	0310	0238	0185	0178
20	6197	0615	0594	0555	0486	0387	0296	0233	0188	0183
30	0616	0614	0585	0529	0454	0363	0283	0229	0196	0190
40	0620	0613	0571	0505	0421	0342	0271	0227	0204	0194
50	0630	0616	0559	0482	0394	0328	0265	0233	0217	0211
60	0646	0619	0554	0463	0378	0318	0265	0242	0232	0225
70	0657	0612	0540	0449	0366	0315	0272	0258	0252	0245
80	0619	0596	0514	0427	0352	0313	0279	0271	0269	0261
90	0580	0586	0496	0415	0350	0323	0299	0294	0296	0290

Table a. 1. continued

α, degrees	ϑ, degrees									
	0	20	40	60	80	100	120	140	160	180
Polyethylene, δ=16 *см* (×10⁻⁵)										
0	0904	0921	1027	2131	0978	0724	0471	0322	0272	0292
10	0935	0954	1020	0142	0910	0671	0447	0334	0287	0296
20	0967	0983	1012	0985	0838	0625	0428	0341	0303	0298
30	0998	1010	1008	0928	0772	0579	0416	0345	0316	0310
40	1050	1044	0991	0876	0702	0540	0406	0350	0330	0318
50	1114	1087	0975	0821	0641	0515	0410	0368	0351	0345
60	1191	1123	0968	0771	0601	0501	0419	0387	0373	0367
70	1250	0114	0947	0728	0571	0501	0440	0418	0407	0400
80	1190	1126	0900	0682	0547	0503	0458	0443	0434	0427
90	1113	1118	0862	0652	0542	0525	0498	0486	0479	0473
Polyethylene, δ =29 *см* (×10⁻⁶)										
0	0984	1019	1200	1352	0283	0854	0499	0350	0337	0321
10	1042	1080	1200	1275	0191	0789	0481	0367	0345	0336
20	1107	1138	1201	1190	1003	0726	0472	0380	0352	0349
30	1161	1182	1202	1116	0917	0668	0463	0390	0367	0363
40	1242	1239	1186	1049	0826	0621	0456	0399	0384	0372
50	1341	1309	1168	0975	0747	0591	0468	0423	0407	0403
60	1459	1367	1161	0907	0694	0577	0482	0448	0434	0429
70	1549	1396	1138	0847	0654	0579	0512	0486	0473	0467
80	1476	1391	1080	0787	0624	0583	0536	0517	0504	0498
90	1384	1387	1032	0748	0618	0613	0586	0570	0558	0553
Concrete, δ=5 *см* (×10⁴)										
0	2960	2870	2749	2651	2439	1981	1543	1150	0793	0761
10	2897	2831	2698	2541	2285	1864	1468	1125	0824	0793
20	2845	2799	2644	2430	2150	1759	1396	1091	0855	0825
30	2793	2767	2592	2328	2020	1655	1327	1062	0889	0859

Table a. 1. continued

α, degrees	ϑ, degrees									
	0	20	40	60	80	100	120	140	160	180
40	2767	2731	2524	2233	1890	1564	1259	1049	0924	0877
50	2762	2702	2467	2143	1786	1501	1233	1068	0988	0955
60	2783	2682	2440	2080	1723	1456	1211	1101	1052	1016
70	2791	2628	2377	2033	1678	1436	1236	1169	1146	1107
80	2618	2542	2264	1949	1621	1422	1259	1225	1223	1181
90	2451	2486	2181	1900	1612	1463	1343	1324	1342	1309
Concrete, δ=15 *см* ($\times 10^{-4}$)										
0	8551	8464	9529	8998	8204	6219	4166	3331	2447	2400
10	8605	8551	8598	8612	7592	5831	4074	3274	2551	2500
20	8645	8634	8532	8195	7084	5441	3986	3224	2666	2599
30	8679	8700	8472	7769	6527	5078	3854	3187	2773	2704
40	8853	8823	8316	7369	6024	4779	3721	3179	2893	2783
50	9168	9007	8162	6961	5575	4587	3695	3283	3082	3006
60	9657	9170	8088	6612	5298	4470	3724	3414	3280	3198
70	9996	9196	7889	6319	5098	4451	3863	3650	3574	3484
80	9497	9054	7484	5975	4900	4441	3984	3842	3813	3717
90	8899	8962	7182	9767	4864	4510	4295	4182	4197	4121
Concrete, δ=25 *см* ($\times 10^{-5}$)										
0	2954	2961	2992	3194	2910	2189	1554	1119	0871	0836
10	3001	3014	3021	3057	2704	2067	1473	1110	0908	0877
20	3047	3061	3056	2908	2507	1940	1408	1106	0940	0918
30	3090	3101	3023	2756	2327	1807	1355	1103	0977	0955
40	3182	3152	2962	2617	2139	1692	1306	1109	1020	0976
50	3303	3222	2906	2474	1980	1615	1298	1152	1086	1063
60	3456	3283	2881	2353	1877	1570	1310	1204	1156	1130
70	3567	3284	2817	2252	1799	1561	1361	1292	1260	1231
80	3372	3225	2680	2128	1727	1558	1405	1363	1344	1314
90	3160	3185	2576	2050	1715	1618	1517	1490	1481	1457

Table a. 2.

BARRIER TRANSMISSION FACTORS FOR SCATTERED NEUTRONS FROM A NUCLEAR EXPLOSION
$\Lambda_{n,s}$, (δ, θ, α) FOR VARIOUS MATERIALS

α, degrees	θ, degrees									
	0	20	40	60	80	100	120	140	160	180
Iron, δ=16 *см* ($\times 10^{-4}$)										
0	0840	0934	0952	0937	0861	0685	0607	0403	0297	0228
10	0813	0822	0843	0836	0796	0719	0569	0415	0336	0211
20	0796	0775	0796	0784	0750	0611	0541	0409	0354	0210
30	0776	0770	0724	0695	0595	0553	0415	0372	0294	0247
40	0773	0763	0704	0618	0518	0419	0342	0286	0252	0253
50	0776	0759	0708	0614	0526	0411	0374	0305	0290	0264
60	0787	0758	0701	0596	0513	0409	0375	0320	0314	0283
70	0794	0744	0685	0582	0501	0406	0384	0340	0342	0309
80	0743	0722	0655	0560	0490	0403	0398	0358	0365	0329
90	0698	0708	0645	0556	0483	0398	0423	0375	0383	0351
Iron, δ=20 *см* ($\times 10^{-4}$)										
0	0576	0568	0542	1521	0477	0363	0285	0222	0166	0156
10	0575	0567	0545	0509	0460	0355	0274	0217	0169	0162
20	0571	0567	0542	0499	0430	0343	0261	0211	0172	0167
30	0566	0563	0534	0482	0410	0326	0258	0208	0179	0173
40	0566	0560	0520	0461	0375	0317	0252	0209	0186	0177
50	0572	0560	0509	0439	0361	0303	0241	0213	0198	0192
60	0583	0560	0504	0423	0345	0292	0240	0221	0212	0205
70	0591	0552	0491	0411	0334	0289	0248	0235	0230	0223
80	0556	0530	0468	0394	0321	0287	0251	0246	0246	0238
90	0521	0529	0453	0383	0320	0297	0269	0267	0272	0266

Table a. 2. continued

α, degrees	ϑ, degrees									
	0	20	40	60	80	100	120	140	160	180
	Polyethylene, δ=16 *см* (×10⁻³)									
0	0864	0881	0977	0971	0918	0684	0441	0312	0262	0282
10	0895	0914	0970	0937	0860	0631	0417	0324	0267	0286
20	0927	0943	0972	0935	0788	0585	0398	0331	0293	0288
30	0958	0970	0968	0888	0732	0549	0396	0335	0306	0300
40	1000	0994	0951	0836	0672	0520	0396	0340	0320	0308
50	1064	1037	0935	0781	0611	0495	0390	0358	0341	0335
60	1131	1073	0928	0741	0571	0481	0399	0367	0363	0357
70	1190	1090	0907	0698	0541	0481	0420	0398	0387	0380
80	1130	1076	0860	0652	0527	0483	0438	0423	0414	0407
90	1063	1068	0822	0622	0522	0505	0478	0466	0459	0453
	Polyethylene, δ=29 *см* (×10⁻⁶)									
0	0964	0999	1180	1322	0990	0834	0489	0341	0329	0313
10	1022	1060	1180	1245	0988	0769	0471	0359	0337	0328
20	1087	1318	1181	1170	0973	0706	0462	0372	0344	0341
30	1141	1162	1182	1096	0897	0659	0453	0381	0359	0355
40	1222	1219	1166	1029	0816	0611	0366	0390	0375	0363
50	1311	1279	1148	0955	0737	0581	0458	0413	0393	0394
60	1429	1337	1141	0887	0684	0567	0472	0438	0424	0419
70	1519	1366	1118	0827	0644	0569	0502	0476	0463	0457
80	1446	1361	1060	0777	0614	0573	0526	0507	0494	0488
90	1354	1357	1012	0738	0608	0603	0576	0560	0548	0543
	Concrete, δ=5 *см* (×10⁻⁴)									
0	1291	1017	0868	0801	0716	0611	0315	0315	0162	0289
10	1292	1207	1026	0881	0691	0599	0312	0267	0182	0356
20	1295	1272	1059	0874	0646	0523	0291	0244	0191	0391
30	1269	1255	1167	0936	0836	0537	0490	0292	0267	0343

Table a. 2. continued

α, degrees	ϑ, degrees									
	0	20	40	60	80	100	120	140	160	180
40	1254	1233	1137	1008	0857	0721	0563	0458	0398	0346
50	1244	1213	1067	0927	0730	0670	0455	0438	0379	0398
60	1239	1198	1052	0898	0694	0623	0440	0440	0391	0434
70	1231	1168	1022	0878	0670	0610	0444	0466	0427	0461
80	1152	1124	0966	0836	0631	0598	0438	0485	0452	0494
90	1078	1095	0941	0829	0640	0640	0494	0547	0520	0581
Concrete, δ=15 *см* ($\times 10^{-5}$)										
0	4400	4250	3358	2817	2527	1906	1236	1705	1007	0963
10	4595	4368	3971	3428	2341	2009	1008	1460	1180	1130
20	4676	4520	4119	3384	2160	1700	0985	1408	1288	1222
30	4457	4390	4063	3701	2952	1886	1730	1435	1331	1272
40	4275	4281	3970	3556	3060	2609	2071	1670	1382	1324
50	4196	4185	3883	3298	2565	2417	1663	1584	1481	1413
60	4264	4120	3833	3179	2457	2253	1604	1605	1577	1503
70	4326	4040	3705	3105	2401	2216	1611	1681	1717	1638
80	4060	3922	3505	2962	2265	1171	1584	1737	1833	1748
90	3801	3849	3375	2967	2289	2306	1726	1937	2091	1937
Concrete, δ=25 *см* ($\times 10^{-5}$)										
0	2111	2125	1969	1931	1724	1311	1082	0798	0580	0546
10	2200	2178	2092	2007	1616	1288	0863	0765	0631	0600
20	2255	2238	2164	1940	1489	1172	0803	0760	0661	0640
30	2245	2236	2125	1917	1591	1162	0947	0764	0686	0666
40	2262	2231	2073	1834	1540	1262	0980	0804	0715	0678
50	2292	2235	2029	1733	1373	1181	0886	0812	0763	0741
60	2339	2242	2009	1666	1305	1122	0877	0842	0812	0788
70	2367	2212	1961	1616	1257	1107	0899	0898	0885	0858
80	2226	2151	1869	1536	1198	1095	0910	0942	0944	0916
90	2085	2110	1802	1501	1198	1143	0993	1041	1051	1015

APPENDIX 2

Table a. 3.

BARRIER TRANSMISSION FACTORS FOR TOTAL DOSE OF FRAGMENT γ RADIATION OF NUCLEAR EXPLOSION $\Lambda^{f}_{\gamma t}(\delta, \theta, \alpha)$ FOR IRON

α, degrees	θ, degrees									
	0	20	40	60	80	100	120	140	160	180
	δ=5 *см* (×10⁻⁴)									
0	0150	0254	0396	0653	0699	0771	0519	0313	0193	0175
10	0244	0322	0528	0787	0756	0768	0488	0306	0188	0172
20	0421	0491	0714	0752	0827	0645	0434	0280	0183	0160
30	0578	0694	0865	0780	0835	0512	0347	0226	0181	0167
40	0906	0989	0952	0910	0763	0446	0337	0253	0223	0206
50	1289	1274	1077	0875	0567	0332	0291	0242	0219	0205
60	1888	1692	1387	0763	0451	0272	0279	0228	0227	0222
70	2652	1984	1328	0611	0376	0259	0288	0264	0245	0233
80	2270	2300	1384	0614	0384	0246	0287	0264	0244	0229
90	2134	2652	1375	0532	0328	0204	0238	0218	0202	0191
	δ=10 *см* (×10⁻⁵)									
0	0140	0301	0564	1065	1053	1333	0759	0347	0175	0160
10	0288	0438	0892	1492	1293	1418	0724	0352	0171	0158
20	0577	0764	1325	1344	1472	1066	0572	0279	0173	0160
30	0848	1149	1640	1381	1500	0745	0395	0217	0164	0153
40	1505	1735	1710	1674	1258	0570	0347	0234	0204	0189
50	2340	2394	1954	1600	0803	0365	0283	0223	0200	0188
60	3740	3322	2716	1101	0700	0300	0275	0232	0208	0204
70	5727	3997	2506	0887	0409	0244	0272	0245	0225	0214
80	4395	4666	2537	0916	0436	0229	0272	0245	0223	0210
90	4379	5959	2747	0934	0385	0186	0226	0202	0185	0175

Table a. 3. continued

α, degrees	ϑ, degrees									
	0	20	40	60	80	100	120	140	160	180
	δ=20 см (×10⁻⁶)									
0	0005	0023	0138	0427	0346	0602	0194	0030	0018	0017
10	0016	0056	0268	0731	0534	0683	0182	0034	0018	0017
20	0074	0184	0579	0593	0658	0382	0107	0025	0018	0017
30	0157	0334	0768	0596	0669	0185	0048	0021	0017	0016
40	0443	0624	0718	0750	0425	0099	0038	0025	0021	0020
50	0891	1042	0800	0666	0190	0043	0032	0024	0021	0204
60	1808	1532	1253	0435	0102	0028	0031	0023	0022	0022
70	2272	1922	1105	0227	0050	0024	0033	0027	0024	0023
80	2061	2385	1012	0216	0048	0023	0033	0027	0024	0022
90	2173	3479	1185	0224	0042	0019	0028	0023	0020	0019

Table a. 4.

BARRIER TRANSMISSION FACTORS FOR SCATTERED DOSE OF FRAGMENT γ RADIATION OF NUCLEAR EXPLOSION $\Lambda^{f}_{\gamma\ s}(\delta, \theta, \alpha)$ FOR IRON

α, degrees	0	20	40	60	80	100	120	140	160	180
	δ=5 см									
0	0113	0160	0243	0403	0452	0473	0340	0236	0170	0155
10	0155	0186	0290	0424	0452	0439	0313	0221	0166	0152
20	0240	0271	0379	0431	0486	0390	0299	0200	0163	0150
30	0328	0378	0458	0449	0482	0327	0263	0192	0160	0147
40	0497	0530	0526	0498	0454	0304	0278	0220	0196	0181
50	0696	0674	0587	0469	0367	0255	0250	0211	0193	0181
60	0991	0879	0707	0441	0321	0216	0243	0200	0200	0195

Table a. 4. continued

α, degrees	0	20	40	60	80	100	120	140	160	180
70	1286	1024	0708	0378	0286	0219	0253	0231	0216	0205
80	1255	1190	0751	0354	0276	0211	0252	0231	0215	0202
90	1133	1229	0676	0300	0224	0173	0209	0191	0178	0168
					δ=10 *см* ($\times 10^{-5}$)					
0	0132	0269	0406	0688	0735	0818	0560	0319	0164	0150
10	0263	0361	0594	0855	0818	0827	0537	0320	0160	0147
20	0488	0559	0795	0819	0898	0712	0465	0259	0161	0150
30	0656	0798	0955	0851	0912	0557	0350	0203	0154	0143
40	1024	1135	1064	1007	0856	0465	0317	0218	0190	0176
50	1481	1442	1225	0990	0608	0322	0262	0207	0187	0176
60	2155	1944	1585	0853	0550	0270	0254	0210	0194	0190
70	2942	2250	1500	0648	0359	0227	0252	0227	0210	0200
80	2616	2611	1584	0675	0386	0214	0252	0208	0203	0196
90	2540	3003	1634	0683	0339	0174	0209	0188	0173	0163
					δ=20 *см* ($\times 10^{-6}$)					
0	0005	0022	0111	0283	0244	0376	0155	0029	0017	0017
10	0015	0050	0216	0428	0342	0403	0145	0033	0017	0017
20	0065	0144	0356	0378	0406	0265	0091	0025	0018	0017
30	0131	0253	0461	0383	0409	0146	0045	0021	0017	0016
40	0343	0435	0463	0462	0304	0084	0037	0024	0021	0020
50	0640	0659	0528	0428	0152	0040	0031	0024	0021	0020
60	1135	0988	0777	0304	0085	0027	0030	0022	0022	0021
70	1823	1220	0707	0175	0046	0023	0032	0026	0023	0023
80	1383	1450	0703	0171	0046	0027	0032	0027	0024	0022
90	1432	1928	0798	0177	0041	0018	0027	0022	0019	0018

APPENDIX 3

Table a. 5

BARRIER TRANSMISSION FACTORS FOR TOTAL DOSE OF CAPTURE γ RADIATION PRODUCED IN AIR FOR NUCLEAR EXPLOSION $\Lambda^{c}_{\gamma t}(\delta, \theta, \alpha)$ FOR IRON

α, degrees	θ, degrees									
	0	20	40	60	80	100	120	140	160	180
	δ=5 *см* (×10⁻⁴)									
0	0274	0400	0472	0643	0661	0662	0488	0322	0150	0132
10	0399	0468	0581	0712	0659	0627	0440	0288	0126	0114
20	0809	0643	0739	0779	0727	0633	0439	0254	0139	0125
30	0928	1265	0979	0959	1216	0685	0377	0185	0132	0120
40	1067	1112	1009	0920	0757	0474	0296	0190	0162	0150
50	1423	1386	1178	1002	0630	0348	0234	0175	0159	0145
60	1792	1650	1397	0861	0501	0299	0214	0179	0169	0156
70	2264	1815	1422	0819	0507	0560	0206	0186	0180	0170
80	2180	2095	1285	0811	0480	0239	0207	0187	0181	0170
90	2100	2142	1290	0810	0480	0242	0221	0188	0184	0175
	δ=10 *см* (×10⁻⁵)									
0	0235	0409	0736	1236	1188	1399	0810	0357	0168	0157
10	0402	0557	1047	1516	1329	1375	0720	0323	0145	0134
20	0798	0915	1406	1640	1516	1232	0622	0286	0158	0146
30	1272	2222	2180	2125	2886	1089	0464	0213	0150	0140
40	1924	2095	2006	1882	1391	0653	0365	0226	0187	0176
50	3025	3015	2387	1993	1007	0429	0291	0211	0184	0170
60	4243	3793	3007	1546	0705	0343	0270	0221	0196	0183
70	5829	3910	3102	1561	0651	0288	0267	0231	0211	0201
80	5067	4925	2727	1228	0560	0263	0270	0234	0211	0198
90	5330	5784	2590	1021	0582	0210	0299	0241	0207	0198

Table a. 5. continued

α, Degrees	ϑ, degrees									
	0	20	40	60	80	100	120	140	160	180
	δ=20 *см* (×10⁻⁶)									
0	0034	0041	0214	0577	0459	0736	0242	0034	0017	0016
10	0035	0088	0392	0838	0636	0765	0216	0032	0015	0014
20	0111	0225	0617	0851	0764	0539	0133	0028	0016	0015
30	0283	0777	0971	1157	1688	0335	0064	0020	0015	0015
40	0669	0877	0960	0963	0554	0136	0042	0024	0020	0019
50	1350	1561	1150	0980	0296	0060	0032	0023	0019	0018
60	2413	2046	1579	0620	0151	0037	0031	0024	0021	0019
70	0304	2712	1382	0542	0166	0045	0032	0026	0022	0021
80	2869	2933	1241	0344	0069	0026	0032	0026	0022	0021
90	3377	2723	1480	0371	0068	0026	0031	0025	0226	0025

Table a. 6.

BARRIER TRANSMISSION FACTORS OF SCATTERED DOSE OF CAPTURE γ RADIATION FROM AIR FOR NUCLEAR EXPLOSION $\Lambda^{c}_{\gamma s}(\delta, \theta, \alpha)$ FOR IRON

α, degrees	ϑ, degrees									
	0	20	40	60	80	100	120	140	160	180
	δ=5 *см* (×10⁻⁵)									
0	2065	2660	2774	3441	3745	3401	2949	2307	1286	1127
10	2643	2849	3061	3320	3367	2992	2594	1956	1083	0968
20	4011	3745	3744	3779	3691	3336	2740	1874	1194	1063
30	5292	6327	4640	4409	5111	3885	2583	1486	1136	1025
40	5554	5492	4949	4440	4040	2995	2228	1582	1387	1280
50	6639	6219	5607	4744	3644	2447	1872	1467	1357	1238

Table a. 6. continued

α, degrees	ϑ, degrees									
	0	20	40	60	80	100	120	140	160	180
60	7498	7133	6297	4591	3277	2227	1762	1500	1440	1324
70	8414	7543	7081	4664	3397	2112	1713	1550	1535	1440
80	8843	7644	6420	4637	3268	1952	1722	1558	1540	1443
90	8881	7832	6481	4612	3215	1968	1746	1574	1562	1468
	$\delta=10$ см ($\times10^{-5}$)									
0	0217	0350	0506	0738	0776	0783	0569	0352	0157	0146
10	0347	0441	0662	0797	0776	0723	0503	0286	0135	0125
20	0645	0665	0839	0908	0866	0749	0482	0260	0148	0136
30	0938	1412	1130	1136	1451	0755	0399	0198	0140	0131
40	1244	1275	1159	1041	0880	0508	0328	0211	0175	0164
50	1775	1635	1368	1118	0712	0364	0268	0197	0172	0159
60	2178	2016	1617	0969	0548	0306	0250	0205	0183	0174
70	2651	2264	1651	0981	0524	0262	0247	0215	0197	0187
80	2687	2465	1608	0866	0481	0244	0250	0217	0197	0185
90	2590	2702	1592	0739	0497	0202	0273	0226	0198	0187
	$\delta=20$ см ($\times10^{-6}$)									
0	0031	0038	0165	0341	0266	0405	0183	0033	0017	0016
10	0033	0075	0279	0439	0370	0400	0162	0031	0015	0014
20	0099	0175	0386	0488	0431	0342	0108	0027	0016	0015
30	0227	0566	0558	0654	0918	0248	0058	0019	0015	0014
40	0492	0561	0565	0536	0364	0111	0040	0023	0019	0018
50	0908	0886	0685	0567	0220	0053	0031	0022	0019	0018
60	1315	1186	0890	0400	0122	0036	0030	0023	0020	0019
70	1696	1454	0915	0345	0157	0044	0031	0025	0027	0021
80	1683	1575	0794	0265	0065	0025	0031	0025	0027	0020
90	1854	1300	0801	0282	0066	0240	0030	0023	0025	0023

APPENDIX 4

Table a. 7

BARRIER TRANSMISSION FACTORS FOR TOTAL DOSE OF γ RADIATION OF RADIOACTIVE FALLOUT FROM NUCLEAR EXPLOSION $\Delta^{r}_{\gamma t}(\delta, \theta, \alpha)$ FOR IRON

Time Following Explosion	θ, degrees									
	0	20	40	60	80	100	120	140	160	180
	δ=5 *см* (×10⁻⁴)									
1,12 hr	0012	0103	0190	0427	0613	0667	0550	0522	0792	0484
23,8 hr	0011	0099	0172	0240	0404	0531	0604	0563	0604	0491
4,57 days	0011	0097	0165	0250	0300	0343	0345	0274	0262	0361
9,8 days	0012	0100	0188	0385	0587	0634	0500	0512	0893	0612
	δ=10 *см* (×10⁻⁵)									
1,12 hr	0015	0146	0354	0655	1085	1153	0849	0889	1675	0982
23,8 hr	0014	0130	0189	0255	0476	0672	0763	0727	0807	0567
4,57 days	0014	0125	0205	0313	0405	0452	0424	0345	0374	0514
9,8 days	0015	0143	0327	0604	1050	1113	0764	0934	1962	1322
	δ=20 *см* (×10⁻⁷)									
1,12 hr	0009	0167	0413	1013	2917	3211	1617	1035	2610	1531
23,8 hr	0009	0087	0144	0254	0771	1017	1624	1014	2630	1524
4,57 days	0009	0141	0223	0264	0574	0684	0492	0413	0517	0703
9,8 days	0009	0167	0425	0994	2715	2931	1537	1093	3230	2617

Table a. 8.

BARRIER TRANSMISSION FACTORS OF DOSE OF SCATTERED γ RADIATION FROM RADIOACTIVE FALLOUT FROM NUCLEAR EXPLOSION $\Lambda^{r}_{\gamma s}(\delta, \theta, \alpha)$ FOR IRON

Time Following Explosion	θ, degrees									
	0	20	40	60	80	100	120	140	160	180
	δ=5 *см* (×10⁻⁴)									
1,12 hr	0012	0101	0164	0315	0430	0461	0384	0433	0733	0431
23,8 hr	0011	0098	0141	0205	0321	0425	0482	0477	0523	0420
4,57 days	0011	0096	0142	0215	0234	0262	0260	0231	0233	0345
9,8 »	0012	0098	0162	0323	0450	0471	0383	0443	0815	0524
	δ=10 *см* (×10⁻⁵)									
1,12 hr	0015	0143	0349	0572	0871	0912	0701	0850	1622	0941
23,8 hr	0014	0128	0186	0239	0422	0596	0697	0688	0774	0542
4,57 days	0014	0125	0205	0301	0361	0404	0372	0312	0351	0500
9,8 »	0015	0140	0326	0591	0901	0940	0692	0901	1880	1191
	δ=20 *см* (×10⁻⁷)									
1,12 hr	0009	0165	0409	0901	2509	2704	1410	1007	2519	1520
23,8 hr	0009	0087	0137	0245	0725	0921	1420	1005	2521	1509
4,57 days	0009	0139	0222	0263	0521	0602	0457	0392	0504	0690
9,8 »	0009	0165	0411	0981	2503	2724	1425	1060	2924	2114

APPENDIX 5

Table a. 9.

YIELD OF CAPTURE γ RADIATION OF VARIOUS MATERIALS ON SIDE OPPOSITE SIDE BOMBARDED BY NEUTRONS $A^{3}_{\gamma i}(\delta)$ (rad of γ QUANTA PER 1 rem NEUTRONS FROM NUCLEAR EXPLOSION WITH NORMAL INCIDENCE TO SURFACE OF SHIELD)

Thickness of Barrier, cm	Concrete		Iron		Water	
	Thermal Neutrons	Fast Neutrons	Thermal Neutrons	Fast Neutrons	Thermal Neutrons	Fast Neutrons
2	0,0754	0,0850	0,132	0,0370	0,0630	0,0535
3	0,0954	0,1135	0,122	0,0465	0,0727	0,0690
4	0,1081	0,1352	0,102	0,0526	0,0860	0,0850
6	0,1194	0,1644	0,065	0,0580	0,091	0,1081
8	0,1178	0,1770	0,040	0,058	0,0885	0,1192
10	0,1110	0,1830	0,0248	0,0554	0,0826	0,1276
12	0,1043	0,1796	0,0153	0,0515	0,0768	0,1250
14	0,0910	0,1532	0,0097	0,0471	0,0701	0,1228
16	0,0810	0,1620	0,0061	0,0427	0,0643	0,1178
18	0,0710	0,1503	0,0038	0,0384	0,0593	0,1110
20	0,10622	0,1393	0,0024	0,0343	0,0543	0,1044
24	0,0476	0,1152	0,0010	0,0272	0,0459	0,0994

Table a. 10.

YIELD OF CAPTURE γ RADIATION ON SIDE OPPOSITE INCIDENT NEUTRONS

$\Delta^{3}_{\gamma j}(\theta, \alpha)$ (rel. units) $\times 10^{-4}$

α, degrees \ ϑ, degrees	0	20	40	60	80	100	120	140	160	180
0	3169	3549	3606	3492	3286	2631	2497	1742	1364	1003
10	3458	3491	3577	3514	3343	2682	2483	1876	1575	0925
20	3647	3579	3661	3540	3353	2747	2447	1889	1671	0919
30	3790	3751	3487	3347	2820	2587	1938	1727	1345	1103
40	3970	3923	3587	3728	2611	2078	1661	1331	1121	1134
50	4133	4051	3684	3156	2596	2053	1680	1381	1228	1221
60	4322	4169	3761	3239	2715	2093	1811	1481	1420	1262
70	4462	4202	3858	3244	2696	2075	1848	1567	1543	1377
80	4357	4232	3825	3224	2694	2079	1910	1646	1655	1465
90	4188	4247	3812	3291	2727	2240	1801	1605	1661	1559